U.S. Coast Guard Research and Development Center
1082 Shennecossett Road, Groton, CT 06340-6096

Report No. CG-D-22-99, II

Prediction of ISO 9705 Room/Corner Test Results
(Appendices A, B, and C)

Volume II

FINAL REPORT
NOVEMBER 1999

This document is available to the U.S. public through the
National Technical Information Service, Springfield, VA 22161

Prepared for:

U.S. Department of Transportation
United States Coast Guard
Marine Safety and Environmental Protection (G-M)
Washington, DC 20593-0001

N O T I C E

This document is disseminated under the sponsorship of the Department of Transportation in the interest of information exchange. The United States Government assumes no liability for its contents or use thereof.

The United States Government does not endorse products or manufacturers. Trade or manufacturers' names appear herein solely because they are considered essential to the object of this report.

This report does not constitute a standard, specification, or regulation.

Marc B. Mandler, Ph.D.
Technical Director
United States Coast Guard
Research & Development Center
1082 Shennecossett Road
Groton, CT 06340-6096

Technical Report Documentation Page

1. Report No.	2. Government Accession Number	3. Recipient's Catalog No.
CG-D-22-99, II	ADA378409	

4. Title and Subtitle	5. Report Date
Prediction of ISO 9705 Room/Corner Test Results – Appendices A, B, and C, Volume II	November 1999
	6. Performing Organization Code Project No. 3308.2.77/UDI 215
7. Author(s) Craig L. Beyler, Sean P. Hunt, Brian Y. Lattimer, Naeem Iqbal, Chris Lautenberger, Nicholas Dembsey, Jonathan Barnett, Marc Janssens, Scott Dillon, and Andrew Greiner	**8. Performing Organization Report No.** R&DC –215-99, II
9. Performing Organization Name and Address Hughes Associates, Inc. 3610 Commerce Drive, Suite 817 Baltimore, MD 21227-1652	**10. Work Unit No. (TRAIS)**
U.S. Coast Guard Research and Development Center 1082 Shennecossett Road Groton, CT 06340-6096	**11. Contract or Grant No.** DTCG39-99-F-E00159
12. Sponsoring Organization Name and Address U.S. Dept of Transportation United States Coast Guard Marine Safety and Environmental Protection (G-M) Washington, DC 20593-0001	**13. Type of Report & Period Covered** Final
	14. Sponsoring Agency Code Commandant (G-MSE) U.S. Coast Guard Headquarters Washington, DC 20593-0001

15. Supplementary Notes

The Research and Development Center's technical point of contact is Mr. Brian Dolph: 860-441-2817 or bdolph@rdc.uscg.mil.

16. Abstract

The full-scale International Standards Organization (ISO) 9705 Room/Corner Test is currently used to regulate compartment-lining materials in the High Speed Craft (HSC) Code. This test method involves the use of large amounts of material so that the test method is an impediment in developing new materials. Bench-scale tests like the Cone Calorimeter and the Lateral Ignition Flame Test (LIFT) Apparatus may provide indications of full-scale performance in the ISO 9705. The objective of this work is to assess if correlations and mathematical models based on bench-scale data can predict material performance in the ISO 9705 Test.

The results of this project show that it is possible to learn a great deal about the expected performance of materials in the ISO 9705 Test from bench-scale tests like the Cone Calorimeter and the LIFT Apparatus. Both the simple correlations using the Flammability Parameter deduced from the Cone Calorimeter and the mathematical models using Cone Calorimeter and LIFT data provided clear insights into the burning behavior of materials in the ISO 9705 Test.

The Flammability Parameter deduced from Cone Calorimeter data was able to correlate the heat release rate and time to flashover in the ISO 9705 Test. This provides the opportunity to obtain significant information concerning expected ISO 9705 performance from a few tests of small samples. It is significant that LIFT results are not required to allow correlation of the performance of U.S. Coast Guard (USCG) HSC Materials.

The mathematical models performed well in predicting the heat release rate and time to flashover in the ISO 9705 Test. These more sophisticated methods provide additional confidence in the ability of bench-scale tests to be used to predict the performance of materials in the ISO 9705 Test. Further, these models have the potential to allow prediction of realistic scenarios, which differ from the ISO 9705 Test method.

Neither correlations from the Cone Calorimeter nor the mathematical models adequately predict the smoke generation rates in the ISO 9705 Test. The inability to predict smoke generation is particularly significant for materials that pass the heat release rate criteria in ISO 9705. Significant additional work is needed in this area.

Volume I of this report contains the objectives, approach, test results, and conclusions. Volume II consists of three appendices; a) prediction based on Quintiere's model; b) evaluation of Worcester Polytechnic Institute (WPI) zone model, and c) Hughes Associates/U.S. Navy Corner Flame Spread model and comparison with USCG ISO 9705 Test results.

17. Key Words	18. Distribution Statement
fire growth, fire spread, fire model, high speed craft, Cone Calorimeter	This document is available to the U.S. public through the National Technical Information Service, Springfield, VA 22161.

19. Security Class (This Report)	20. Security Class (This Page)	21. No of Pages	22. Price
UNCLASSIFIED	UNCLASSIFIED	295	

Form DOT F 1700.7 (8/72) Reproduction of form and completed page is authorized.

TABLE OF CONTENTS

Page

Appendix A: Predictions Based on Quintiere's Model of ISO 9705 Room Fire Test Performance of Marine Composites A-1

Appendix B: Evaluation of the WPI Zone Model Flame Spread Algorithm Against Corner Test Data B-1

Appendix C: Hughes Associates, Inc./U.S. Navy Corner Flame Spread Model and Comparison with USCG ISO 9705 Test Results C-1

APPENDIX A – PREDICTIONS BASED ON QUINTIERE'S MODEL OF ISO 9705 ROOM FIRE TEST PERFORMANCE OF MARINE COMPOSITES

ABSTRACT

The purpose of this program was to predict the performance of eight marine composites and one textile wall covering in the ISO 9705 room-corner test using the fire growth model developed by Quintiere [Quintiere, 1993]. Four sets of material properties were developed using data obtained from the Cone Calorimeter and the Lateral Ignition and Flame spread Test (LIFT) apparatus. These properties were input into a FORTRAN version of Quintiere's model previously published by Dillon [Dillon, 1998]. The predicted heat release rate was compared with the actual heat release rate measured in ISO 9705 tests. These initial simulations did not provide acceptable predictions of the heat release rate and the time to flashover (characterized by a measured heat release rate of 1,000 kW).

Quintiere's model was converted to Microsoft® Excel 97, Visual Basic for Applications (VBA), and a validation was conducted to ensure that identical results were obtained as with the FORTRAN version. All modifications to Quintiere's fire growth model were conducted on the VBA version from that point on.

In an attempt to improve the heat release rate predictions by the fire growth model, the material properties were re-examined. It was determined that the convection coefficient, h_c, in the Cone Calorimeter is a function of incident heat flux. To account for this heat flux dependency, a new method had to be developed to obtain ignition properties from the ignition times measured at different heat flux levels. The heat of gasification values appeared to be excessive, and were believed to be the main cause of the poor flashover time predictions with Quintiere's original model. Therefore, the heat release rate algorithm based on the total pyrolysis area, heat of combustion, and heat of gasification was abandoned in favor of the use of an exponentially decaying heat release rate curve derived from Cone Calorimeter data at 50 kW/m².

The fire growth model was also revised to reflect the new properties. The equations used in the original FORTRAN version were replaced by equations previously used by Janssens [Janssens, 1995] in his QBasic version of the Quintiere model. This approach provides a more simplified method with the pyrolysis and burned out areas represented by rectangular areas as opposed to complex trapezoids. The main modification in Janssens' version of the model is an improved algorithm to provide a more realistic characterization of the ignition burner flame. The heat flux to the material in contact with the burner flame is determined based on the heat output of the burner and the temperature of the material, as opposed to simply using a constant flux. Additional modifications were made as described below. The heat

release rate from the burning material was simulated using the aforementioned exponentially decaying curve. As the flame front progresses, the pyrolysis area increases. At every incremental time step, a new area may ignite and start burning. The modified model tracks and sums the heat release rate from each incremental area based on the exponentially decaying heat release rate curve to determine the total heat release rate from the material. This method automatically accounts for burnout, i.e., an incremental area burns out when its heat release rate reaches the end of the exponential curve. An algorithm was added to calculate the emissivity of the upper gas layer as a function of the specific extinction area measured in the Cone Calorimeter (Quintiere assumes the emissivity to be 1.0). A routine was also added to estimate the smoke production rate in the room based on the specific extinction area measured in the Cone Calorimeter.

The results of the prediction using the revised fire growth model are quite reasonable. For materials with flashover times less than 600 (Material Nos. 3, 4, and 8), the model predictions are very close to the experimental data. For materials with flashover times between 600 and 1200 (Material Nos. 5 and 9), the predicted flashover times fall within the same 300-kW exposure period. For the remaining four materials, the model consistently predicts that flashover does not occur. The model also correctly predicts that the heat release rate criteria for fire restricting materials are not exceeded. However, two of these four materials (Material Nos. 1 and 6) failed marginally on smoke production in the tests, while the model predicts that all four materials would meet the smoke requirements.

Based on the predictions achieved, the fire growth model presented in this report represents a simple method for predicting material performance in the ISO 9705 Room-Corner Test based on a limited amount of test requirements and input parameters. A single Cone Calorimeter run at 50 kW/m^2, supplemented with surface temperature measurements, is all that is needed. However, it is recommended to perform at least two or three runs to improve the confidence in the input data (and, hence, the predictions). More work is needed to improve the smoke predictions, and to validate the conjecture that the surface temperature at ignition can be determined experimentally, in lieu of being inferred from the analysis of ignition data obtained at different heat flux levels.

TABLE OF CONTENTS

1.0 INTRODUCTION A-5

2.0 ORIGINAL MATERIAL PROPERTIES AND MODEL SIMULATIONS A-6

2.1 Ignition Properties A-6

2.1.1 LIFT Ignition Data A-6

2.1.2 Cone Calorimeter Ignition Data A-6

2.2 Flame Spread Properties A-8

2.2.1 LIFT Flame Spread Data A-8

2.2.2 IMO Flame Spread Data A-8

2.3 Heat Release Rate Properties A-9

2.4 Model Simulations A-10

2.4.1 FORTRAN Version A-10

2.4.2 VBA Version A-11

3.0 MODIFIED MATERIAL PROPERTIES AND MODEL SIMULATION A-11

3.1 Ignition Properties A-11

3.2 Flame Spread Properties A-14

3.3 Heat Release Rate Properties A-15

3.4 Smoke Release Rate Properties A-16

3.5 Modifications to the Model A-16

3.6 Modified Model Simulations A-18

3.7 Conclusions A-19

4.0 SUMMARY AND RECOMMENDATIONS A-20

5.0 REFERENCES A-21

ATTACHMENT A – ORIGINAL CONE CALORIMETER IGNITION PROPERTIES
ATTACHMENT B – CONE CALORIMETER CONVECTION HEAT TRANSFER COEFFICIENT DETERMINATION
ATTACHMENT C – ORIGINAL CONE CALORIMETER HEAT OF GASIFICATION DATA
ATTACHMENT D – ORIGINAL MODEL PREDICTIONS
ATTACHMENT E – MODIFIED CONE CALORIMETER IGNITION PROPERTIES
ATTACHMENT F – MODIFIED HEAT RELEASE RATE PROPERTIES
ATTACHMENT G – MODIFIED MODEL PREDICTIONS

1.0 INTRODUCTION

This report presents the results of a program that was conducted at Southwest Research Institute (SwRI) for Hughes Associates Inc. in Baltimore, MD, under subcontract No. E00150-4, and covers part of the work to be performed by Hughes for the U.S. Coast Guard under Contract No. DTCG39-97-D-E00150.

The performance of eight marine composite materials and one textile wall covering, previously tested in accordance with ISO 9705 "Fire tests—full-scale room test for surface products" (also referred to as the room-corner test), was predicted using a fire growth model developed by Quintiere [Quintiere, 1993]. The nine materials considered are presented in Table A-1.

Table A-1. Marine Composite Materials.

Material No.	Generic Name
1	FR Phenolic
2	Fire-Restricting Material
3	FR Polyester
4	FR Vinylester
5	FR Epoxy
6	Coated FR Epoxy
7	Wall Covering Material
8	Polyester
9	FR Modified Acrylic

Originally, a FORTRAN version of Quintiere's model was used to predict the performance of the materials. However, the calculations were in poor agreement with the experimental data. Therefore, the model was revised to include new methods for determining ignition and flame spread properties, as well as new algorithms for the ignition burner exposure, heat release and smoke production rate predictions, and the emissivity of the upper layer.

2.0 ORIGINAL MATERIAL PROPERTIES AND MODEL SIMULATIONS

2.1 Ignition Properties

2.1.1 LIFT Ignition Data

The ignition times obtained in the Lateral Ignition and Flamespread Test (LIFT) apparatus are reported in Appendix E2 of USCG R&D Center Report No. CG-D-22-98 [Janssens, Garabedian & Gray, 1998]. The ignition temperature, T_{ig}, and the thermal inertia, $k\rho c$, were calculated from these data using the procedures outlined in American Society for Testing and Materials (ASTM) Standard E 1321 "Standard Test Method for Determining Material Ignition and Flamespread Properties." The results are presented in Section 7 of the aforementioned report. The ignition property values required for input into the fire growth model are repeated in Table A-2 below. Note that no ignition properties could be obtained for Material Nos. 1 and 2 because the samples did not ignite at the highest heat flux that can be obtained in the LIFT apparatus.

Table A-2. Ignition Properties Derived from LIFT Ignition Data.

Material No.	T_{ig} (°C)	$k\rho c$ ($kW^2 \cdot s/m^4 \cdot K^2$)
1	—	—
2	—	—
3	375	1.65
4	370	1.89
5	453	1.73
6	643	8.00
7	647	0.27
8	337	0.74
9	385	1.72

2.1.2 Cone Calorimeter Ignition Data

The nine materials were tested in the Cone Calorimeter in accordance with ISO 5660-1:1993 "Fire Tests—Reaction to fire–Heat release rate of building products," with smoke production measurements made in accordance with the draft version of ISO 5660-2. A portion of the Cone Calorimeter ignition data is reported on the standard data sheets presented in Appendix C of USCG R&D Center Report No.

CG-D-22-98. Ignition times were obtained at additional heat flux levels, but these times are not presented in the USCG report. The complete set of Cone Calorimeter time to ignition data, including the minimum heat flux necessary for ignition, $\dot{q}''_{0,ig}$, is presented in Attachment A of this report. Material properties were obtained using the same calculation procedure described in ASTM E 1321 as used for the LIFT data. However, the convection coefficient of h_c = 15 W/m²·K, that is applicable to the LIFT apparatus, was not used. A coefficient applicable to the Cone Calorimeter for specimens exposed in the horizontal orientation with the retainer frame was determined and used for the calculations. This coefficient was obtained on the basis of a heat transfer analysis of a 12.7-mm thick calcium silicate board exposed at different heat flux levels, and instrumented with fine thermocouples on the exposed and unexposed surfaces. This analysis is described in detail in Attachment B of this report. Note that the convection coefficient appears to be a function of the heat flux. Therefore, the convection coefficient evaluated at the critical heat flux was used to calculate the surface temperature at ignition, T_{ig}. This value was also used to calculate the thermal inertia, kρc, from the slope b, which is conservative. The resulting material ignition properties are listed in Table A-3.

Table A-3. Ignition Properties Derived from ASTM E 1354 Cone Calorimeter Ignition Data.

Material No.	T_{ig} (°C)	kρc (kW/m²-K)²s
1	603	2.23
2	632	1.61
3	398	1.29
4	398	1.99
5	408	1.83
6	518	1.02
7	453	1.91
8	389	0.83
9	408	2.84

2.2 Flame Spread Properties

2.2.1 LIFT Flame Spread Data

Flamespread data were also obtained according to the procedures described in ASTM Standard E 1321. The results are reported in Appendix E3 of the USCG report. The corresponding flame spread properties (flame heating parameter, ϕ, and minimum temperature for lateral spread, $T_{s,\,min}$) are repeated in Table A-4. Note that for five of the nine materials, lateral flame spread data could not be obtained from the LIFT apparatus.

Table A-4. Lateral Flame Spread Properties Derived from LIFT Data.

Material No.	ϕ (kW^2/m^3)	$T_{s,min}$ (°C)
1	—	—
2	—	—
3	19.5	325
4	6.3	428
5	—	—
6	—	—
7	—	—
8	19.1	234
9	32.9	307

2.2.2 IMO Flame Spread Data

A second set of lateral flame spread properties was obtained using the same calculation procedure as for the LIFT data, but based on flame spread data obtained according to International Maritime Organization (IMO) Resolution A.653(16) "Recommendation on Improved Fire Test Procedures for Surface Flammability of Bulkhead, Ceiling, and Deck Finish Materials." The flamespread data obtained from the IMO surface flammability test are presented in Table A-5. As in the LIFT, flame spread data could not be obtained for five of the materials.

Table A-5. Lateral Flamespread Properties Derived from IMO Resolution A.653(16) Test Data.

Material No.	ϕ (kW^2/m^3)	$T_{s,min}$ (°C)
1	—	—
2	—	—
3	4.8	406
4	18.4	419
5	—	—
6	—	—
7	—	—
8	18.9	177
9	13.6	284

2.3 Heat Release Rate Properties

Representative values of the effective heat of combustion, ΔH_C, and total heat released per unit area, Q", were obtained for each material. These values were calculated as the average of all values measured for that material when tested in the Cone Calorimeter. In addition, the heat of gasification, L, was calculated according to a procedure recommended by Quintiere [Quintiere, 1993]. The heat of gasification values were obtained by plotting the maximum 30-sec average heat release rate, $HRR_{30,\,max}$, with respect to the external heat flux from the Cone heater, $\dot{q}''_e$. An effective heat of gasification was calculated based on the slope of a liner fit through the data:

$$L = \frac{\Delta H_C}{slope} \tag{A1}$$

The $HRR_{30,\,max}$ values were obtained from Section 5.4 of the USCG report and are presented in Attachment C of this report. The graphs of $HRR_{30,\,max}$ plotted with respect to $\dot{q}''_e$ and the slopes of the best-fit lines used to obtain the heat of gasification can also be found in Attachment C. The resulting heat release rate properties are presented in Table A-6.

Table A-6. Heat Release Rate Properties Derived from Cone Calorimeter Data.

Material No.	ΔH_C (MJ/kg)	Q" (MJ/m²)	L (MJ/kg)
1	7.7	15.9	9.4
2	9.7	8.1	16.6
3	11.3	35.6	17.6
4	13.4	49.0	13.3
5	8.2	12.6	19.5
6	7.6	11.7	15.2
7	9.1	5.8	8.4
8	21.6	61.5	6.8
9	12.3	41.1	13.5

2.4 Model Simulations

2.4.1 FORTRAN Version

Simulations of the ISO 9705 room-corner tests were performed for the nine materials, using the most current FORTRAN version of Quintiere's model that was available. This version has been previously published by Dillon [Dillon, 1998]. Detailed descriptions of the Quintiere's model and the computer-based FORTRAN version are available in the literature [Quintiere, 1993; Dillon, 1998; Janssens, 1995; Haynes, 1996; Quintiere, 1995; Quintiere, Haynes & Rhodes, 1995] and will not be repeated in this report.

The FORTRAN model requires the input of the seven material properties (T_{ig}, $k\rho c$, ϕ, $T_{s,\,min}$, ΔH_C, Q", and L), a description of the compartment geometry, characteristics of the ignition burner, as well as several modeling parameters. A maximum of four sets of property data were developed using combinations of the different sets of data presented in Sections 2.1 through 2.3. For the materials for which no flame spread data could be obtained (Material Nos. 1, 2, 5, 6, and 7) a flame heating parameter of $\phi = 0$ kW²/m³, and a minimum surface temperature for spread of $T_{s,\,min} = 20$ °C were chosen.

Predictions of the heat release rate from the materials were performed for each set of property data. Graphical comparisons of the measured and predicted heat release rate curves are presented in Attachment D.

2.4.2 VBA Version

After predicting the performance of the materials using the FORTRAN version of Quintiere's model, the source code was converted to Microsoft® Excel 97, Visual Basic for Applications (VBA). The use of VBA provides a user-friendly interface with which to run the model. The source code of the model is run as a macro with the material properties, room dimensions, burner characteristics, model parameters, *etc*. entered into a windows-based user form.

A validation was conducted to ensure that identical results were obtained with both the FORTRAN and VBA versions. All additional modifications to the model from this point on were performed using the VBA version.

3.0 MODIFIED MATERIAL PROPERTIES AND MODEL SIMULATION

3.1 Ignition Properties

Procedures to obtain material properties from piloted ignition data at different heat flux levels commonly assume that the surface heat losses partly involve Newtonian cooling which is characterized by a constant convection coefficient. It is shown in Attachment B that the convection coefficient in the Cone Calorimeter, for specimens in the horizontal orientation tested with the retainer frame, can be expressed as a linear function of the external heat flux from the Cone heater:

$$h_c \equiv h_0 + h_1 \dot{q}''_e \qquad \text{(A2)}$$

where h_0 = 11.8 W/m²·K and h_1 = 0.00034 1/K at heat flux levels below 50 kW/m², and h_0 = 25.5 W/m^2·K and h_1 = 0.000065 1/K at heat flux levels equal to or greater than 50 kW/m².

Consider a semi-infinite solid with constant properties k, ρ, and c exposed to a constant radiant heat flux, $\dot{q}''_e$, with radiative and convective heat losses from the surface:

$$\rho c \frac{\partial T}{\partial t} = k \frac{\partial^2 T}{\partial x^2} \qquad \text{(A3.a)}$$

with

$$T = T_\infty \qquad t = 0, \text{ and } x \geq 0 \tag{A3.b}$$

and

$$\varepsilon \dot{q}''_e = h_c(T_s - T_\infty) + \varepsilon\sigma(T_s^4 - T_\infty^4) \tag{A3.c}$$

where T_s is the temperature at the surface (x = 0), and T_∞ is the initial and ambient temperature. The solution of Equations (A3.a)-(A3.c) can be expressed by the following relationship between the time t_{ig},to reach surface temperature $T_s = T_{ig}$, and the incident heat flux $\dot{q}''_e$ [Janssens, 1991]:

$$\dot{q}''_e = \sigma(T_{ig}^4 - T_\infty^4) + \frac{h_c}{\varepsilon}(T_{ig} - T_\infty) + \frac{0.71(T_{ig} - T_\infty)}{\varepsilon}\left(\frac{k\rho c}{t_{ig}}\right)^{0.5} \tag{A4}$$

Substitution of Equation (A2) into Equation (A4), after rearranging, leads to

$$\left(\frac{k\rho c}{t_{ig}}\right)^{0.5} = C_1\dot{q}''_e - C_0 \tag{A5.a}$$

where

$$C_1 = \frac{\varepsilon}{0.71(T_{ig} - T_\infty)} - \frac{h_1}{0.71} \tag{A5.b}$$

and

$$C_0 = \frac{\varepsilon\sigma(T_{ig}^4 - T_\infty^4)}{0.71(T_{ig} - T_\infty)} - \frac{h_0}{0.71} \tag{A5.c}$$

Equation (A5.a) suggests that $(1/t_{ig})^{0.5}$ be plotted as a function of $\dot{q}''_e$. The intercept of a straight line fitted through the data points is equal to C_0/C_1, which can be used to determine T_{ig}. Once the surface temperature at ignition is known, kρc can be calculated from the slope of the linear fit. Because h_0 and h_1 have different values for heat fluxes below and above 50 kW/m², the slope of the linear fit is slightly smaller at heat fluxes below 50 kW/m². This is illustrated for Material Nos.1 and 2 on pages AE-1 and AE-2 of Attachment E, respectively. These two materials did not ignite at heat fluxes below 50 kW/m², and the ignition properties were estimated from a correlation of ignition data at heat fluxes at 50 kW/m² and higher (solid line in the graphs). Based on the resulting T_{ig} and kρc values, the location of the Equation (A5.a) was calculated for heat fluxes below 50 kW/m² (dashed line in the graphs).

A different approach was used for the remaining materials, all of which ignited at heat flux levels below 50 kW/m². Because the samples generally do not exhibit semi-infinite solid behavior at low heat flux levels, the data points do not fall on a straight line, and Equation (A5.a) cannot be used to determine T_{ig} by extrapolation [Janssens, 1991]. T_{ig} can be determined experimentally, by instrumenting some of the ignition test specimens with fine surface thermocouples. This approach will be recommended in Section 4.0 for future work, because it significantly reduces the number of small-scale tests that are needed to obtain the material properties needed to estimate ISO 9705 (or other) room-corner test performance. In the absence of experimental ignition temperatures, it was assumed that the critical heat flux for ignition was 5 kW/m² below the lowest heat flux level at which ignition was observed within a 20-min period of exposure. This critical flux value was used to estimate T_{ig}, and kρc was then calculated from the slope of a line connecting the estimated critical heat flux on the abscissa, and the average of the data points at 50 kW/m². The correlations are shown in Attachment E, pages AE-3 through AE-9. Ignition data for Material Nos. 3 through 9, obtained at lower heat flux levels, are presented in the graphs of Attachment E, however the values are not used in the determination of kρc. The resulting ignition properties are summarized in Table A-7.

Table A-7. Modified Cone Calorimeter Ignition Properties.

Material No.	T_{ig} (°C)	$k\Delta c$ ($kW^2 \cdot s/m^4 \cdot K^2$)
1	450	1.5252
2	380	2.9935
3	337	1.1547
4	337	1.3283
5	393	1.1169
6	483	0.1615
7	412	0.1973
8	323	0.6061
9	349	1.4393

3.2 Flame Spread Properties

The ASTM E 1321 LIFT data analysis procedure specifies that $1/\sqrt{V(x)}$ be plotted as a function of $\dot{q}''_e(x)$, and a straight line be fitted through the data points. The flame heating parameter ϕ is calculated from the slope C as follows:

$$\phi = \frac{k\rho c}{C^2 h_{ig}^2} \tag{A6}$$

Since the ignition properties have changed, the flame heating parameter was recalculated. The results are presented in Table A-8.

Table A-8. Modified Flame Spread Properties.

Material No.	h_{ig} (W/m·K)	$k\Delta c$ ($kW^2 \cdot s/m^4 \cdot K^2$)	C	N (kW^2/m^3)
3	37.8	1.1547	0.22	16.7
4	37.8	1.3283	0.42	5.3
8	36.4	0.6061	0.16	17.9
9	39.1	1.4393	0.26	13.9

3.3 Heat Release Rate Properties

The simulation data presented in Attachment D indicate that the original model generally underestimates fire growth. This is attributed, at least in part, to high heat of gasification values. To eliminate this problem, it was decided to use actual Cone Calorimeter heat release rate curves, instead of heat release properties derived from Cone data. The Cone Calorimeter data show that heat flux effects are not significant for most materials, and the experimental data at 50 kW/m² were selected for (an initial) analysis. Quintiere [Quintiere, 1993] uses an incident heat flux of 60 kW/m² for the ISO 9705 ignition burner flames and 30 kW/m² for a vertical wall flame. However, experiments by Dillon [Dillon, 1998] and calculations by Janssens [Janssens, 1995] indicate that a heat flux of 45 to 50 kW/m² may be more appropriate for the ISO 9705 burner with an output of 100 kW. Therefore, the selection of Cone Calorimeter data at 50 kW/m² is reasonable for this analysis. Because there were no heat release data at 50 kW/m² for Material Nos. 2 and 5, the Cone Calorimeter results at 75 kW/m² were used instead. The average heat release curve for all runs conducted at 50 (or 75 kW/m²) was approximated by an exponentially decaying function, as shown below:

$$\begin{aligned} 0 \le t - t_{ig} \le 30 \quad &: \quad \dot{Q}'' = HRR_{30,max} \\ 30 \le t - t_{ig} \le t_b \quad &: \quad \dot{Q}'' = HHR_{30,max} e^{-\lambda(t - t_{ig} - 30)} \\ t - t_{ig} > t_b \quad &: \quad \dot{Q}'' = 0 \end{aligned} \tag{A7}$$

The decay parameter λ is determined such that the area under the curve is equal to the average total heat release rate measured in the Cone Calorimeter experiments. The resulting fitting parameters are given in Table A-9 and the exponential heat release rate curves are presented in Attachment F. The idea to use an exponentially decaying function was based on earlier work by Magnusson and Sundström [Magnusson & Sundström, 1985]. The maximum 30-sec sliding average heat release rate was used instead of the peak, because the former has been proposed as one of the criteria to qualify fire-restricting materials on the basis of Cone Calorimeter data.

The Cone Calorimeter heat release rate curves presented in Attachment F represent an average of the measured heat release rates from the tests conducted. To average the data, the data was synchronized such that the ignition times corresponded to the to the average ignition time and an average value was taken at each time step.

Table A-9. Heat Release Rate Fitting Parameters.

Material No.	$HRR_{30, max}$ (kW/m²)	t_b (s)	8 (1/s)
1	30	241	0.00630
2	***32***	***265***	***0.00179***
3	109	720	0.00194
4	124	978	0.00150
5	***80***	***431***	***0.00430***
6	25	50	0.14000
7	39	143	0.00000
8	350	355	0.00474
9	118	1008	0.00243

Bold Italic: Values at 75 kW/m²

3.4 Smoke Release Rate Properties

A method was developed to obtain a rough estimate of the smoke production rate in the ISO 9705 room-corner test. The heat release rate of the wall material is divided by the heat of combustion (based on Cone Calorimeter data obtained at 50 or 75 kW/m^2). The resulting mass loss rate is multiplied with the specific extinction area, σ, measured in the Cone calorimeter to determine the smoke production rate. The heat of combustion and specific extinction area data are provided in Table A-10.

3.5 Modifications to the Model

The VBA input data forms and associated code were modified to include the heat release rate and smoke production rate calculations described above. The geometry of the burning area was simplified based on equations previously used by Janssens [Janssens, 1995] in his QBasic version of the Quintiere model. The pyrolysis and burned out areas are represented by rectangular areas as opposed to complex trapezoids. This approach provides a simple means for calculating and tracking flamespread, heat release, and burnout.

Table A-10. Heat of Combustion and Specific Extinction Area Data.

Material No.	)H_c (kJ/g)	Φ (m^2/kg)
1	4.9	84
2	***11.3***	***20***
3	11.4	594
4	12.9	742
5	***8.8***	***219***
6	11.4	391
7	6	48
8	21.3	746
9	13	68

Bold Italic: Values at 75 kW/m^2

Algorithms were also included that better describe the geometry and thermal environment created by the ignition source. The heat flux to the material in contact with the burner flame is determined based on the heat output of the burner and the temperature of the material, as opposed to simply using a constant flux.

Equations to estimate heat release rate on the basis of the heat of combustion, heat of gasification, and net heat flux were replaced with calculations on the basis of the exponentially decaying curve. The total heat release rate from the wall material at time t is given by

$$\mathrm{HRR}(t) = \sum_{i=1}^{t} (A_i - A_{i-1})\dot{Q}''(t-i) \qquad \text{(A8)}$$

where A_i and A_{i-1},are the burning areas at time i and i-1 seconds, respectively.

As the flame front progresses, the pyrolysis area increases. At every incremental time step, a new area may ignite and start burning. The modified model tracks and sums the heat release rate from each incremental area based on the exponentially decaying heat release rate curve to determine the total heat release rate from the material. This method automatically accounts for burnout, i.e., an incremental area burns out when its heat release rate reaches the end of the exponential curve.

Routines were also added to estimate the smoke production rate, SPR, and the corresponding emissivity of the hot gas layer, ε_g. The smoke production rate is calculated as the heat release rate divided by the heat of combustion and multiplied by the specific extinction area measured in the Cone Calorimeter.

The emissivity of the upper gas layer is also calculated as a function of the specific extinction area. Quintiere's original model assumes $\varepsilon_g = 1$, which appears to be overly conservative for low smoke producing materials. The emissivity of a hot and smoky gas layer can be estimated from [Seader & Einhorn, 1976]

$$\varepsilon_g = 1 - \exp\left(-(0.33 + 0.47C_s)(H - Z_i)\right) \tag{A9}$$

where C_s is the concentration of soot particles (g/m^3), H is the room height (m), and Z_i is the layer interface height (m). The soot concentration can be estimated from

$$C_s = \frac{SPR}{k_m \dot{V}_o} = \frac{\sigma HRR(t)}{k_m \dot{V}_o \Delta H_c} \tag{A10}$$

where k_m = 7.6 m^2/g based on data by Seader and Einhorn for flaming wood and plastics fires [Seader & Einhorn, 1976]. The layer depth was set equal to 1 m, based on observations in the ISO 9705 tests. To obtain a conservative (high) estimate of ε_g, a volumetric vent flow of 0.5 m^3/s was chosen. The resulting ε_g estimates vary between 0.4 and 1.0.

3.6 Modified Model Simulations

The results of the simulations with the modified model are presented in Attachment G. A comparison is provided between the calculated and measured heat release rate, upper gas layer temperature, smoke production rate, and heat flux to the floor. Comparisons with the experimental temperature data are based on the readings of the ceiling thermocouple opposite the burner. The floor flux was calculated on the basis of radiation from the upper gas layer, *i.e.*, the heat flux from the flames was ignored. As a result, the model underestimates the floor flux for materials with low heat release rate.

The heat release predictions are quite reasonable. For the materials with flashover times less than 600 s (Nos. 3, 4, 8), the model predictions are very close to the measured heat release rate. For materials with flashover times between 600 and 1200 s (Nos. 5 and 9), the predicted flashover times fall within the

same 300-kW exposure period. For the remaining materials, the model correctly predicts that flashover does not occur. Measured and predicted flashover times (times to 1 MW total heat release rate, except where noted) are compared in Table A-11. The measured and predicted average heat release and smoke production rates used to qualify fire restricting materials are presented in Table A-12. For the materials that did not flash over, the model correctly predicts that the heat release criteria for fire restricting materials are not exceeded. However, two of the four materials (No. 1 and No. 6) failed marginally on smoke, while the model predicts that all four materials would meet the smoke requirements.

Table A-11. Comparison of Measured and Predicted Flashover Times.

Material No.	Experimental (s)	Model (s)
3	342	345
4	306	305
5	***978***	***666***
8	102	56
9	672	611

Bold Italic: Time to 750 kW

3.7 Conclusions

The modified model does a reasonable job in predicting flashover times and heat release rates. However, the model underestimates smoke production, and more work is needed to address this problem.

Table A-12. Measured and Predicted Average Heat Release and Smoke Production Rates.

Material No.	Experimental Data				Model Predictions			
	HRR_{avg} (kW)	HRR_{30s} (kW)	SPR_{avg} (m^2/s)	SPR_{60s} (m^2/s)	HRR_{avg} (kW)	HRR_{30s} (kW)	SPR_{avg} (m^2/s)	SPR_{60s} (m^2/s)
1	62	159	***1.5***	5.4	36	120	0.6	2.0
2	31	129	0.2	0.5	47	134	0.1	0.2
6	28	134	***1.5***	3.5	8	193	0.3	4.5
7	17	131	0.1	0.2	48	194	0.4	1.5
Criteria	≤ 100	≤ 500	≤ 1.4	≤ 8.3	≤ 100	≤ 500	≤ 1.4	≤ 8.3

Bold Italic: Marginal failure

4.0 SUMMARY AND RECOMMENDATIONS

A modified version of Quintiere's fire growth model was developed to predict performance of wall and ceiling linings in the ISO 9705 room-corner test. Good quantitative agreement was found between the predicted and measured heat release rates for a set of eight marine composite materials and one textile wall covering.

The results of this analysis indicate that a minimal amount of small-scale data are required to run the model. A single Cone Calorimeter test at 50 kW/m² is all that is needed. However, it is recommended to perform at least two or three runs to improve the confidence in the input data (and, hence, the predictions). The choice of using Cone data at 50 kW/m² is based on a maximum heat flux to the walls of approximately 45 to 50 kW/m² from the flames of the ISO burner at 100 kW. However, the heat flux, from the burner with an output of 300 kW can range between 50 kW/m² to approximately 80 to 90 kW/m² near the wall-ceiling interface and approximately 100 kW/m² to the ceiling just above the burner (Dillon, 1998). Therefore, after 10 minutes it would seem reasonable to use Cone Calorimeter data at a higher incident heat flux. Only Material Nos. 5 and 9 produced flashover conditions after 10 minutes, but the model conservatively predicted flashover faster than the experiments. This indicates that the simple model presented in this report may be reasonable for predicting flashover for a variety of materials. However, further analysis of this of scenario is clearly warranted.

Although the flamespread data were developed, it was found that lateral flamespread was insignificant to the predictions of material performance in the ISO 9705 test. Therefore, it is suggested that LIFT and IMO surface flammability test data are unnecessary for performing predictions by the method presented in this report. This can be advantageous due to the high cost of lateral flamespread tests in comparison with Cone Calorimeter tests.

A first attempt was made at estimating the smoke production rate on the basis of the specific extinction area measured in the Cone Calorimeter. The smoke predictions are in qualitative agreement with the measurement, but in some cases they err on the unconservative side. Therefore, additional work is needed to improve the smoke predictions.

It has been suggested that the critical heat flux for ignition can be determined on the basis of supplementary surface temperature measurements. However, since the tests conducted were not provided with surface mounted thermocouples, the materials should be re-tested to verify this conjecture.

5.0 REFERENCES

1. Quintiere, J. G., "A Model for Fire Growth on Materials in a Room-Corner Test," *Fire Safety Journal*, Vol. 20, 1993, pp. 313-339.

2. Dillon S. E., "Analysis of the ISO 9705 Room/Corner Test: Simulations, Correlations and Heat Flux Measurements," NIST-GCR-98-756, National Institute of Standards and Technology, Gaithersburg, MD, August 1998.

3. Janssens, M., "Predictions of ISO 9705 Room/Corner Test Using a Simple Model," Interscience Communications Limited, Fire and Materials, Proceedings of the 4th International Conference and Exhibition, 1995, pp.73-83.

4. Janssens, M. L, Garabedian, A. S. & Gray, W., "Establishment of International Standards Organization (ISO) 5660 Acceptance Criteria for Fire-Restricting Materials Used on High-Speed Craft," Report No. CG-D-22-98, U.S. Coast Guard R & D Center, Groton, CT, 1998.

5. Haynes, G. A., "Analysis of a Model to Predict Flame Spread Over a PMMA Wall in a Compartment," M.S. Thesis, Department of Fire Protection Engineering, University of Maryland, College Park, Maryland, 1996.

6. Quintiere, J. G., "Estimating Fire Growth on Compartment Interior Finish Materials," Department of Fire Protection Engineering, University of Maryland, College Park, MD, 1995.

7. Quintiere J. G., Haynes G. & Rhodes B. T. "Applications of a Model to Predict Flame Spread Over Interior Finish Materials in a Compartment," *Journal of Fire Protection Engineering*, 7 (1) 1995 pp.1-13.

8. Janssens, M.L., "Thermophysical Properties of Wood and their Role in Enclosure Fire Growth," Ph.D. Thesis, University of Ghent, Belgium, 1991.

9. Quintiere, J., "Growth of Fire in Building Compartments", *Fire Standards and Safety, ASTM STP 614*, A.F. Robertson, Ed., American Society For Testing and Materials, 1977, pp. 131-167.

10. Magnusson, S. E. & and Sundström, B, "Combustible Linings and Room Fire Growth—A First Analysis," *Fire Safety Science: Science and Engineering, ASTM STP 882*, T. Z. Harmathy, Ed., American Society for Testing and Materials, Philadelphia, 1985, pp. 45-69.

11. Seader, J.D., and I.N. Einhorn, 16th Symposium (Int) on Combustion, Pittsburg, PA, 1976.

[This page intentionally left blank]

ATTACHMENT A

ORIGINAL CONE CALORIMETER IGNITION PROPERTIES

(CONSISTING OF 10 PAGES)

Original Cone Calorimeter Ignition Properties

MATERIAL NO. 1

$\dot{q}''_{o,ig}$ = 48 kW/m²

$\dot{q}''_e$ (kW/m²)	t_{ig} (s)	$\frac{\dot{q}''_{o,ig}}{\dot{q}''_e}$	$t_{ig}^{1/2}$ ($s^{1/2}$)
100	17	0.480	4.123
100	15	0.480	3.873
95	8	0.505	2.828
90	10	0.533	3.162
85	12	0.565	3.464
75	77	0.640	8.775
75	78	0.640	8.832
65	140	0.738	11.832
60	210	0.800	14.491
55	211	0.873	14.526
50	324	0.960	18.000
50	166	0.960	12.884
50	380	0.960	19.494
49	218	0.980	14.765
47	NI	1.021	N/A
45	NI	1.067	N/A
25	NI	1.920	N/A

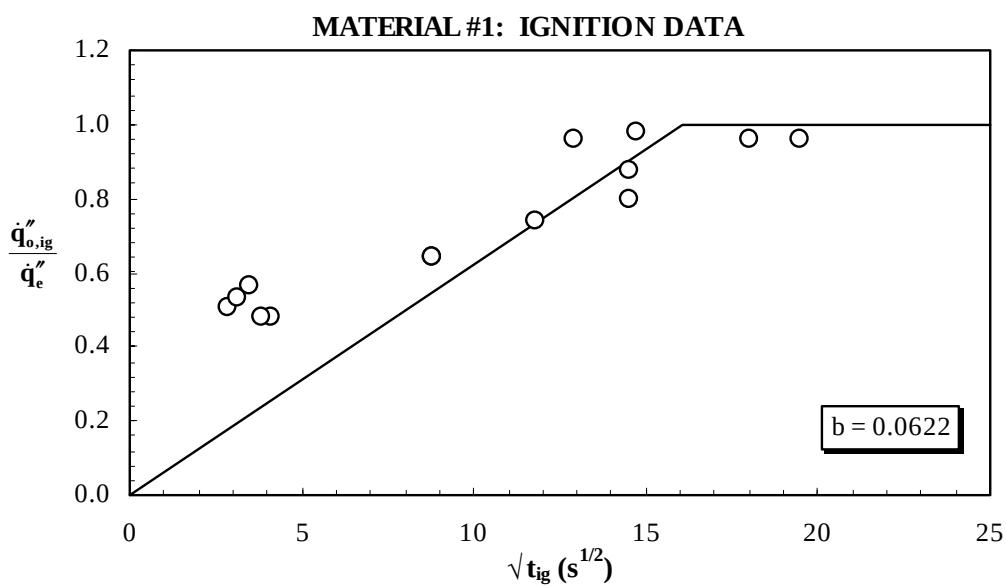

Original Cone Calorimeter Ignition Properties

MATERIAL NO. 2

$\dot{q}''_{o,ig}$ = 54 kW/m²

$\dot{q}''_e$ (kW/m²)	t_{ig} (s)	$\frac{\dot{q}''_{o,ig}}{\dot{q}''_e}$	$t_{ig}^{1/2}$ ($s^{1/2}$)
100	13	0.540	3.606
100	13	0.540	3.606
95	8	0.568	2.828
90	14	0.600	3.742
85	19	0.635	4.359
75	72	0.720	8.485
75	83	0.720	9.110
70	107	0.771	10.344
65	138	0.831	11.747
60	163	0.900	12.767
55	192	0.982	13.856
54	198	1.000	14.071
53	NI	1.019	N/A
50	NI	1.080	N/A

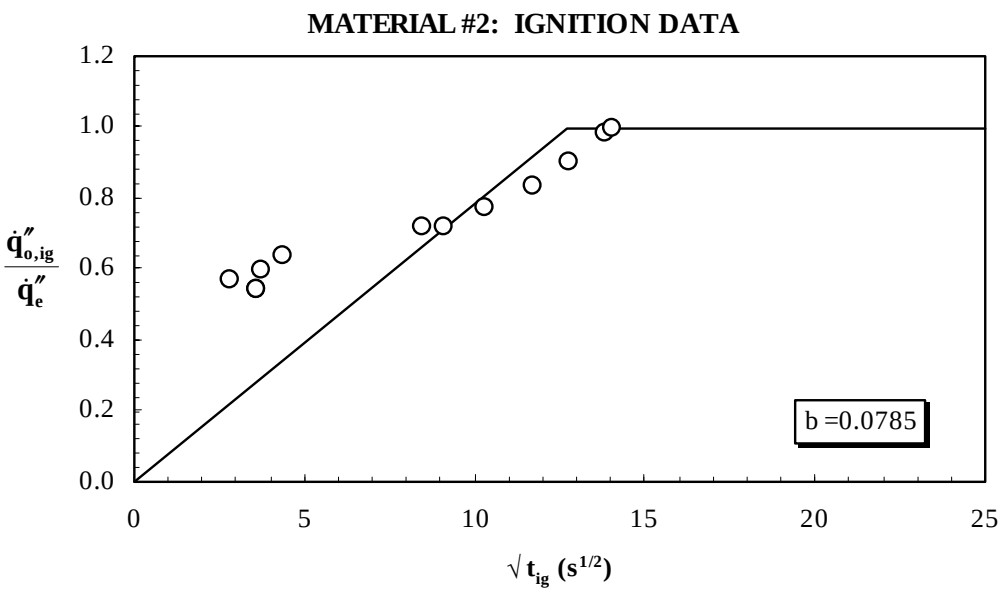

Original Cone Calorimeter Ignition Properties

MATERIAL NO. 3

$\dot{q}''_{o,ig}$ = 18 kW/m²

$\dot{q}''_e$ (kW/m²)	t_{ig} (s)	$\frac{\dot{q}''_{o,ig}}{\dot{q}''_e}$	$t_{ig}^{1/2}$ ($s^{1/2}$)
100	14	0.180	3.742
95	16	0.189	4.000
90	17	0.200	4.123
75	25	0.240	5.000
75	28	0.240	5.292
50	71	0.360	8.426
50	59	0.360	7.681
25	248	0.720	15.748
25	250	0.720	15.811
18	397	1.000	19.925
17	NI	1.059	N/A
15	NI	1.200	N/A

MATERIAL #3: IGNITION DATA

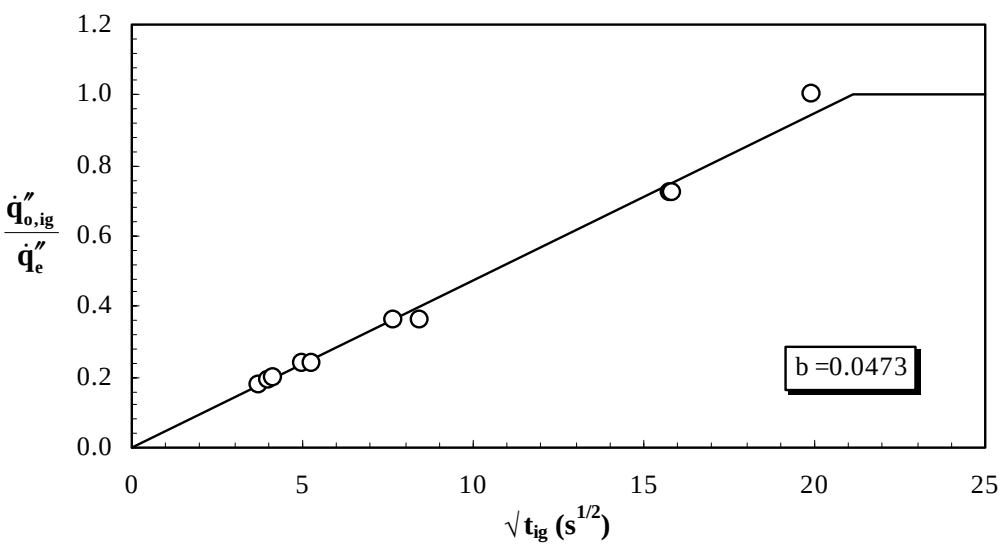

Original Cone Calorimeter Ignition Properties

MATERIAL NO. 4

$\dot{q}''_{o,ig}$ = 18 kW/m²

$\dot{q}''_e$ (kW/m²)	t_{ig} (s)	$\frac{\dot{q}''_{o,ig}}{\dot{q}''_e}$	$t_{ig}^{1/2}$ ($s^{1/2}$)
100	13	0.180	3.606
95	14	0.189	3.742
90	15	0.200	3.873
75	35	0.240	5.916
75	32	0.240	5.657
50	79	0.360	8.888
50	70	0.360	8.367
25	265	0.720	16.279
25	355	0.720	18.841
20	667	0.900	25.826
18	735	1.000	27.111
17	NI	1.059	N/A
15	NI	1.200	N/A

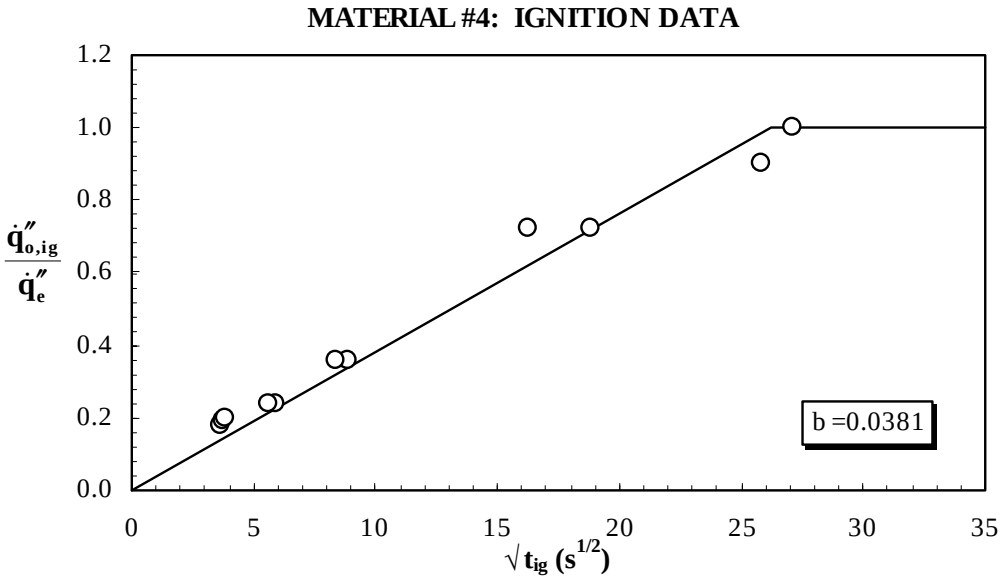

Original Cone Calorimeter Ignition Properties

MATERIAL NO. 5

$\dot{q}''_{o,ig}$ = 19 kW/m²

$\dot{q}''_e$ (kW/m²)	t_{ig} (s)	$\frac{\dot{q}''_{o,ig}}{\dot{q}''_e}$	$t_{ig}^{1/2}$ ($s^{1/2}$)
100	36	0.190	6.000
95	38	0.200	6.164
90	39	0.211	6.245
85	49	0.224	7.000
75	58	0.253	7.616
75	60	0.253	7.746
50	135	0.380	11.619
50	110	0.380	10.488
35	134	0.543	11.576
30	205	0.633	14.318
25	349	0.760	18.682
23	930	0.826	30.496
20	407	0.950	20.174
18	NI	1.056	N/A
15	NI	1.267	N/A

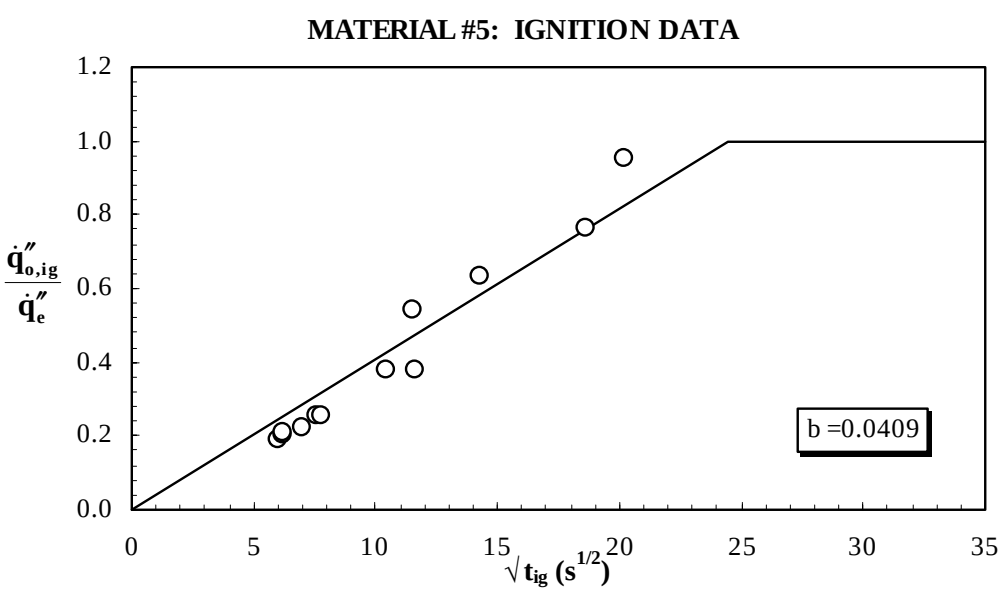

Original Cone Calorimeter Ignition Properties

MATERIAL NO. 6

$\dot{q}''_{o,ig}$ = 33 kW/m²

$\dot{q}''_e$ (kW/m²)	t_{ig} (s)	$\frac{\dot{q}''_{o,ig}}{\dot{q}''_e}$	$t_{ig}^{1/2}$ ($s^{1/2}$)
100	22	0.330	4.690
100	20	0.330	4.472
95	19	0.347	4.359
90	21	0.367	4.583
85	27	0.388	5.196
75	30	0.440	5.477
57	57	0.579	7.550
50	68	0.660	8.246
45	71	0.733	8.426
40	84	0.825	9.165
38	122	0.868	11.045
36	205	0.917	14.318
34	218	0.971	14.765
32	NI	1.031	N/A
25	NI	1.320	N/A

MATERAL #6: IGNITION DATA

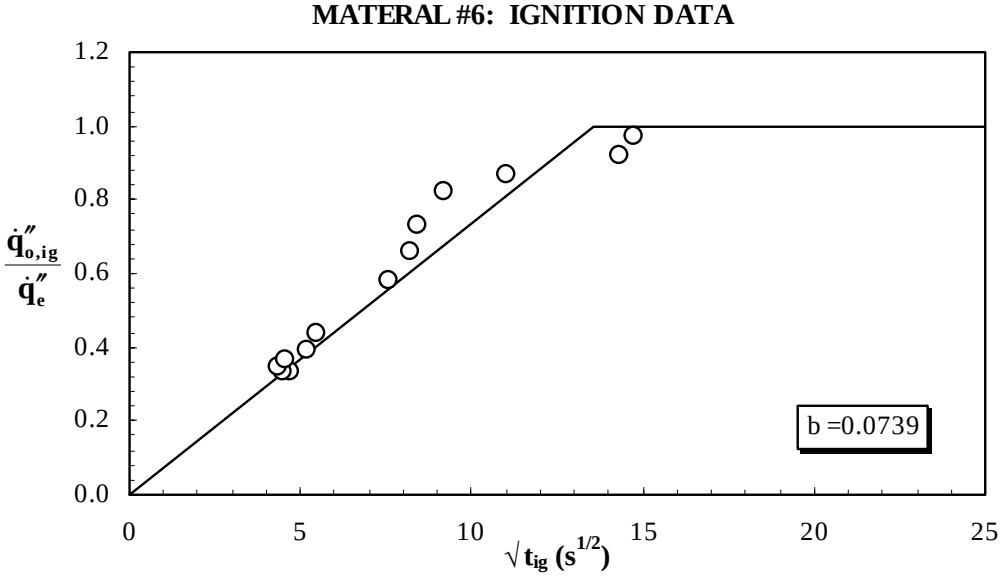

Original Cone Calorimeter Ignition Properties

MATERIAL NO. 7

$\dot{q}''_{o,ig}$ = 24 kW/m²

$\dot{q}''_e$ (kW/m²)	t_{ig} (s)	$\frac{\dot{q}''_{o,ig}}{\dot{q}''_e}$	$t_{ig}^{1/2}$ ($s^{1/2}$)
75	14	0.320	3.742
75	13	0.320	3.606
70	14	0.343	3.742
65	16	0.369	4.000
60	18	0.400	4.243
50	26	0.480	5.099
50	29	0.480	5.385
25	1165	0.960	34.132
25	690	0.960	26.268
23	NI	1.043	N/A
22	NI	1.091	N/A
20	NI	1.200	N/A

MATERIAL #7: IGNITION DATA

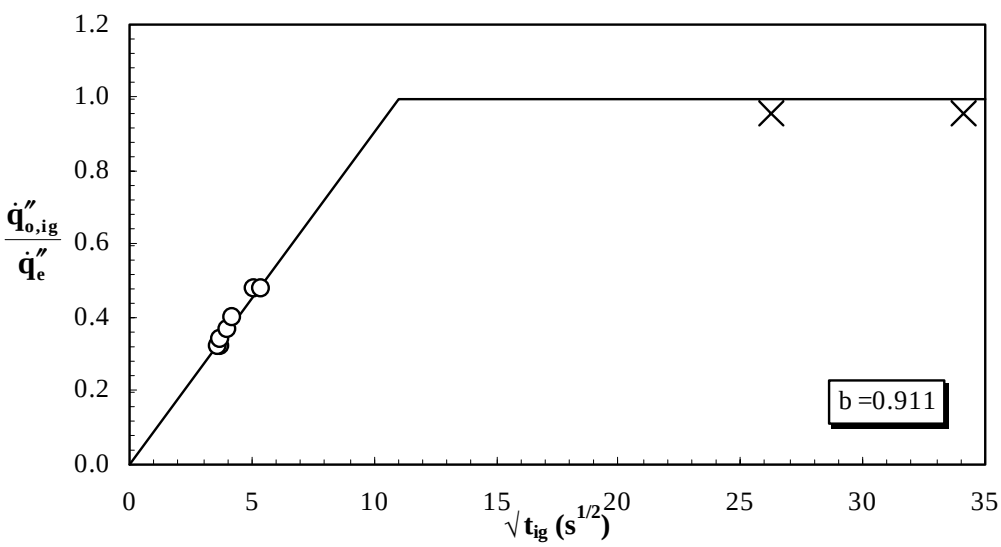

Note: × indicates data points that were neglected in the determination of the best-fit line.

Original Cone Calorimeter Ignition Properties

MATERIAL NO. 8

$\dot{q}''_{o,ig}$ = 17 kW/m²

$\dot{q}''_e$ (kW/m²)	t_{ig} (s)	$\frac{\dot{q}''_{o,ig}}{\dot{q}''_e}$	$t_{ig}^{1/2}$ ($s^{1/2}$)
85	11	0.200	3.317
80	11	0.213	3.317
75	16	0.227	4.000
75	15	0.227	3.873
70	13	0.243	3.606
65	14	0.262	3.742
50	33	0.340	5.745
50	26	0.340	5.099
25	100	0.680	10.000
25	145	0.680	12.042
20	161	0.850	12.689
18	381	0.944	19.519
17	880	1.000	29.665
16	NI	1.063	N/A
15	NI	1.133	N/A

MATERIAL #8: IGNITION DATA

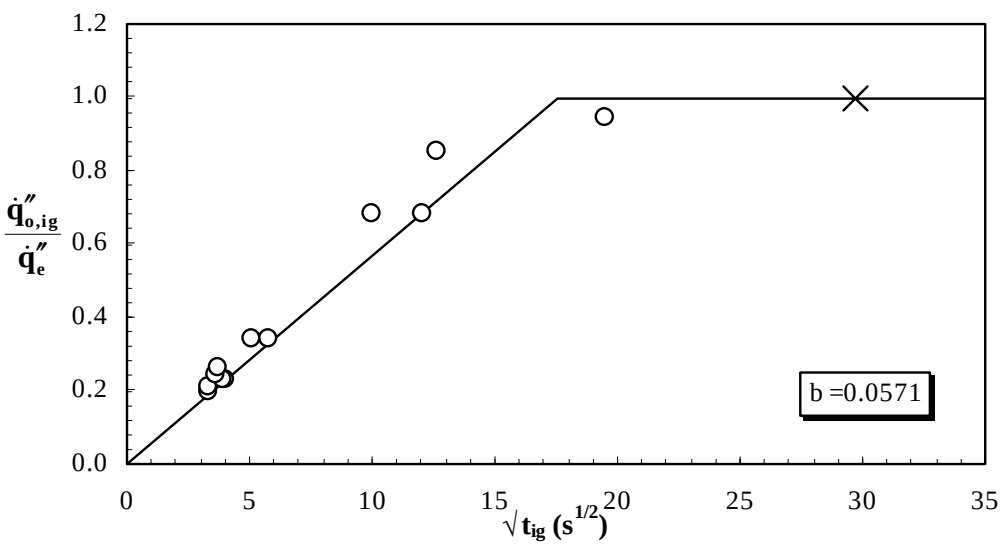

Note: × indicates a data point that was neglected in the determination of the best-fit line.

Original Cone Calorimeter Ignition Properties

MATERIAL NO. 9

$\dot{q}''_{o,ig}$ = 19 kW/m²

$\dot{q}''_e$ (kW/m²)	t_{ig} (s)	$\frac{\dot{q}''_{o,ig}}{\dot{q}''_e}$	$t_{ig}^{1/2}$ ($s^{1/2}$)
100	20	0.190	4.472
95	24	0.200	4.899
90	24	0.211	4.899
85	43	0.224	6.557
75	65	0.253	8.062
75	55	0.253	7.416
75	65	0.253	8.062
50	85	0.380	9.220
50	105	0.380	10.247
50	90	0.380	9.487
25	540	0.760	23.238
25	420	0.760	20.494
25	425	0.760	20.616
20	998	0.950	31.591
19	1104	1.000	33.226
18	NI	1.056	N/A

MATERIAL #9: IGNITION DATA

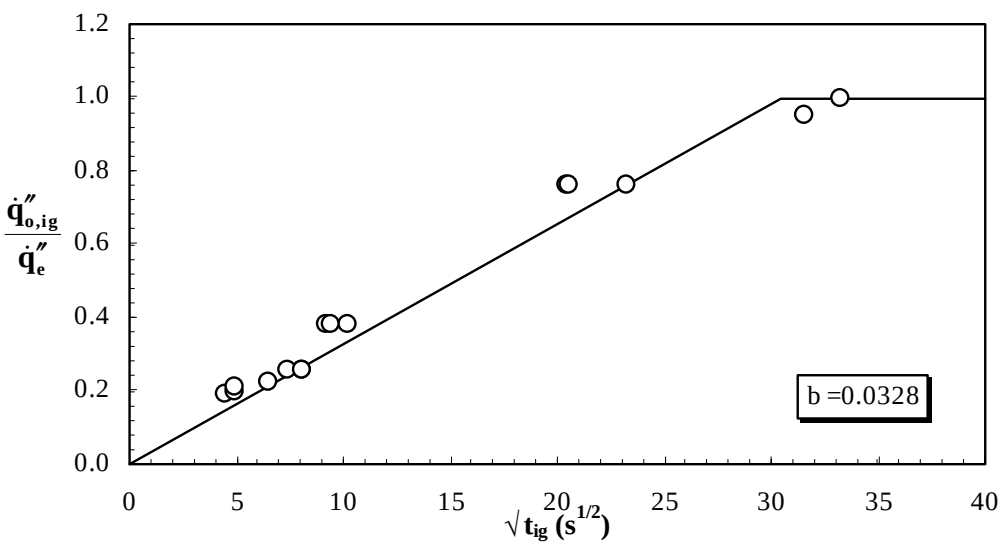

ATTACHMENT B

CONE CALORIMETER CONVECTIVE HEAT TRANSFER COEFFICIENT DETERMINATION

(CONSISTING OF 6 PAGES)

Cone Calorimeter Convection Heat Transfer Coefficient Determination

The convective heat transfer coefficient, h_c, for materials tested horizontally in the Cone Calorimeter with the sample retainer frame was determined by exposing a piece of calcium silicate (Ca-Si) board to the radiant flux of the cone heater and measuring the temperatures of the exposed and unexposed surfaces. The temperatures of the two surfaces were used to calculate the net heat flux into the calcium silicate board by a finite difference method using the material properties presented in Table AB-1. The net heat flux was then used to calculate the convective heat transfer coefficient based on the following expression:

$$h_c = \frac{\varepsilon\, \dot{q}''_e - \varepsilon\sigma\, (T_s^4 - T_\infty^4) - \dot{q}''_{net}}{(T_s - T_\infty)} \cdot 10^3 \qquad \text{(AB-1)}$$

where h_c = convective heat transfer coefficient, W/m²·K

$\dot{q}''_e$ = external heat flux from the cone heater, kW/m²

ε = surface emissivity of the test specimen

σ = Stefan-Boltzmann constant, 5.67×10^{-11} kW/m²·K⁴

T_s = surface temperature, K

T_∞ = ambient temperature, K

$\dot{q}''_{net}$ = net heat flux into the specimen, kW/m²

Table AB-1. Properties of Marinite I Calcium Silicate Board (BNZ Materials, Inc.).

Thermal Conductivity, k	0.12 W/m·K
Density, ρ	737 kg/m³
Specific Heat, c	1.17 kJ/kg·°C @ 93°C 1.25 kJ/kg·°C @ 205°C 1.34 kJ/kg·°C @ 316°C 1.42 kJ/kg·°C @ 425°C

The test specimen was a 100 x 100 mm (4 x 4 in.) x 12.7 mm (1/2 in.) thick piece of "Marinite I" Ca-Si board obtained from BNZ Materials, Inc. Prior to testing, the specimen was heated to 200°C in a muffle furnace for approximately 12 hours to remove any trapped moisture and stored with drierite to maintain a moisture free specimen. A 10-mil diameter, Type K, thermocouple (TC) was used to measure the exposed surface temperature. The TC was fixed to the board by drilling small holes through the board

approximately 13 mm on either side of the center (along the diagonal) and running the TC wires through the holes with the TC bead securely against the sample surface. A 10-mil diameter Inconel sheathed thermocouple was attached to the bottom surface to measure the unexposed surface temperature. The test specimen was backed with refractory blanket and placed in a standard Cone Calorimeter sample holder with the sample retainer frame. The specimen was exposed to radiant heat fluxes of 10 to 100 kW/m² in a horizontal orientation and the surface temperatures were measured and recorded every 0.5 sec for approximately 25 to 40 min.

In order to calculate the convective heat transfer coefficient using Equation (AB-1), the surface emissivity, ε, of the Ca-Si board was required. The emissivity was not available in the material literature, so it was determined based on the measured surface temperature. After heating the surface of the calcium silicate board to approximately 700°C in the Cone Calorimeter, the specimen was removed and allowed to cool, in the sample holder, in a vertical orientation. The surface temperature at the center of the board was measured for over 35 minutes using the surface TC as well as an infrared pyrometer set to an emmissivity of ε = 1.0. The surface emissivity was calculated based on the two measured temperatures. The surface temperatures of the Ca-Si board and the calculated surface emissivity values are plotted with respect to time in Figure AB-1. The figure indicates that the average surface emissivity for Marinite I calcium silicate board is 0.88 over a range of 40 to 700°C.

The measured temperatures of the exposed and unexposed surfaces of the calcium silicate board were used to calculate the net heat flux and the associated convective heat transfer coefficient. The experimentally determined surface emissivity was used along with $\dot{q}''_{net}$ in Equation (AB-1), to calculate h_c for horizontal specimens as a function of time over a range of external heat flux levels: 10 to 100 kW/m². An example of the result of such a calculation is presented graphically in Figure AB-2. Average h_c values were determined for all the heat flux exposures and are presented numerically in Table B-2 and graphically with respect to the external heat flux in Figure AB-3. Based on the data presented in Figure AB-3, an exponential expression for the convective heat transfer coefficient was developed:

$$h_c = 6.56 \cdot \dot{q}''^{0.35}_{e} \qquad \text{(AB-2)}$$

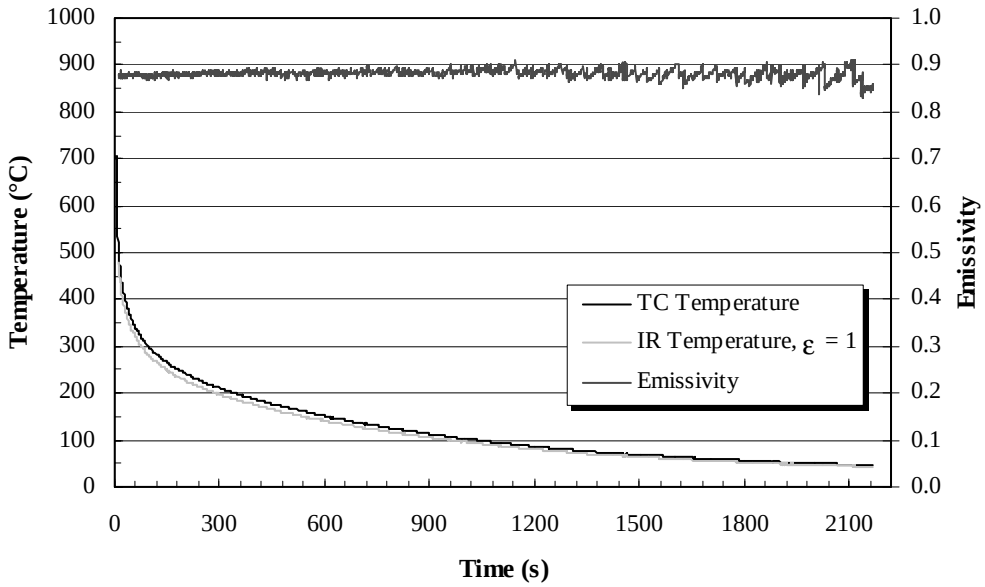

Figure AB-1. Emissivity, ε, of Marinite I, Calcium Silicate Board (BNZ Materials, Inc.).

The critical heat flux for ignition, $\dot{q}''_{o,ig}$, was used in Equation (AB-2) to calculate the correct h_c value in the determination of the temperature for material ignition, T_{ig}, in Section 2.1.2.

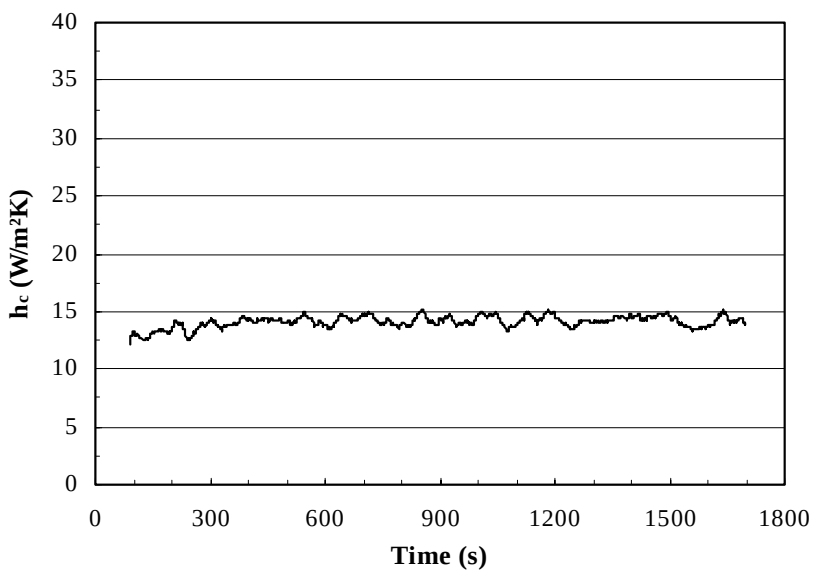

Figure AB-2. Example of the Convective Heat Transfer Coefficient, h_c, in the Cone Calorimeter Calculated with Respect to Time: $\dot{q}''_e$ = 10 kW/m².

Table AB-2. Convective Heat Transfer Coefficients for Horizontal Specimens with the Sample Retainer Frame in SwRI's Cone Calorimeter.

$\dot{q}''_e$ (kW/m²)	$h_{c,\,avg}$ (W/m²·K)
10	14.2
18	18.2
25	21.8
25	19.8
50	28.2
62	28.9
75	29.4
100	33.1
100	31.7

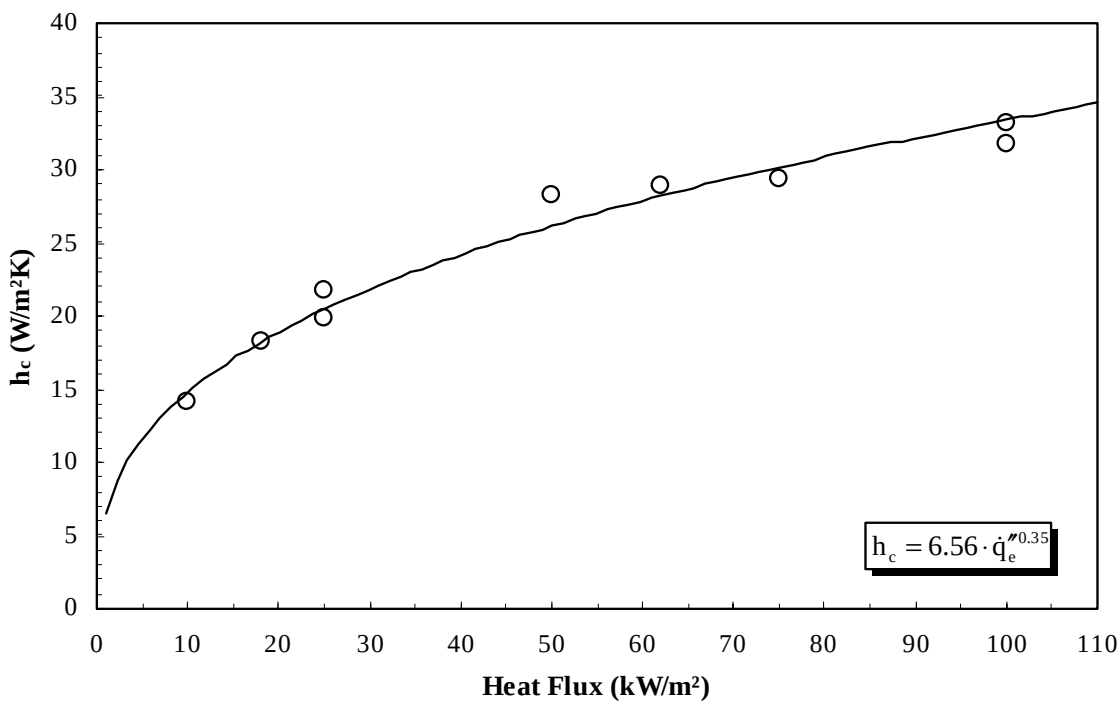

Figure AB-3: Convective Heat Transfer Coefficient, h_c, Plotted with Respect to the External Flux for Horizontal Specimens Tested in the Cone Calorimeter with the Sample Retainer Frame.

Cone Calorimeter Convection Heat Transfer Coefficient Determination

In order to calculate the modified ignition properties in Section 3.1, the exponential expression determined in Figure AB-3 was simplified to produce two linear expressions for h_c based on the external heat flux (see Figure AB-4):

$$h_c = 0.34 \cdot \dot{q}''_e + 11.8 \qquad \dot{q}''_e < 50 \text{ kW/m}^2$$
$$h_c = 0.065 \cdot \dot{q}''_e + 25.5 \qquad \dot{q}''_e \geq 50 \text{ kW/m}^2 \qquad \text{(AB-3)}$$

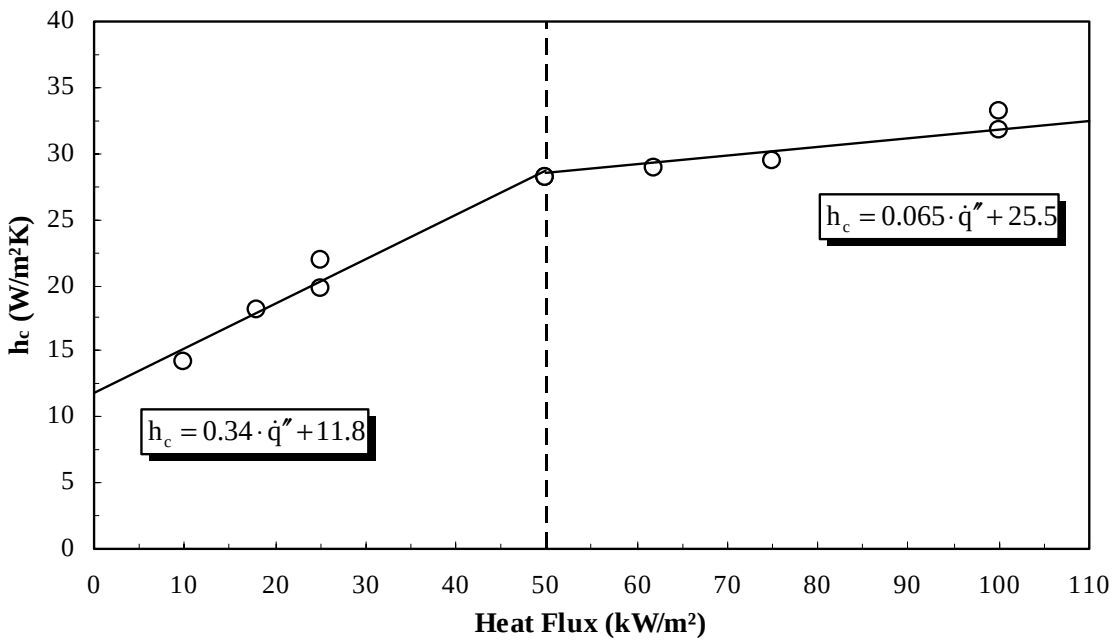

Figure AB-4: Convective Heat Transfer Coefficient, h_c, with Respect to the External Flux for Horizontal Specimens Tested in the Cone Calorimeter with the Sample Retainer Frame.

ATTACHMENT C

ORIGINAL CONE CALORIMETER HEAT OF GASIFICATION DATA

(CONSISTING OF 10 PAGES)

Original Cone Calorimeter Heat of Gasification Data

MATERIAL NO. 1

$\dot{q}''_e$ (kW/m²)	$HRR_{30,\ max}$ (kW/m²)
50	30
75	76
75	63
100	60
100	91

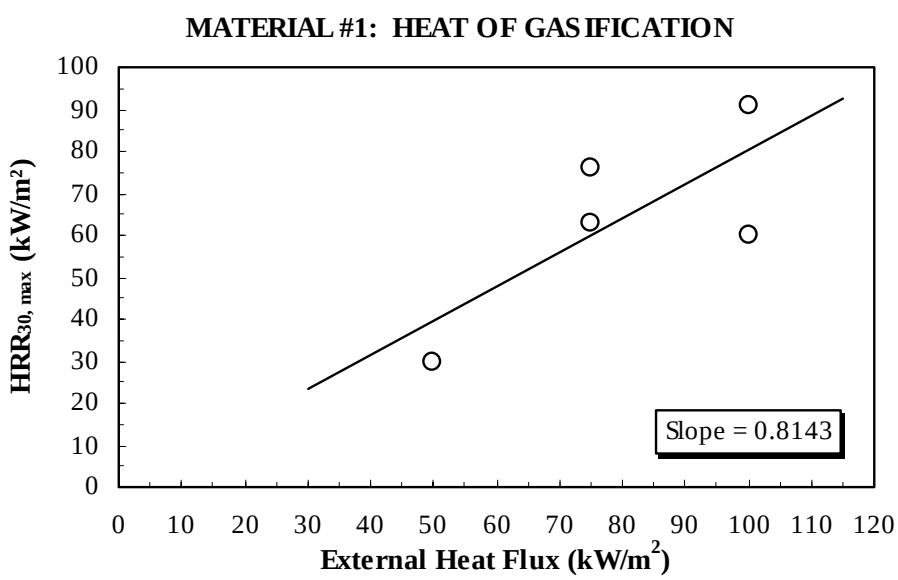

Original Cone Calorimeter Heat of Gasification Data

MATERIAL NO. 2

$\dot{q}''_e$ (kW/m²)	$HRR_{30,\ max}$ (kW/m²)
75	36
75	27
100	43
100	49

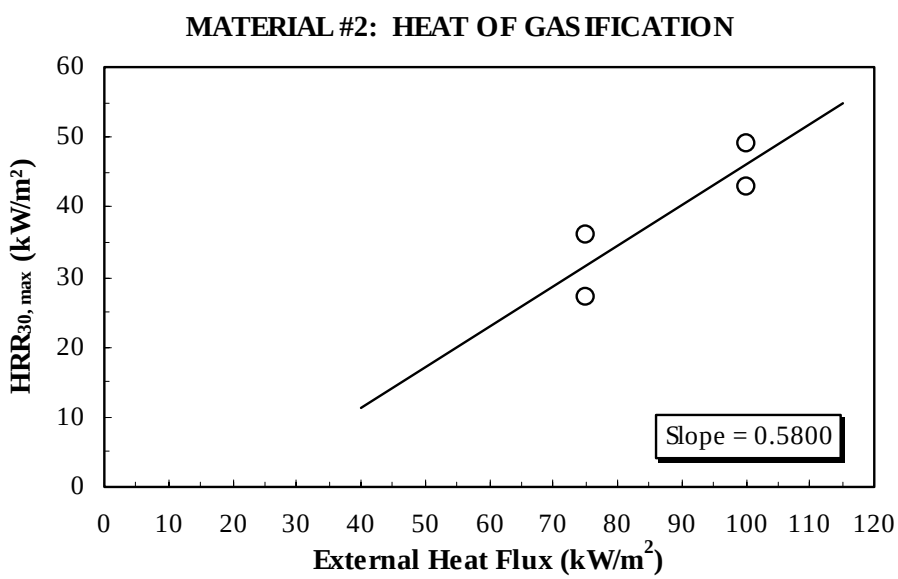

Original Cone Calorimeter Heat of Gasification Data

MATERIAL NO. 3

$\dot{q}''_e$ (kW/m²)	$HRR_{30,\ max}$ (kW/m²)
25	93
25	94
50	113
50	104
75	125
75	126

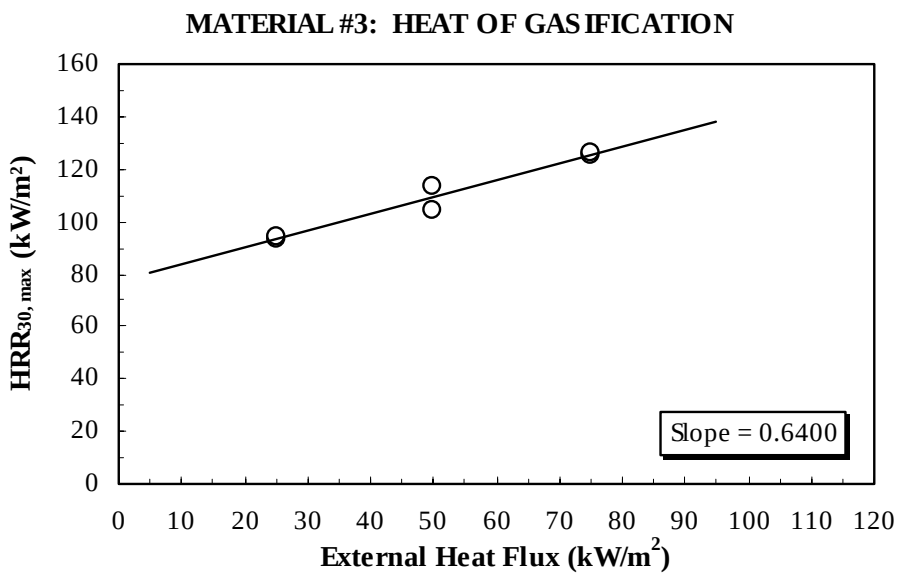

Original Cone Calorimeter Heat of Gasification Data

MATERIAL NO. 4

$\dot{q}''_e$ (kW/m²)	$HRR_{30,\ max}$ (kW/m²)
25	89
25	104
50	121
50	126
75	154
75	140

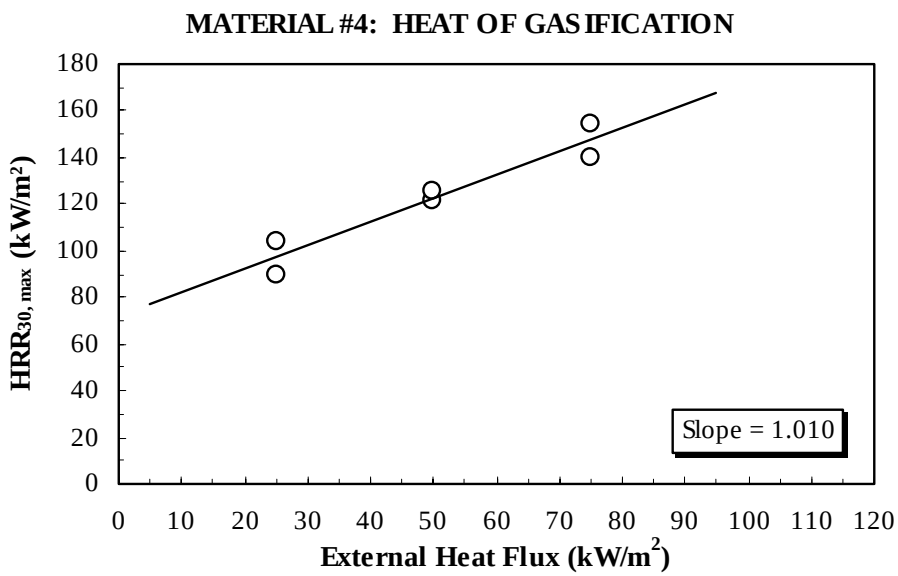

Original Cone Calorimeter Heat of Gasification Data

MATERIAL NO. 5

$\dot{q}''_e$ (kW/m²)	$HRR_{30,\ max}$ (kW/m²)
50	54
50	75
75	85
75	74
100	84

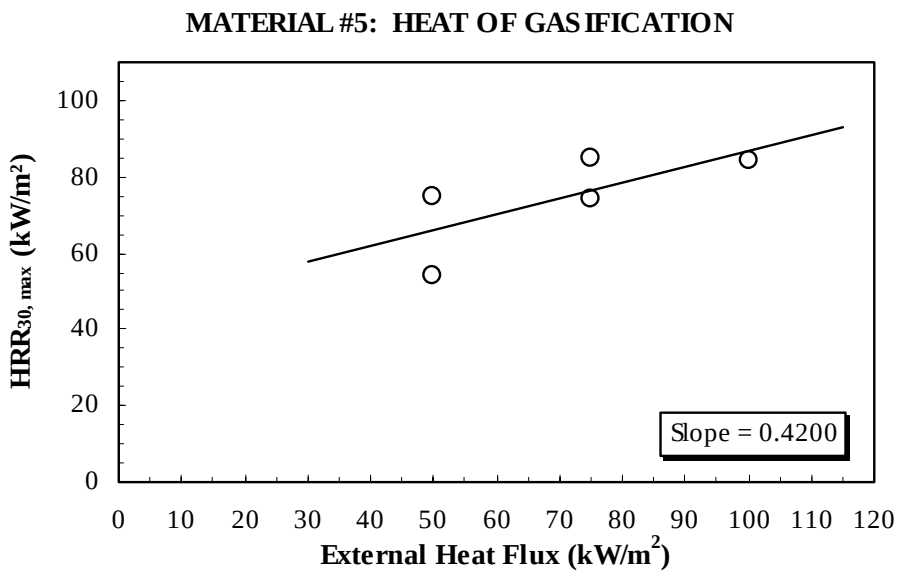

Original Cone Calorimeter Heat of Gasification Data

MATERIAL NO. 6

$\dot{q}''_e$ (kW/m²)	$HRR_{30,\ max}$ (kW/m²)
50	27
75	77
75	15
100	53
100	54

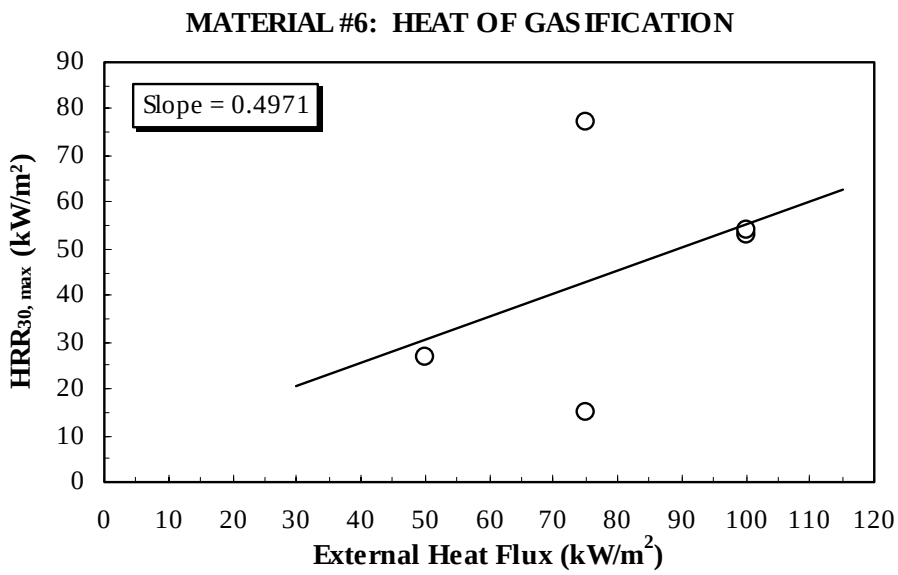

Original Cone Calorimeter Heat of Gasification Data

MATERIAL NO. 7

$\dot{q}''_e$ (kW/m²)	$HRR_{30,\ max}$ (kW/m²)
25	38
25	34
50	58
50	65
75	46
75	134

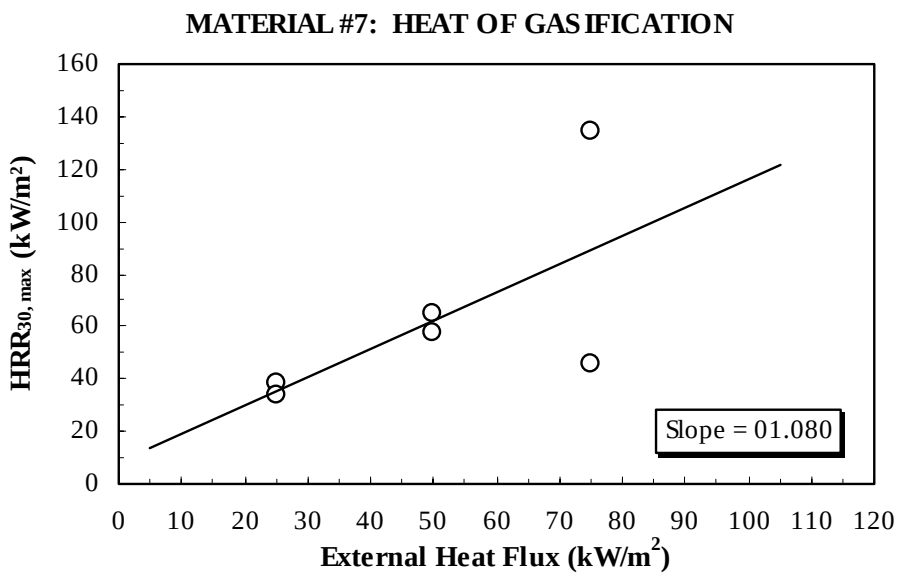

Original Cone Calorimeter Heat of Gasification Data

MATERIAL NO. 8

$\dot{q}''_e$ (kW/m²)	$HRR_{30,\ max}$ (kW/m²)
25	245
25	288
50	370
50	330
75	451
75	399

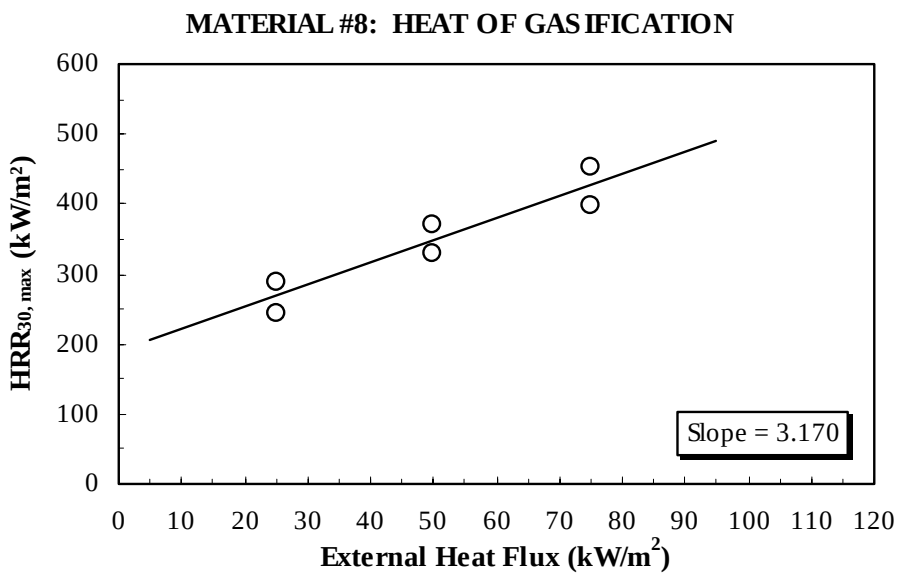

Original Cone Calorimeter Heat of Gasification Data

MATERIAL NO. 9

$\dot{q}''_e$ (kW/m²)	$HRR_{30,\ max}$ (kW/m²)
25	87
25	91
25	103
50	106
50	120
50	129
75	127
75	152
75	139

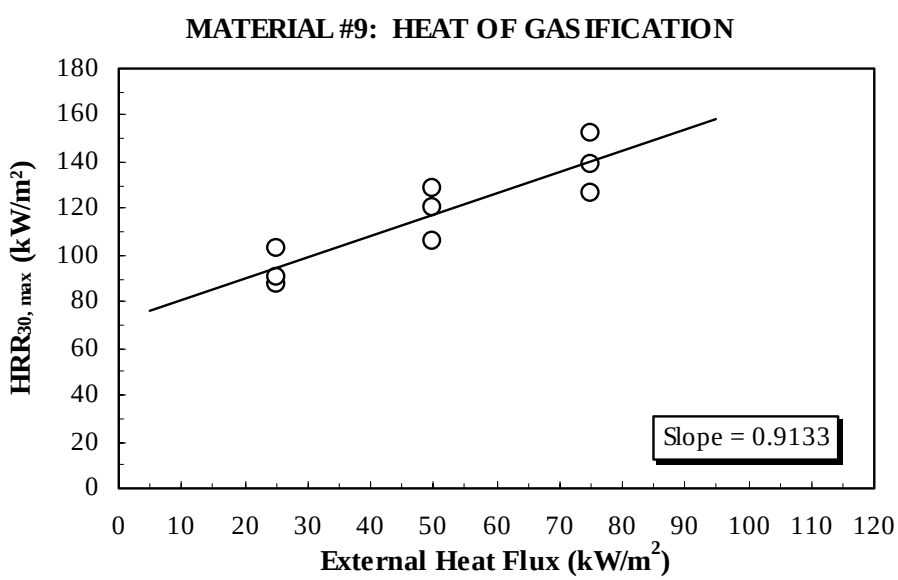

ATTACHMENT D

ORIGINAL MODEL PREDICTIONS

(CONSISTING OF 7 PAGES)

Original Model Predictions

Predictions of the performance of the nine USCG materials in the ISO 9705 Room-Corner test were made using the material properties presented in Section 2.0 input into Quintiere's fire growth model. Predictions were made using the ignition data from the Cone Calorimeter and the Lateral Ignition and Flamespread Test (LIFT) apparatus and flamespread data from the LIFT apparatus and the International Maritime Organization (IMO) Surface Flammability Test.

The predictions for the USCG materials are presented below. The legend of the graphical presentations of the material performance indicates the material properties that were used for each prediction. The first term indicates the ignition properties and the second term indicates the flame spread properties. For example "Cone & IMO (CI)" indicates that the ignition data from the Cone Calorimeter and flamespread data from the IMO Surface Flammability Test were used. For materials where no flamespread data were available, only the set of ignition data used is presented. For example "Cone" simply indicates that there were no flame spread data available and the Cone Calorimeter ignition data were used. For such a material the flame heating parameter, Φ, was input as 0 kW^2/m^3 and the minimum temperature for lateral flame spread, $T_{s,\,min}$, was input as 20°C (293 K), in order to indicate that no flamespread should be calculated by the prediction model.

Original Model Predictions

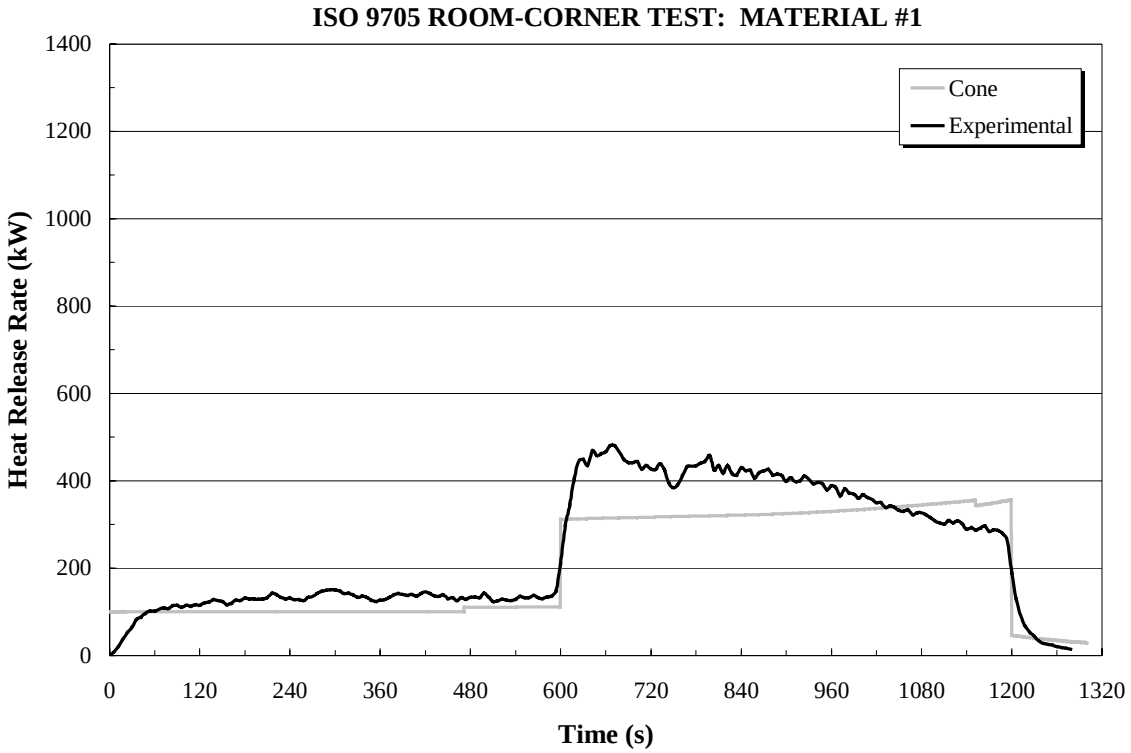

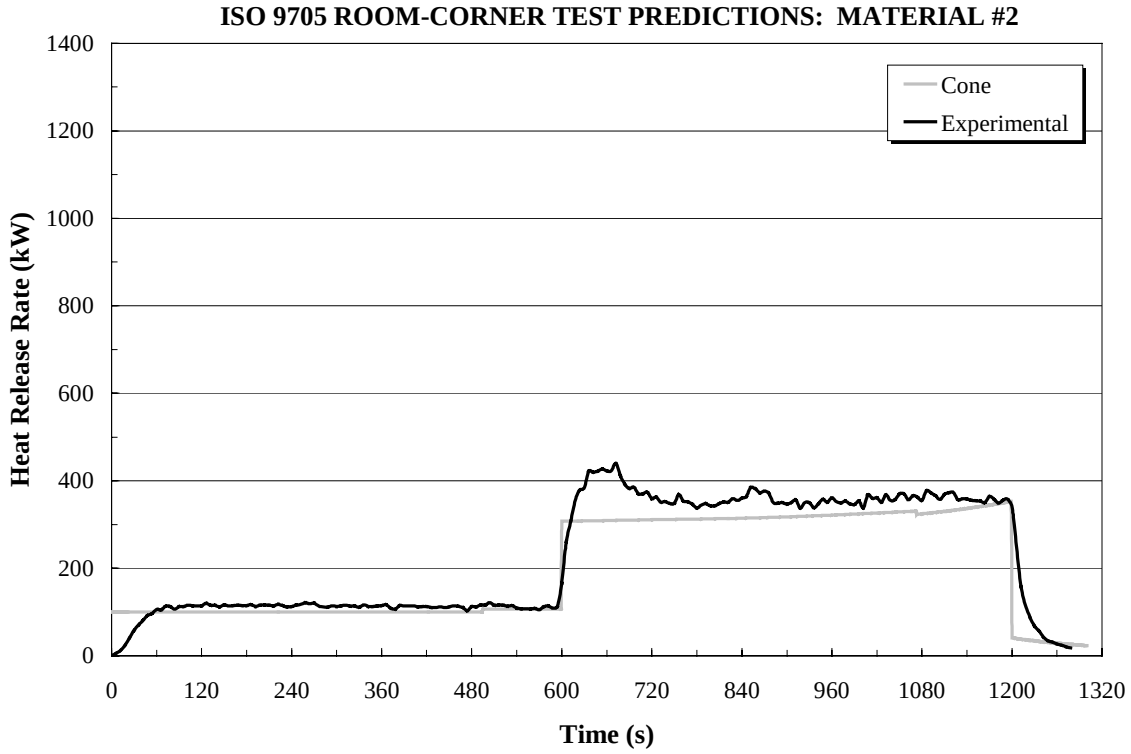

Original Model Predictions

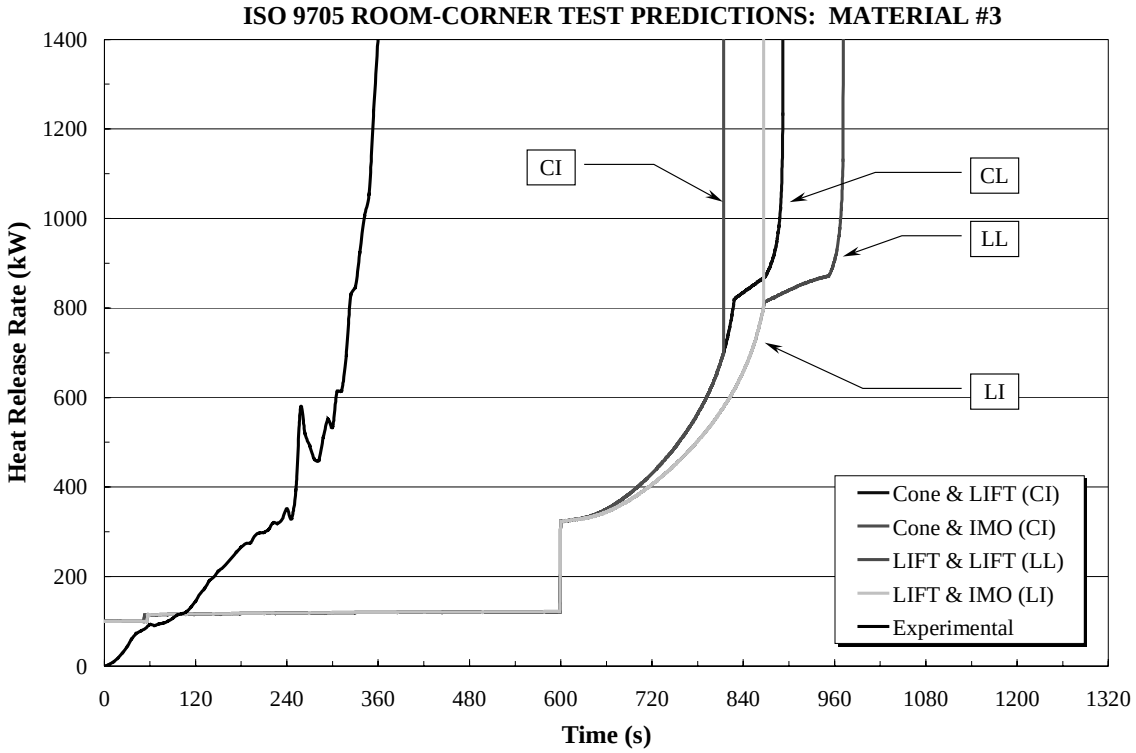

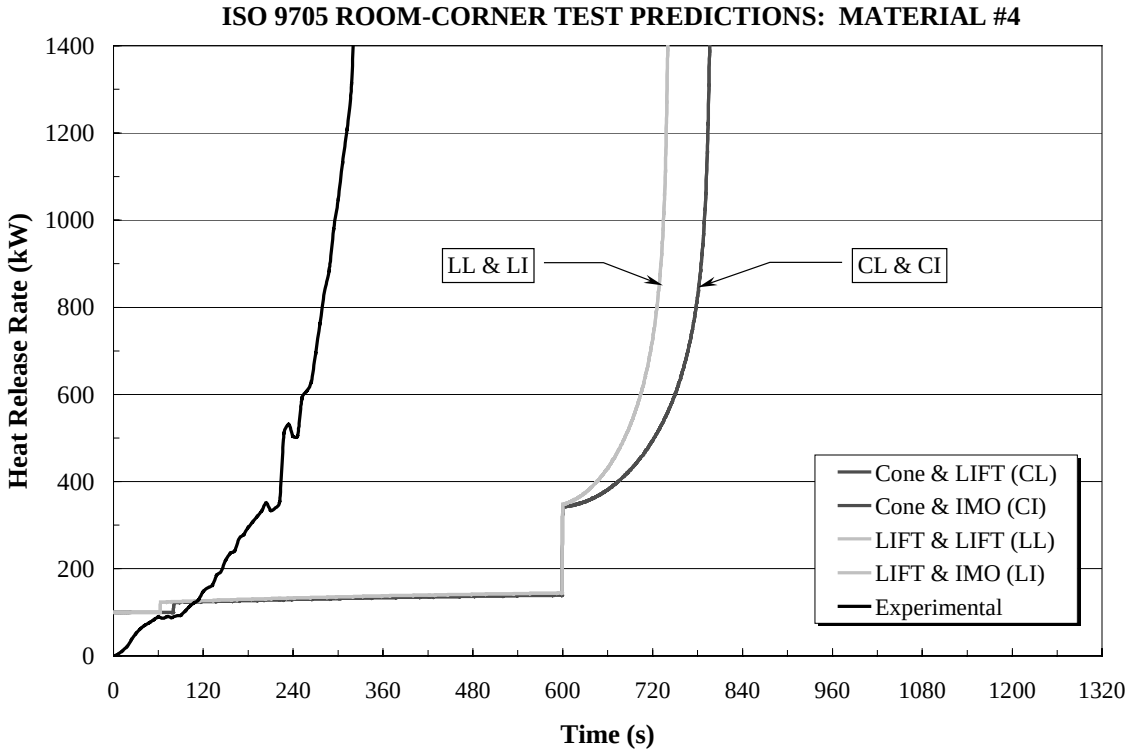

Original Model Predictions

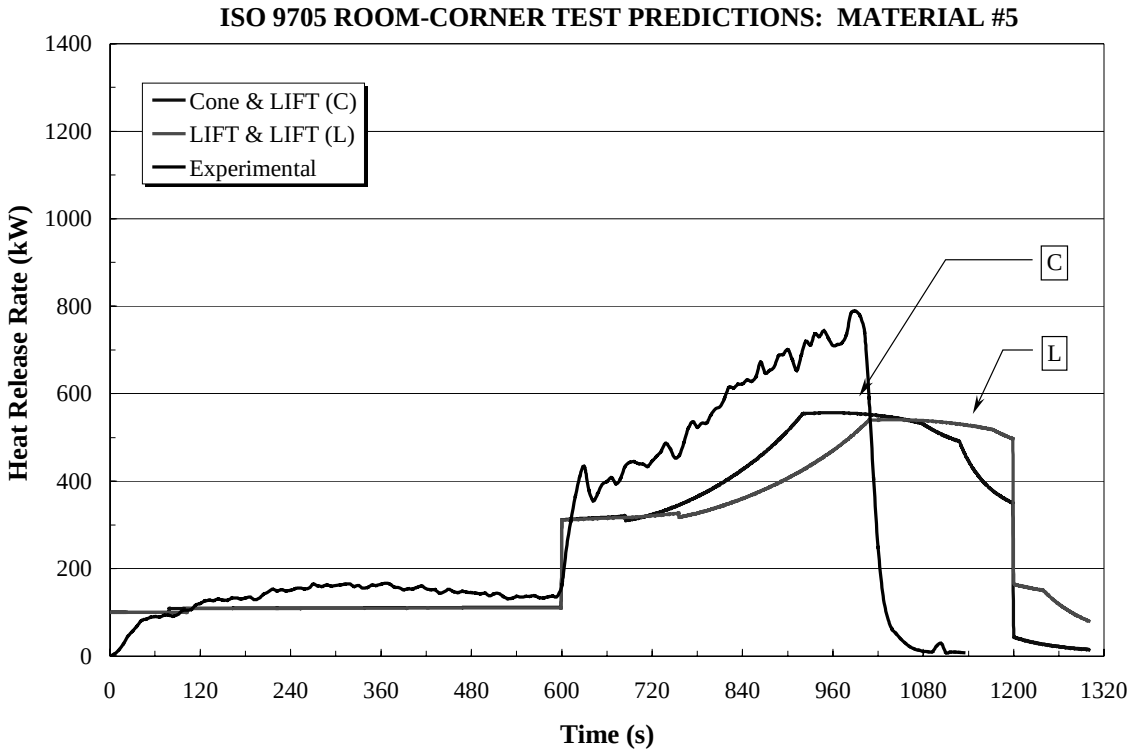

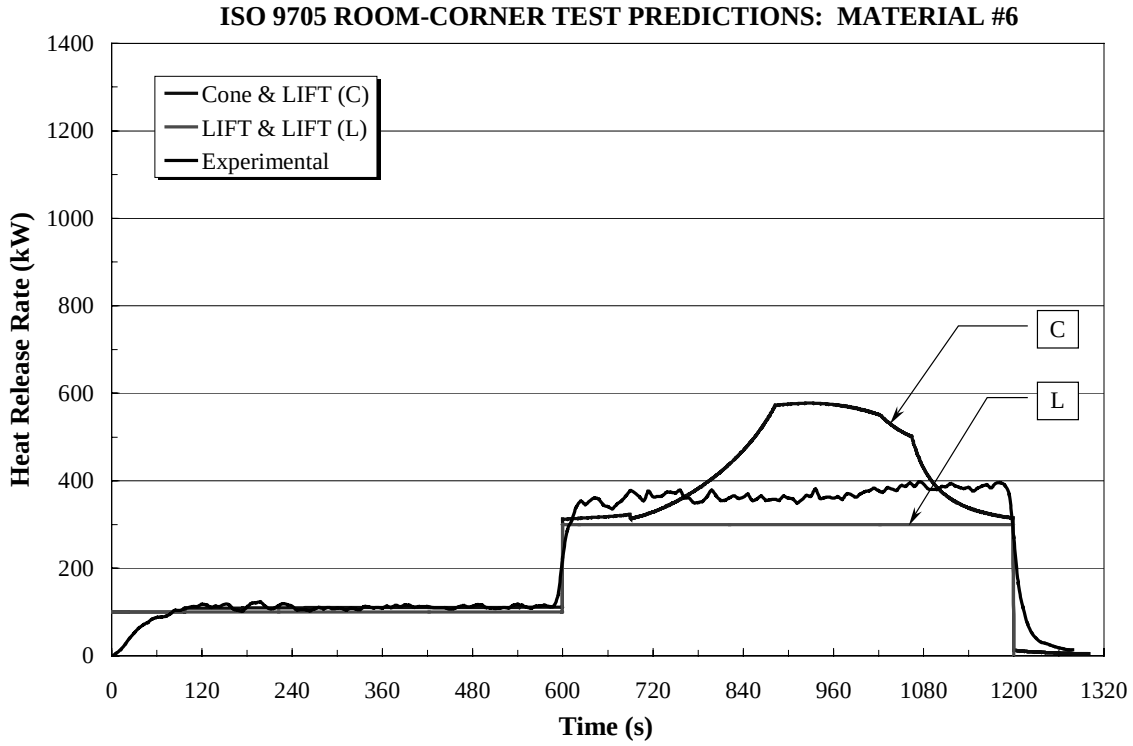

Original Model Predictions

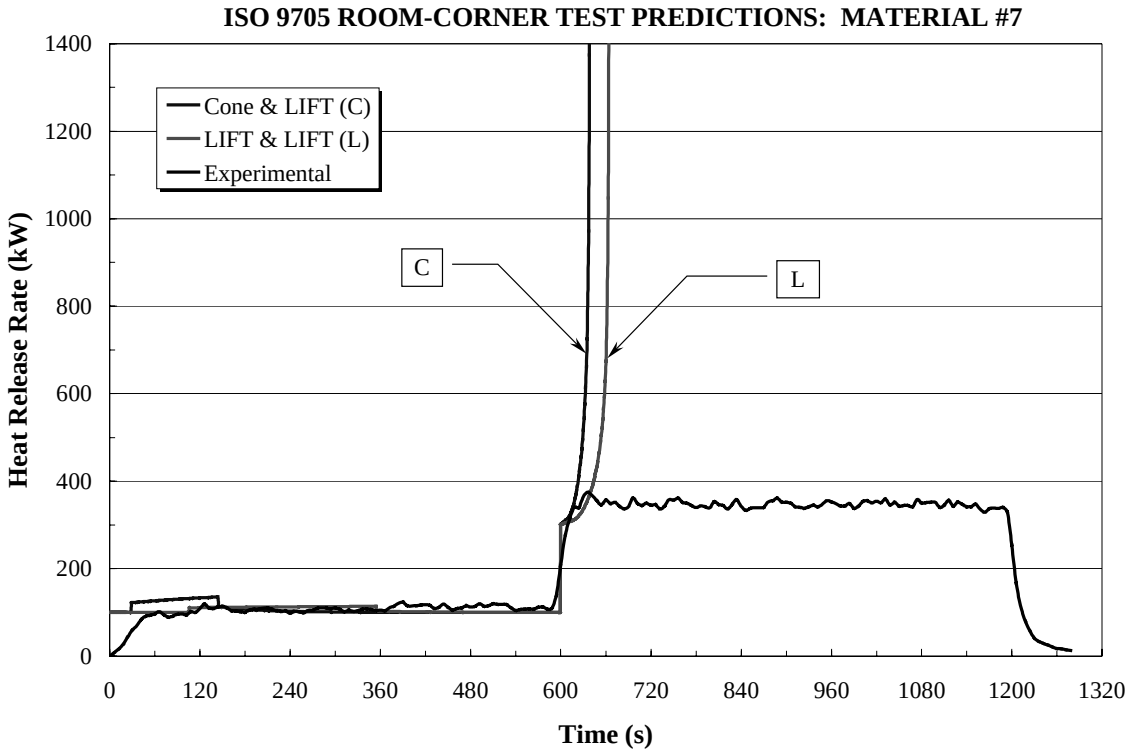

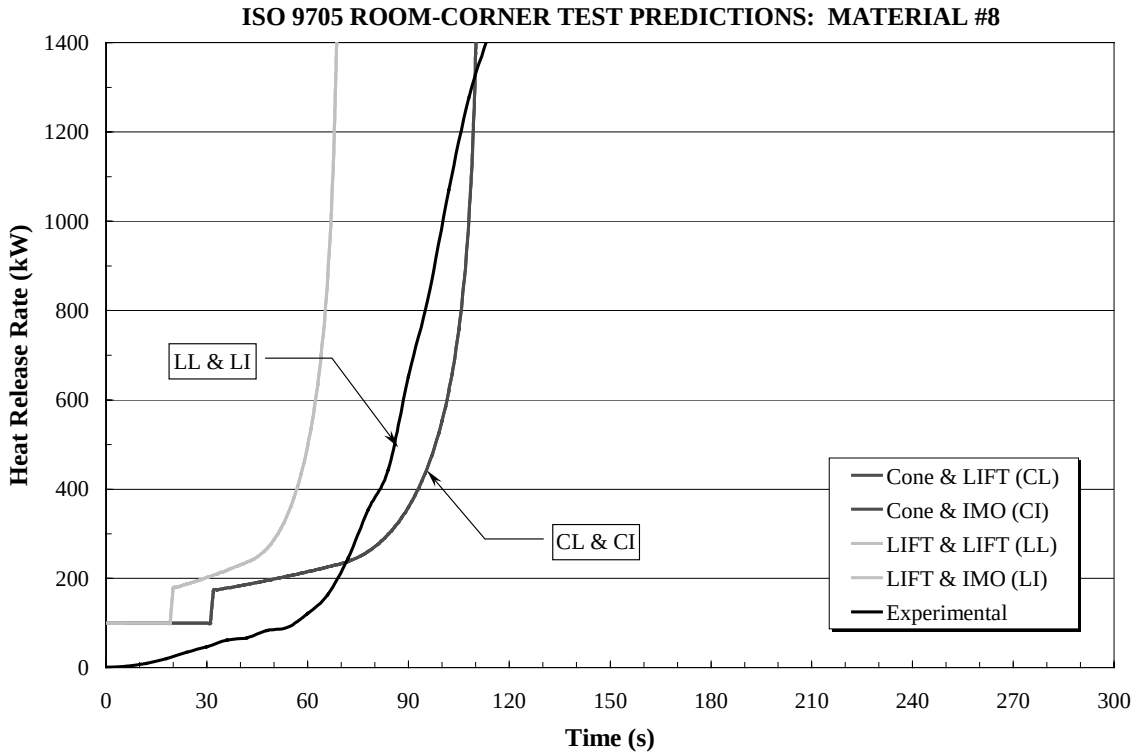

Original Model Predictions

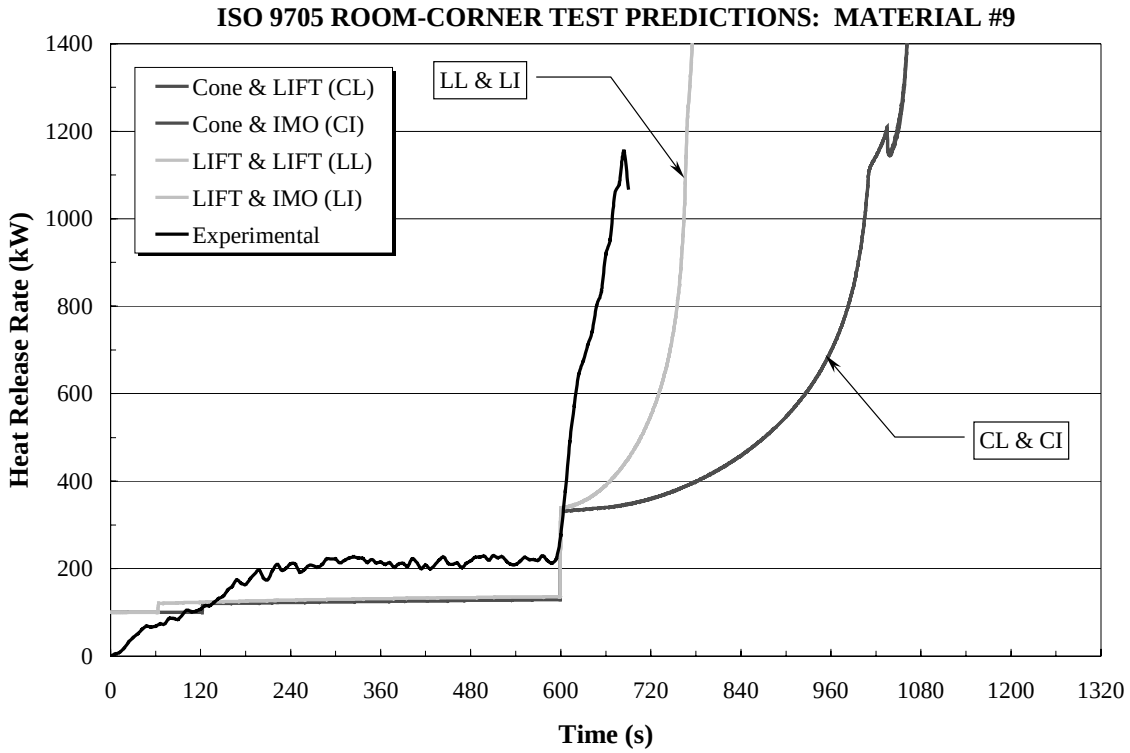

ATTACHMENT E

MODIFIED CONE CALORIMETER IGNITION PROPERTIES

(CONSISTING OF 10 PAGES)

Modified Cone Calorimeter Ignition Properties

MATERIAL NO. 1

Heat Flux (kW/m^2)	t_{ig} (s)	$(1/t_{ig})^{0.5}$ ($s^{-0.5}$)	$(k\rho c/t_{ig})^{0.5}$ ($kW/m^2 \cdot K$)	Fit
75	77	0.1140	0.1378	0.1116
75	78	0.1132	0.1378	0.1116
65	140	0.0845	0.1086	0.0879
60	210	0.0690	0.0940	0.0761
55	211	0.0688	0.0794	0.0643
50	324	0.0556	0.0648	0.0524
50	380	0.0513	0.0648	0.0524
27.84		0.0000	0.0000	0.0000

ε = 0.92

Intercept (> 50) = 27.84 kW/m^2

h_c = 27.3 $W/m^2 \cdot K$

h_{ig} = 59.6 $W/m^2 \cdot K$

T_{ig} = 450 °C

$k\rho c$ = 1.5252 $kW^2 \cdot s/m^4 \cdot K^2$

Intercept (< 50) = 24.48 kW/m^2

Minimum Flux = 47.0 kW/m^2

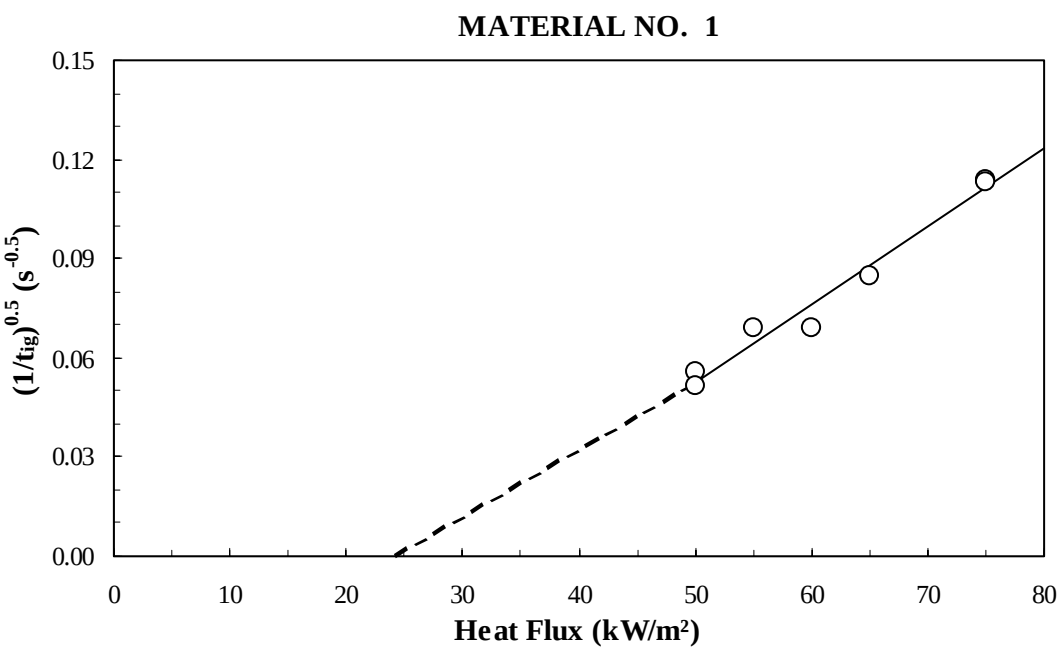

Modified Cone Calorimeter Ignition Properties

MATERIAL NO. 2

Heat Flux (kW/m^2)	t_{ig} (s)	$(1/t_{ig})^{0.5}$ ($s^{-0.5}$)	$(k\rho c/t_{ig})^{0.5}$ ($kW/m^2 \cdot K$)	Fit
75	72	0.1179	0.1915	0.1107
75	83	0.1098	0.1915	0.1107
70	107	0.0967	0.1740	0.1006
65	138	0.0851	0.1565	0.0904
60	163	0.0783	0.1389	
55	192	0.0722	0.1214	
54	198	0.0711	0.1179	
20.40		0.0000	0.0000	0.0000

ε =	0.92
Intercept (> 50) =	20.4 kW/m^2
h_c =	26.8 $W/m^2 \cdot K$
h_{ig} =	52.1 $W/m^2 \cdot K$
T_{ig} =	380 °C
$k\rho c$ =	2.9935 $kW^2 \cdot s/m^4 \cdot K^2$
Intercept (< 50) =	16.74 kW/m^2
Minimum Flux =	53.0 kW/m^2

MATERIAL NO. 2

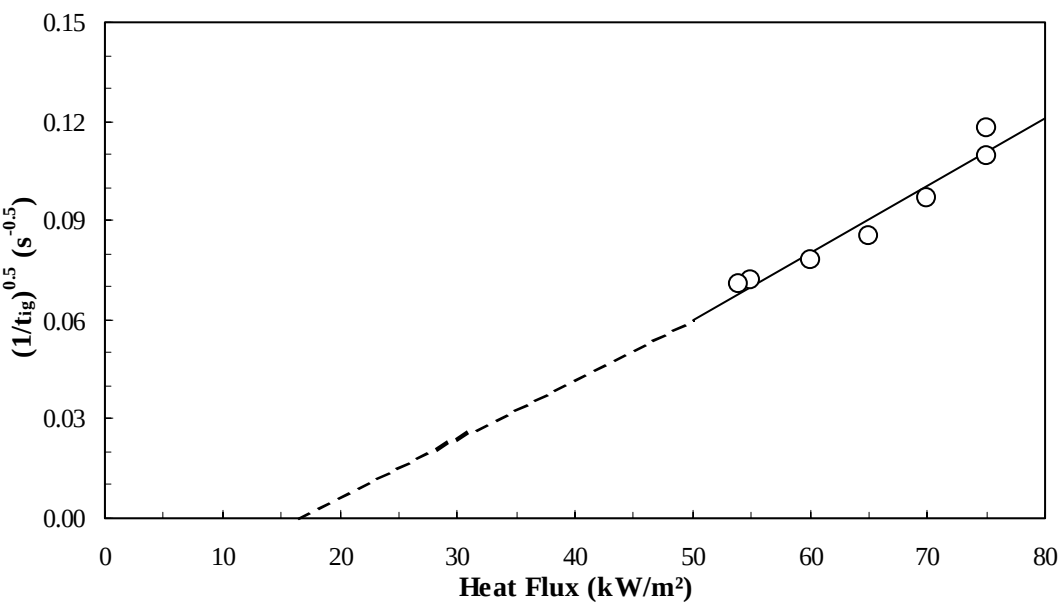

Modified Cone Calorimeter Ignition Properties

MATERIAL NO. 3

Heat Flux (kW/m^2)	t_{ig} (s)	$(1/t_{ig})^{0.5}$ ($s^{-0.5}$)	$(k\rho c/t_{ig})^{0.5}$ ($kW/m^2 \cdot K$)	Fit
50	71	0.1187	0.1337	0.1244
50	59	0.1302	0.1337	0.1244
25	248	0.0635		
25	250	0.0632		
18	397	0.0502		
13		0.0000	0.0000	0.0000

ε = 0.92

Critical Flux = 13.0 kW/m^2

h_c = 16.2 $W/m^2 \cdot K$

h_{ig} = 37.8 $W/m^2 \cdot K$

T_{ig} = 337 °C

$k\rho c$ = 1.1547 $kW^2 \cdot s/m^4 \cdot K^2$

Minimum Flux = 17.0 kW/m^2

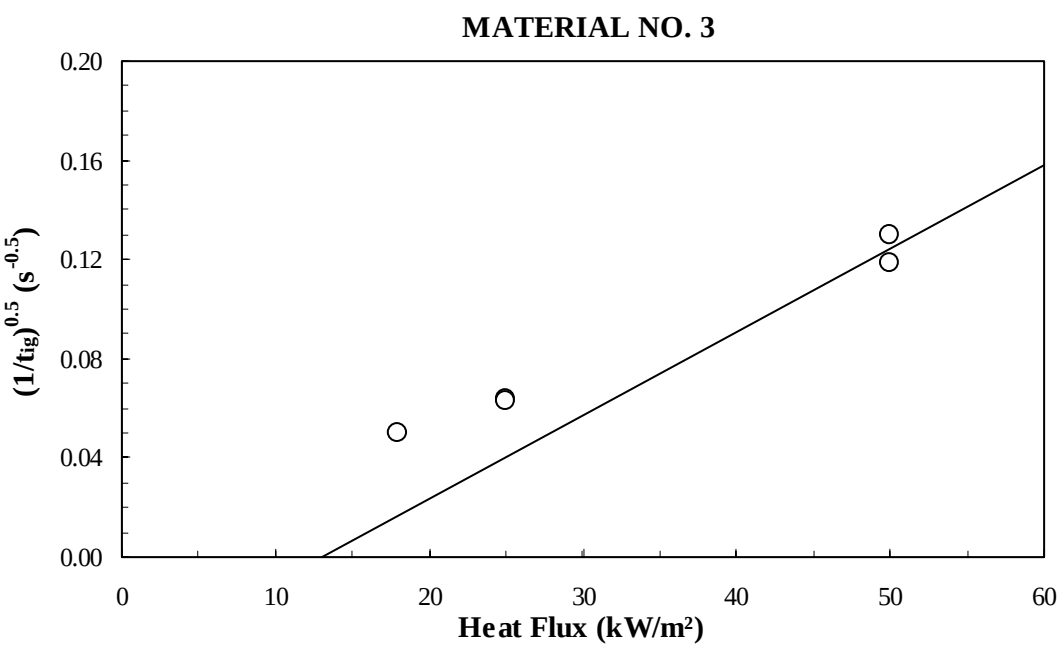

Modified Cone Calorimeter Ignition Properties

MATERIAL NO. 4

Heat Flux (kW/m^2)	t_{ig} (s)	$(1/t_{ig})^{0.5}$ ($s^{-0.5}$)	$(k\rho c/t_{ig})^{0.5}$ ($kW/m^2 \cdot K$)	Fit
50	79	0.1125	0.1337	0.1160
50	70	0.1195	0.1337	0.1160
25	265	0.0614		
25	355	0.0531		
20	667	0.0387		
18	397	0.0502		
13		0.0000	0.0000	0.0000

ε = 0.92

Critical Flux = 13.0 kW/m^2

h_c = 16.2 $W/m^2 \cdot K$

h_{ig} = 37.8 $W/m^2 \cdot K$

T_{ig} = 337 °C

$k\rho c$ = 1.3283 $kW^2 \cdot s/m^4 \cdot K^2$

Minimum Flux = 17.0 kW/m^2

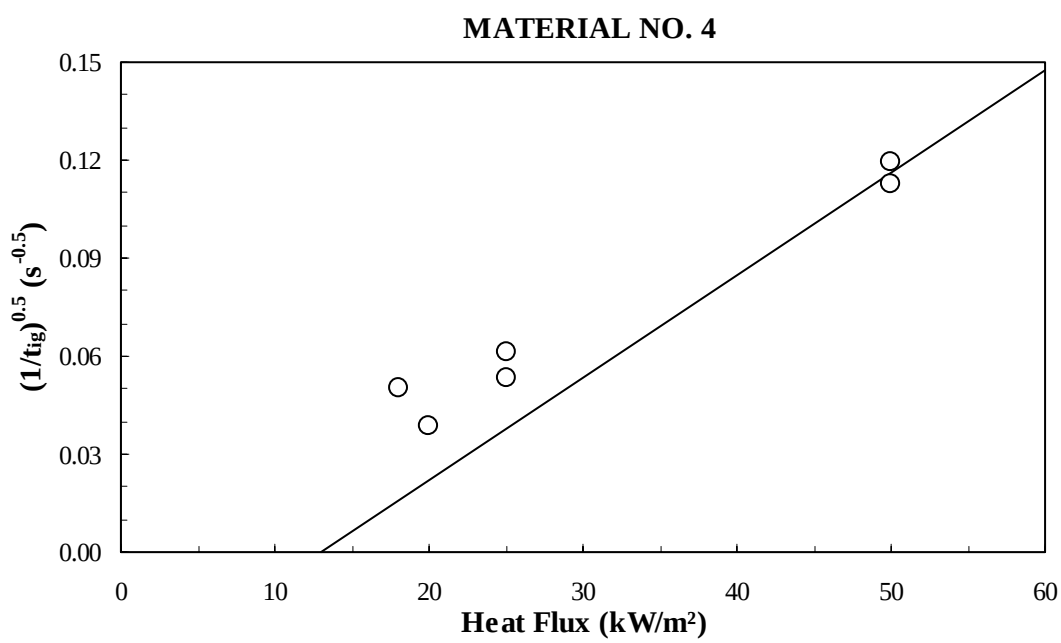

Modified Cone Calorimeter Ignition Properties

MATERIAL NO. 5

Heat Flux (kW/m^2)	t_{ig} (s)	$(1/t_{ig})^{0.5}$ ($s^{-0.5}$)	$(k\rho c/t_{ig})^{0.5}$ ($kW/m^2 \cdot K$)	Fit
50	135	0.0861	0.0959	0.0907
50	110	0.0953	0.0959	0.0907
35	134	0.0864		
30	205	0.0698		
25	349	0.0535		
23	930	0.0328		
18		0.0000	0.0000	0.0000

ε = 0.92

Critical Flux = 18.0 kW/m^2

h_c = 17.9 $W/m^2 \cdot K$

h_{ig} = 44.4 $W/m^2 \cdot K$

T_{ig} = 393 °C

$k\rho c$ = 1.1169 $kW^2 \cdot s/m^4 \cdot K^2$

Minimum Flux = 22.0 kW/m^2

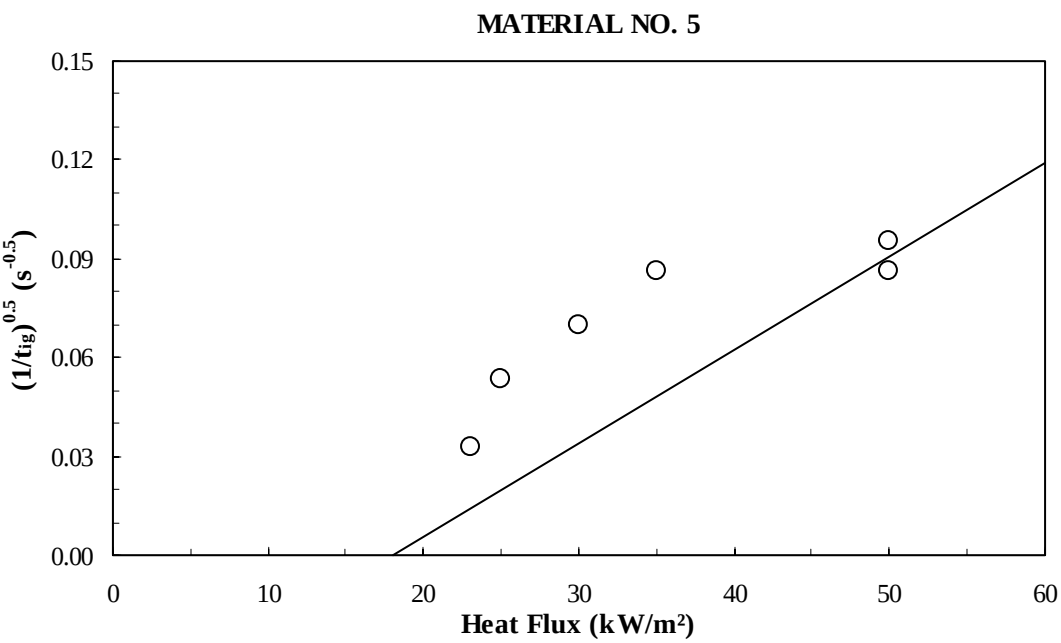

Modified Cone Calorimeter Ignition Properties

MATERIAL NO. 6

Heat Flux (kW/m^2)	t_{ig} (s)	$(1/t_{ig})^{0.5}$ ($s^{-0.5}$)	$(k\rho c/t_{ig})^{0.5}$ ($kW/m^2 \cdot K$)	Fit
50	68	0.1213	0.0487	0.1213
45	71	0.1187		
40	84	0.1091		
38	122	0.0905		
36	205	0.0698		
34	218	0.0677		
29		0.0000	0.0000	0.0000

ε = 0.92

Critical Flux = 29.0 kW/m^2

h_c = 21.7 $W/m^2 \cdot K$

h_{ig} = 57.6 $W/m^2 \cdot K$

T_{ig} = 483 °C

$k\rho c$ = 0.1615 $kW^2 \cdot s/m^4 \cdot K^2$

Minimum Flux = 32.0 kW/m^2

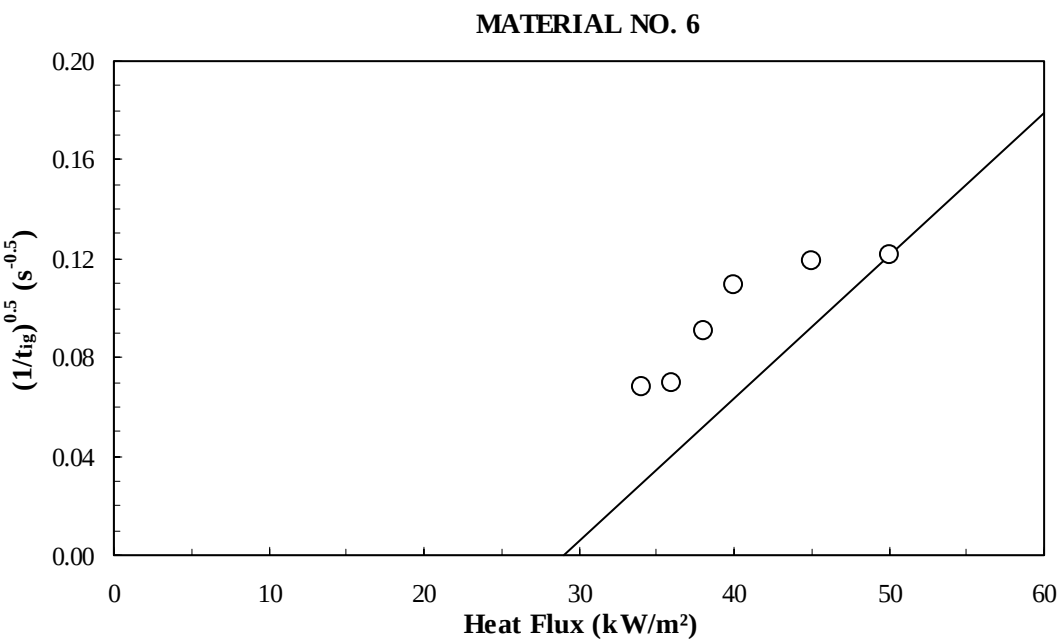

Modified Cone Calorimeter Ignition Properties

MATERIAL NO. 7

Heat Flux (kW/m^2)	t_{ig} (s)	$(1/t_{ig})^{0.5}$ ($s^{-0.5}$)	$(k\rho c/t_{ig})^{0.5}$ ($kW/m^2 \cdot K$)	Fit
50	26	0.1961	0.0848	0.1909
50	29	0.1857	0.0848	0.1909
25	1165	0.0293		
25	690	0.0381		
20		0.0000	0.0000	0.0000

ε = 0.92

Critical Flux = 20.0 kW/m^2

h_c = 18.6 $W/m^2 \cdot K$

h_{ig} = 46.9 $W/m^2 \cdot K$

T_{ig} = 412 °C

$k\rho c$ = 0.1973 $kW^2 \cdot s/m^4 \cdot K^2$

Minimum Flux = 23.0 kW/m^2

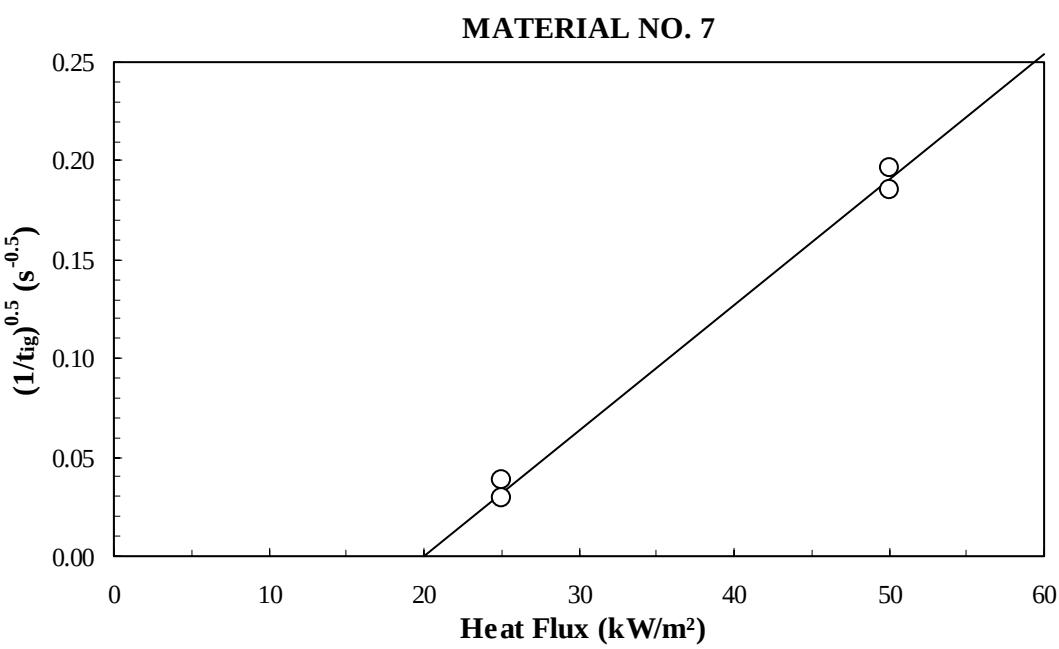

Modified Cone Calorimeter Ignition Properties

MATERIAL NO. 8

Heat Flux (kW/m^2)	t_{ig} (s)	$(1/t_{ig})^{0.5}$ ($s^{-0.5}$)	$(k\rho c/t_{ig})^{0.5}$ ($kW/m^2 \cdot K$)	Fit
50	33	0.1741	0.1441	0.1851
50	26	0.1961	0.1441	0.1851
25	100	0.1000		
25	145	0.0830		
20	161	0.0788		
18	381	0.0512		
17	880	0.0337		
12		0.0000	0.0000	0.0000

ε = 0.92

Critical Flux = 12.0 kW/m^2

h_c = 15.9 $W/m^2 \cdot K$

h_{ig} = 36.4 $W/m^2 \cdot K$

T_{ig} = 323 °C

$k\rho c$ = 0.6061 $kW^2 \cdot s/m^4 \cdot K^2$

Minimum Flux = 16.0 kW/m^2

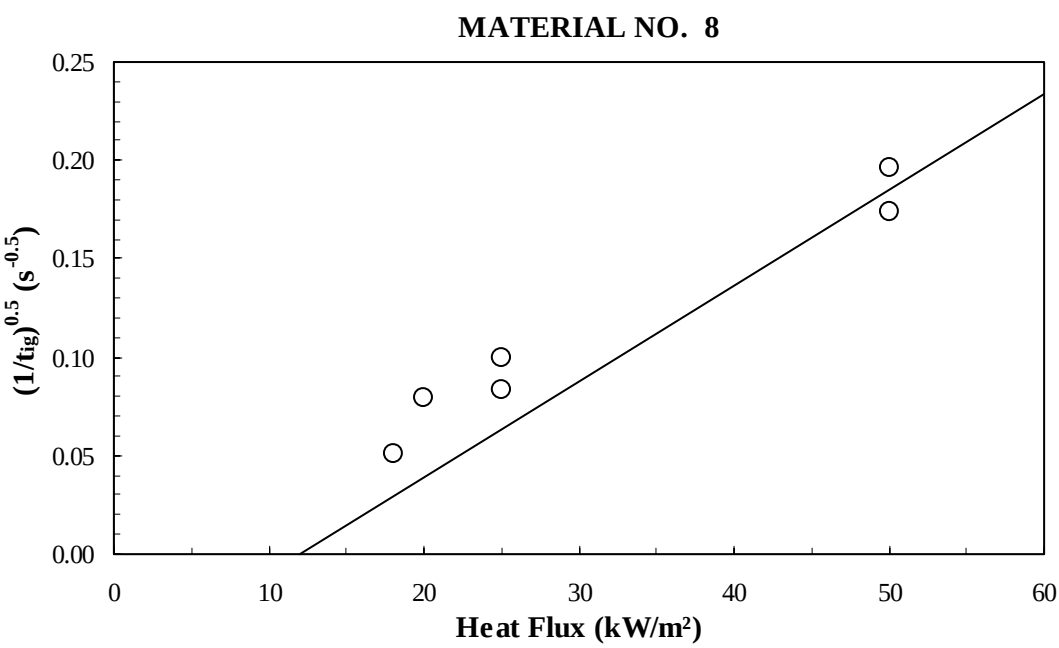

Modified Cone Calorimeter Ignition Properties

MATERIAL NO. 9

Heat Flux (kW/m^2)	t_{ig} (s)	$(1/t_{ig})^{0.5}$ ($s^{-0.5}$)	$(k\rho c/t_{ig})^{0.5}$ ($kW/m^2 \cdot K$)	Fit
50	85	0.1085	0.1246	0.1038
50	105	0.0976	0.1246	0.1038
50	90	0.1054	0.1246	0.1038
25	540	0.0430		
25	420	0.0488		
25	425	0.0485		
20	998	0.0317		
19	1104	0.0301		
14		0.0000	0.0000	0.0000

ε = 0.92

Critical Flux = 14.0 kW/m^2

h_c = 16.6 $W/m^2 \cdot K$

h_{ig} = 39.1 $W/m^2 \cdot K$

T_{ig} = 349 °C

$k\rho c$ = 1.4393 $kW^2 \cdot s/m^4 \cdot K^2$

Minimum Flux = 18.0 kW/m^2

MATERIAL NO. 9

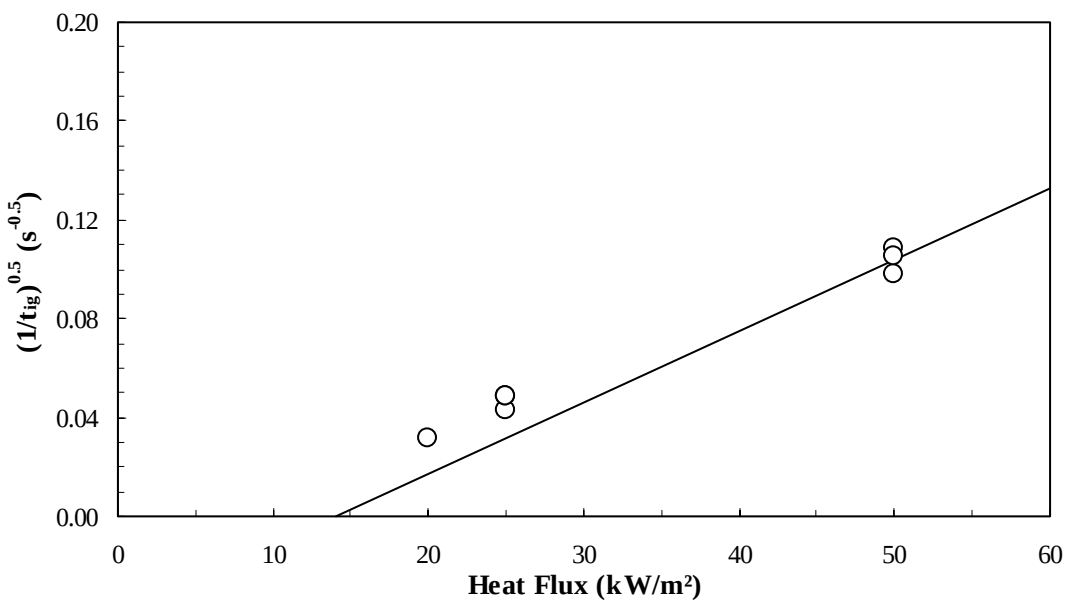

ATTACHMENT F

MODIFIED HEAT RELEASE RATE PROPERTIES

(CONSISTING OF 7 PAGES)

Modified Heat Release Rate Properties

HEAT RELEASE RATE - 50 kW/m²

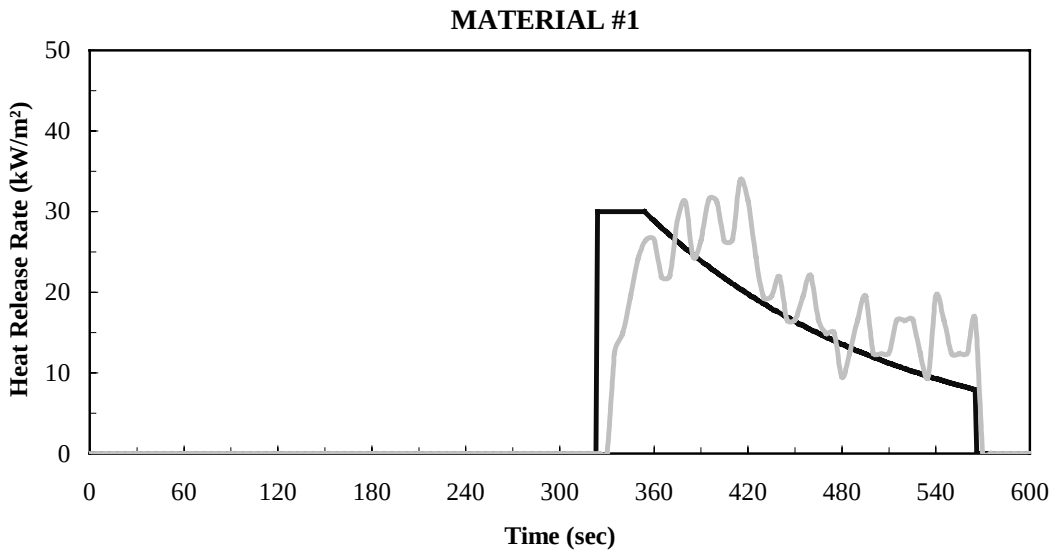

t_{ig}	t_b	HRR_{30max}	THR	λ
324 s	241 s	30 kW/m²	4.40 MJ/m²	0.00630

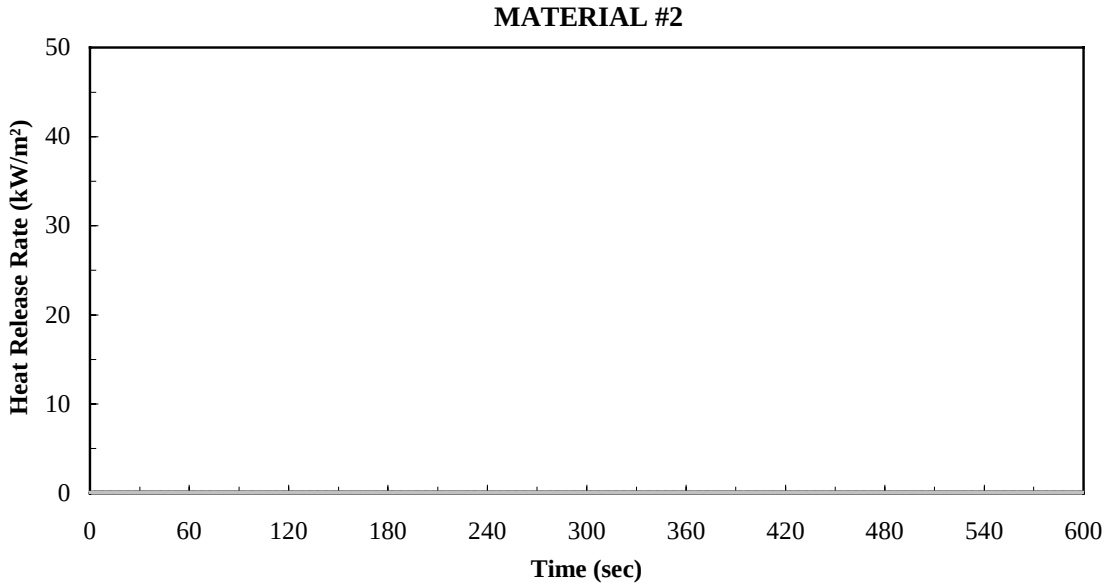

t_{ig}	t_b	HRR_{30max}	THR	λ
NI	NI	---	0.00 MJ/m²	0

Modified Heat Release Rate Properties

HEAT RELEASE RATE - 50 kW/m²

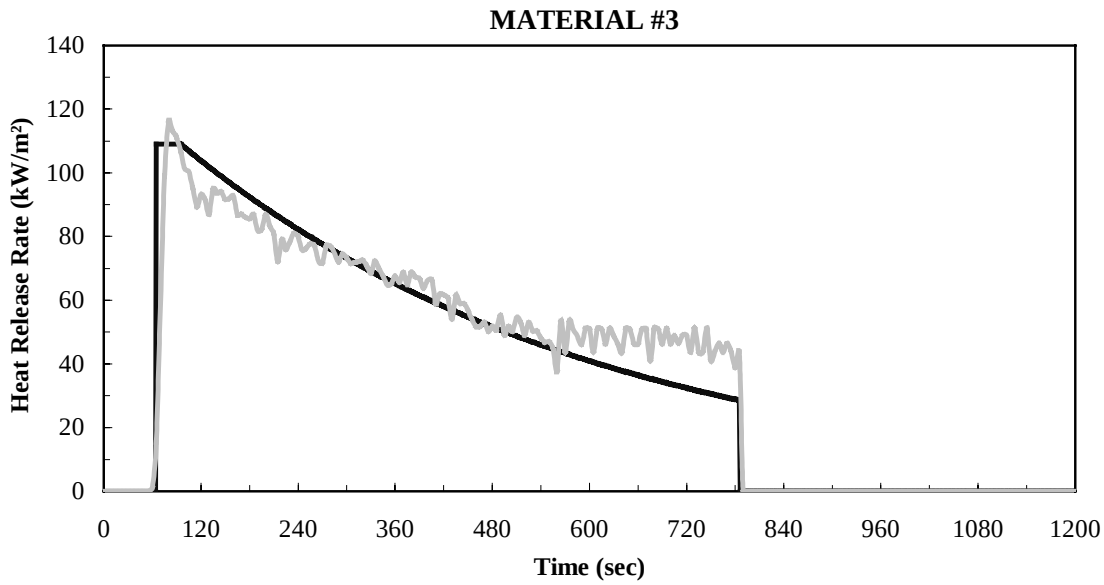

t_{ig}	t_b	HRR_{30max}	THR	λ
65 s	720 s	109 kW/m²	44.72 MJ/m²	0.00194 1/s

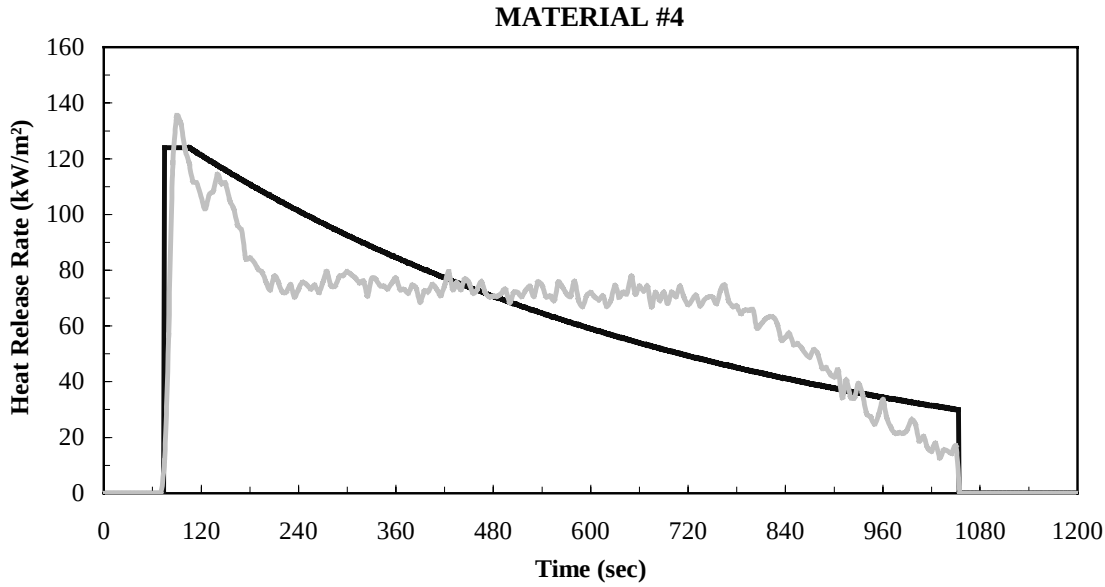

t_{ig}	t_b	HRR_{30max}	THR	λ
75 s	978 s	124 kW/m²	66.44 MJ/m²	0.0015 1/s

Modified Heat Release Rate Properties

HEAT RELEASE RATE - 50 kW/m²

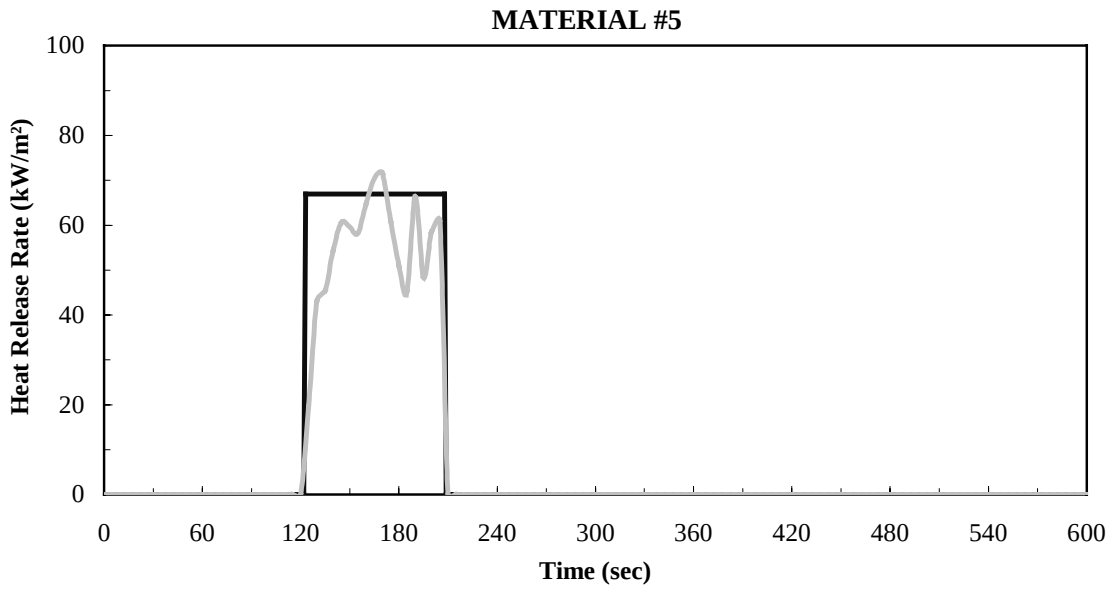

t_{ig}	t_b	HRR_{30max}	THR	λ
123 s	85 s	67 kW/m²	5.69 MJ/m²	0.00000 1/s

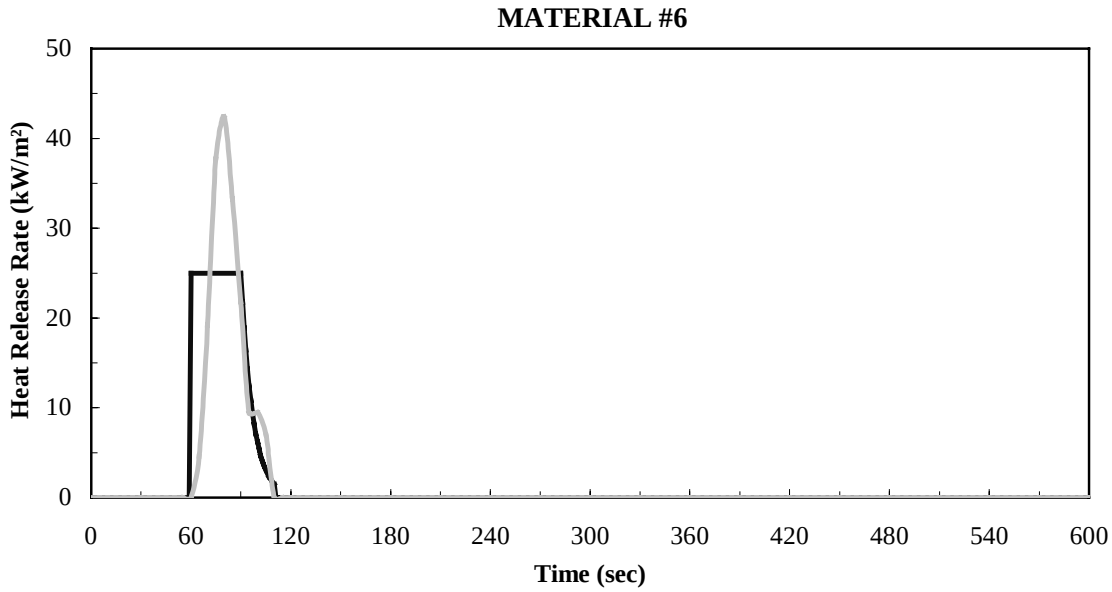

t_{ig}	t_b	HRR_{30max}	THR	λ
60 s	50 s	25 kW/m²	0.92 MJ/m²	0.140 1/s

Modified Heat Release Rate Properties

HEAT RELEASE RATE - 50 kW/m²

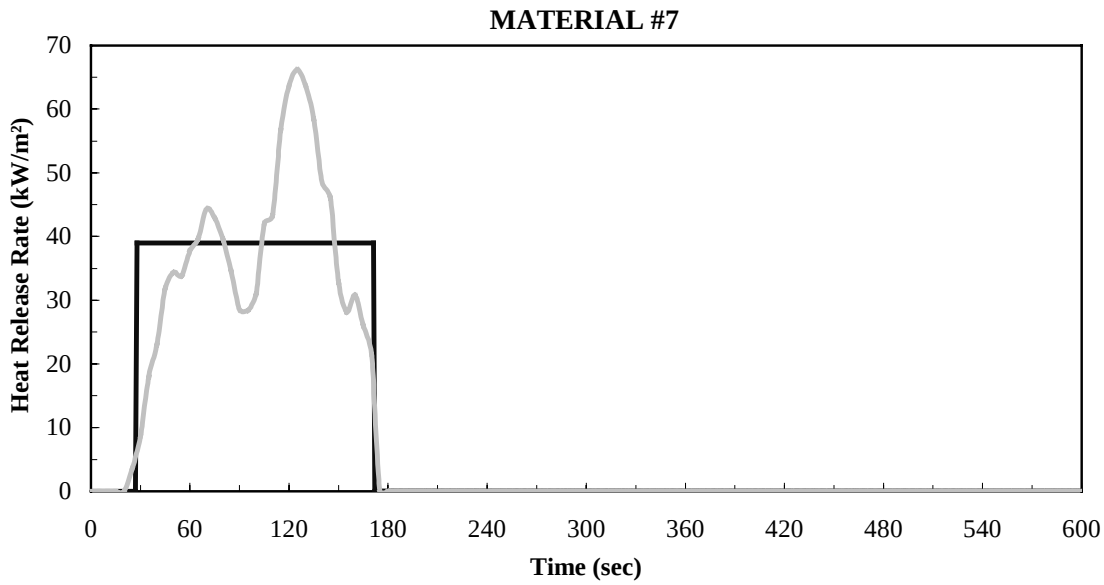

t_{ig}	t_b	HRR_{30max}	THR	λ
28 s	143 s	39 kW/m²	5.58 MJ/m²	1E-15 1/s

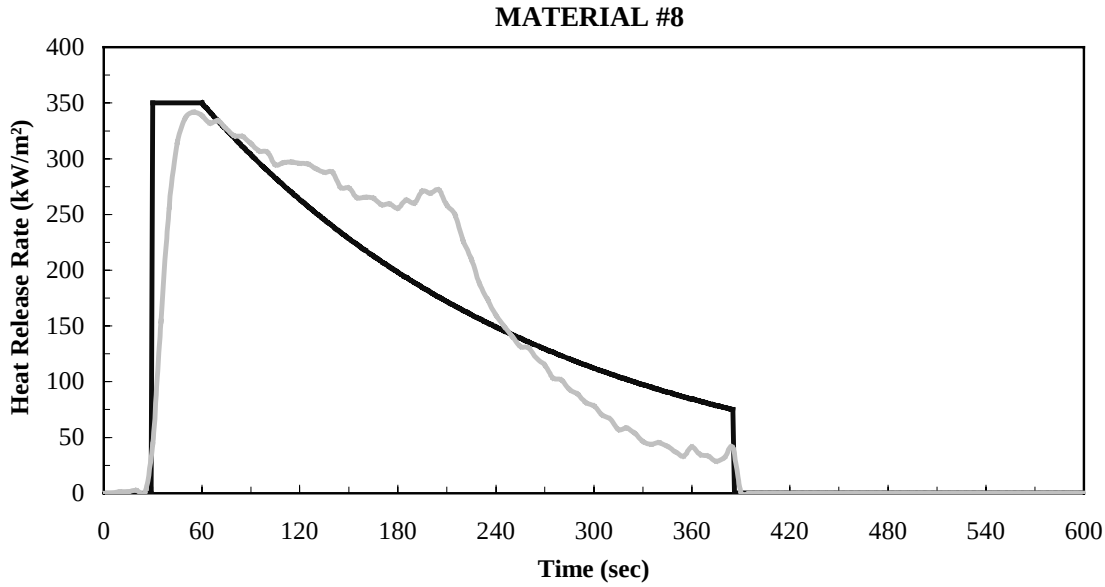

t_{ig}	t_b	HRR_{30max}	THR	λ
30 s	355 s	350 kW/m²	68.52 MJ/m²	0.00474 1/s

Modified Heat Release Rate Properties

HEAT RELEASE RATE - 50 kW/m²

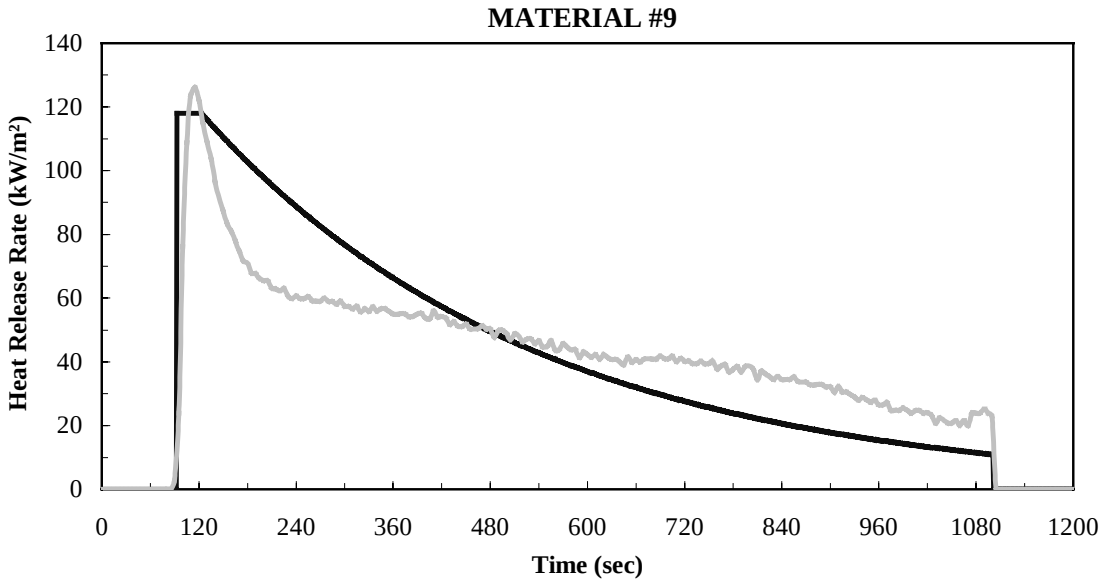

t_{ig}	t_b	HRR_{30max}	THR	λ
93 s	1008 s	118 kW/m²	47.59 MJ/m²	0.00243 1/s

Modified Heat Release Rate Properties

HEAT RELEASE RATE - 75 kW/m²

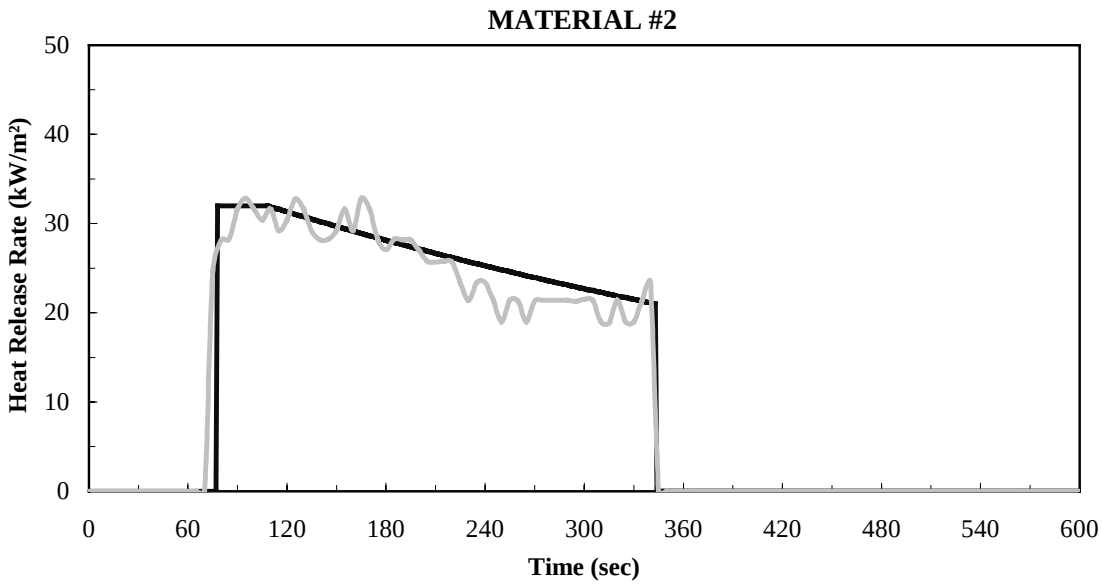

t_{ig}	t_b	HRR_{30max}	THR	λ
78 s	265 s	32 kW/m²	7.10 MJ/m²	0.00179 1/s

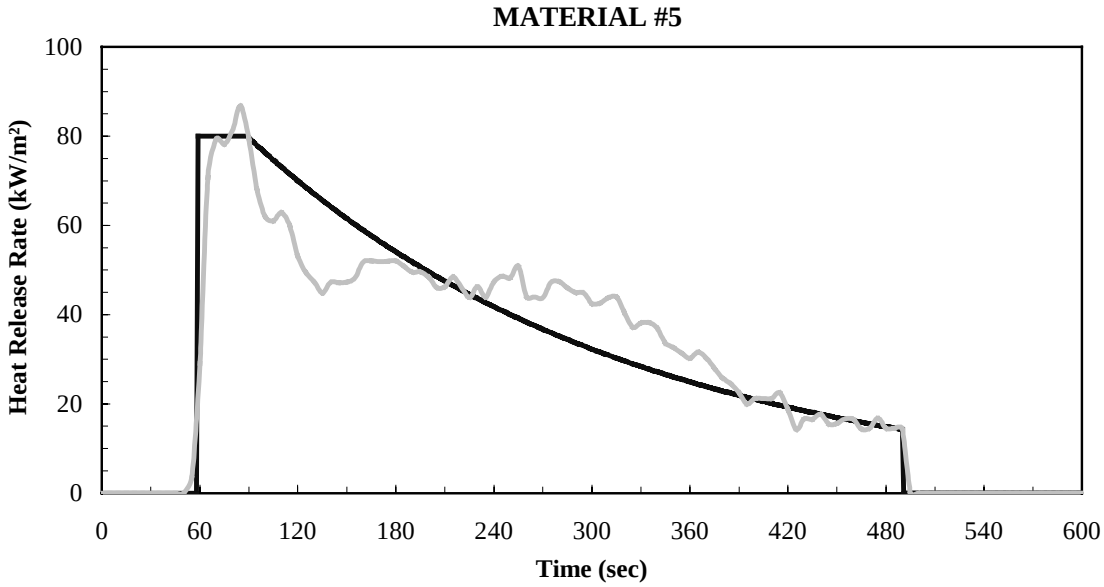

t_{ig}	t_b	HRR_{30max}	THR	λ
59 s	431 s	80 kW/m²	17.69 MJ/m²	0.00430 1/s

ATTACHMENT G

MODIFIED MODEL PREDICTIONS

(CONSISTING OF 19 PAGES)

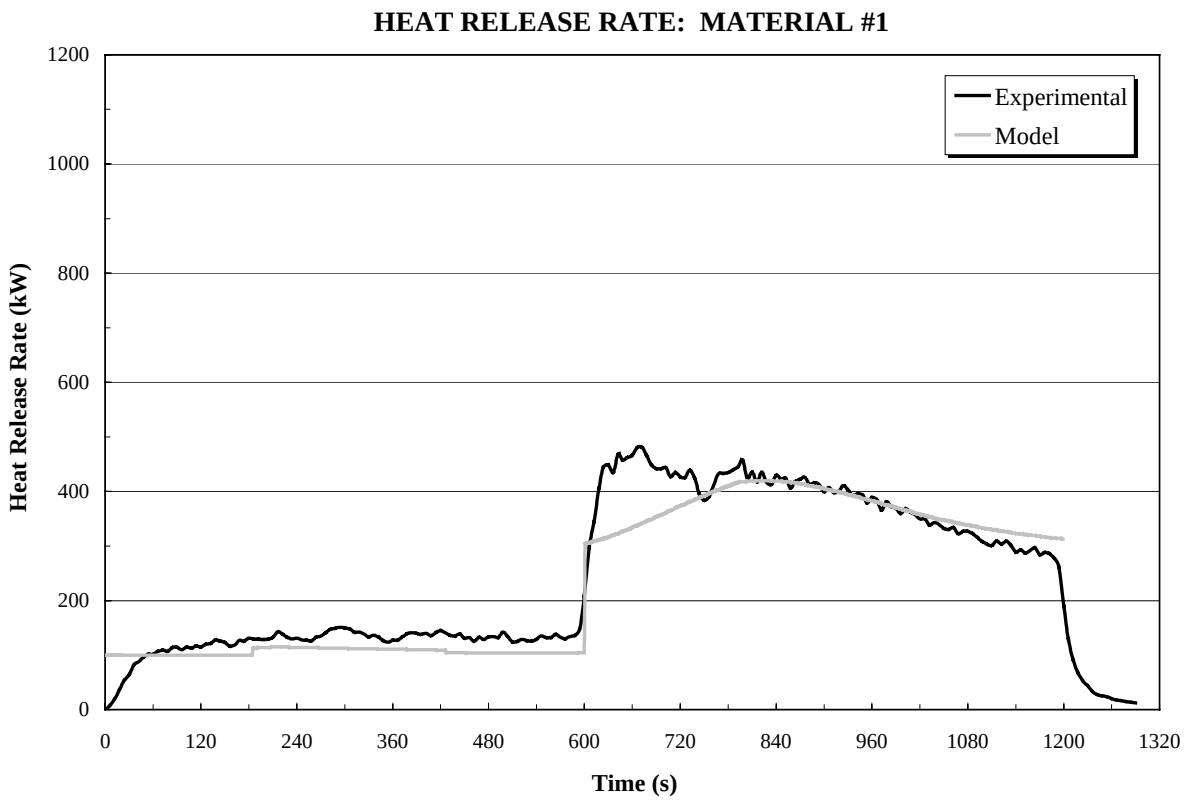
HEAT RELEASE RATE: MATERIAL #1
Experimental
Model
Heat Release Rate (kW)
0
200
400
600
800
1000
1200
0
120
240
360
480
600
720
840
960
1080
1200
1320
Time (s)

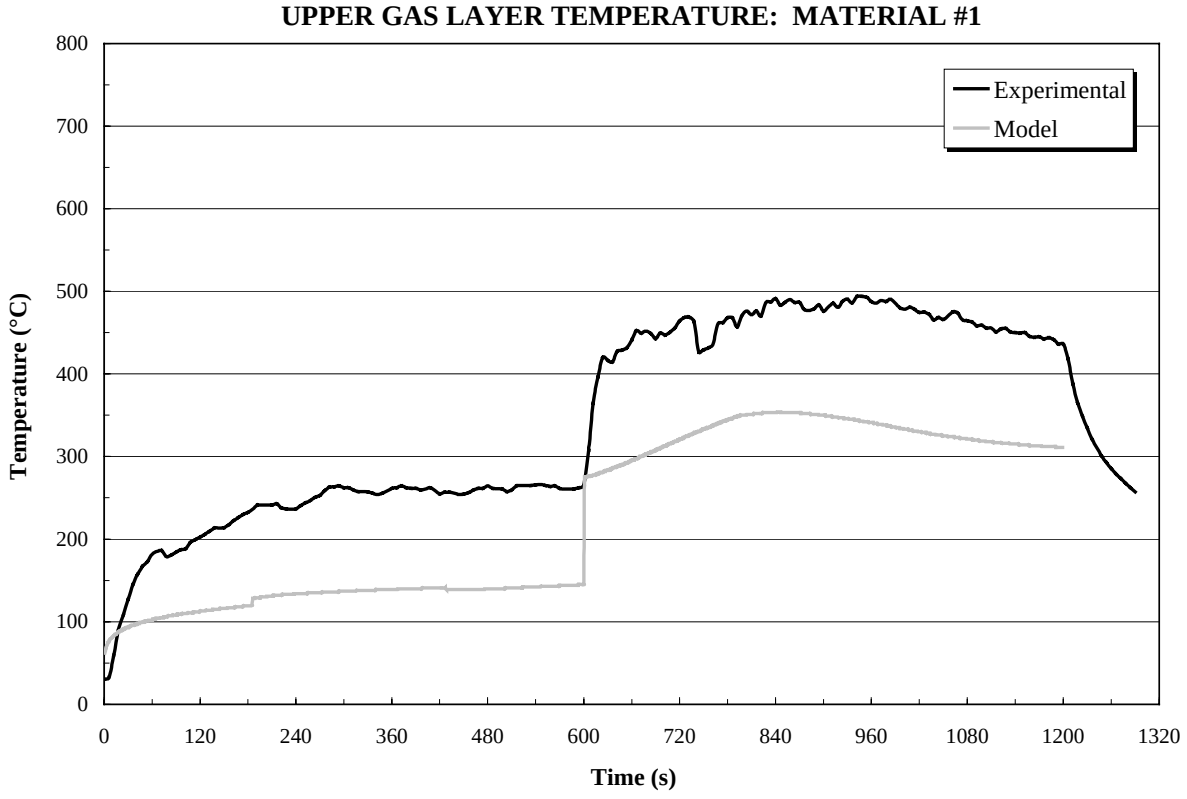
UPPER GAS LAYER TEMPERATURE: MATERIAL #1
Experimental
Model
Temperature (°C)
0
100
200
300
400
500
600
700
800
0
120
240
360
480
600
720
840
960
1080
1200
1320
Time (s)

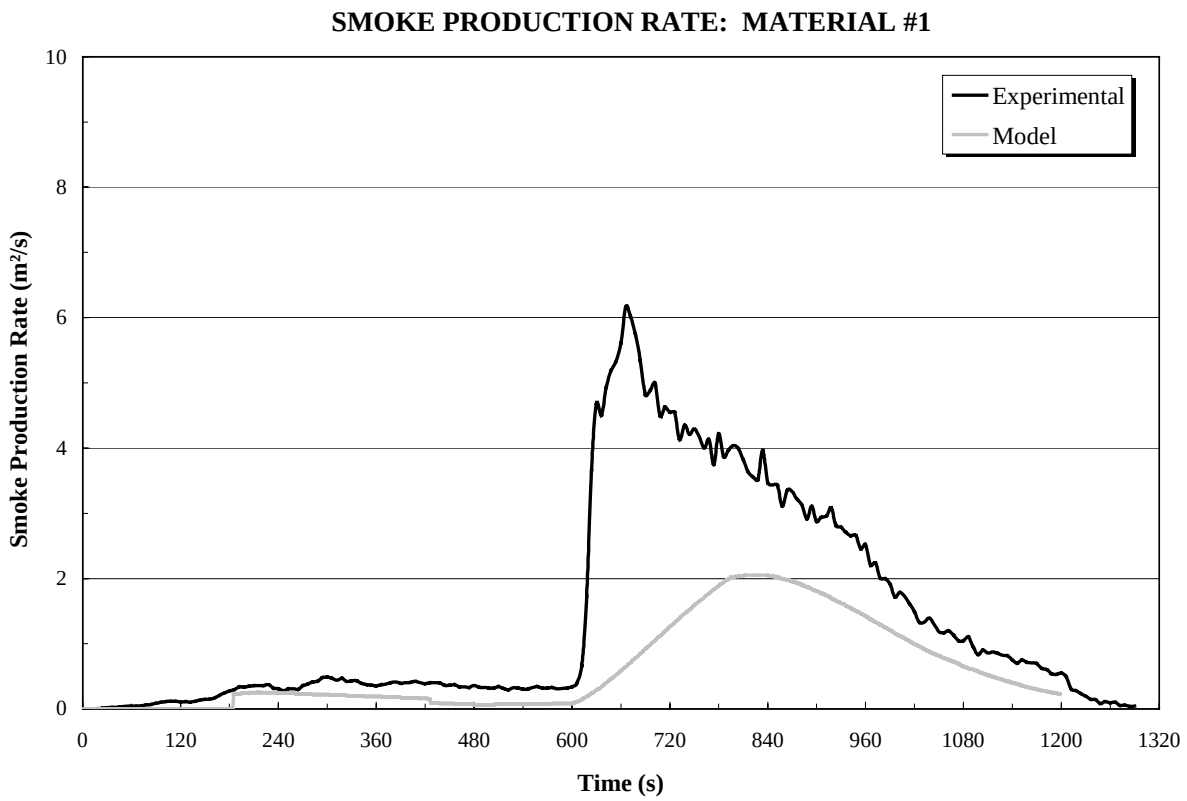
SMOKE PRODUCTION RATE: MATERIAL #1
Experimental
Model
Smoke Production Rate (m²/s)
0
2
4
6
8
10
0
120
240
360
480
600
720
840
960
1080
1200
1320
Time (s)

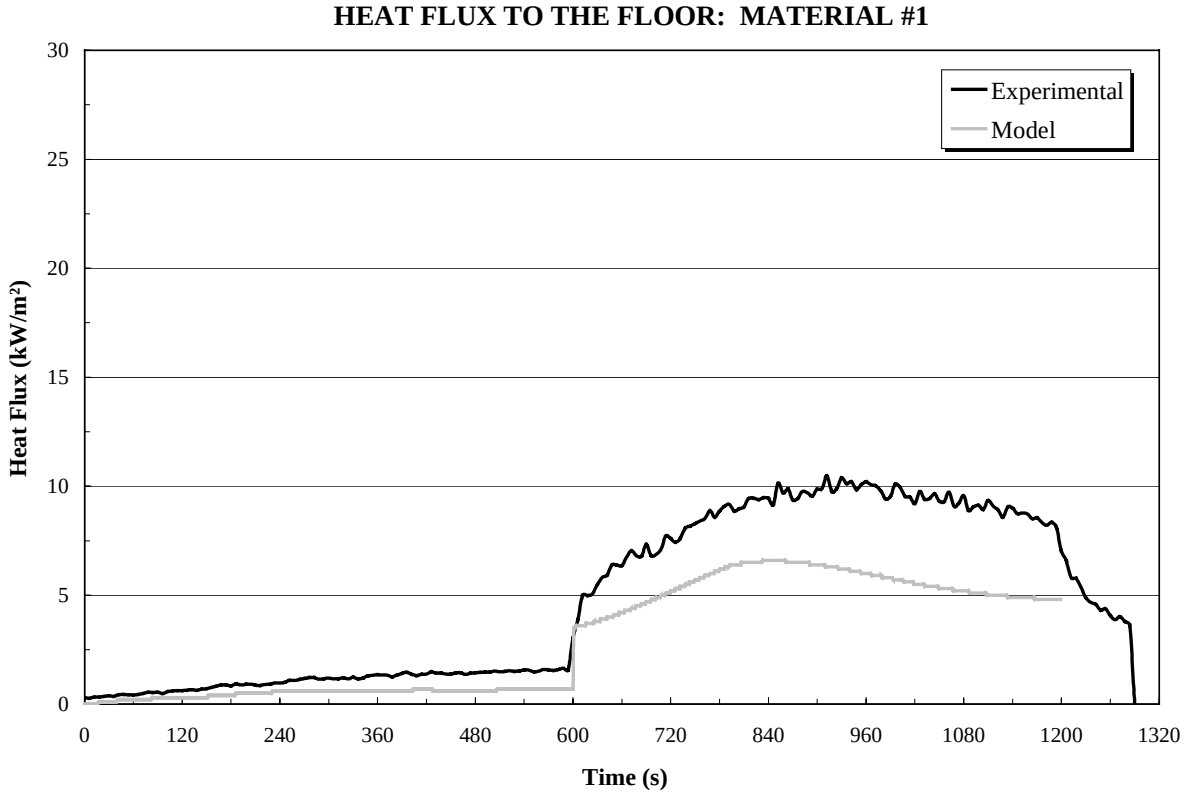
HEAT FLUX TO THE FLOOR: MATERIAL #1
Experimental
Model
Heat Flux (kW/m²)
0
5
10
15
20
25
30
0
120
240
360
480
600
720
840
960
1080
1200
1320
Time (s)

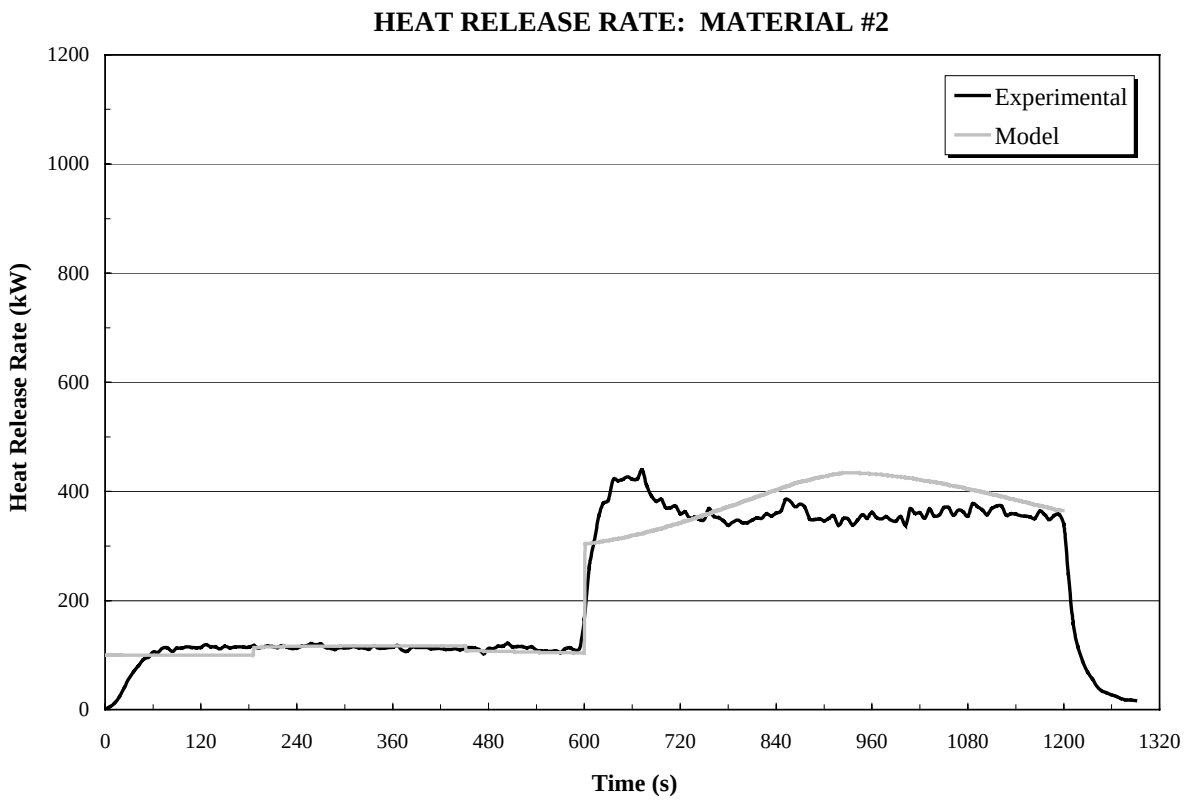
HEAT RELEASE RATE: MATERIAL #2
Experimental
Model
Heat Release Rate (kW)
0
200
400
600
800
1000
1200
0
120
240
360
480
600
720
840
960
1080
1200
1320
Time (s)

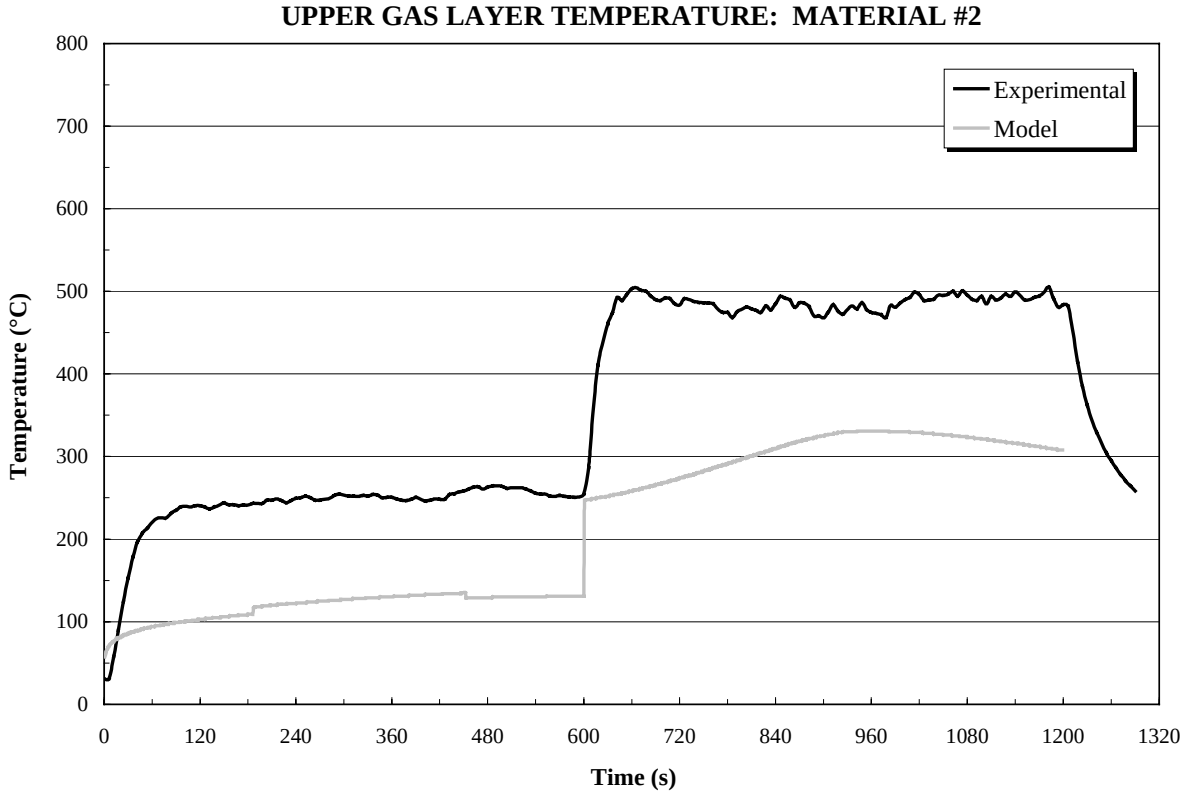
UPPER GAS LAYER TEMPERATURE: MATERIAL #2
Experimental
Model
Temperature (°C)
0
100
200
300
400
500
600
700
800
0
120
240
360
480
600
720
840
960
1080
1200
1320
Time (s)

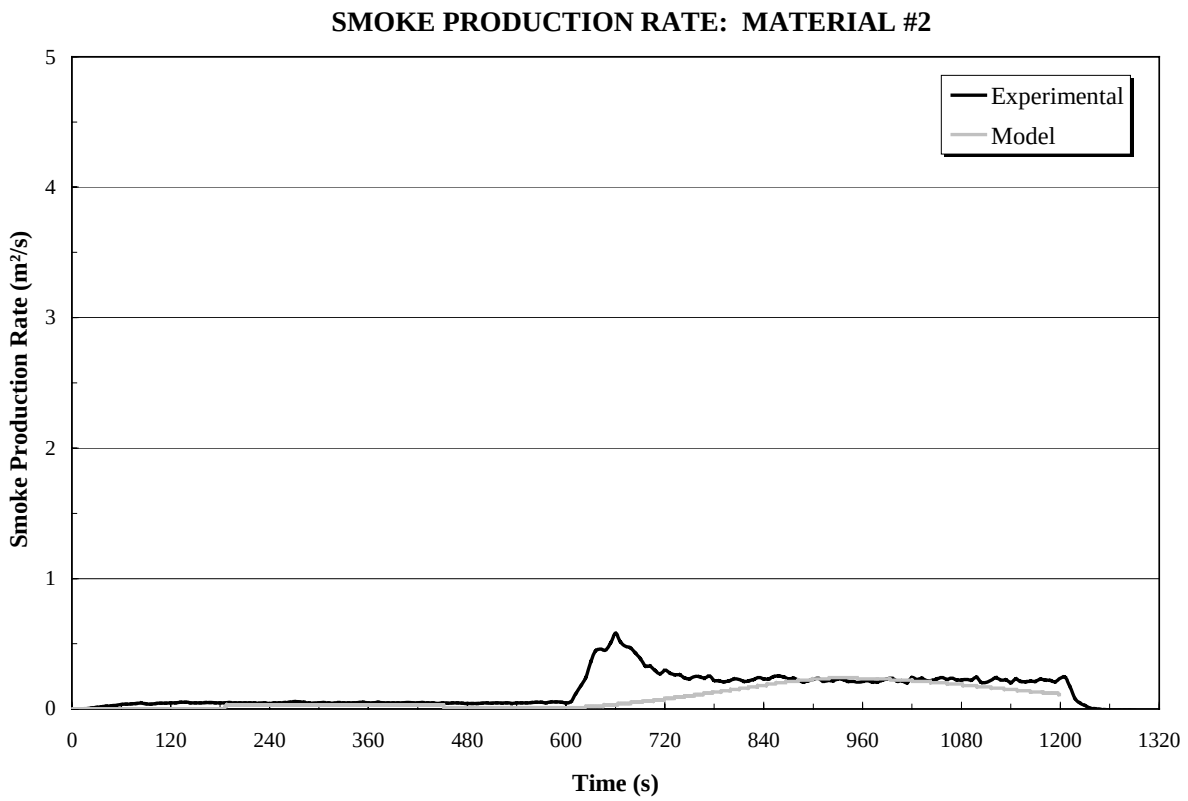
SMOKE PRODUCTION RATE: MATERIAL #2
Experimental
Model
Smoke Production Rate (m²/s)
0
1
2
3
4
5
0
120
240
360
480
600
720
840
960
1080
1200
1320
Time (s)

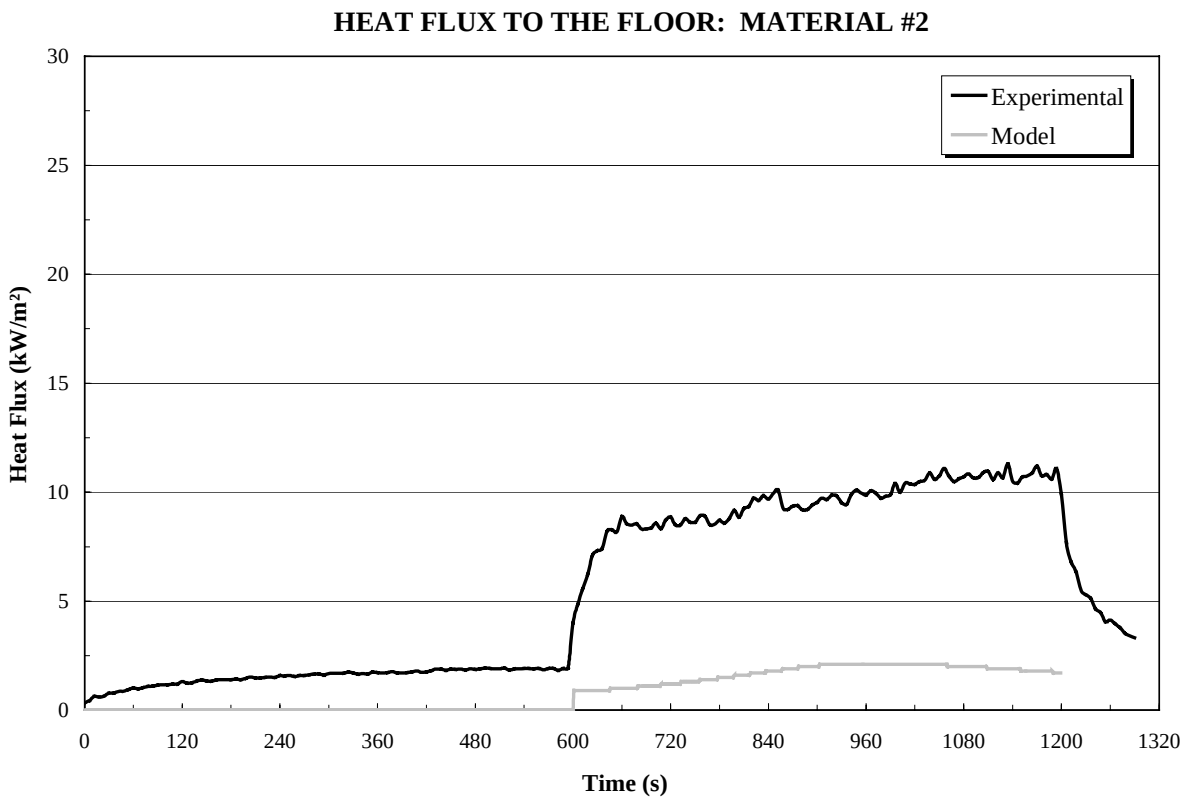
HEAT FLUX TO THE FLOOR: MATERIAL #2
Experimental
Model
Heat Flux (kW/m²)
0
5
10
15
20
25
30
0
120
240
360
480
600
720
840
960
1080
1200
1320
Time (s)

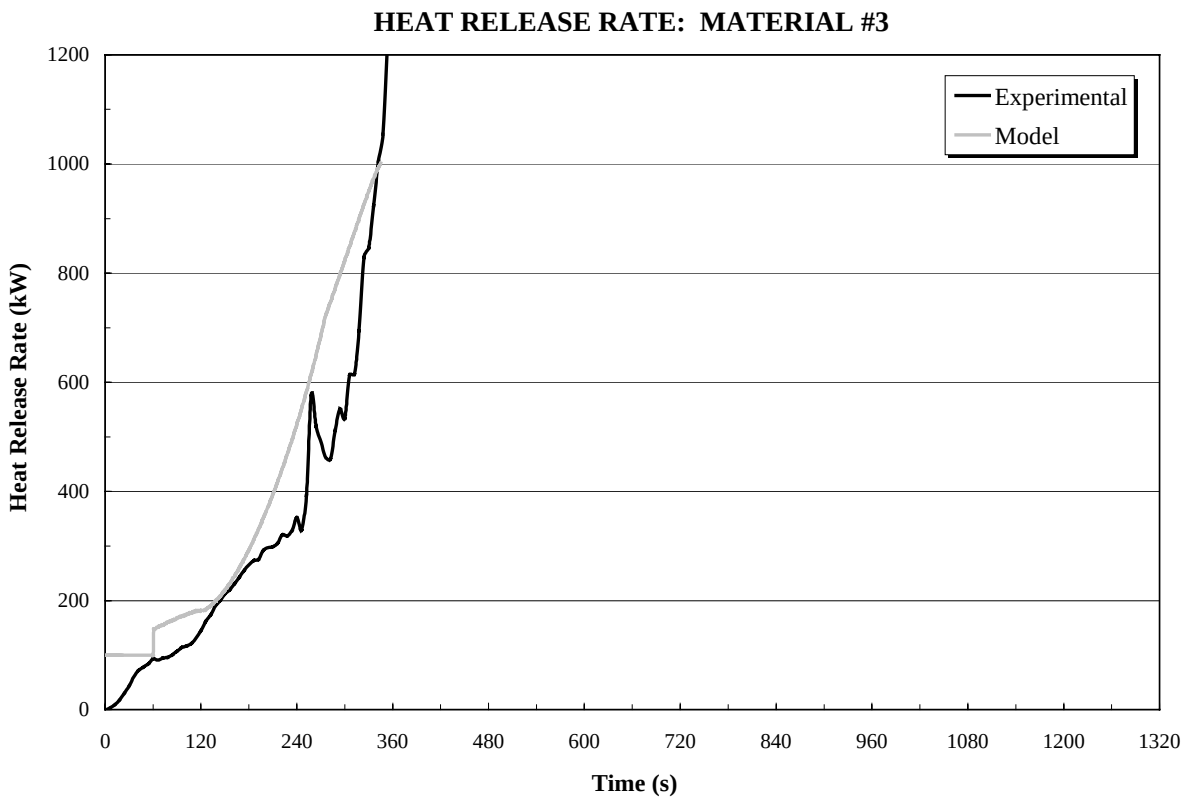
HEAT RELEASE RATE: MATERIAL #3
Heat Release Rate (kW)
Time (s)
Experimental
Model
0
200
400
600
800
1000
1200
0
120
240
360
480
600
720
840
960
1080
1200
1320

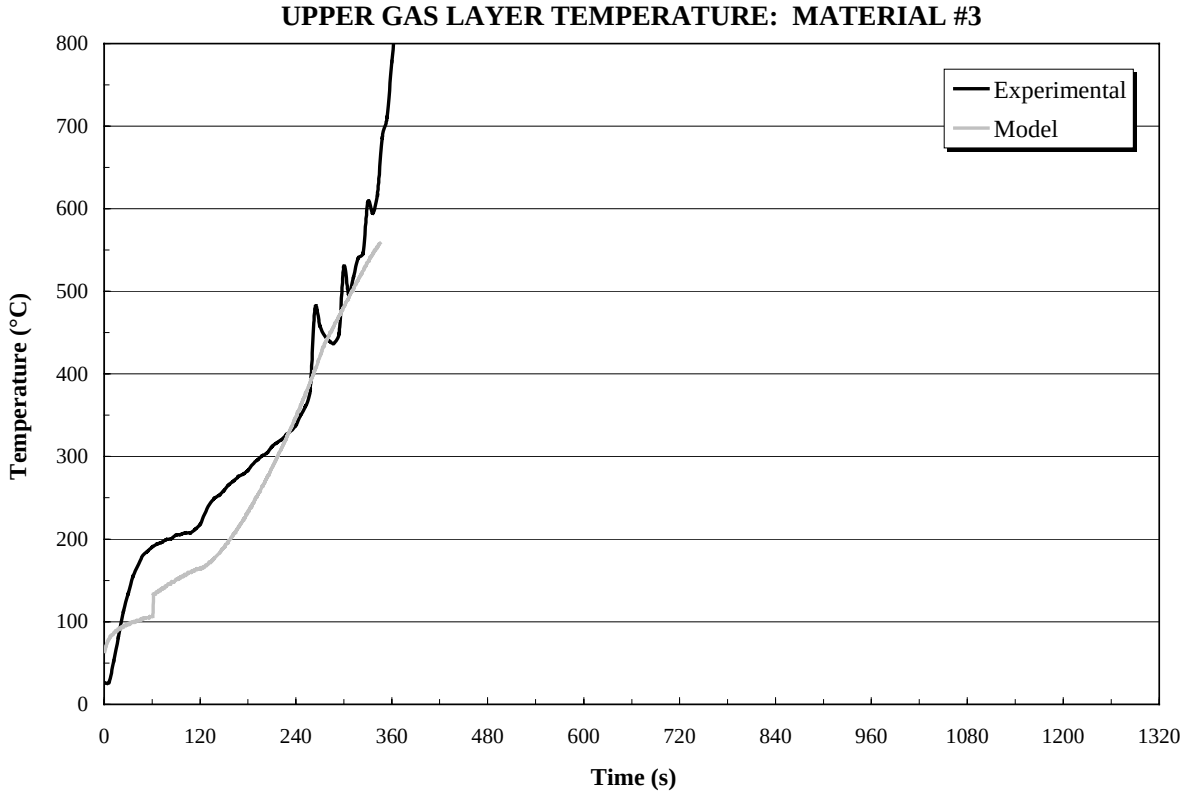
UPPER GAS LAYER TEMPERATURE: MATERIAL #3
Temperature (°C)
Time (s)
Experimental
Model
0
100
200
300
400
500
600
700
800
0
120
240
360
480
600
720
840
960
1080
1200
1320

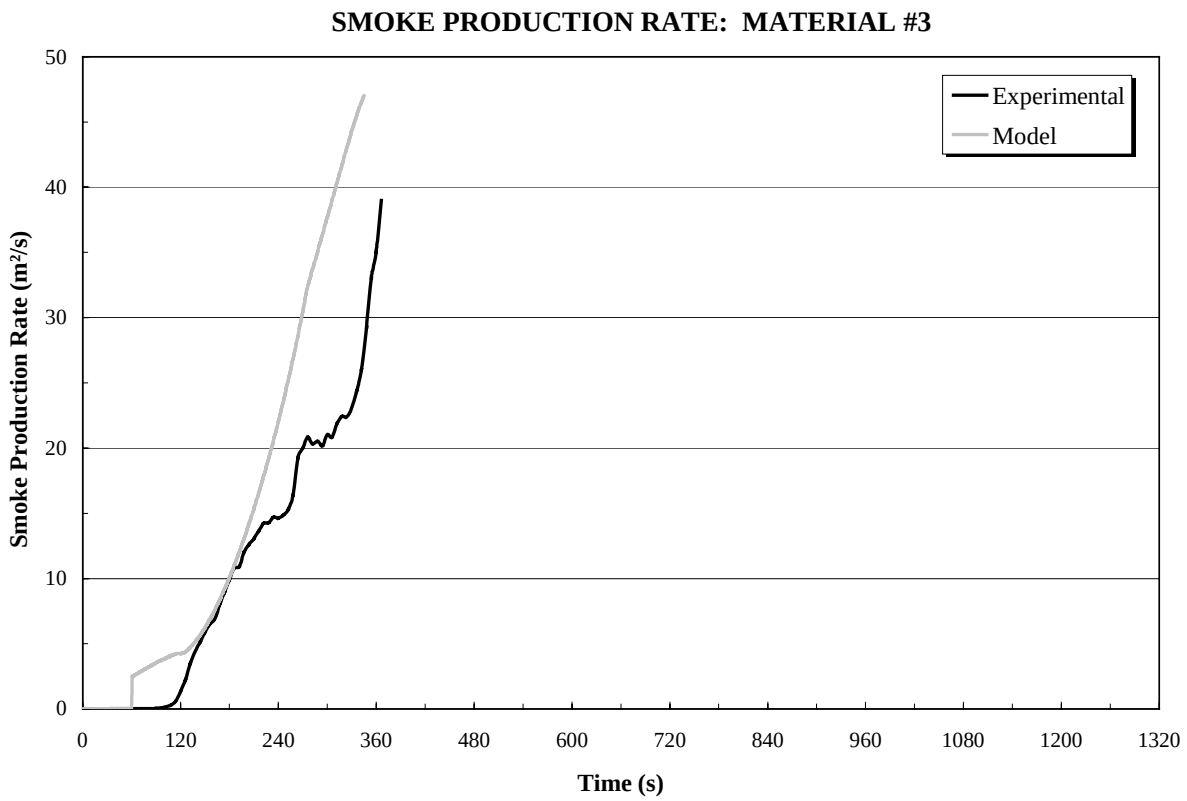
SMOKE PRODUCTION RATE: MATERIAL #3
Experimental
Model
Smoke Production Rate (m²/s)
0
10
20
30
40
50
0
120
240
360
480
600
720
840
960
1080
1200
1320
Time (s)

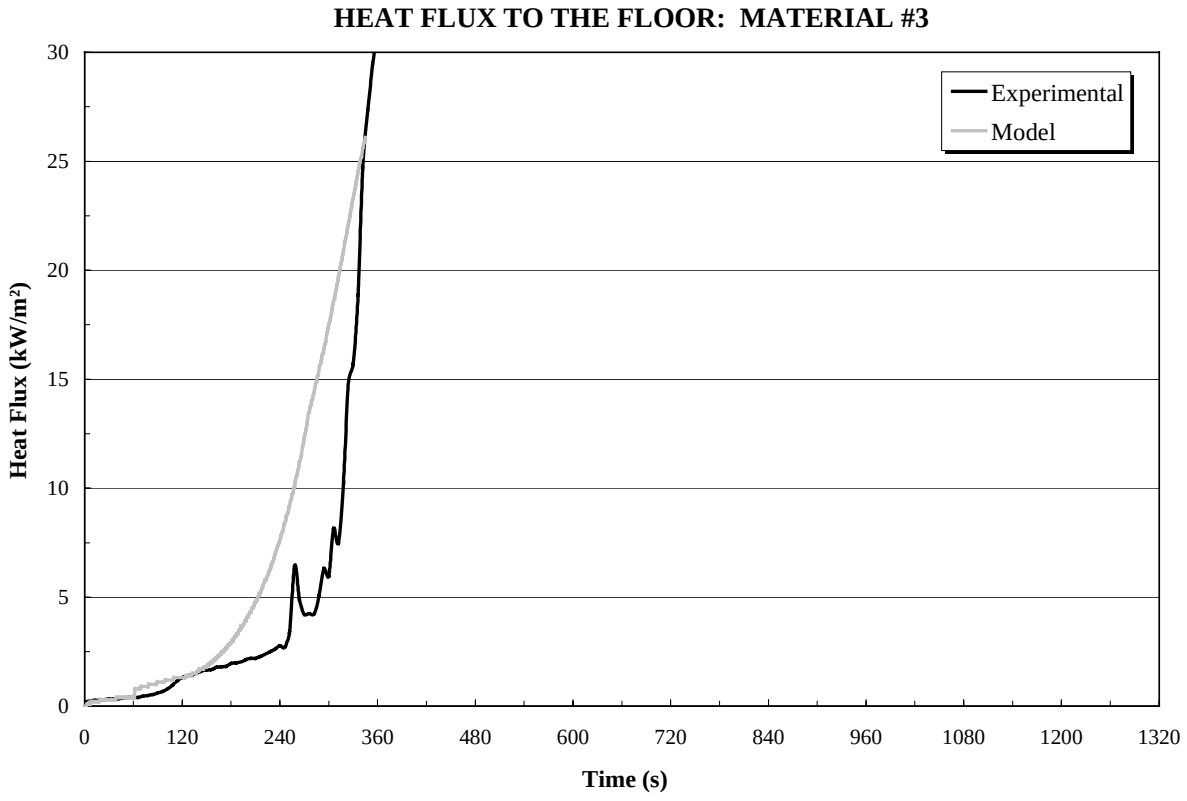
HEAT FLUX TO THE FLOOR: MATERIAL #3
Experimental
Model
Heat Flux (kW/m²)
0
5
10
15
20
25
30
0
120
240
360
480
600
720
840
960
1080
1200
1320
Time (s)

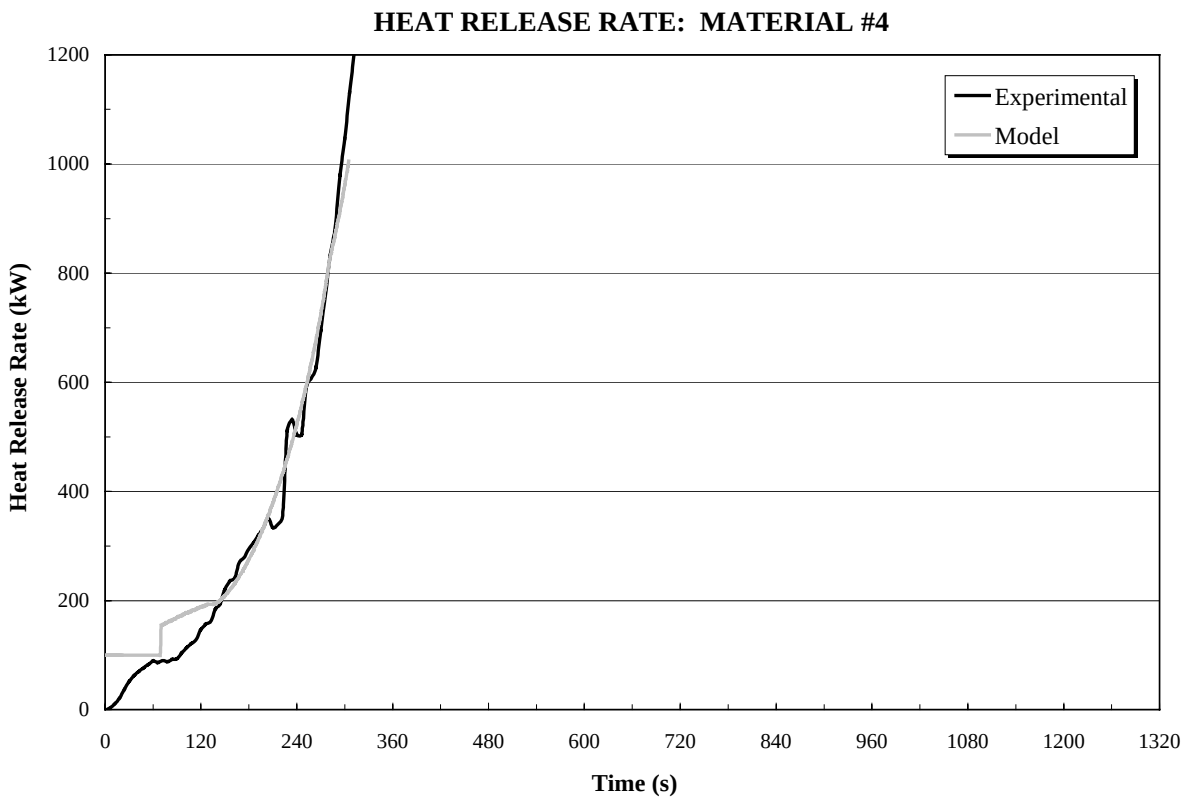
HEAT RELEASE RATE: MATERIAL #4
Heat Release Rate (kW)
Time (s)
Experimental
Model
0
200
400
600
800
1000
1200
0
120
240
360
480
600
720
840
960
1080
1200
1320

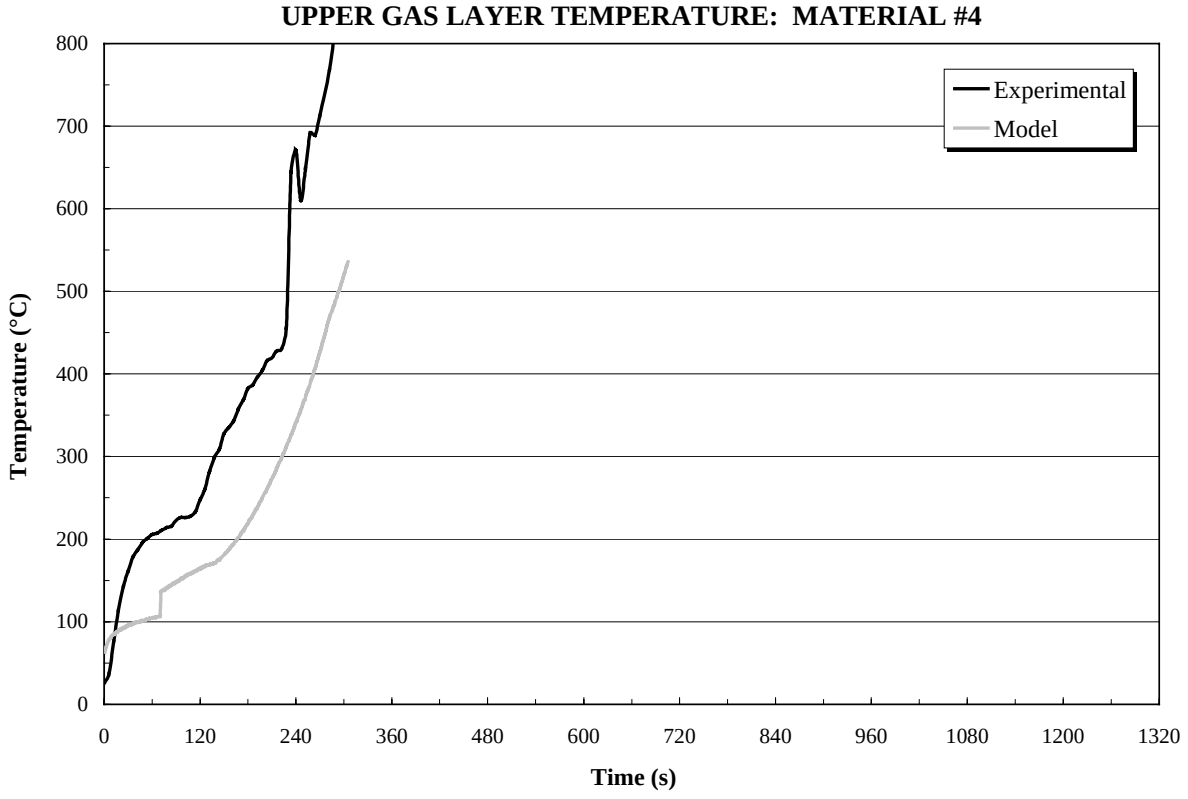
UPPER GAS LAYER TEMPERATURE: MATERIAL #4
Temperature (°C)
Time (s)
Experimental
Model
0
100
200
300
400
500
600
700
800
0
120
240
360
480
600
720
840
960
1080
1200
1320

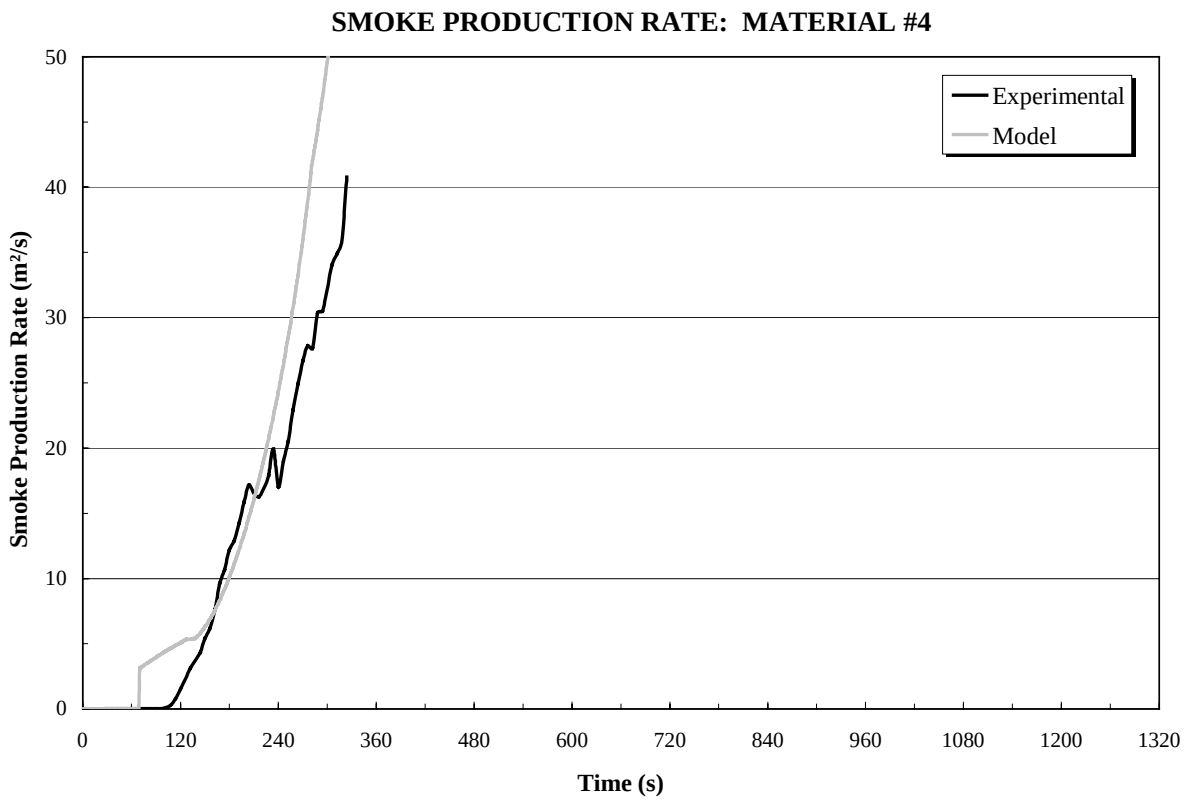
SMOKE PRODUCTION RATE: MATERIAL #4
Experimental
Model
Smoke Production Rate (m²/s)
0
10
20
30
40
50
0
120
240
360
480
600
720
840
960
1080
1200
1320
Time (s)

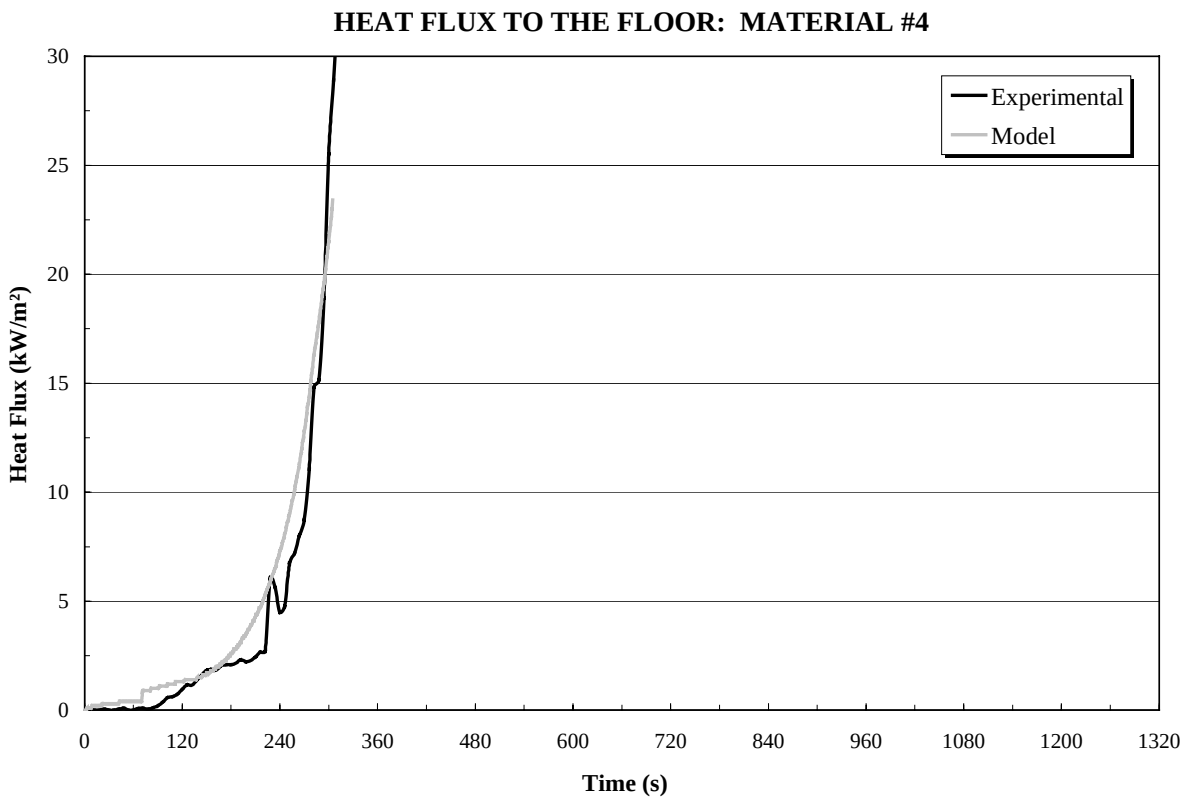
HEAT FLUX TO THE FLOOR: MATERIAL #4
Experimental
Model
Heat Flux (kW/m²)
0
5
10
15
20
25
30
0
120
240
360
480
600
720
840
960
1080
1200
1320
Time (s)

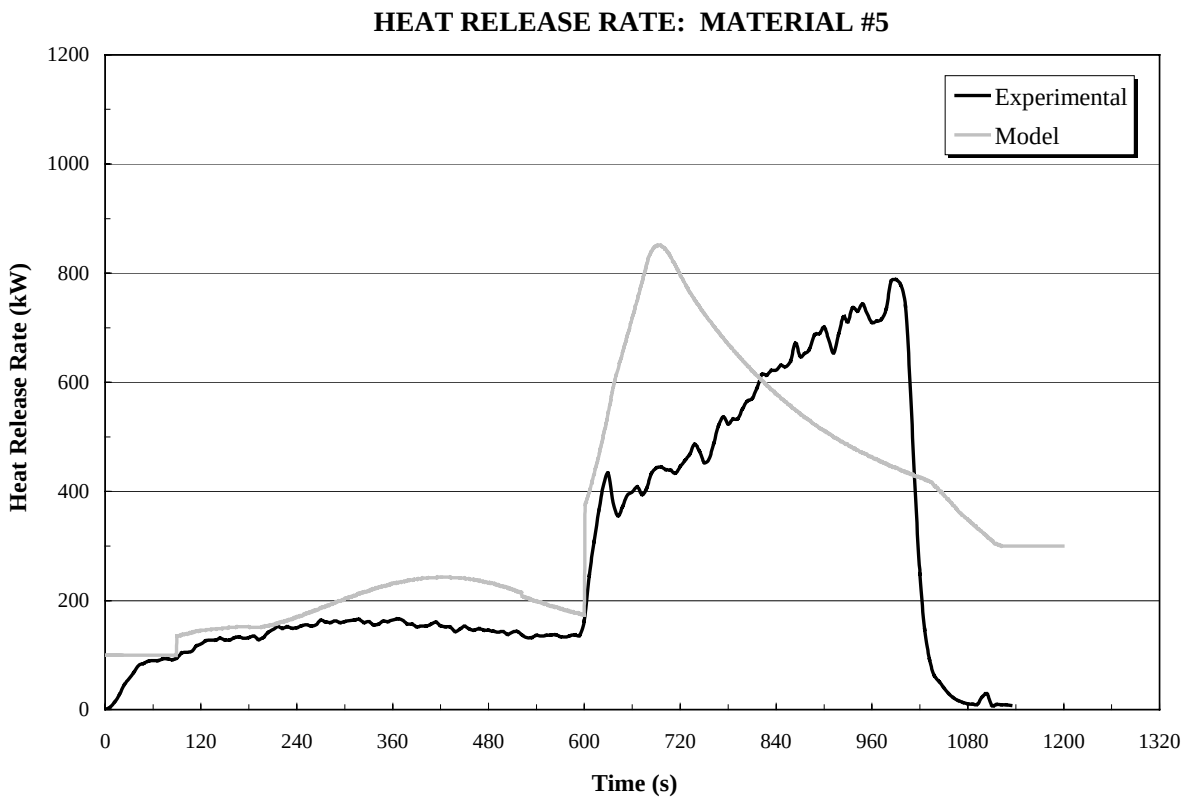
HEAT RELEASE RATE: MATERIAL #5
Experimental
Model
Heat Release Rate (kW)
Time (s)
0
200
400
600
800
1000
1200
0
120
240
360
480
600
720
840
960
1080
1200
1320

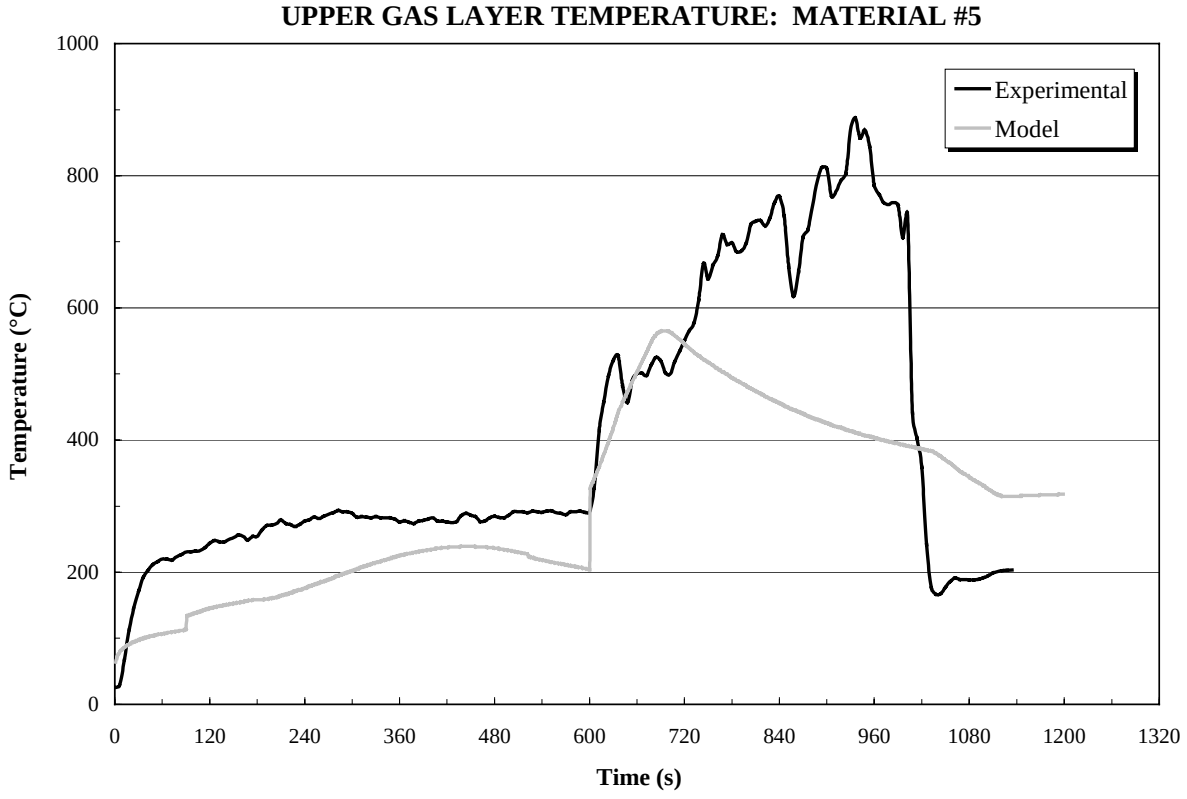
UPPER GAS LAYER TEMPERATURE: MATERIAL #5
Experimental
Model
Temperature (°C)
Time (s)
0
200
400
600
800
1000
0
120
240
360
480
600
720
840
960
1080
1200
1320

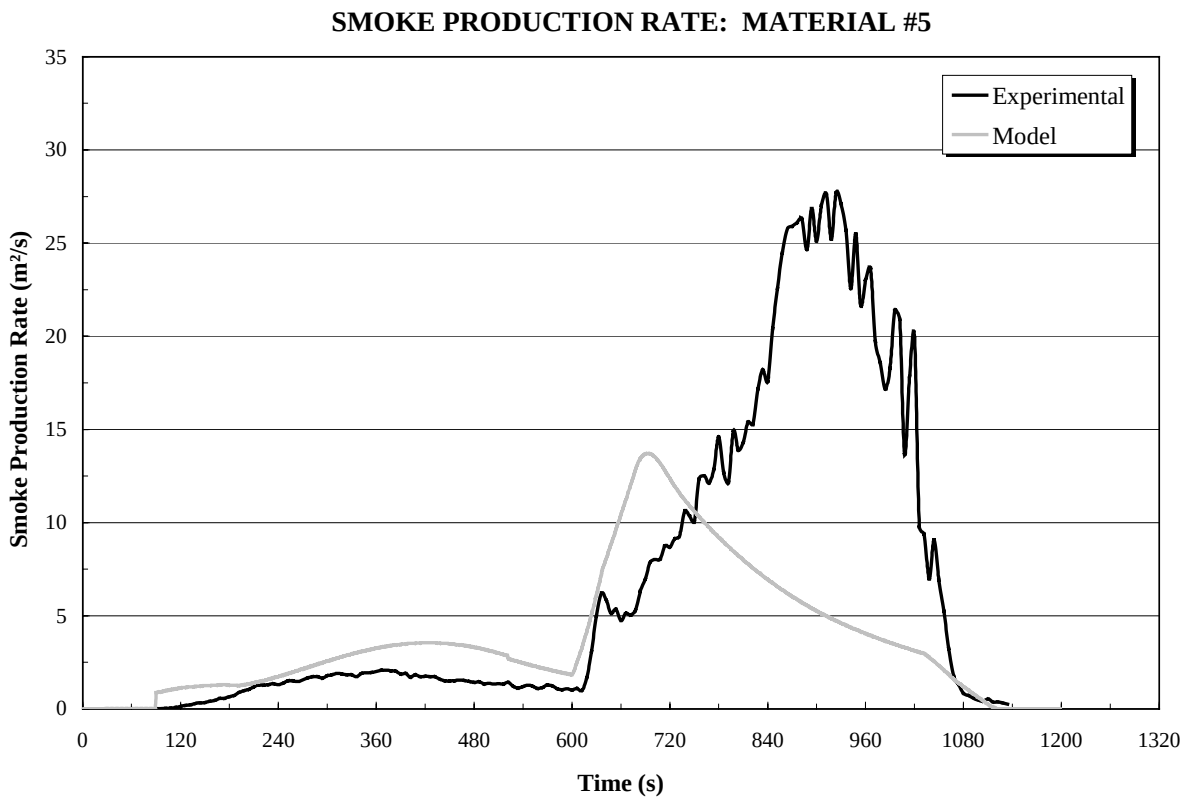
SMOKE PRODUCTION RATE: MATERIAL #5
Experimental
Model
Smoke Production Rate (m²/s)
Time (s)
0
5
10
15
20
25
30
35
0
120
240
360
480
600
720
840
960
1080
1200
1320

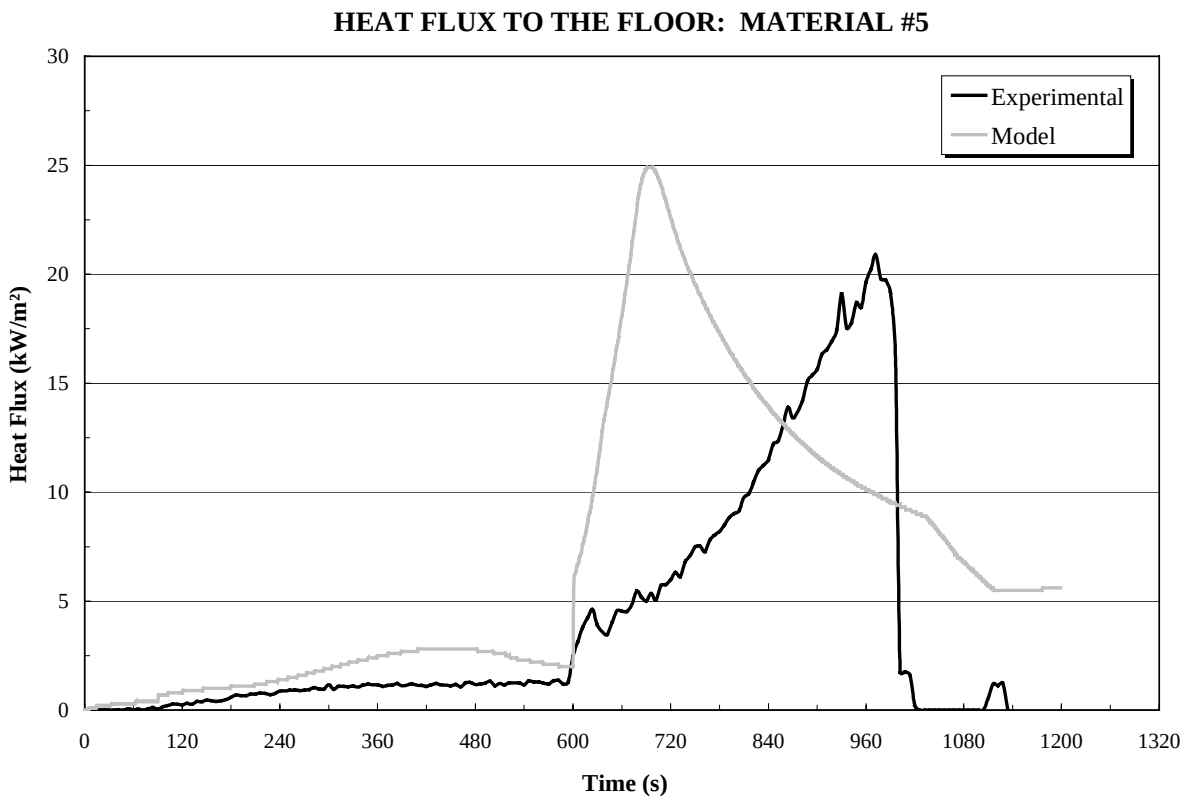
HEAT FLUX TO THE FLOOR: MATERIAL #5
Experimental
Model
Heat Flux (kW/m²)
Time (s)
0
5
10
15
20
25
30
0
120
240
360
480
600
720
840
960
1080
1200
1320

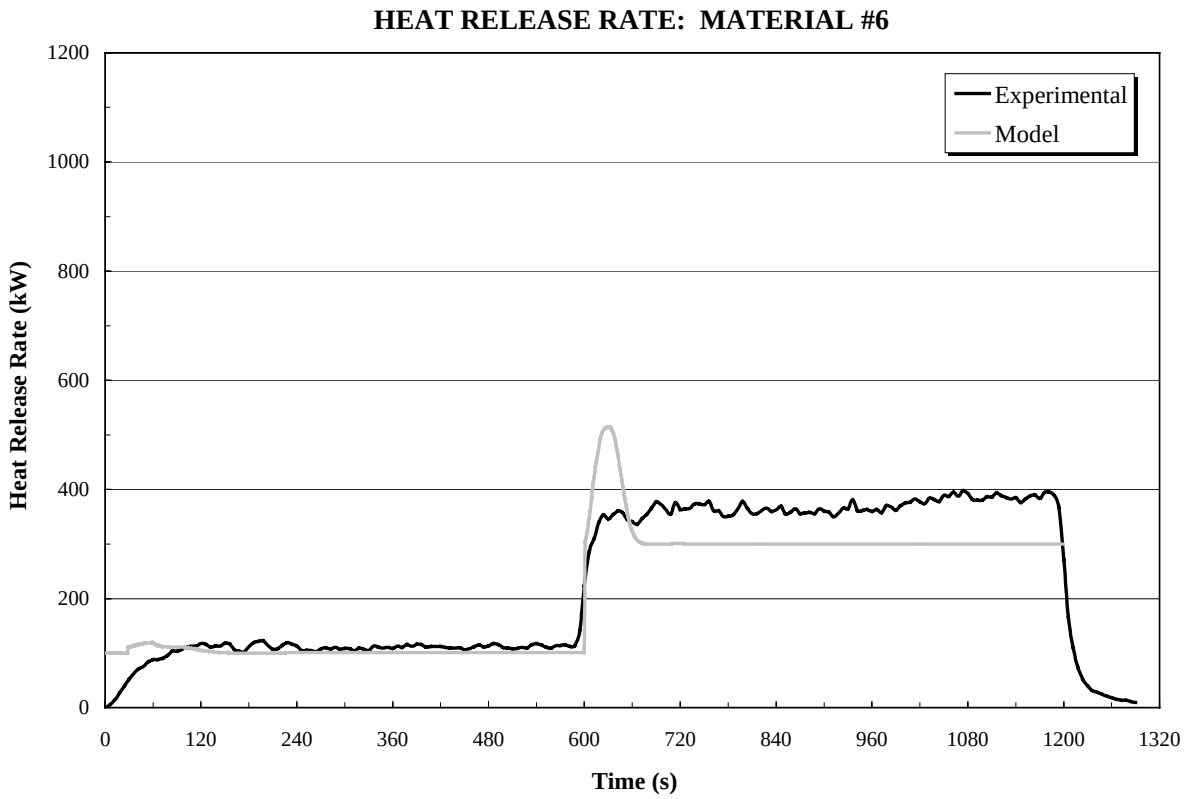
HEAT RELEASE RATE: MATERIAL #6
Experimental
Model
Heat Release Rate (kW)
0
200
400
600
800
1000
1200
0
120
240
360
480
600
720
840
960
1080
1200
1320
Time (s)

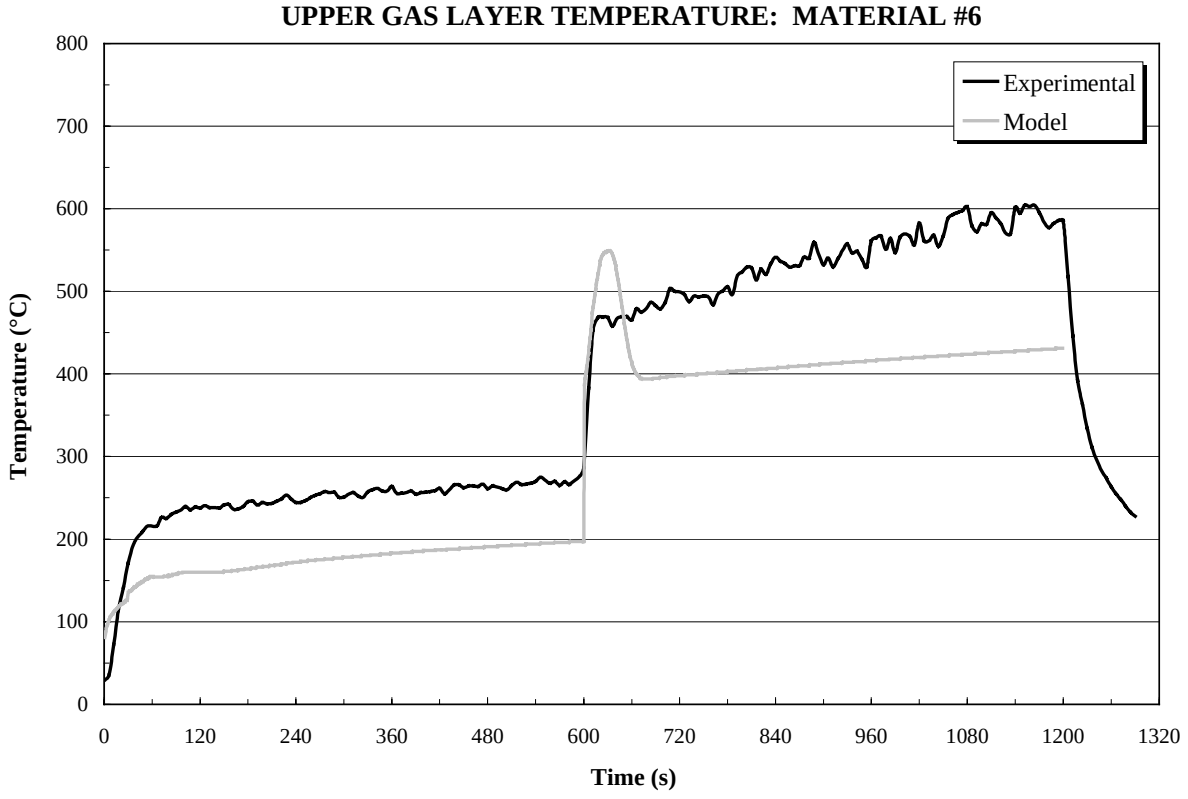
UPPER GAS LAYER TEMPERATURE: MATERIAL #6
Experimental
Model
Temperature (°C)
0
100
200
300
400
500
600
700
800
0
120
240
360
480
600
720
840
960
1080
1200
1320
Time (s)

SMOKE PRODUCTION RATE: MATERIAL #6

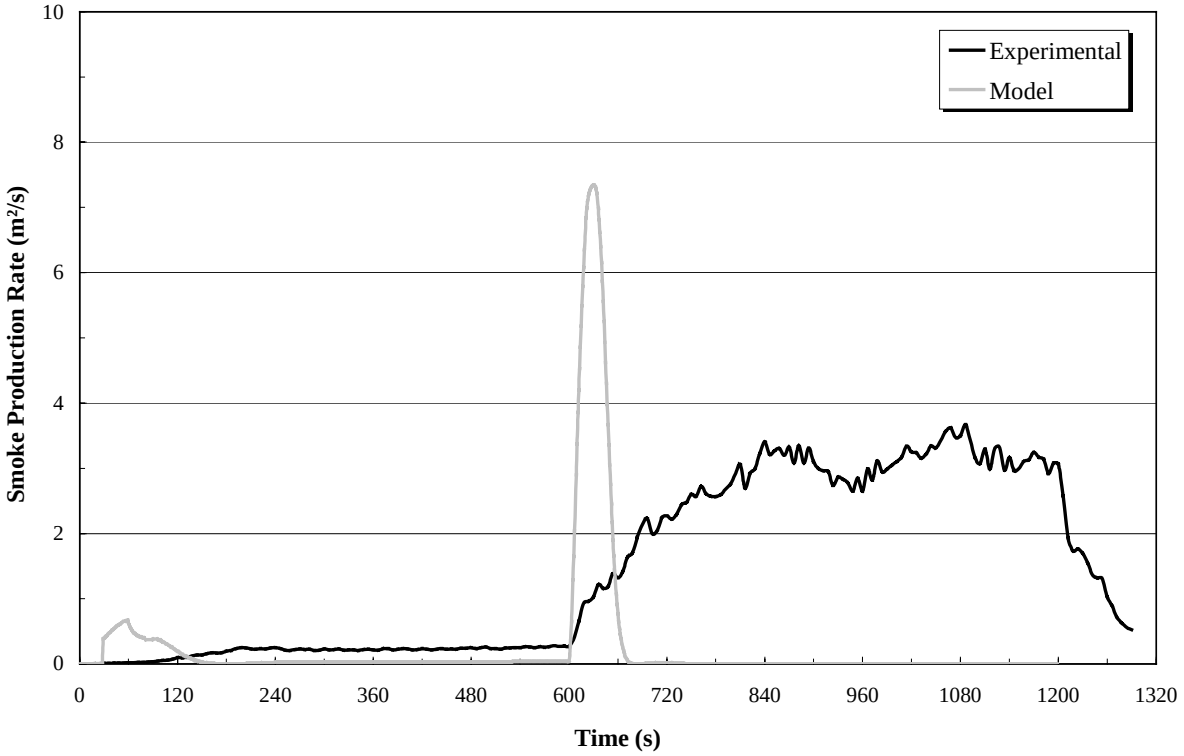

HEAT FLUX TO THE FLOOR: MATERIAL #6

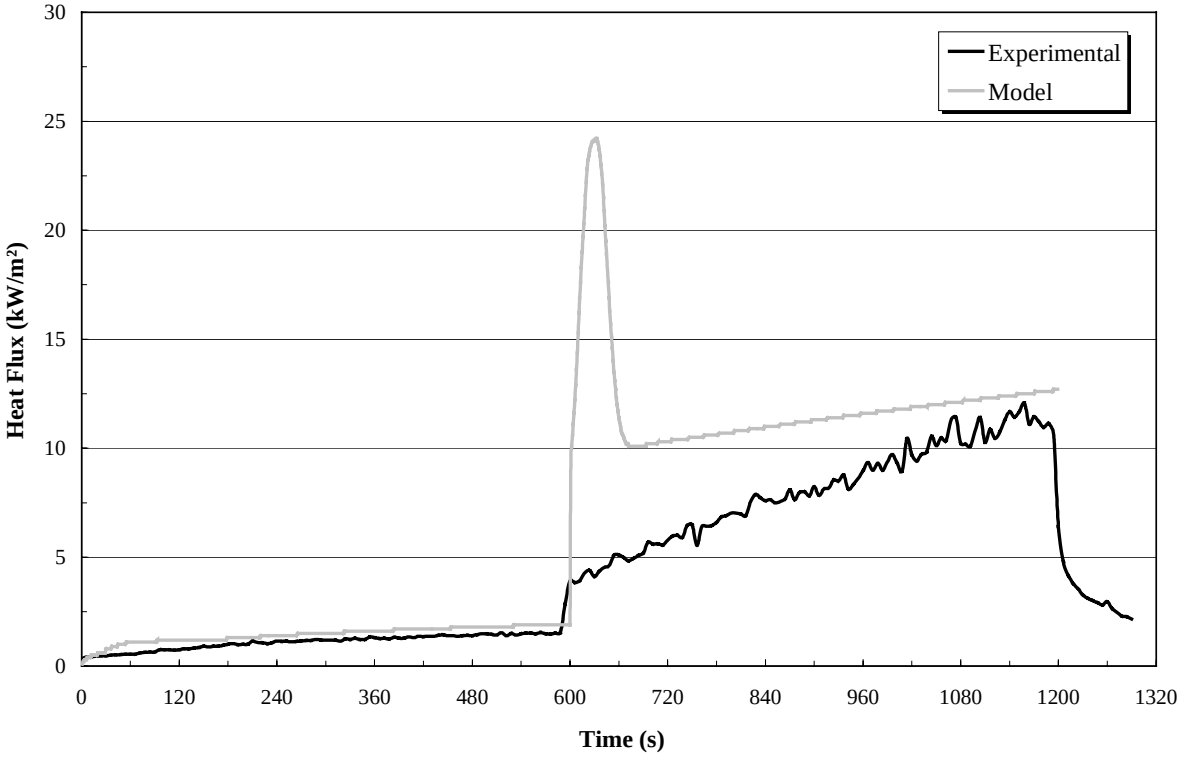

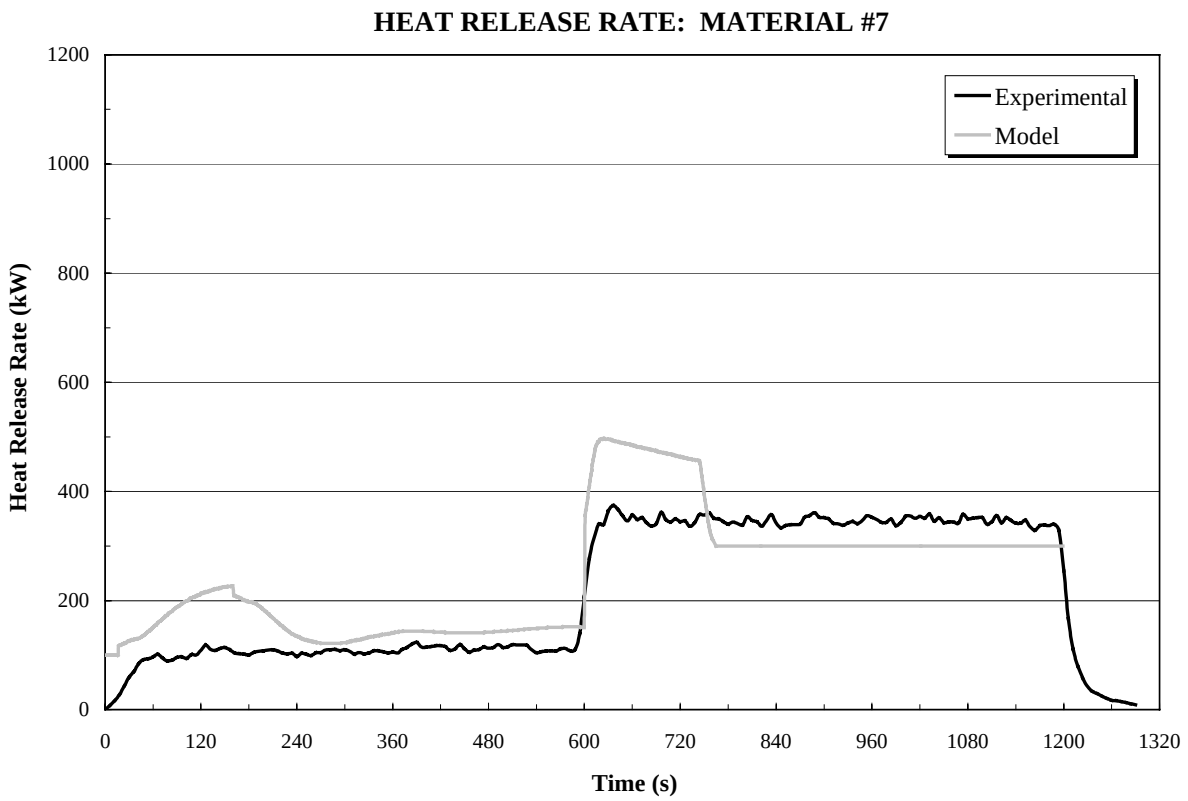
HEAT RELEASE RATE: MATERIAL #7
Experimental
Model
Heat Release Rate (kW)
0
200
400
600
800
1000
1200
0
120
240
360
480
600
720
840
960
1080
1200
1320
Time (s)

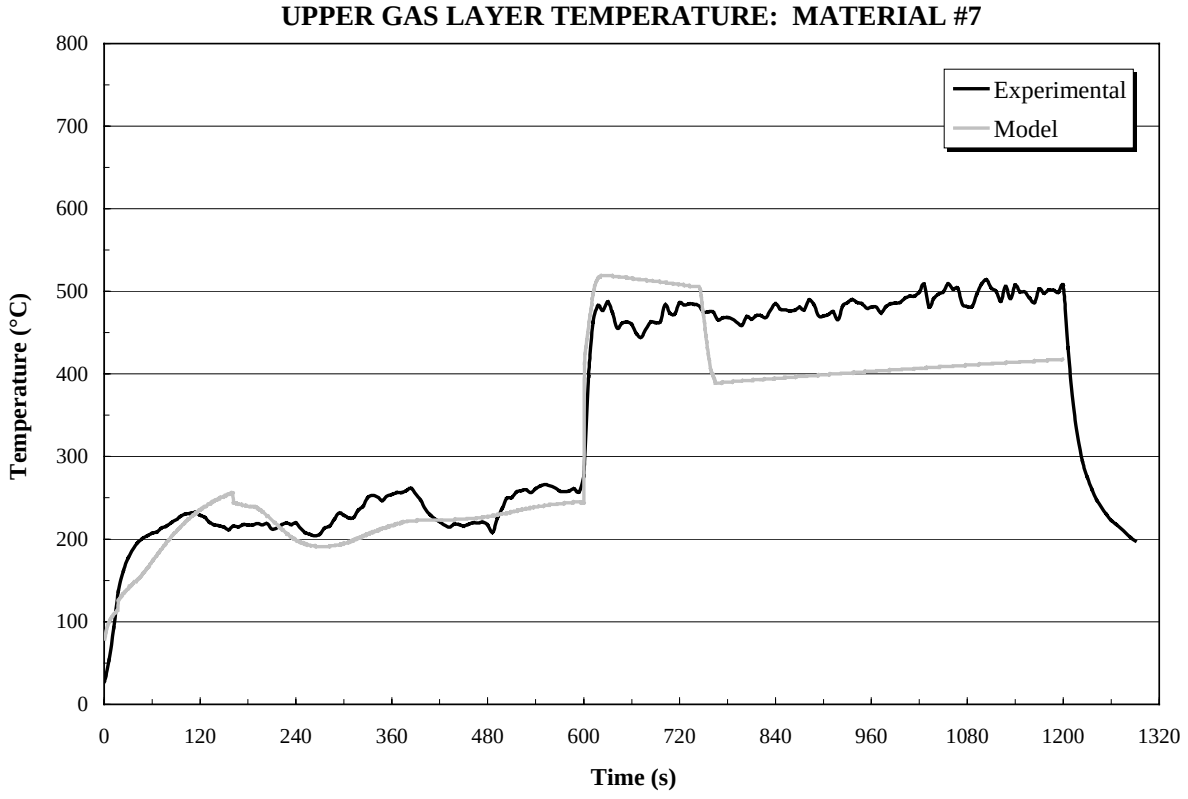
UPPER GAS LAYER TEMPERATURE: MATERIAL #7
Experimental
Model
Temperature (°C)
0
100
200
300
400
500
600
700
800
0
120
240
360
480
600
720
840
960
1080
1200
1320
Time (s)

SMOKE PRODUCTION RATE: MATERIAL #7

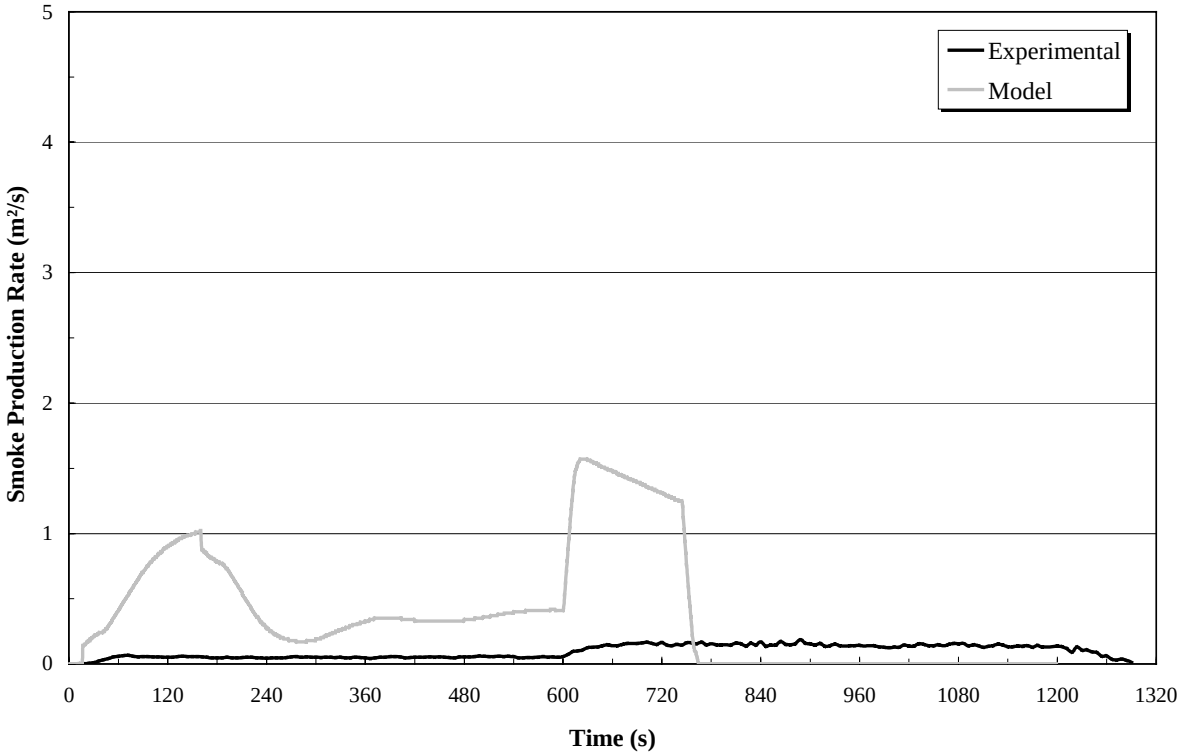

HEAT FLUX TO THE FLOOR: MATERIAL #7

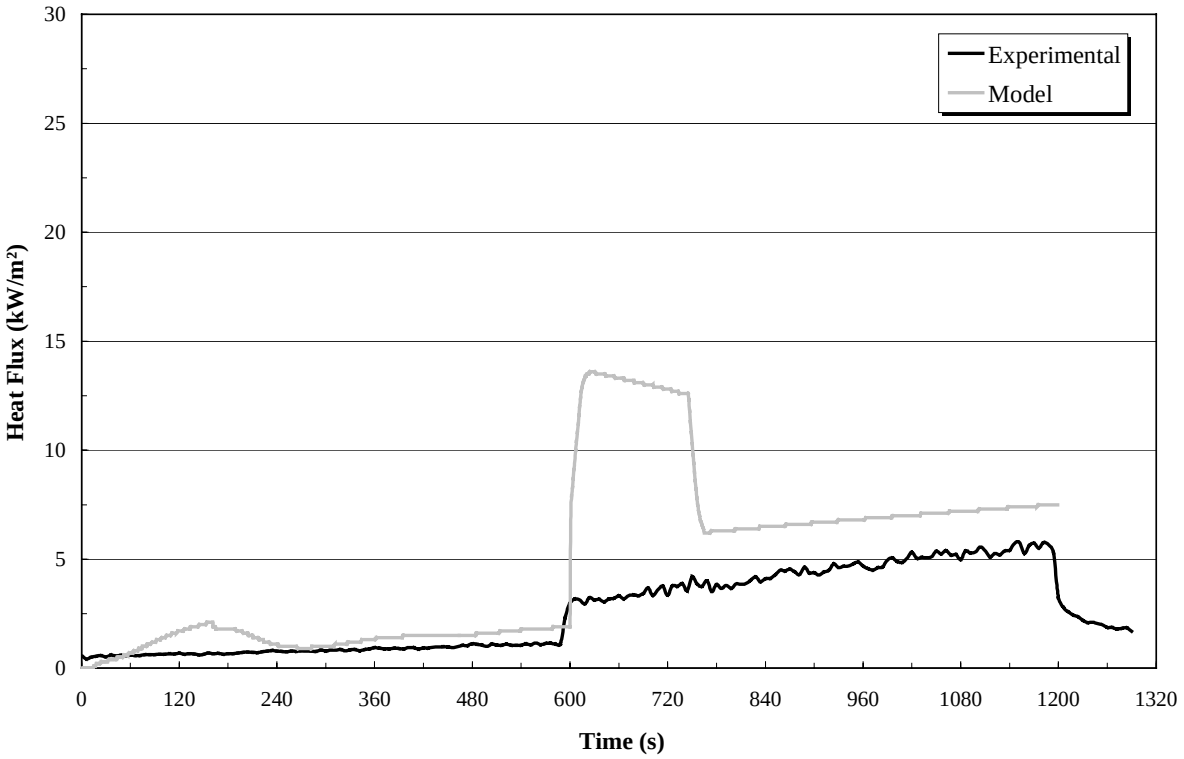

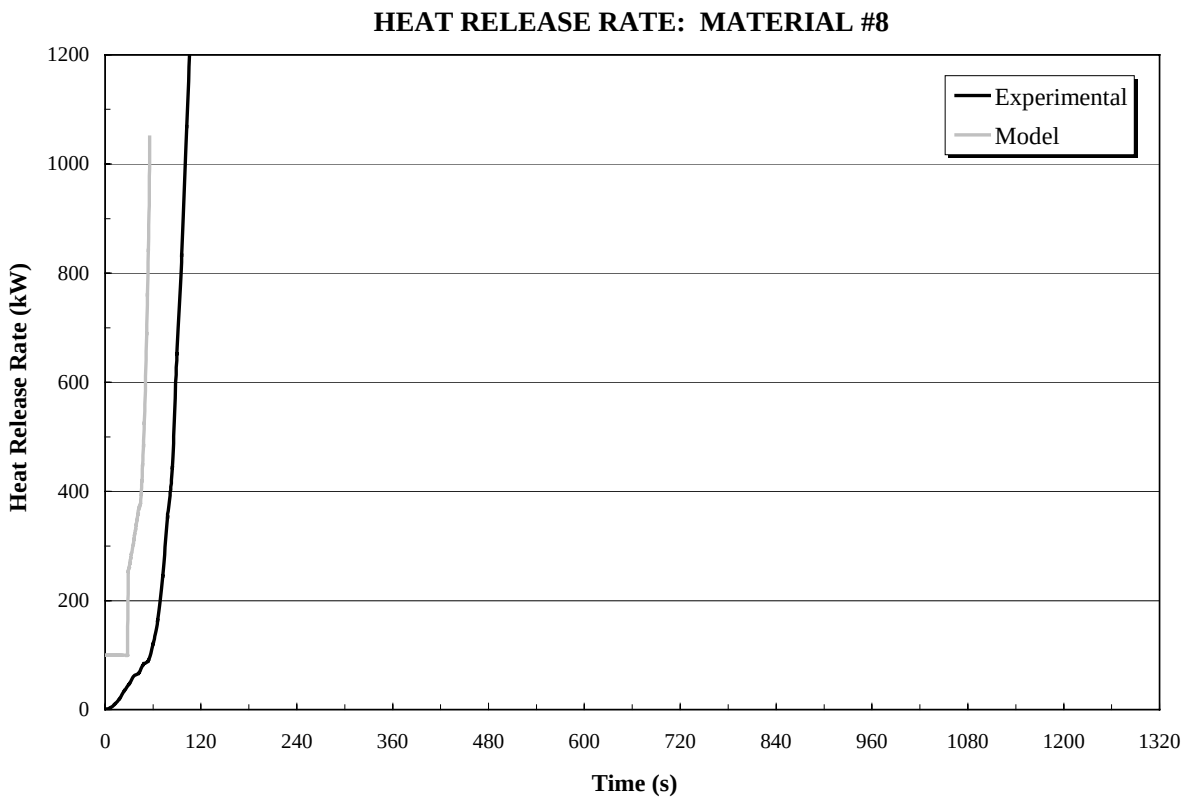
HEAT RELEASE RATE: MATERIAL #8
Heat Release Rate (kW)
Time (s)
Experimental
Model
0
200
400
600
800
1000
1200
0
120
240
360
480
600
720
840
960
1080
1200
1320

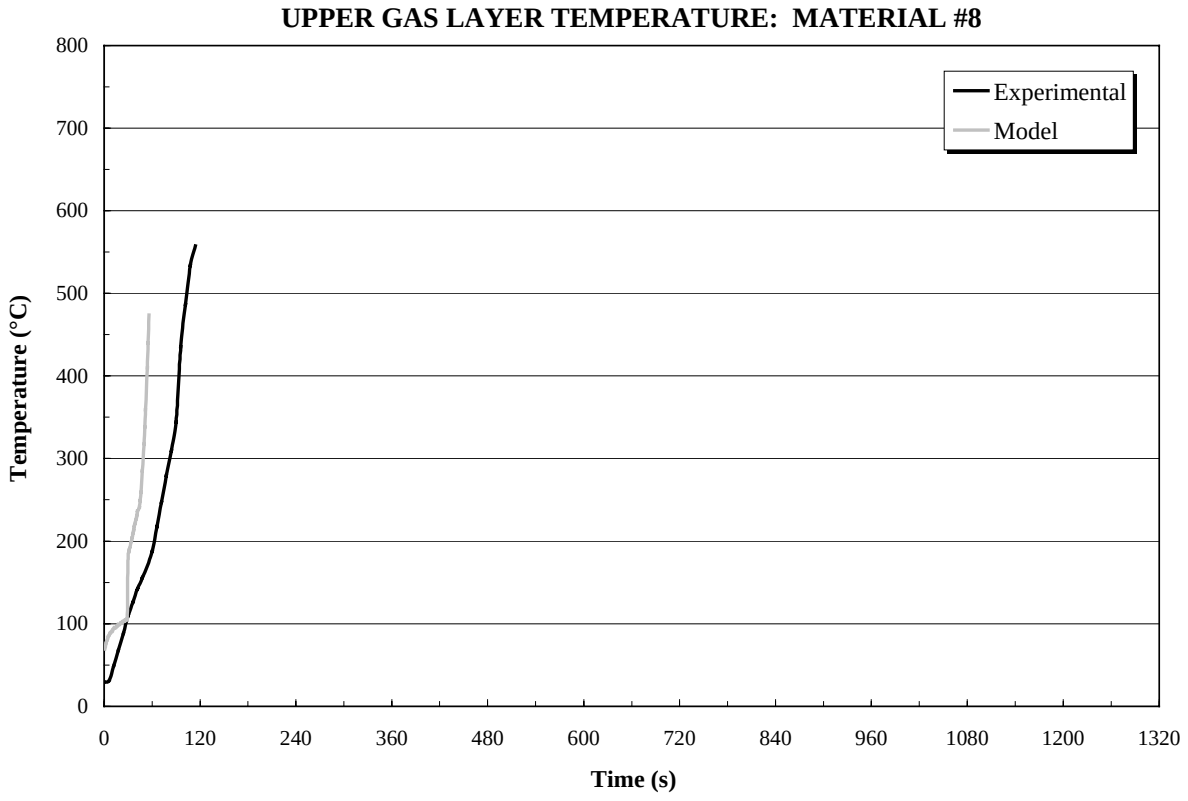
UPPER GAS LAYER TEMPERATURE: MATERIAL #8
Temperature (°C)
Time (s)
Experimental
Model
0
100
200
300
400
500
600
700
800
0
120
240
360
480
600
720
840
960
1080
1200
1320

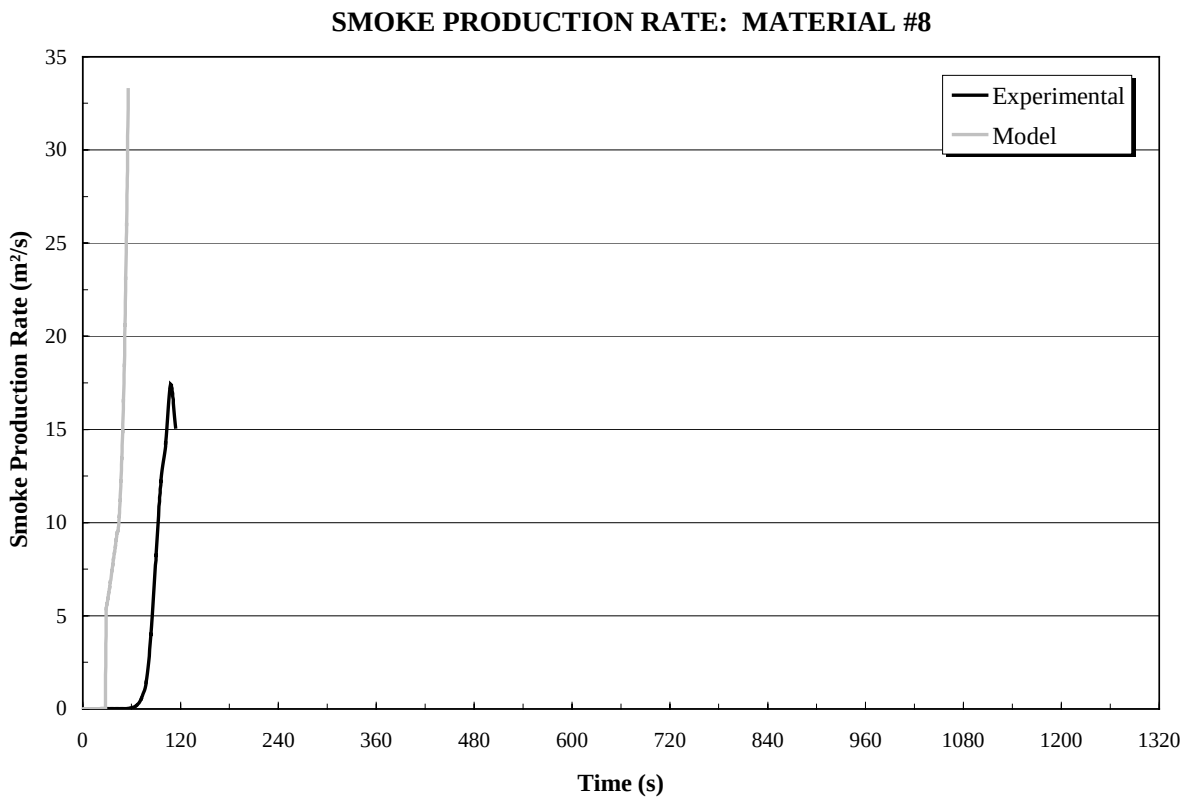
SMOKE PRODUCTION RATE: MATERIAL #8
Experimental
Model
Smoke Production Rate (m²/s)
0
5
10
15
20
25
30
35
0
120
240
360
480
600
720
840
960
1080
1200
1320
Time (s)

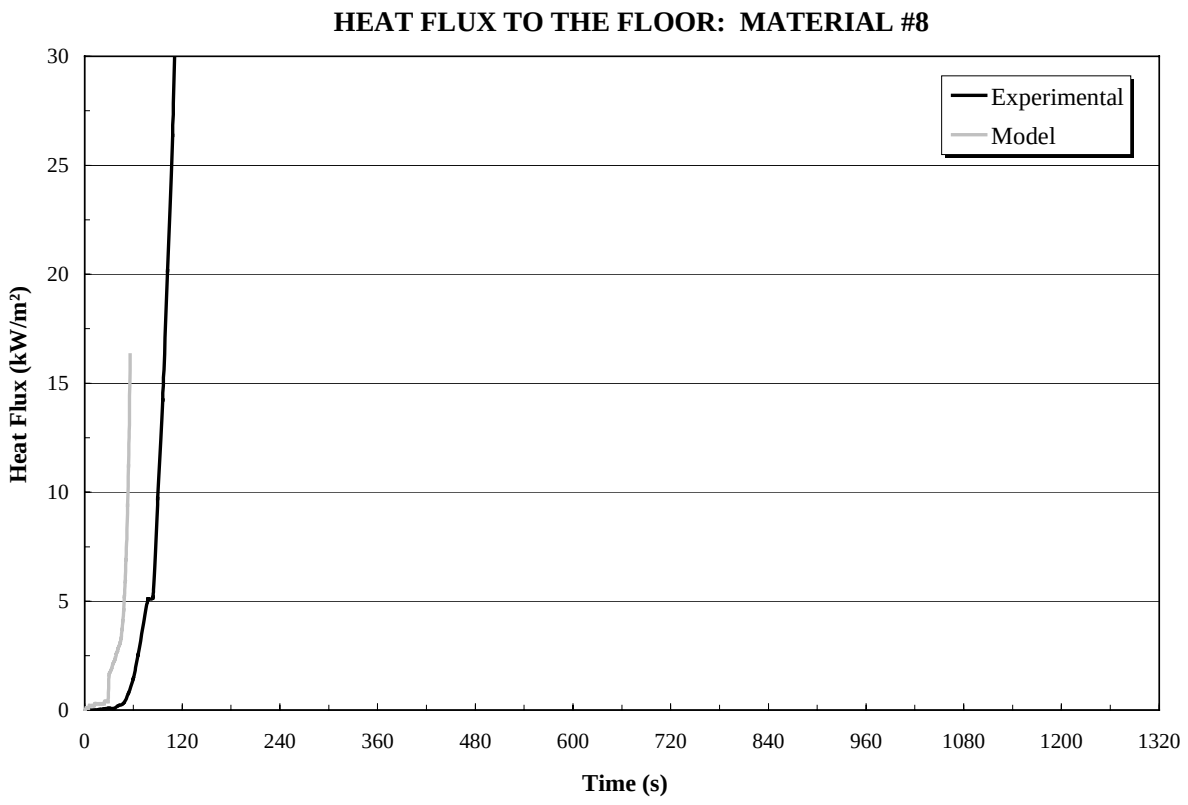
HEAT FLUX TO THE FLOOR: MATERIAL #8
Experimental
Model
Heat Flux (kW/m²)
0
5
10
15
20
25
30
0
120
240
360
480
600
720
840
960
1080
1200
1320
Time (s)

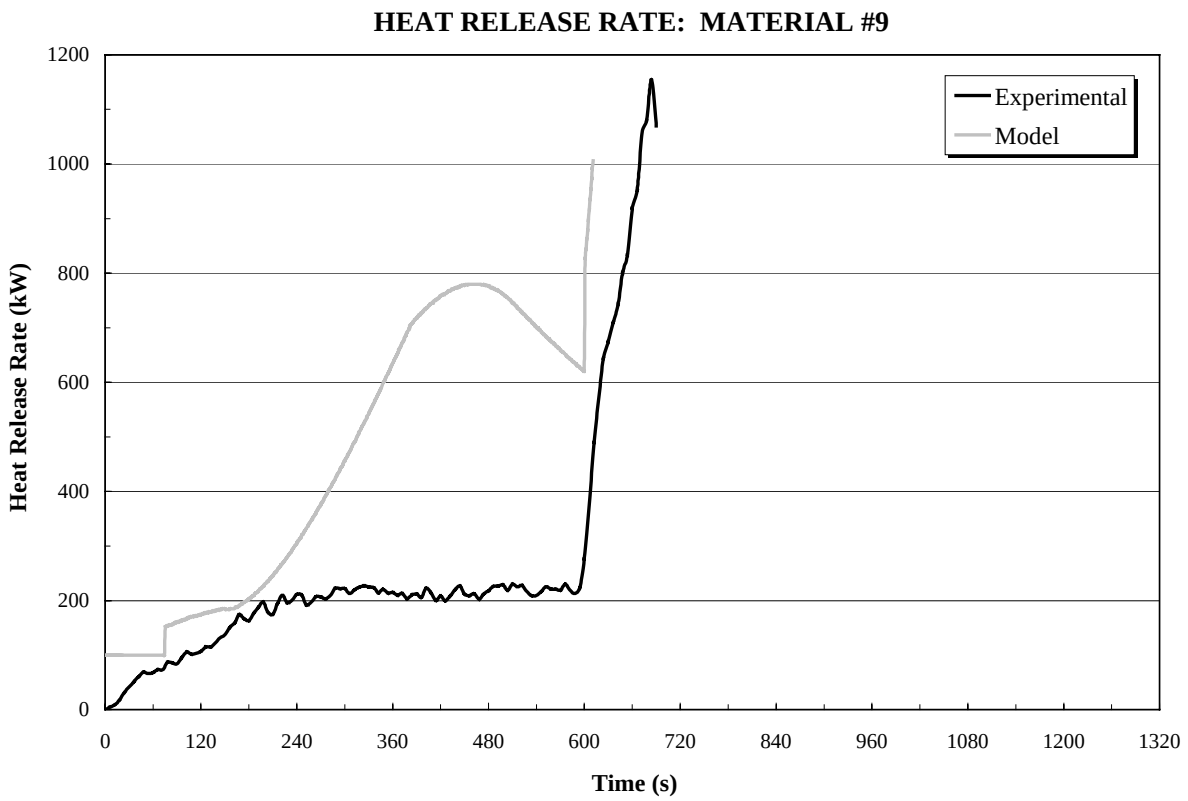
HEAT RELEASE RATE: MATERIAL #9
Heat Release Rate (kW)
Time (s)
Experimental
Model
0
200
400
600
800
1000
1200
0
120
240
360
480
600
720
840
960
1080
1200
1320

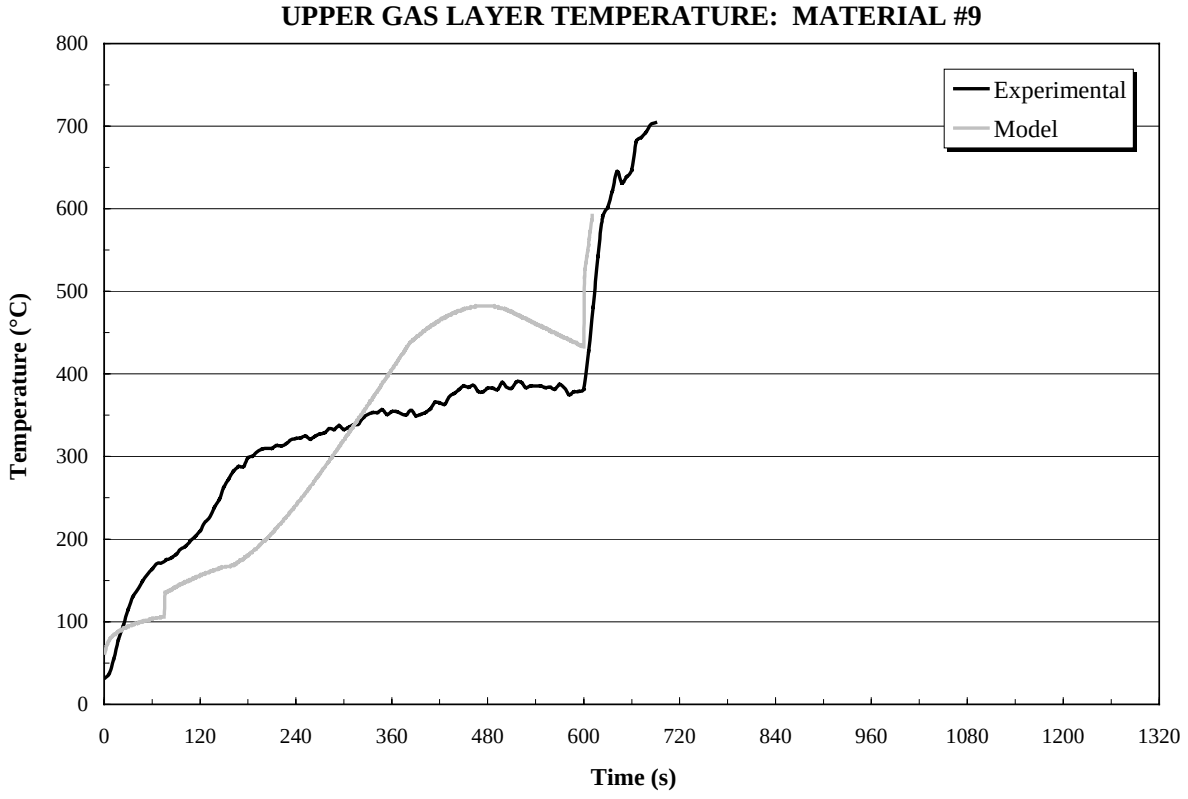
UPPER GAS LAYER TEMPERATURE: MATERIAL #9
Temperature (°C)
Time (s)
Experimental
Model
0
100
200
300
400
500
600
700
800
0
120
240
360
480
600
720
840
960
1080
1200
1320

SMOKE PRODUCTION RATE: MATERIAL #9

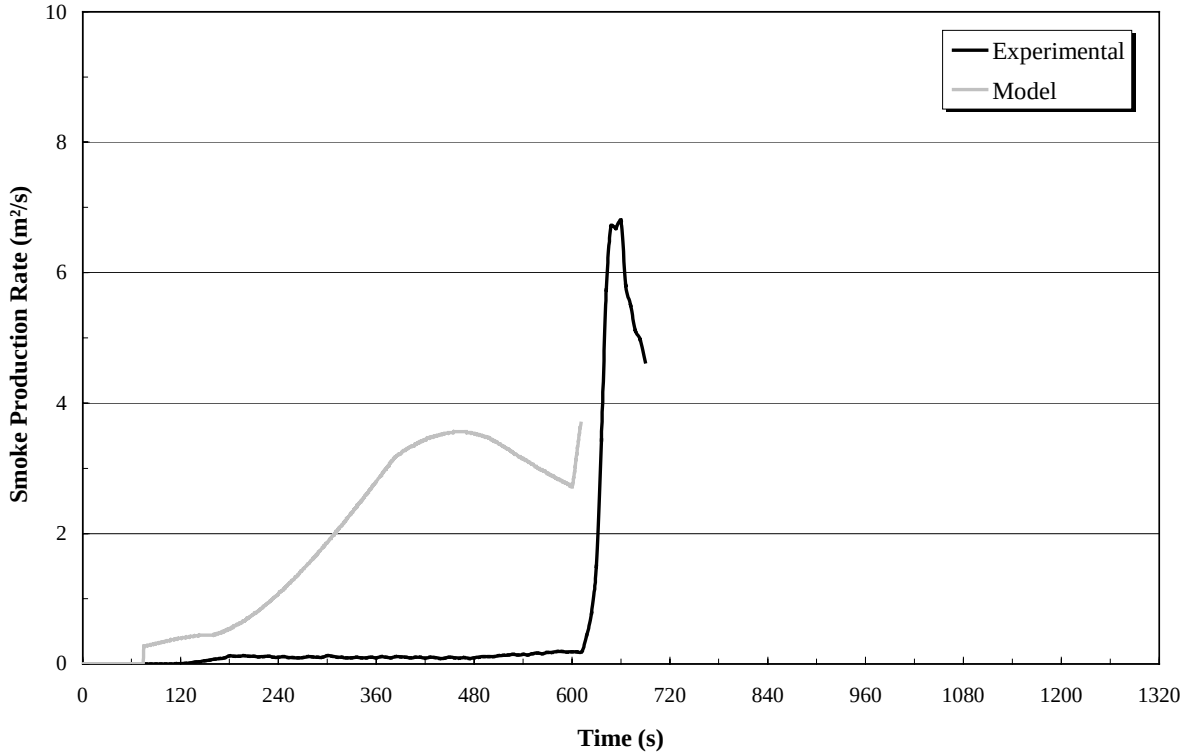

HEAT FLUX TO THE FLOOR: MATERIAL #9

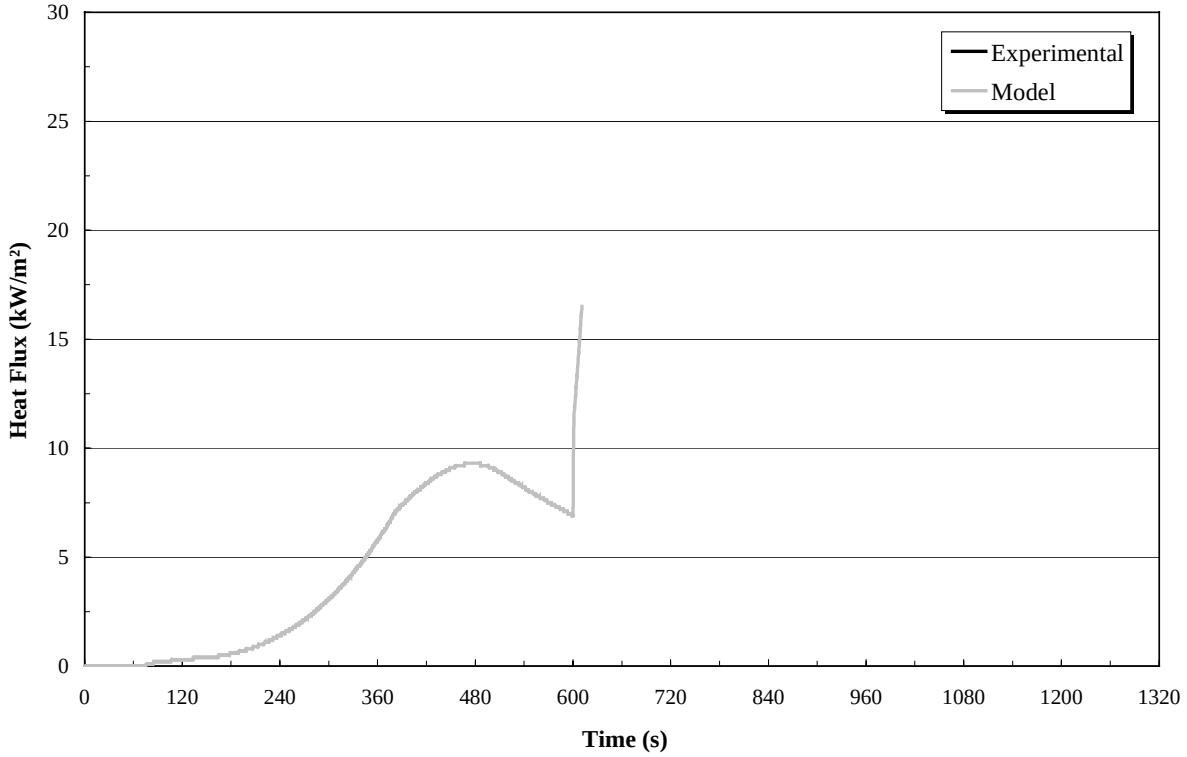

[This page intentionally left blank.]

APPENDIX B – EVALUATION OF THE WPI ZONE MODEL FLAME SPREAD ALGORITHM AGAINST CORNER TEST DATA

TABLE OF CONTENTS

Page

1.0 INTRODUCTION B-7

2.0 MODIFICATIONS TO ORIGINAL FLAME SPREAD ALGORITHM B-7

2.1 CHANGE IN GEOMETRY FOR CORNER CONFIGURATION B-7
2.2 CORNER FLAME HEIGHT CORRELATION B-8
2.3 ENHANCED RADIATIVE EXCHANGE IN THE CORNER B-8
2.4 EXPERIMENTAL CORNER HEAT FLUX MAP B-10
2.5 MULTIPLE PYROLYSIS ZONES B-10
2.6 INSERTION INTO CFAST B-10

3.0 DEVELOPMENT OF INPUT PARAMETERS B-11

3.1 SPECIFIC HEAT AND THERMAL CONDUCTIVITY B-11
3.2 NET HEAT OF COMPLETE COMBUSTION AND COMBUSTION EFFICIENCY B-11
3.3 RADIATIVE FRACTION OF HEAT RELEASE RATE B-12
3.4 EMISSIVITY B-12
3.5 FLAME TRANSMISSIVITY B-12
3.6 LATERAL FLAME SPREAD PROPERTIES B-13
3.7 CONE CALORIMETER CURVE AT MULTIPLE IRRADIANCES B-13

4.0 SIMULATION RESULTS AND MODEL VALIDATION B-14

4.1 INTERPRETATION OF THE PYROLYSIS/BURNOUT FRONT GRAPH B-15
4.2 HEAT RELEASE RATE B-16
4.3 UPPER LAYER GAS TEMPERATURE B-22
4.4 SMOKE PRODUCTION RATE B-25
4.5 HEAT FLUX TO THE FLOOR B-26

5.0 SENSITIVITY ANALYSIS B-27

5.1 SELECTION OF PARAMETERS FOR VARIATION IN SENSITIVITY ANALYSIS B-28
5.2 VARIATION OF THERMAL CONDUCTIVITY B-30
5.3 CONE CALORIMETER CURVE AT MULTIPLE IRRADIANCES B-31
5.4 VARIATION OF EMISSIVITY AND FLAME TRANSMISSIVITY B-33
5.5 VARIATION OF IGNITION TEMPERATURE B-35

5.6 VARIATION OF LATERAL FLAME SPREAD INPUTS B-35
5.7 FLAME SPREAD BEHAVIOR ON FIRE-RETARDANT MATERIALS B-35
5.8 ADDITIONAL VARIATIONS B-40
5.8.1 Compartment size and ventilation B-40
5.8.2 Initial temperature B-42

6.0 CONCLUSIONS B-46
6.1 STRENGTHS OF MODEL B-46
6.2 WEAKNESSES OF MODEL B-47
6.3 RECOMMENDATIONS FOR FUTURE WORK B-48

7.0 INPUTS TO THE ALGORITHM B-50

8.0 BASELINE HRR RESULTS B-71

9.0 BASELINE UPPER LAYER GAS TEMPERATURE RESULTS B-76

10.0 BASELINE SMOKE PRODUCTION RATE RESULTS B-81

11.0 BASELINE FLOOR HEAT FLUX RESULTS B-86

12.0 REFERENCES B-91

LIST OF FIGURES

Page

Figure B2-1 – Geometry of the elements used in radiation network B-9
Figure B3-1 – Sample cone calorimeter data B-14
Figure B4-1 – Example of pyrolysis and burnout front graph B-16
Figure B4-2 – Baseline heat release rate for material #8 ..... B-17
Figure B4-3 – Baseline heat release rate for material #1 ..... B-18
Figure B4-4 – Baseline heat release rate for material #3 ..... B-19
Figure B4-5 – Baseline heat release rate for material #4 ..... B-19
Figure B4-6 – Baseline heat release rate for material #5 ..... B-20
Figure B4-7 – Baseline heat release rate for material #9 ..... B-20
Figure B4-8 – Total flux versus distance for material #4 ..... B-21
Figure B4-9 – Pyrolysis and burnout fronts for material #4 ..... B-22
Figure B4-10 – Upper layer gas temperature for material #8 ..... B-23
Figure B4-11 – Upper layer gas temperature for material #1 ..... B-24
Figure B4-12 – Upper layer gas temperature for material #9 ..... B-24
Figure B4-13 – Smoke production rate material #1 ..... B-26
Figure B4-14 – Smoke production rate material #8 ..... B-26
Figure B4-15 – Heat flux to the floor for material #1 ..... B-27
Figure B5-1 – Variation of thermal conductivity for material #3 ..... B-30
Figure B5-2 – Variation of cone calorimeter curves for material #4 ..... B-32
Figure B5-3 – Pyrolysis and burnout fronts for material #4 at 25kW/m^2 ..... B-32
Figure B5-4 – Cone calorimeter curve for material #4 at 25kW/m^2 ..... B-33
Figure B5-5 – Variation of material emissivity for material #9 ..... B-34
Figure B5-6 – Variation of flame transmissivity for material #9 ..... B-34
Figure B5-7 – Variation of ignition temperature for material #3 ..... B-35
Figure B5-8 – Possible fire-retardant activity for material #3 and #4 ..... B-37
Figure B5-9 – Change of cone calorimeter curve for material #3 ..... B-37
Figure B5-10 – Change of cone calorimeter curve for material #4 ..... B-38
Figure B5-11 – Results from non-FR cone calorimeter curve for material #3 ..... B-38
Figure B5-12 - Results from non-FR cone calorimeter curve for material #4 ..... B-39
Figure B5-13 – Effect of compartment size on HRR for material #3 ..... B-40
Figure B5-14 – Effect of compartment size on T_{gu} for material #3 ..... B-41
Figure B5-15 – Compartment ventilation effect on HRR for material #9 ..... B-42
Figure B5-16 – Compartment ventilation effect on T_{gu} for material #9 ..... B-42

LIST OF FIGURES (continued)

Page

Figure B5-17 – Effect of initial temperature on heat release rate for material #8 ..... B-43
Figure B5-18 – Effect of initial temperature on heat release rate for material #9 ..... B-44
Figure B5-19 – Effect of initial temperature on heat release rate for material #9 ..... B-45

LIST OF TABLES

Page

Table B4-1 – Comparison of predicted HRR and SPR to experimental data B-15
Table B4-2 – Time to flashover B-15
Table B5-1 – Sensitivity analysis matrix B-29

NOMENCLATURE

Symbols

c_p	J/kg-K or kJ/kg-K	Specific heat at constant pressure
D	m	Characteristic dimension of ignition burner
ΔH_{ch}	kJ/g	Chemical heat of combustion
ΔH_{eff}	kJ/g	Effective heat of combustion
$\Delta H_{net,c}$	kJ/g	Net heat of complete combustion
ΔH_{rad}	kJ/g	Radiative heat of combustion
k	W/m-K or kW/m-K	Material thermal conductivity
$\dot{q}''_{crit}$	W/m^2 or kW/m^2	Critical heat flux for ignition
$\dot{Q}^*_D$	†	Non-dimensional heat release rate
S	m	Mean beam length
T_{ig}	K	Material ignition temperature
$T_{s,min}$	K	Minimum surface temperature for lateral flame spread
Z_f	m	Flame height (used in flame height correlation)

Greek Symbols

α_{flame}	†	Flame Absorptivity
χ_A	†	Combustion efficiency
χ_R	†	Radiative fraction of heat release rate
δ	m	Material thickness
ε_{flame}	†	Emissivity of flames from the burning material
ε_g	†	Emissivity of the upper gas layer
ε_k	†	Material surface emissivity of element k
ε_t	†	Total emissivity of upper gas layer
Φ	kW^2/m^3	Lateral flame spread parameter
κ	1/m	Mean absorption coefficient (0.47)
κ_s	1/m	Absorption coefficient of the soot in the upper layer
ρ	kg/m^3	Material density
τ_{flame}	†	Flame transmissivity

Notes:
† Dimensionless variable

1.0 INTRODUCTION

This report contains an evaluation of an enhanced version of the flamespread algorithm of Mitler (Mitler, 1993, 1994) as implemented in CFAST (Peacock, 1993, 1997) by WPI FPE MS student Mark Wright. It is based on his thesis (Wright, 1999) which discusses the material contained in this report in greater detail. The changes that were made to the original algorithm of Mitler (Mitler, 1993, 1994) are discussed and the processes through which material input properties are derived from bench-scale experimental data are explained. The flame spread algorithm has been evaluated against the data provided by Janssens (Janssens, 1998). A sensitivity analysis was conducted to better understand the dynamics of the model with the intention of identifying areas that may require higher precision. This sensitivity analysis also focuses on quantifying the effects of cone calorimeter (ISO 5660), and LIFT apparatus (IMO Resolution A.653, ASTM E 1321-97-a) data interpretation methods on the predictions of the model. Additionally the model's strengths and weakness are identified, and suggestions are made as to how research should proceed to improve upon the model.

2.0 MODIFICATIONS TO ORIGINAL FLAME SPREAD ALGORITHM

The original flame spread algorithm (Mitler, 1993, 1994) was designed to simulate flame spread along a side-wall with the burner located at a distance from the corner such that the corner effects were negligible. The algorithm has been modified to simulate the ISO 9705 test configuration. Several aspects of the algorithm required modification to extend the model to the corner configuration. These modifications are discussed in the following sections.

2.1 Change in Geometry for Corner Configuration

The change in geometry of flame spread on the walls themselves requires little modification when altering the algorithm for the corner configuration. The area of spread is "folded" into the corner along its centerline. The change in geometry of flame spread across the ceiling is more difficult to define. The two corner walls constrain the flame spread across the ceiling, creating a more bounded geometry. It is necessary to define the shape of flame spread across the ceiling in order to properly track the pyrolysis and burnout front positions on the ceiling and to calculate the enhanced radiative exchange between the walls and ceiling in the corner.

A quarter-circular geometry was used to represent the shape of the pyrolysis and burnout fronts on the ceiling. This was done primarily because the geometry of spread is intuitively realistic and the radiation calculations are slightly easier with the quarter-circular geometry of spread as opposed to a

triangular or square geometry. With this geometry, the pyrolysis and burnout fronts spread radially from the corner, with growth of the pyrolysis area simplified as a radial progression.

2.2 Corner Flame Height Correlation

The height of flames from a burner in a compartment corner is different from those against the center of a compartment wall (Drysdale, 1999). Therefore, it was necessary to develop an alternate expression for flame height in the corner. Several correlations for square burners in a corner were examined using the standard non-dimensional group $\dot{Q}_D^*$ (Drysdale, 1999). The first was developed by Hasemi and Tokunaga (Hasemi, 1984) for square burners in an open corner configuration. The next correlation (identified by Dillon (Dillon, 1998)) was developed by Kokkala. The last correlation for a square burner flame height in a compartment corner (also identified by Dillon (Dillon, 1998)) was originally developed by Heskestad and revised by Kokkala.

Values of Z_f/D versus $\dot{Q}_D^*$ were calculated for each of the three individual correlations. These three curves were then collapsed into one by taking the arithmetic mean of all three correlations for Z_f/D versus $\dot{Q}_D^*$ in order to arrive at an approximation of flame height from a square burner in a corner. A power law curve-fit was backed out of this arithmetic mean and the resulting expression, as given by Equation (B2-1), replaces Mitler's original flame height correlation.

$$\frac{Z_f}{D} = -1.7 + 5.8\left(\dot{Q}_D^*\right)^{1/2} \qquad \text{(B2-1)}$$

2.3 Enhanced Radiative Exchange in the Corner

The incident radiation distribution to the wall and ceiling in the corner configuration is different as compared to the side-wall configuration because the geometry allows for radiative exchange between the two corner walls and also between the corner walls and the ceiling. The total incident flux is enhanced, and this flux in turn controls the mass loss rate for a pyrolyzing region or adds to the degree of preheating for a non-pyrolyzing region.

A subroutine was added that calculates the radiative exchange among the walls, ceiling, and the hot upper gas layer in the corner. The radiative fluxes from the burner and wall flames are also added as external fluxes. A factor to attenuate radiation as it passes through a flame is included. It is assumed that both the walls and the upper layer gas are gray bodies with uniform properties. The emissivity of the gas layer without soot (ε_g) is calculated in the usual way, using the partial pressures of H_2O and CO_2, beam

length, and the Hottel (Tien, 1995) charts. A subroutine was borrowed directly from the source code of the WPI/Fire model (Satterfield, 1990) for this purpose. The equation used to calculate the emissivity of the hot upper gas layer is from Tien, *et al.* (Tien, 1995) and is given as Equation (B2-2):

$$\varepsilon_t = \left(1 - e^{-\kappa_S S}\right) + \varepsilon_g e^{-\kappa_S S} \tag{B2-2}$$

The walls are discretized into strips with a width of approximately 0.12m because this element size was found to provide adequate resolution while allowing acceptable execution times. The geometry of the corner was broken into five separate zones and the upper gas layer, as shown in Figure B2-1. View factor algebra and reciprocity were used to generate a radiation network. The resulting matrix is solved by LU factorization and the overall radiative exchange is calculated between wall elements on opposing sides of the corner, as well as between wall and ceiling elements. The main output of this subroutine is the incident radiant flux at each element.

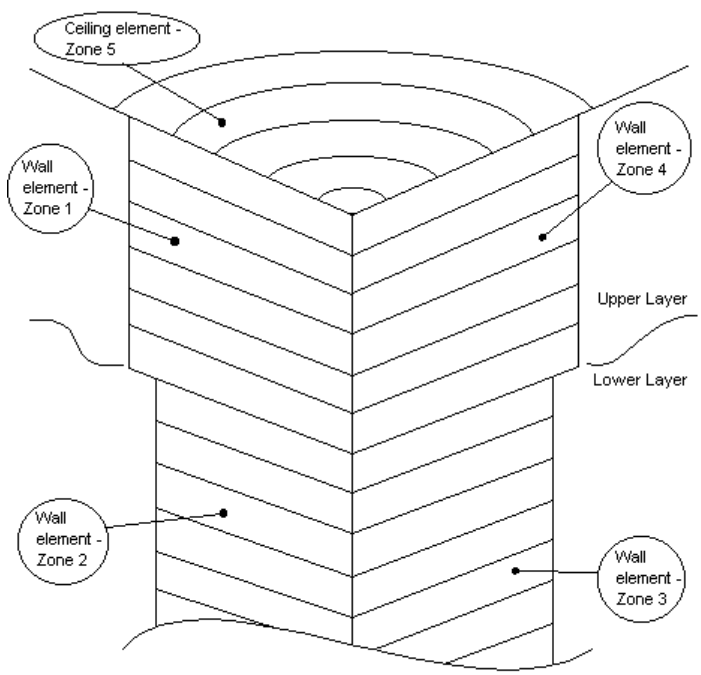

Figure B2-1. – Geometry of the elements used in radiation network.

2.4 Experimental Corner Heat Flux Map

The original flame spread algorithm (Mitler, 1993, 1994) simulated the heat flux from a line burner to a sidewall by adding separate theoretical expressions for convective and radiative heat transfer to calculate a total flux. A different approach was used in the modified algorithm. Experimental information on the flux distribution in the ISO 9705 configuration was recorded by Dillon (Dillon, 1998). His graphs provide two-dimensional distributions for the total (i.e., convective and radiative) flux; however, the model only requires a one-dimensional distribution of the flux. For this reason, the flux distribution maps were translated to a one-dimensional analogue.

The original flux distributions caused the model to behave somewhat unrealistically. Ignition always occurred on the wall just below the ceiling at the location of highest flux, but general observation on corner fire experiments indicates that sustained ignition occurs farther down the wall. As a result of this discrepancy, the flux distributions were altered to ensure ignition at the area of elevated flux on the wall behind the burner flame. For the 100 kW burner distribution, the flux was decreased to 30 kW/m^2 at a height of approximately 1.3-m and set constant until the 30-kW/m^2 boundary was reached on the ceiling. A similar procedure was followed for the 300 kW burner distribution, except the cutoff was 60kW/m^2 at a height of approximately 1.7-m.

2.5 Multiple Pyrolysis Zones

Provisions were made to track multiple pyrolysis zones in the modified flame spread algorithm. The original algorithm allowed only one pyrolysis zone at any given time in the simulation. All elements below a node at which burn-out occurred were marked as non-burning. This often led to the situation where a significant number of elements were extinguished even though there was still available fuel. The shift in the lower pyrolysis bound at burn-out was removed to correct this problem. Burn-out is now controlled by the remaining fuel at each node. Once multiple pyrolysis zones exist and they are sufficiently far apart, the validity of the flame height and heat flux calculations is questionable because the algorithm was written to simulate only one pyrolysis zone.

2.6 Insertion Into CFAST

The modified flame spread algorithm was incorporated into the zone model CFAST (Peacock, 1993, 1997). Gas temperatures, wall temperatures, interface height, etc. are calculated internally by the zone model. CFAST has the ability to simulate the burning of multiple objects within a compartment.

The time at which ignition occurs can be specified, or CFAST can dynamically determine when ignition occurs based on the localized attainment of an ignition criterion, such as T_{ig} or $\dot{q}''_{crit}$. The burning of an object is governed by its thermophysical properties as specified in CFAST's integrated thermal and object databases. CFAST tracks the combustion of a burning object and calculates its effect on the overall compartmental conditions. The new flame spread algorithm was inserted into CFAST (Peacock, 1993, 1997) as a new object type, designated as object type five.

3.0 DEVELOPMENT OF INPUT PARAMETERS

The data used to derive the input parameters required by the flame spread algorithm were provided by Southwest Research Institute (San Antonio, TX). These data were the basis of a report (Janssens, 1998) that described the testing of seven fire-retardant (FR) woven glass composite materials, a textile wall covering material, and one non-fire-retardant composite material. Each material was tested in the cone calorimeter (ISO 5660), LIFT apparatus (IMO Resolution A.653, ASTM E 1321-97-a), and full-scale room scenario (ISO 9705). The material ignition and lateral flame spread properties were derived using the procedure described in ASTM E 1321. Out of the nine materials tested, four produced complete sets of material data. The other five were missing values for the minimum temperature for lateral flame spread ($T_{s,min}$), and the lateral flame spread parameter (Φ). This section describes the input parameters required by the flamespread algorithm and explains how they are derived from experimental data.

3.1 Specific Heat and Thermal Conductivity

The available experimental data provided a value for each material's thermal inertia ($k\rho c_p$); however, the input routine of the flame spread algorithm requires the individual specification of thermal conductivity (k), density (ρ), and specific heat (c_p). The experimental data provided a separate value for material density (ρ). A study by Grenier (Grenier, 1998) on similar composite materials was consulted to obtain a value for specific heat (c_p) of 1000 J/kg-K. The value for thermal conductivity was backed out from $k\rho c_p$, using the known values for ρ and c_p.

3.2 Net Heat of Complete Combustion and Combustion Efficiency

The algorithm is set up to use an effective heat of combustion by multiplying a net heat of complete combustion by a combustion efficiency as follows:

$$\Delta H_{eff} = \left(\chi_A\right)\left(\Delta H_{net,c}\right) \tag{B3-1}$$

The primary material that is consumed during combustion of composite materials is the resin that binds the glass together. For this reason, the net heat of complete combustion for the resin material alone is used with an appropriate combustion efficiency to arrive at the effective heat of combustion derived from the cone calorimeter tests. The net heat of complete combustion for these materials was taken from Tewarson (Tewarson, 1995). If no data could be found on a particular material, a combustion efficiency of 0.5 was assumed and an appropriate net heat of complete combustion was used to arrive at the experimentally determined effective heat of combustion.

3.3 Radiative Fraction of Heat Release Rate

The radiative fraction of heat release rate (χ_R) was derived in a similar manner as the combustion efficiency, using the radiative heat of combustion and the chemical heat of combustion:

$$\chi_R = \frac{\Delta H_{rad}}{\Delta H_{ch}} \qquad \text{(B3-2)}$$

The chemical heat of combustion of the resin material *alone* was used in this case instead of the value for the overall composite material provided by Janssens (Janssens, 1998). If these values could not be found, a radiative fraction of 0.3 was assumed because this is a nominal value for most fuels (Drysdale, 1999).

3.4 Emissivity

The emissivity of these materials was not determined during testing. Based on Grenier's study of similar materials (Grenier, 1998), an emissivity of 0.9 was assumed to be reasonable for these simulations.

3.5 Flame Transmissivity

A value for flame transmissivity was also not determined during testing of the composite materials, and little guidance on this value was found in the literature. The only basis found was from Karlsson (Karlsson, 1992), where he assumed a flame emissivity of 0.5. If the assumption is made that $\varepsilon_{flame} = \alpha_{flame}$, and $\alpha_{flame} = (1 - \tau_{flame})$, then τ_{flame} is 0.5. This is the value currently used for these materials.

3.6 Lateral Flame Spread Properties

Two sets of the values governing lateral flame spread ($T_{s,min}$ and Φ) were available for each material. This is due to the fact that data on $T_{s,min}$ and Φ were reduced following two different experimental procedures, specifically IMO Resolution A.653, and ASTM E 1321-97-a. The average values from the two data reduction methods were used in the simulations.

3.7 Cone Calorimeter Curve at Multiple Irradiances

Several cone calorimeter tests were performed on each material. Generally, two tests were completed at each of three irradiance levels. The ignition times of the two curves were aligned and the arithmetic mean of heat release per unit area versus time was found at each discrete time for which data were available. This created an average heat release rate curve for each material at each irradiance level. In some cases, the burn-time of one cone calorimeter test was significantly longer than that of the other, leading to a possible spike (i.e., a curve that is discontinuous in the first derivative) when the shorter curve ends. In order to resolve this issue, the newly created average curve was extended via extrapolation from the time corresponding to the end of the shorter cone curve. More specifically, the tail end of the longer cone curve was shifted vertically upward or vertically downward to avoid discontinuity at the point where the shorter cone curve ends, as shown in Figure B3-1 at 730 seconds.

Once the corrected average curve had been developed, a number of points (typically on the order of five to twenty points, depending on the complexity of the curve) were selected that captures the overall behavior of the cone calorimeter curve. A simple five-point moving average was used to help select points when the corrected average curve exhibited a significant degree of noise. These are the points that are provided to the flamespread algorithm as input. An example is shown in Figure B3-1. These are provided in Section 7 for all nine materials.

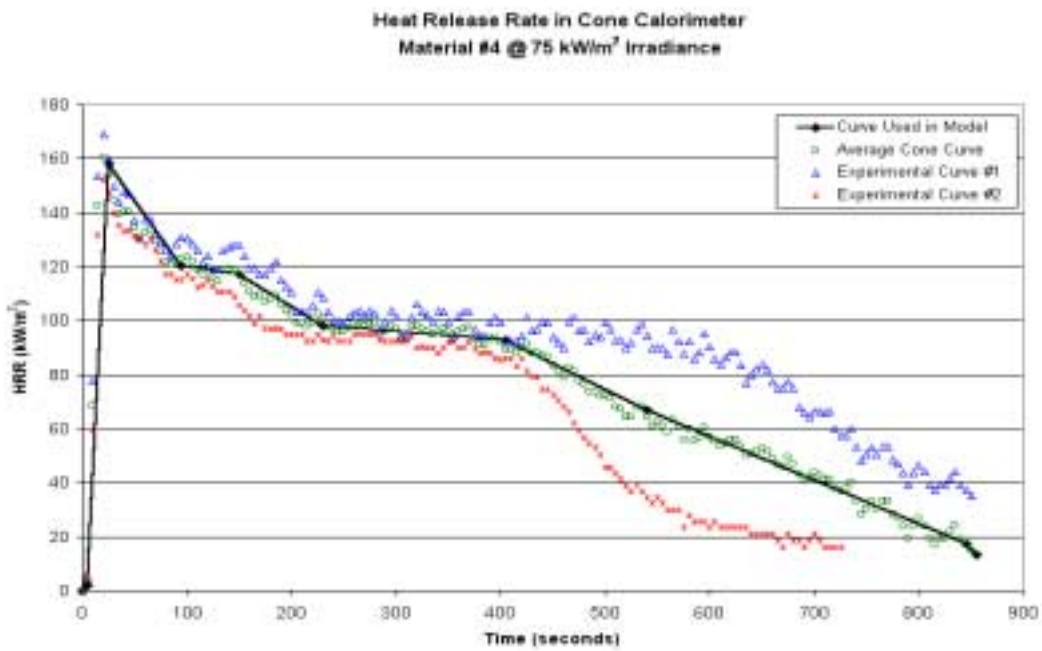

Figure B3-1. – Sample cone calorimeter data.

4.0 SIMULATION RESULTS AND MODEL VALIDATION

This section presents selected results generated by the modified flame spread algorithm and compares them to experimental data. Heat release rate, upper layer gas temperature, smoke production rate, and heat flux to the floor of the compartment were selected as validation criteria and are discussed in this section. Although graphical data from individual runs are presented, the results are discussed from a holistic point of view because the qualitative relationships among the four validation criteria are consistent for all materials. The baseline results for all nine materials are given in Sections 8 through 11. A summary of the simulation results compared to experimental data is given in Table B4-1 and the times to flashover are given in Table B4-2. A total heat release rate of 1000 kW was used as the criterion for flashover except for material #5 where 750 kW was used because flames were seen to come from the door during full-scale testing at a heat release rate of approximately 750 kW. In Table B4-1, “Net Avg.” refers to the average net HRR (i.e., burner HRR has been subtracted) over the entire test, “Net 30s Avg Max” is the maximum net 30-second (or 60-second) sliding average, and “Net Max” is the highest instantaneous net heat release rate that was predicted during the simulation.

Table B4-1. – Comparison of predicted HRR and SPR to experimental data.

Material	Heat Release Rate (kW)					Smoke Production Rate (m^2/s)				
	Experimental		Simulation			Experimental		Simulation		
	Net Avg	Net 30s Avg Max	Net Avg	Net 30s Avg Max	Net Max	Net Avg	Net 60s Avg Max	Net Avg	Net 60s Avg Max	Net Max
1	62	62	48	192	194	1.50	5.41	2.51	7.45	7.71
2	31	31	28	109	118	0.15	0.47	1.77	4.33	4.66
3	191	191	119	366	388	10.00	21.70	8.66	23.34	25.05
4	190	190	152	660	693	9.08	32.10	10.17	38.23	41.20
5	115	115	44	218	223	6.39	26.40	5.80	22.69	24.97
6	28	28	67	164	166	1.45	3.46	8.27	18.91	19.25
7	17	17	11	77	82	0.10	0.16	0.91	1.41	1.41
8	170	170	131	361	901	2.28	4.10	3.86	5.30	32.23
9	109	109	109	488	512	0.42	3.81	1.38	3.30	3.51

Table B4-2. – Time to flashover.

Material	Experimental	Model
3	5.8 minutes	N/A
4	5.1 minutes	N/A
5	16.4 minutes*	N/A
8	1.8 minutes	1.4 minutes
9	11.3 minutes	N/A

* Flashover assumed to be total HRR of 750kW

4.1 Interpretation of the Pyrolysis/Burnout Front Graph

The pyrolysis/burnout front graphs presented in the following discussion are somewhat difficult to understand at first glance; therefore, an example is provided as Figure B4-1 for clarity. The arrows indicate the general direction of the fronts, and the hatched area represents burning. The thick dashed line represents the boundary between the wall and the ceiling, with all points above this line being on the ceiling. The height scale does not change for the ceiling, but the length scale on the ceiling is a radius instead of a vertical height. To obtain a radius, the virtual height of the room (ceiling height minus the height of the burner) is subtracted from the value on the graph. This graph can also be used to determine the burning time of a particular element by choosing a height and moving horizontally to estimate the time that elapses between the passage of the pyrolysis and burnout fronts.

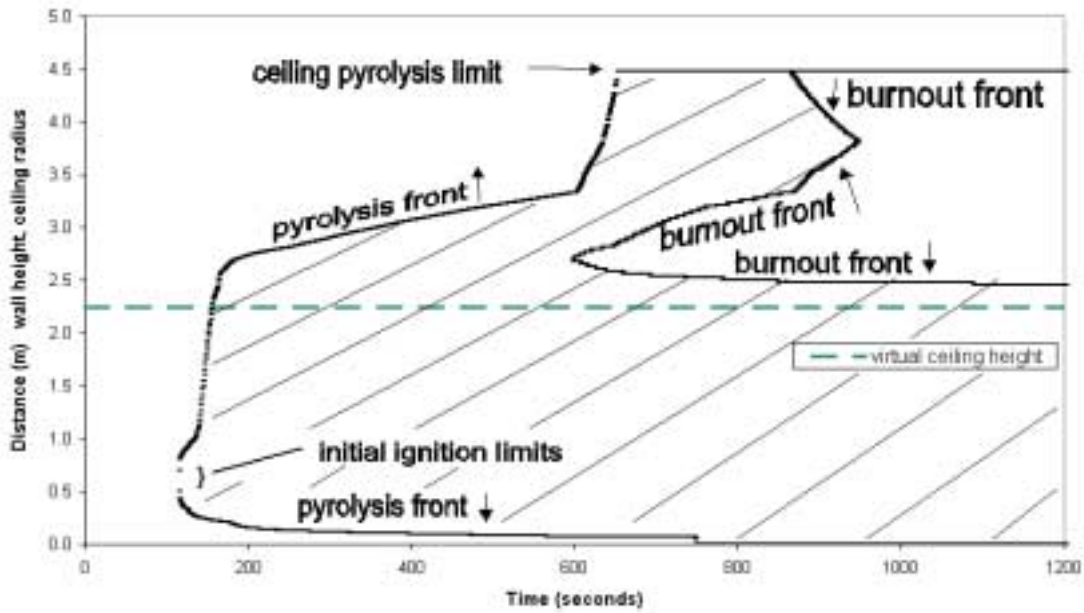

Figure B4-1. – Example of pyrolysis and burnout front graph.

4.2 Heat Release Rate

The simulated heat release rate of the marine grade polyester composite (material #8) follows the experimental curve quite well, as shown by its baseline curve in Figure B4-2. The fire growth on this material is quite rapid, and flashover conditions (heat release rate of 1MW) are reached roughly 40 seconds after ignition. The entire wall is burning and the ceiling ignites about 15 seconds after ignition. The rapid growth after ceiling ignition is a function of the burning nodes quickly reaching the peak burning rate on their cone calorimeter curve combined with rapid growth across the ceiling elements. Unlike the wall elements, the ceiling elements increase in area the further they are from the corner. This characteristic of the algorithm is important to remember when examining spread across the ceiling and the resulting rate of heat release.

The peak heat release rate from the cone calorimeter is quite high for this material (~350kW/m^2), and is probably the most dominant factor in its rapid fire growth. As will be discussed in Section 5, some slight perturbations from the baseline curve occur when varying the parameters in the sensitivity matrix, but the overall curvature of the simulation for material #8 remains similar to the baseline graph shown in Figure B4-2.

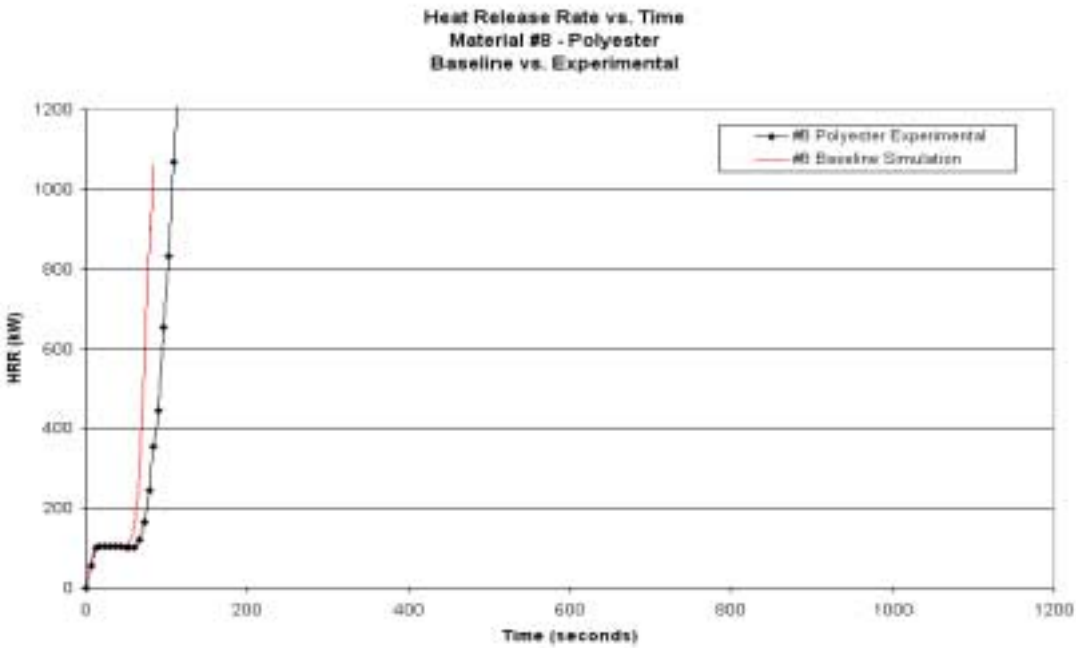

Figure B4-2. – Baseline heat release rate for material #8.

The behavior of the fire-retardant materials is significantly different from the marine grade polyester composite. A total of seven fire-retardant materials were tested, and these materials can be divided into two separate sub-categories. The first category consists of the materials that exhibited little burning during full scale testing. The materials that did now show significant burning are material #1 (FR phenolic), material #2 (fire restricting material), and material #6 (coated FR epoxy). The second sub-category consists of the fire-retardant materials that caused flashover during full-scale testing. These are material #3 (FR polyester), material #4 (FR vinylester), material #5 (FR epoxy), and material #9 (FR acrylic). It should be noted that 1000 kW was used as the criterion for flashover except with material #5. This was necessary because flames were seen to come from the door during full-scale testing of material #5 at a time corresponding to a heat release rate of approximately 750 kW; therefore, this value is the criterion for flashover for material #5. Material #7 was predicted but its results are not considered to be valid because the material was seen to fall on the floor during full-scale testing.

The model captured the general behavior of the materials that did not exhibit significant burning. Figure B4-3 shows a comparison between the experimental data and the model prediction for material #1. This behavior is qualitatively comparable to the remaining cases that did not show significant burning.

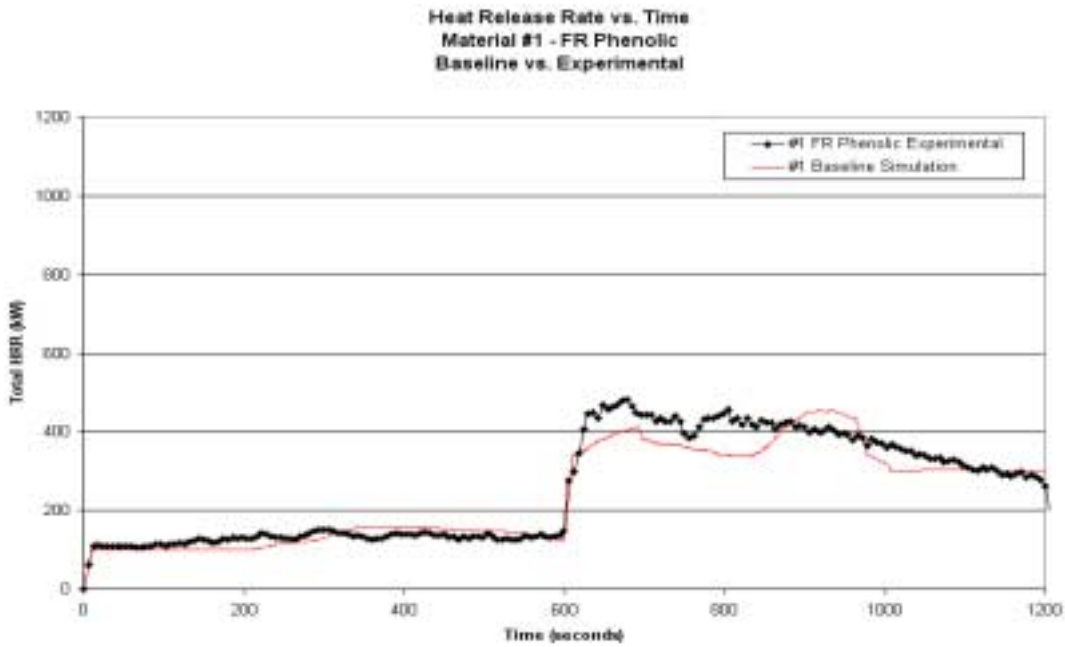

Figure B4-3. – Baseline heat release rate for material #1.

The simulated behavior of the fire-retardant composite materials that went to flashover during full-scale testing is significantly different from the previously discussed cases. The remainder of this section examines the behavior of these materials in detail. The simulations for materials #3 and #4 do not match the experimental curves well except near ignition, as can be seen from Figures 4-4 and 4-5. The total experimental heat release rate of material #5 was seen to approach 800 kW after the ignition burner strength was increased to 300 kW. The model, as shown in Figure B4-6, did not capture this behavior after 600 seconds. The predicted behavior of material #9 follows the experimental results fairly well before 600 seconds but the model does not track the experimental behavior after the burner strength increase, as shown in Figure B4-7.

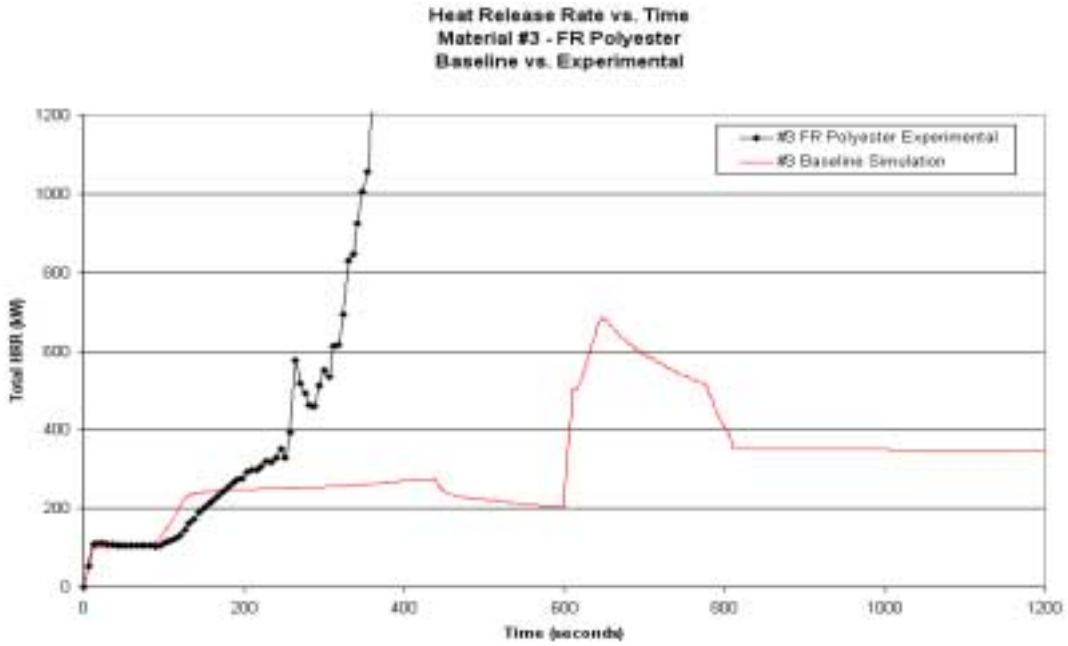

Figure B4-4. – Baseline heat release rate for material #3.

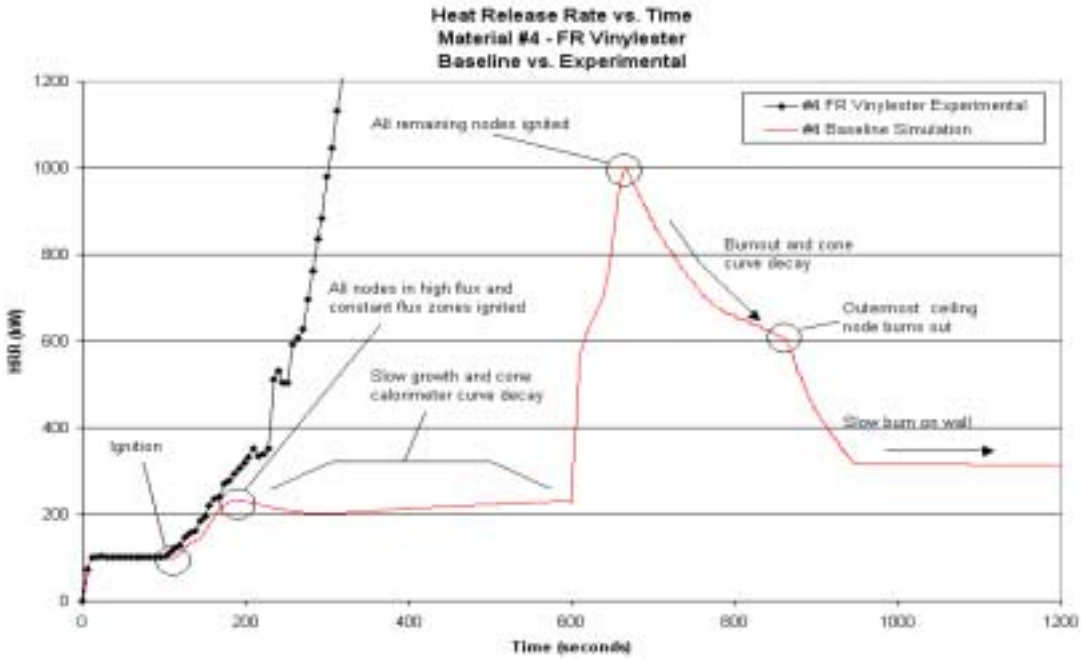

Figure B4-5.– Baseline heat release rate for material #4.

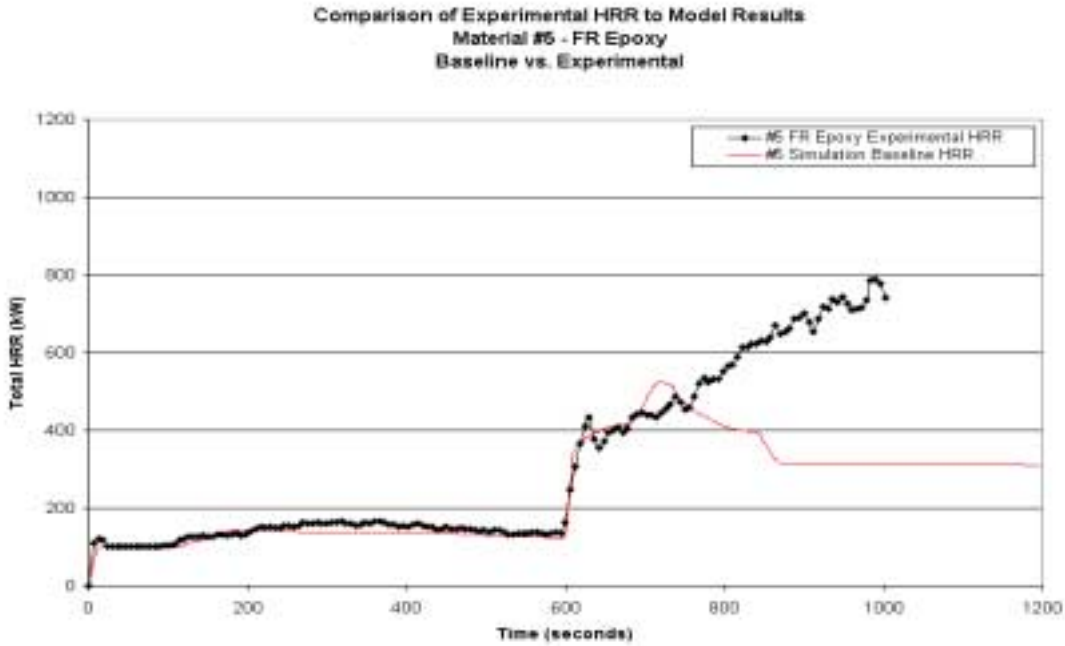

Figure B4-6. – Baseline heat release rate for material #5.

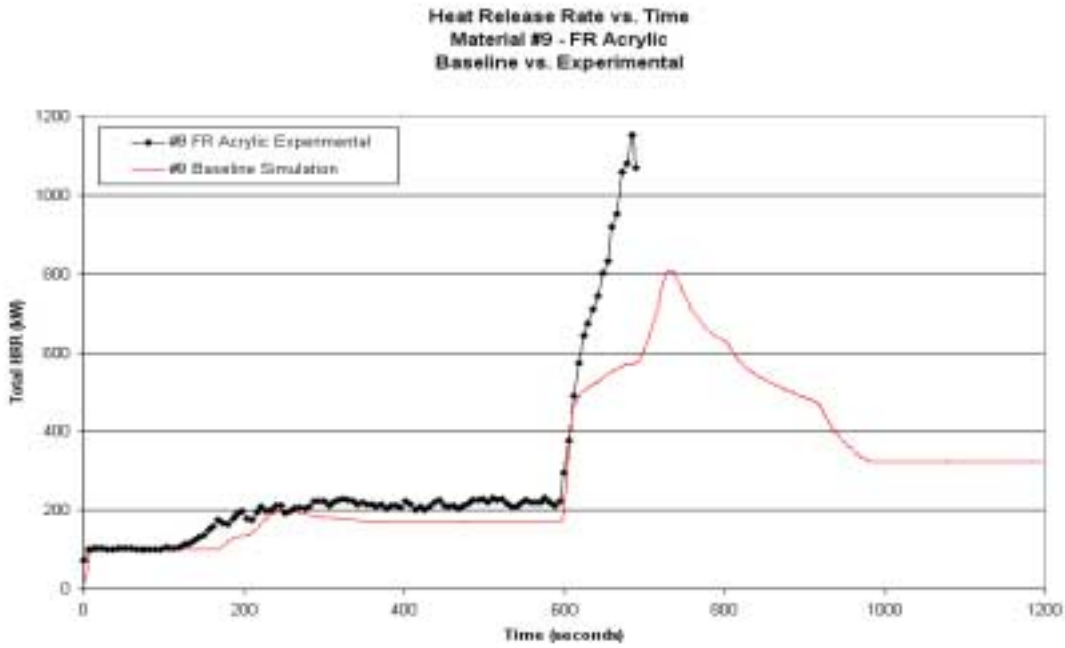

Figure B4-7.– Baseline heat release rate for material #9.

The results from material #4 shown in Figure B4-5 are used to explain the simulated behavior generally exhibited by these fire-retardant materials. After ignition, a period of sustained growth occurs as flame spreads over the area of high heat flux on the wall, followed shortly by the spread of flame over the area of constant heat flux specified by the heat flux map (115 seconds to 180 seconds). Figure B4-8

shows the heat flux distribution at three discrete times for material #4. The area of high flux is followed by an area of constant flux that ends at a height of approximately 2.6-m, corresponding to a radius of 0.35 m on the ceiling. Figure B4-9 shows the pyrolysis and burnout front locations versus time for material #4. The initial rapid growth occurs from 115 seconds to 180 seconds, ending at approximately 2.6 m. Thus, the initial growth is directly related to the initial heat flux distribution.

The section of the curve from 180 to 600 seconds in Figure B4-5 is representative of slow flame spread across the ceiling coupled with nodes beginning to burn with a heat release rate determined by the decay portion of the cone calorimeter curve. This results in a slower rate of growth. The burnout simulated by the algorithm also tends to occur more rapidly on the ceiling as opposed to the wall, i.e., the ceiling releases a greater amount of energy in a shorter period of time.

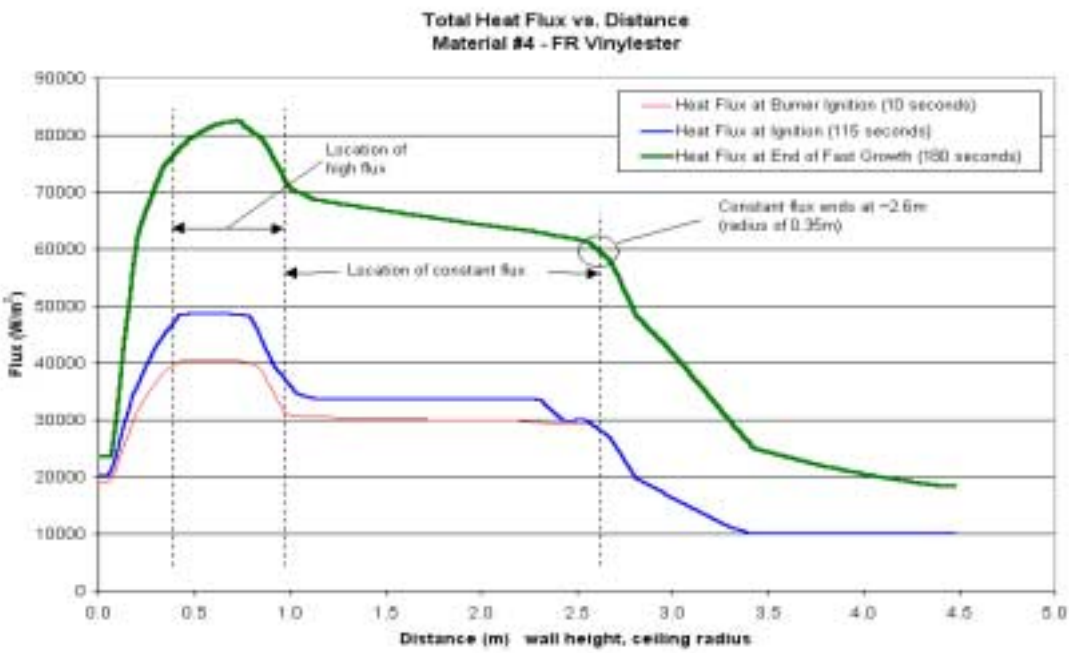

Figure B4-8. – Total flux versus distance for material #4.

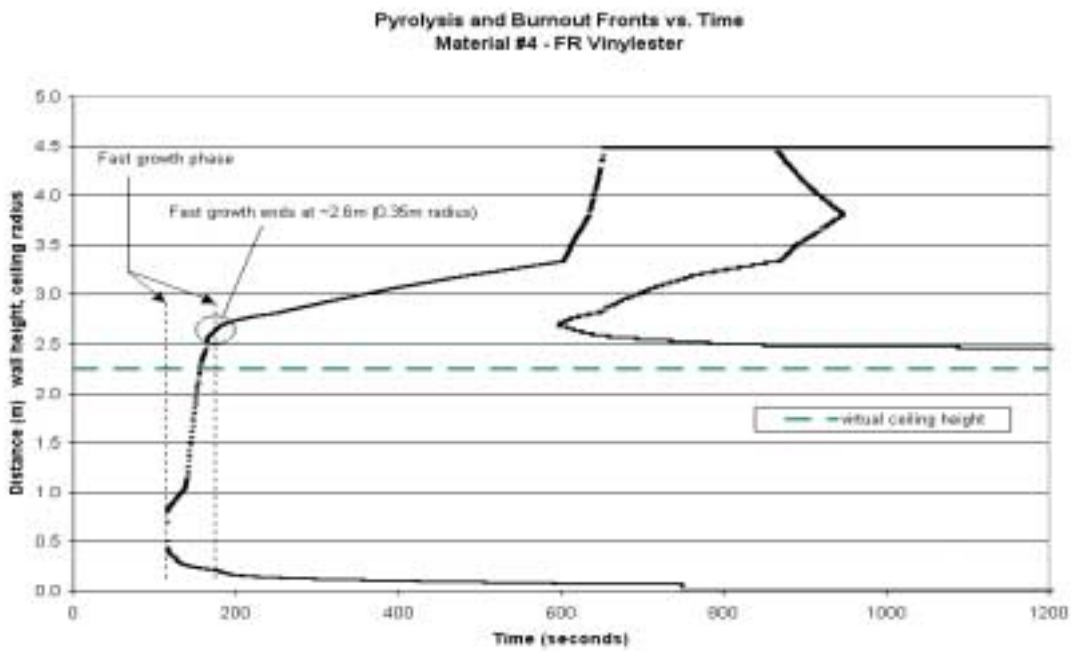

Figure B4-9. – Pyrolysis and burnout fronts for material #4.

The section of the heat release rate curve after 600 seconds in Figure B4-5 shows the behavior of the material after the ignition burner strength is increased from 100 kW to 300 kW. It is typical for the remaining non-burning nodes to ignite in a short span of time, as occurs from 600 to 675 seconds in the sample figure. If initial burnout does not happen before 600 seconds, it generally occurs during this segment of the curve. Note that the slope of heat release rate curve in this segment is also quite high. This is similar to the high slope shown for material #8 in Figure B4-2 after the entire wall has ignited. In Figure B4-5, the rapid growth after the burner output increase is a direct result of the increasing size of the elements across the ceiling as previously described. The segment of the curve in Figure B4-5 from 675 to 1200 seconds is indicative of additional burnout and continued burning of nodes with their heat release rates being determined by the decay portion of the cone calorimeter curve.

4.3 Upper Layer Gas Temperature

The upper and lower layer gas temperatures (as well as wall temperatures) are calculated internally by CFAST. The experimental data provided by Janssens (Janssens, 1998) include temperatures from several thermocouples positioned throughout the test room. It should be noted that these thermocouple readings might not represent a true gas temperature due to radiative losses or gains, depending on their location in the compartment. CFAST calculates the mean temperature of a well-mixed, homogeneous gas layer, whereas these thermocouples record temperature at several discrete

locations in the test room. These thermocouples can be used to estimate the gas temperatures that were present during full-scale testing, but the reading of a single thermocouple is not directly analogous to the temperature of a well-mixed homogeneous gas layer as is reported by CFAST. The model predictions were compared to the temperatures of a thermocouple at the center of the room and a thermocouple in the doorway.

It was generally found that when the heat release rate is over-predicted, the same is true of the upper layer gas temperature. A comparison of experimental to predicted data for material #8 is shown in Figure B4-10. Although the upper layer gas temperature calculated by CFAST is higher than the thermocouple readings, this is consistent with its heat release rate curve which is also over-predicted (see Figure B4-2). It is also generally true that an under-predicted heat release rate corresponds to an under-predicted upper layer gas temperature compared to the thermocouple readings.

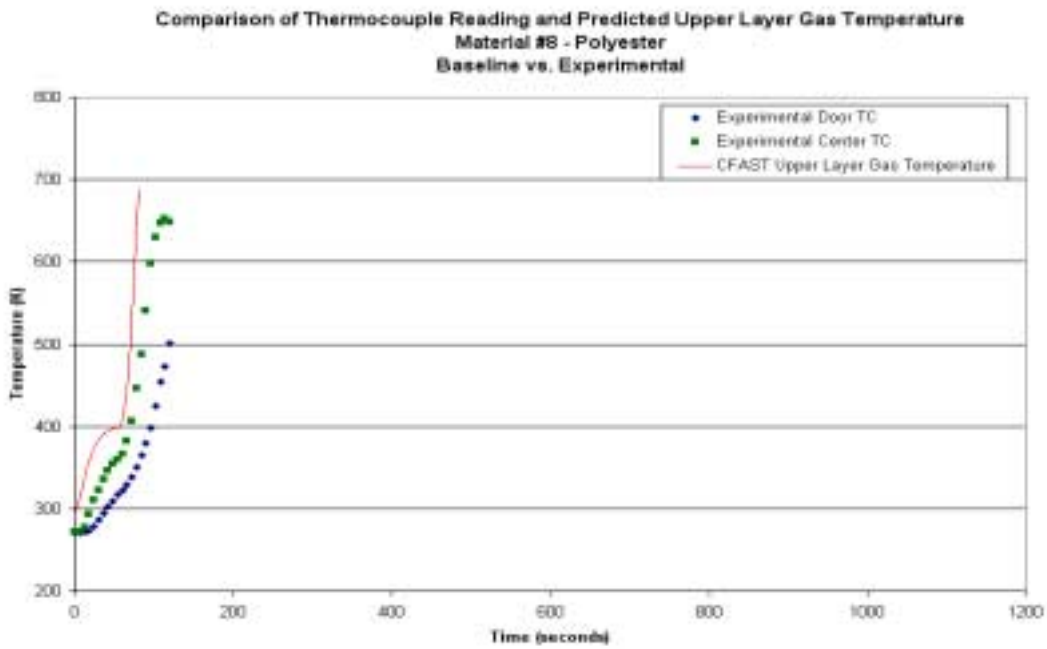

Figure B4-10. – Upper layer gas temperature for material #8.

It was found that the upper layer gas temperature calculated by CFAST was similar to the thermocouple temperatures when the heat release rate predicted by the model was also similar to that observed experimentally. The results for materials #1 and #9 are shown in Figures 4-11 and 4-12,

respectively. These upper layer gas temperatures should be examined concurrently with Figures 4-3 and 4-7, the predicted heat release rate curves for materials #1 and #9.

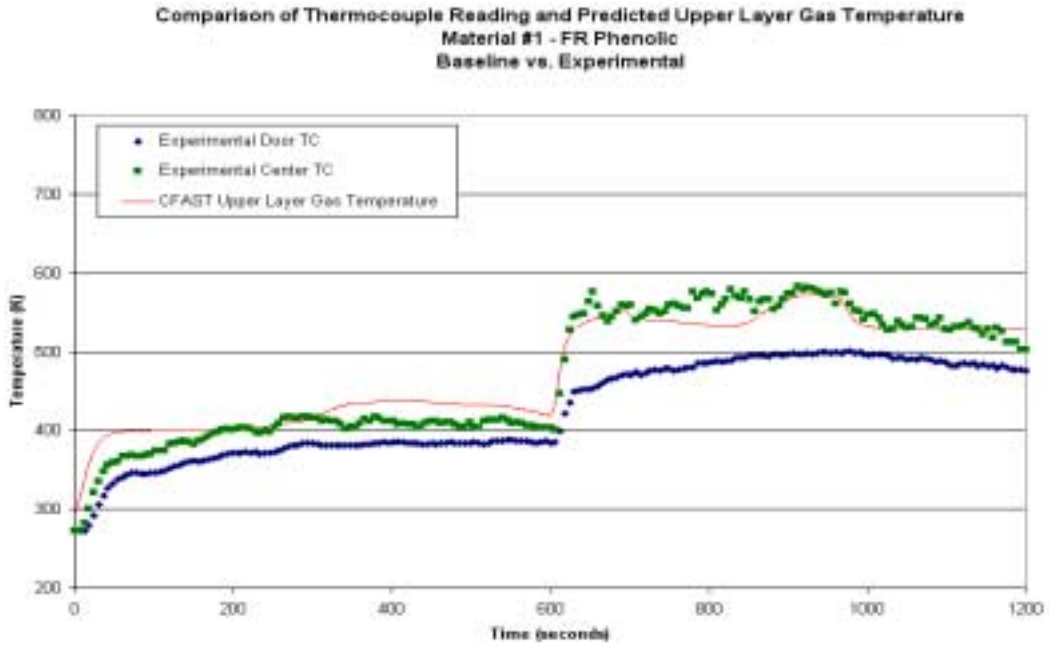

Figure B4-11. – Upper layer gas temperature for material #1.

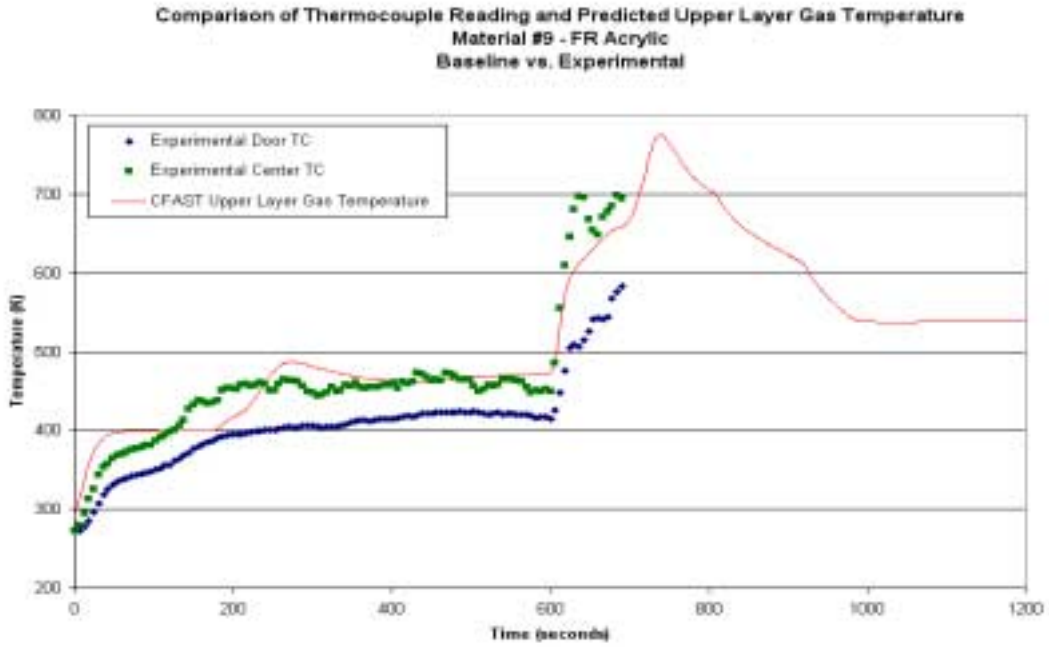

Figure B4-12. Upper layer gas temperature for material #9.

4.4 Smoke Production Rate

The smoke production rate was calculated from the upper layer optical density and vent flow as computed by CFAST. CFAST allows the user to specify the yields of CO, CO_2, soot, and several other chemical species for each individual object in the compartment. The yields given by Tewarson (Tewarson, 1995) for the resin material only (as opposed to a glass-reinforced resin) were used as input to the model. No yield data were found in the literature for vinylester or acrylic. For this reason, cone calorimeter data were used to calculate a soot yield for these two materials. CFAST requires that all species yields be specified as a ratio to the yield of CO_2. The CO_2 yield for PMMA was substituted for that of acrylic, and the CO_2 yield for polyester was substituted for vinylester.

The main CFAST output file contains a time history of species concentrations and optical density in the upper and lower layers. Also given are the temperature of each layer and mass-based vent flows. The mass flow out of the upper layer was converted to a volumetric flowrate using the ideal gas law and upper layer gas temperature. The product of this volumetric flowrate and the upper layer optical density was converted to a smoke production rate using a conversion factor of 2.3.

As was seen with the upper layer gas temperatures, the smoke production rate is consistent with the heat release rate. The shape of the smoke production rate curve follows the heat release rate curve. An over-prediction in the heat release rate generally corresponds to an over-prediction in the smoke production rate. Conversely, the smoke production rate is generally under-predicted when the heat release rate is under-predicted. The smoke production rates for materials #1 and #8 are shown in Figures 4-13 and 4-14. Their corresponding heat release rate curves can be found in Figures 4-3 and 4-2.

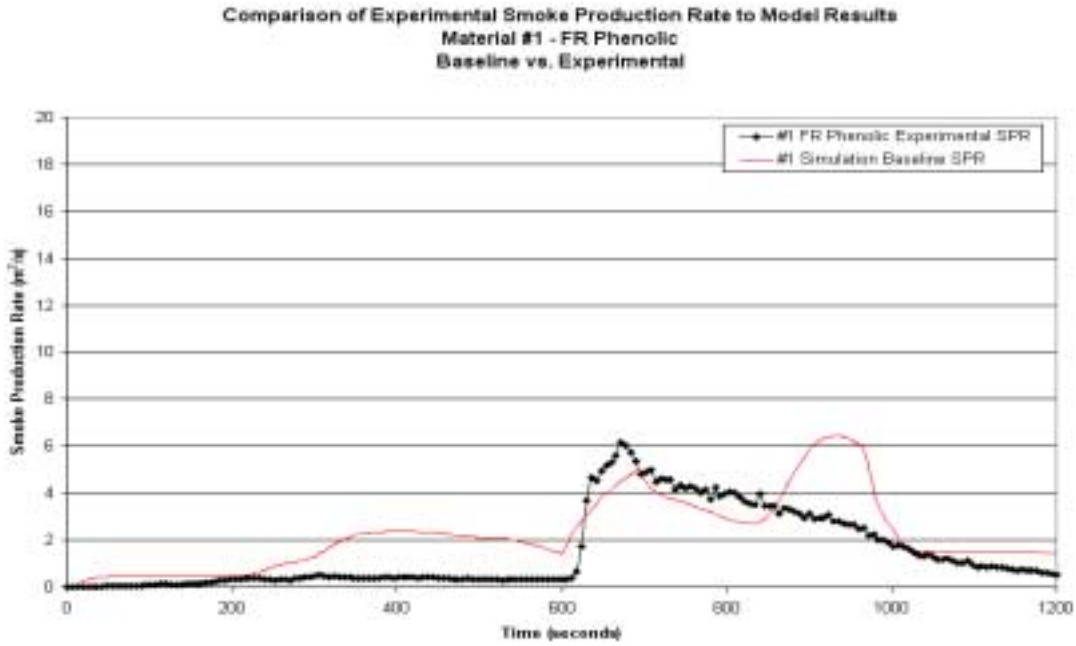

Figure B4-13. – Smoke production rate material #1.

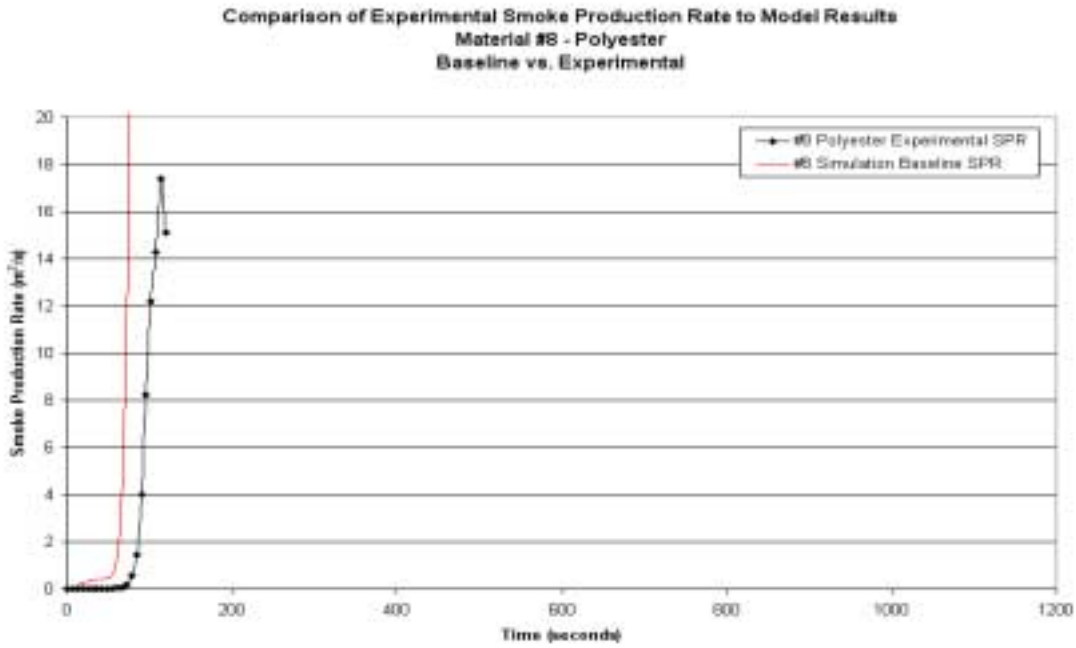

Figure B4-14. – Smoke production rate material #8.

4.5 Heat Flux to the Floor

CFAST allows the user to specify targets at arbitrary locations and orientations throughout the compartment. The flux at these targets is then calculated internally by CFAST. The simulations were run with a target placed at the center of the floor to estimate this heat flux. The results of the simulation show

that the direct radiation from the ignition burner flame and wall flames are not included. The heat flux at this target is primarily due to radiative heat transfer from the hot upper gas layer. For this reason, the heat flux at the center of the floor was consistently underestimated as compared to experimental data. Future versions of the model will include a module to account for direct ignition burner and wall flame radiation to a target on the floor. A typical time history of heat flux to the floor is shown in Figure B4-15. It can be seen that the simulation results are consistent with the upper layer gas temperature, Figure B4-11.

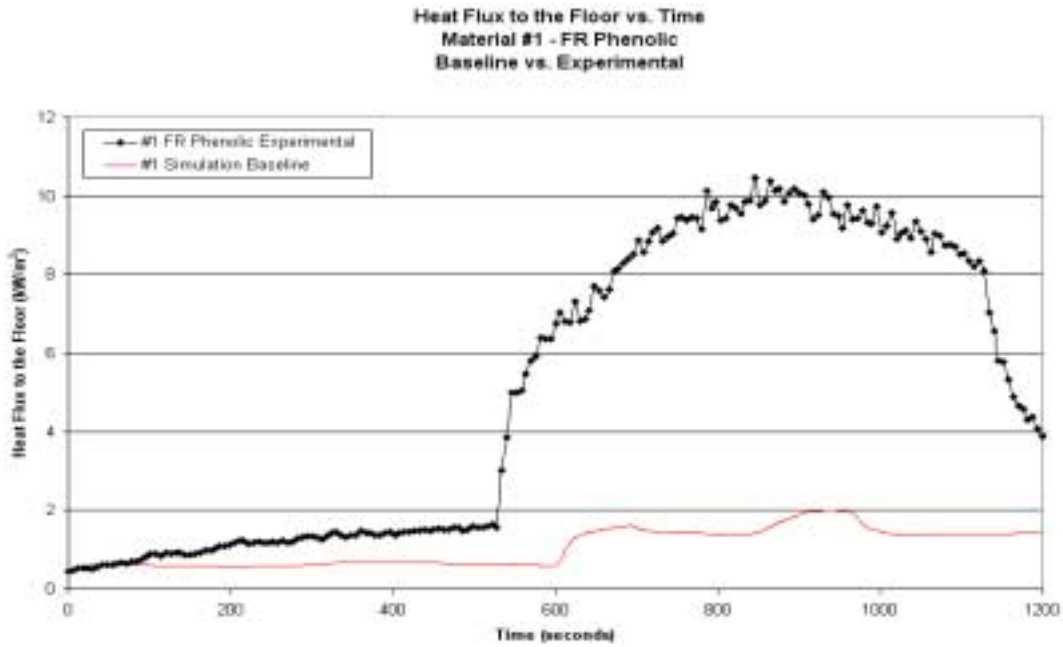

Figure B4-15. – Heat flux to the floor for material #1.

5.0 SENSITIVITY ANALYSIS

A self-consistent set of input data was assembled for each material. A sensitivity matrix was developed and used to quantify the effects of altering various input parameters. The key baseline input parameters can be found on the first page of Section 7, and the complete set of input parameters (including algorithm options) for the nine materials immediately follows. With the intention of keeping this report brief, the sensitivity analysis results from four of the nine materials will be discussed here. It should be noted that the general results discussed in this report extend to all materials for which simulations were run because similar phenomena were observed for all nine materials. The complete set of baseline results can be found in Sections 8 through 11.

5.1 Selection of Parameters for Variation in Sensitivity Analysis

The thermal inertia ($k\rho c_p$) of the lining material affects ignition time, material surface temperature, and fire growth rate; therefore, it is important to examine the effect of varying $k\rho c_p$. A value for density (ρ) was available, and the value for specific heat (c_p) was held constant at 1000 J/kg-K as previously mentioned. For these reasons thermal conductivity (k) was varied, effectively altering the thermal inertia. A factor of two was selected because work conducted by Jacoby (Jacoby, 1998) on similar composite materials showed that the level of uncertainty in calculation of ignition parameters was roughly within a factor of two.

The mass loss rate, and thus the heat release rate, is calculated directly from the cone calorimeter curve that is provided to the model as input. For this reason, examining the effect of using cone calorimeter curves at multiple irradiance levels is important. Average cone calorimeter curves from three irradiance levels were used for all materials apart from material #2, for which there were data at only two irradiance levels. It was decided that the cone calorimeter curves at the median irradiance level would be considered to be the baseline case, although this is somewhat of an arbitrary choice. In the case of material #2, the lower irradiance (75 kW/m^2) was chosen to constitute the baseline. The complete set of average cone calorimeter curves and the individual points that were given to the model as input can be found in Section 7.

The material emissivity (ε) and the flame transmissivity (τ_{flame}) were selected for variation because they are used in the radiation calculations. These variables are used as part of the radiation network used to compute the enhanced radiative exchange in the corner. Their variation is important because few sources were found that suggest baseline values to use for emissivity or flame transmissivity.

The ignition temperature (T_{ig}) has several effects on the simulation results and was therefore selected for variation. The time at which the wall lining material first ignites is dependent upon its ignition temperature. After ignition, the rate of fire growth is affected because a non-burning element is marked as burning when it has been heated to its ignition temperature. Additionally, the degree to which a burning element radiates is proportional to the fourth power of its ignition temperature (i.e., its maximum surface temperature), thus affecting the overall level of radiative exchange in the corner. The variation of ignition temperature was selected as ± 25% to represent a reasonable variation due to experimental error and uncertainties in cone or LIFT data reduction. The minimum temperature at which

lateral flame spread occurs ($T_{s,min}$) was altered proportionally with ignition temperature. This was done because the decreased ignition temperature would generally be lower than the unaltered value of $T_{s,min}$.

It was decided to vary the inputs affecting lateral flame spread to determine the significance of lateral flame spread in the simulations. These variables were the minimum temperature at which lateral flame spread occurs ($T_{s,min}$) and the lateral flame spread parameter (Φ). The variation of each parameter was selected as ± 25% to represent a reasonable variation due to experimental error and uncertainties in cone or LIFT data reduction. The variation of Φ by ± 25% is straightforward; however, some difficulties arise when varying $T_{s,min}$ by + 25% due to its close proximity with the ignition temperature. If $T_{s,min}$ + 25% was greater than the T_{ig}, then $T_{s,min}$ was set to a value infinitesimally smaller than T_{ig}. This prevented the possibility of division by zero but effectively prevented lateral flame spread.

The resulting sensitivity matrix is shown in Table B5-1. The leftmost column describes the manner in which the input data were modified. The next column refers to the particular variation, later referred to as "cases." For example, case 3- refers to the baseline simulation of material #3, and case 6g refers to the simulation of material #6 with the material emissivity set to 0.95.

Table B5-1. – Sensitivity analysis matrix.

		USCG MATERIAL NUMBER								
VARIATION		**1**	**2**	**3**	**4**	**5**	**6**	**7**	**8**	**9**
Baseline	**-**									
k * 0.5	**a**	0.637	3.354	0.391	0.611	0.479	0.267	0.543	0.299	0.756
k * 2	**b**	2.548	13.416	1.564	2.442	1.916	1.068	2.170	1.194	3.022
Cone Curve @ Lowest Irradiance	**c**	50	N/A	25	25	50	50	25	25	25
Cone Curve @ Highest Irradiance	**e**	100	100	75	75	100	100	75	75	75
ε = 0.75	**f**	0.75	0.75	0.75	0.75	0.75	0.75	0.75	0.75	0.75
ε = 0.95	**g**	0.95	0.95	0.95	0.95	0.95	0.95	0.95	0.95	0.95
τ_{flam} = 0.75	**h**	0.75	0.75	0.75	0.75	0.75	0.75	0.75	0.75	0.75
τ_{flam} = 0.25	**i**	0.25	0.25	0.25	0.25	0.25	0.25	0.25	0.25	0.25
T_{ig} + 25% {$T_{s,min}$ + 25%}	**j**	1095 {986}	1131 {1018}	839 {799}	839 {799}	851 {766}	989 {890}	908 {817}	828 {599}	851 {711}
T_{ig} - 25% {$T_{s,min}$ - 25%}	**k**	657 {591}	679 {611}	503 {479}	503 {479}	511 {460}	593 {534}	545 {490}	497 {359}	511 {427}
$T_{s,min}$ + 25%	**l**	876	905	671	671	681	791	726	599	681
$T_{s,min}$ - 25%	**m**	591	611	479	479	460	534	490	359	427
Φ + 25%	**n**	19.49	19.49	15.16	15.39	19.49	19.49	19.49	23.78	29.03
Φ - 25%	**o**	11.69	11.69	9.10	9.24	11.69	11.69	11.69	14.27	17.42

5.2 Variation of Thermal Conductivity

The main effects of changing thermal conductivity for all materials was a delay or advance in the ignition time and a change in the rate of fire growth, as indicated by Figure B5-1. A decrease in thermal conductivity causes ignition to occur at an earlier time and also induces more rapid fire growth after ignition. This is because the diffusion of heat through the wall is inhibited, leading to a more rapid surface temperature increase. This is due to the fact that the cone calorimeter curve exhibits rapid decay after its peak heat release rate has been reached. An increase in thermal conductivity has the opposite effect, as heat readily diffuses through the wall (case 3b in Figure B5-1). The surface temperature rises more slowly, leading to delayed ignition and slower fire growth.

A secondary effect of changing the thermal conductivity also becomes apparent upon examination of Figure B5-1. When ignition is delayed and fire growth is slower, a greater amount of unburned material remains at the time when the ignition burner strength is increased to 300kW. This promotes a longer burning time after the increase in burner strength.

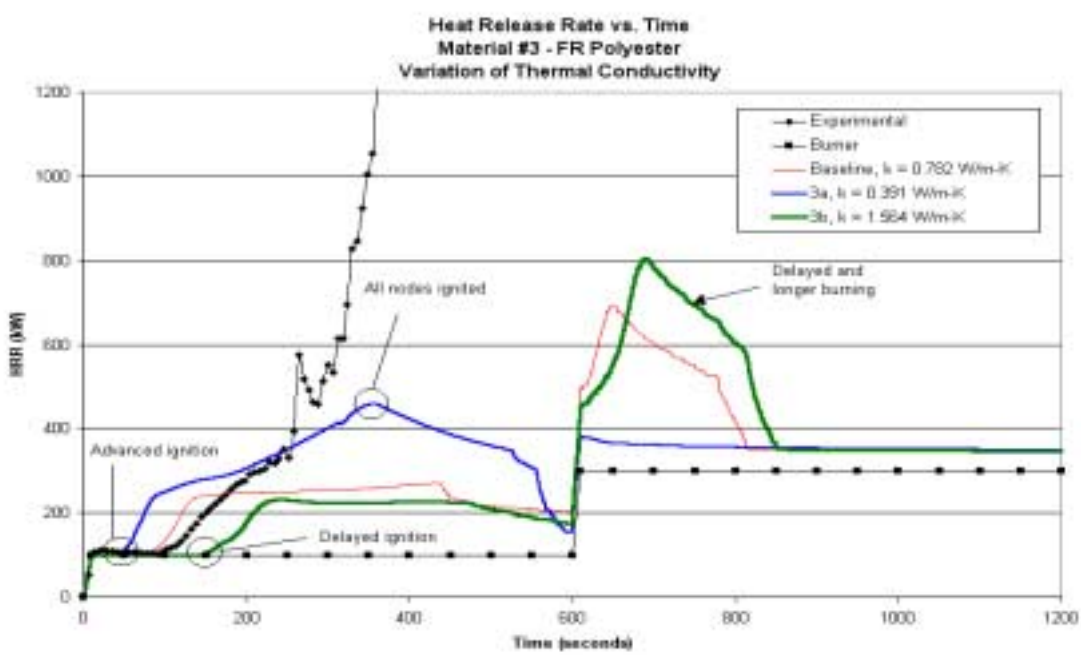

Figure B5-1. – Variation of thermal conductivity for material #3.

5.3 Cone Calorimeter Curve at Multiple Irradiances

From Figure B5-2 it is evident that the predicted results are highly sensitive to the usage of different cone calorimeter curves. Except for the non-fire-retardant polyester based material, all of the low-irradiance cone calorimeter curves produced significant effects similar to the one shown in Figure B5-2. Rapid burnout occurs with lower irradiance levels. Figure B5-3 confirms this observation by showing that the pyrolysis fronts are indeed followed shortly by a burnout front. This rapid burnout is a direct result of the cone calorimeter curve for material #4 at an irradiance of 25kW/m^2, as shown in Figure B5-4. Very little area exists under this curve; therefore, a small amount of fuel is available at each node, inducing rapid burnout.

Also important in this simulation is the relative burn time of the wall in comparison to the ceiling. The material on the ceiling is consumed extremely rapidly, with some nodes burning for less than one minute. Similar results are exhibited with materials #3 and #9, although the effect is less evident with material #9. Material #8 did not show significant variation among the different cone calorimeter curves.

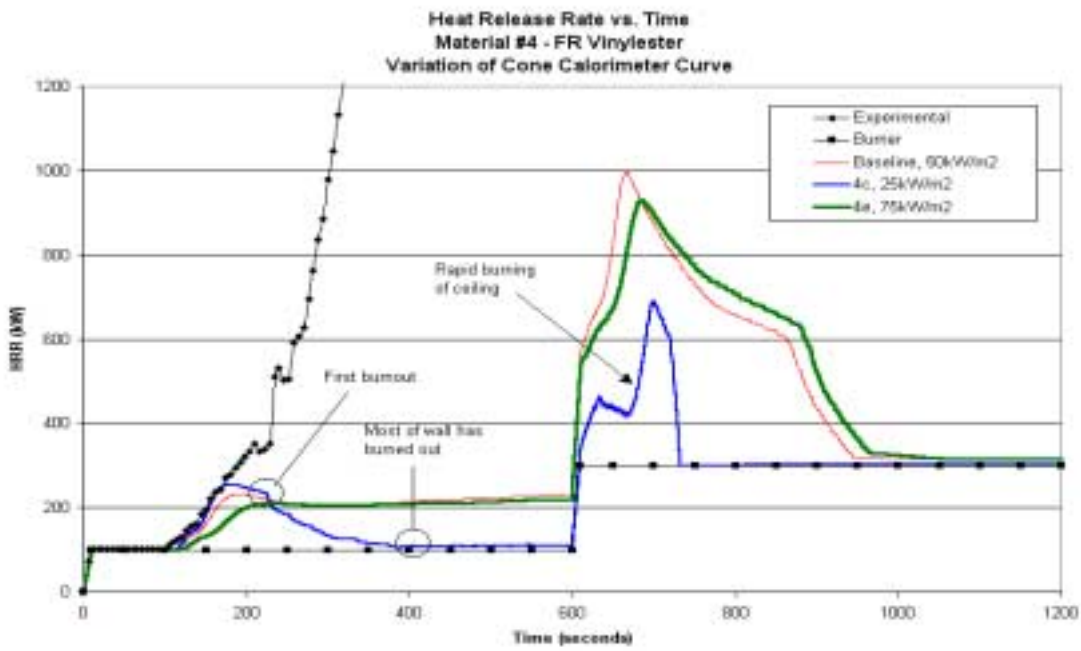

Figure B5-2. – Variation of cone calorimeter curves for material #4.

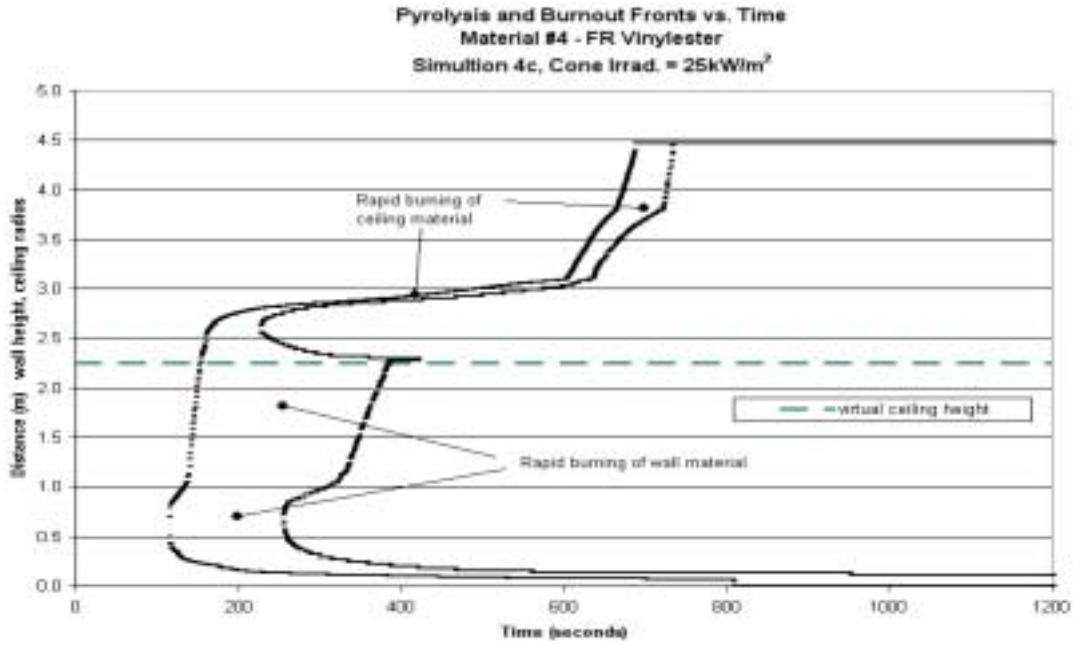

Figure B5-3. – Pyrolysis and burnout fronts for material #4 at 25kW/m^2.

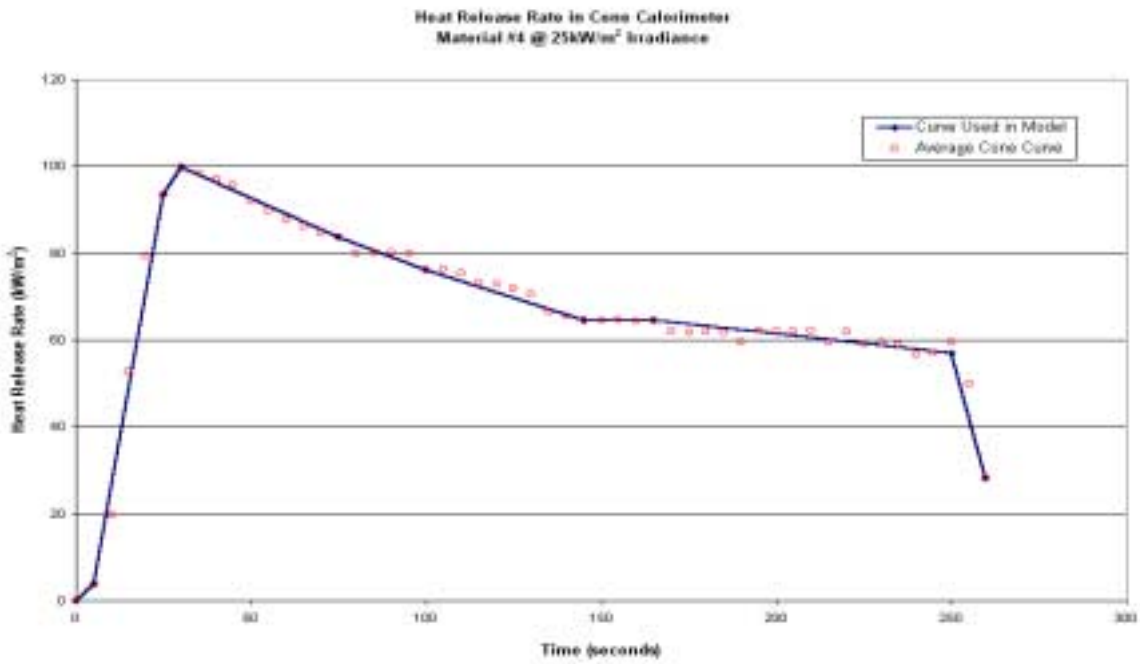

Figure B5-4. – Cone calorimeter curve for material #4 at 25kW/m^2.

5.4 Variation of Emissivity and Flame Transmissivity

Variation of material emissivity and flame transmissivity did not cause a significant change in the shape of the heat release rate curves, but rather small deviations from the baseline case. Figures 5-5 and 5-6 show the variation of these parameters for material #9, where it becomes obvious that altering these variables had little impact. The heat release rate curves for all other materials exhibited similar perturbations from the baseline case when material emissivity and flame transmissivity were varied.

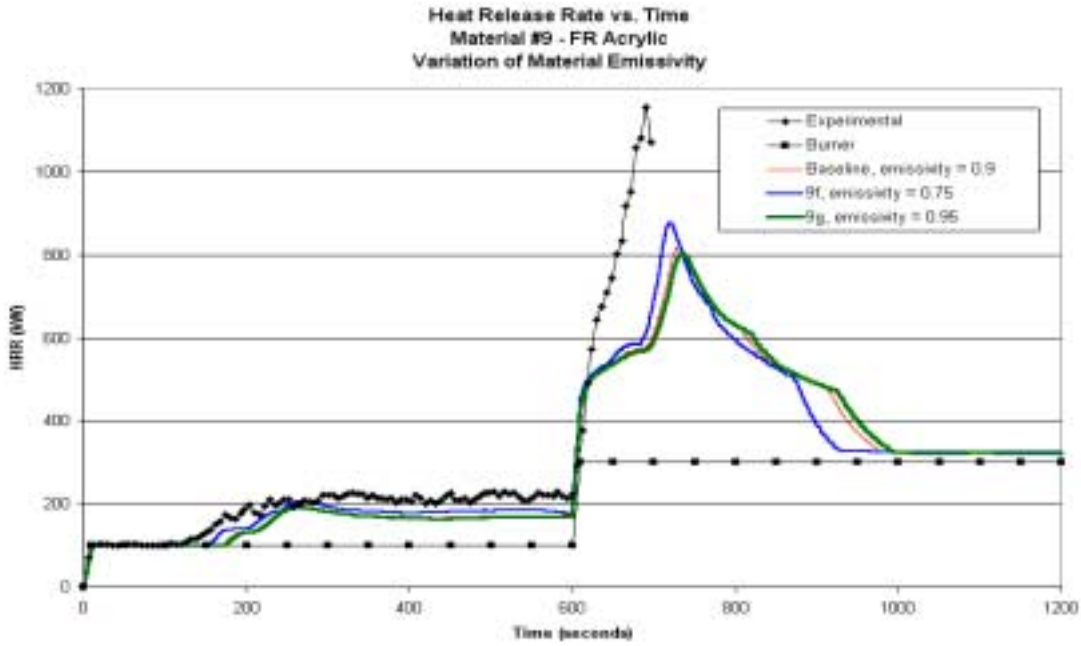

Figure B5-5. – Variation of material emissivity for material #9.

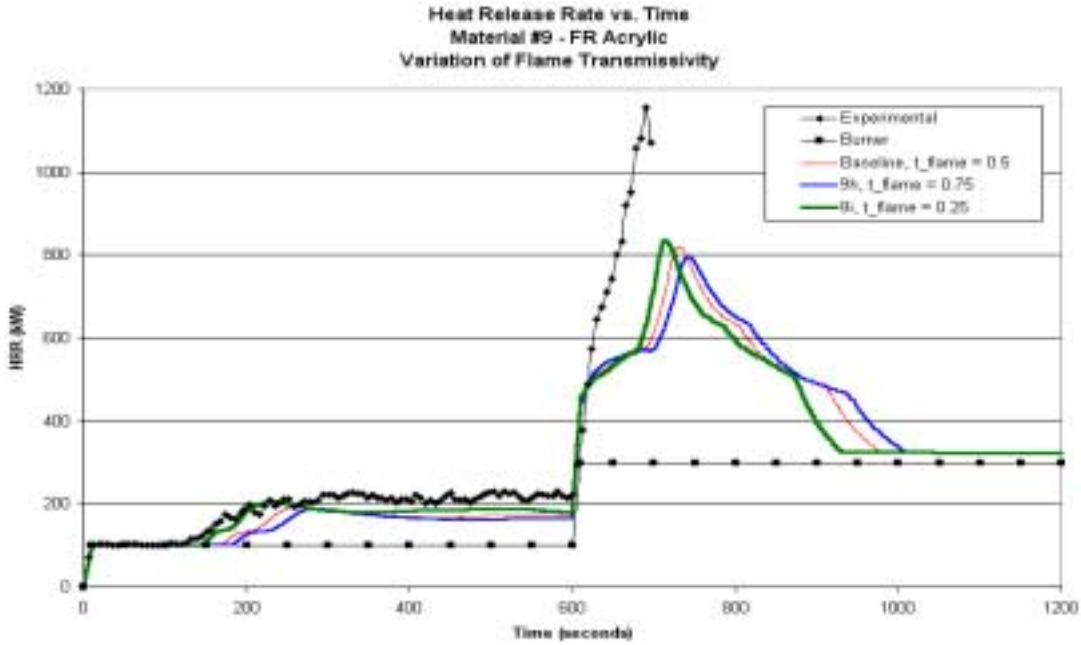

Figure B5-6. – Variation of flame transmissivity for material #9.

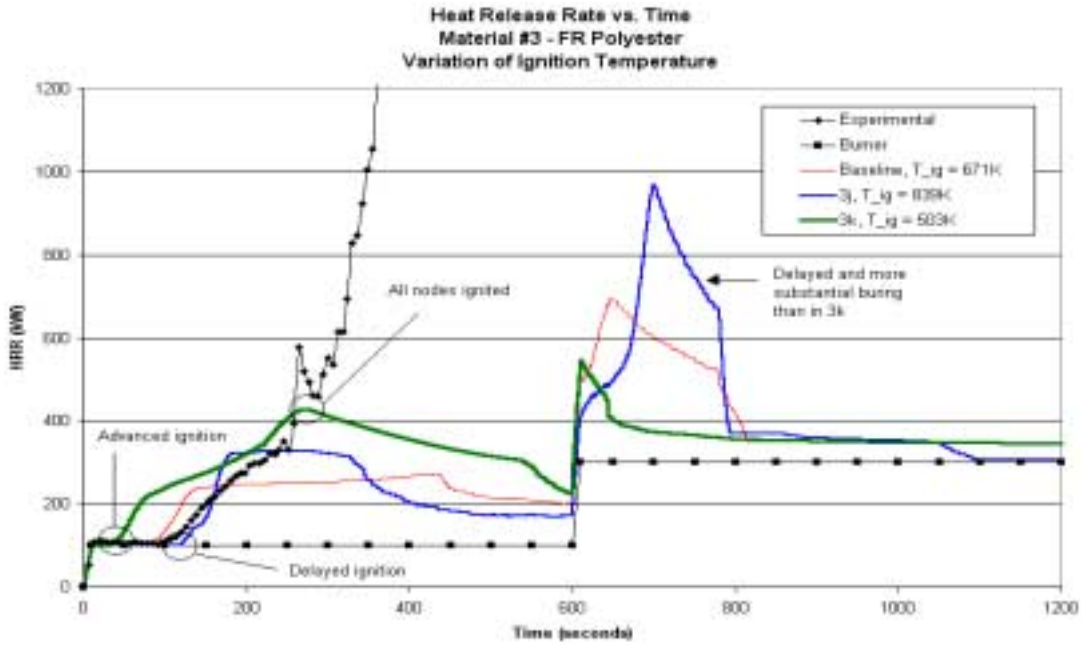

Figure B5-7. – Variation of ignition temperature for material #3.

5.5 Variation of Ignition Temperature

A change in the material ignition temperature produced similar effects as with the variation of thermal conductivity. A lower ignition temperature produced faster ignition, followed by more rapid fire growth and burnout. A higher ignition temperature produced delayed ignition, slower fire growth, and longer burn times. This is shown in Figure B5-7.

5.6 Variation of Lateral Flame Spread Inputs

Variation of the minimum temperature for lateral flame spread and the lateral flame spread parameter showed no effects in the simulations. This is due to the fact that the upper wall temperature as calculated by CFAST never exceeded the minimum temperature for lateral flame spread, even for the cases where $T_{s,min}$ was reduced by 25%. For this reason, no graphs are presented that show the variation of $T_{s,min}$ and Φ as these cases are no different from the baseline examples.

5.7 Flame spread behavior on fire-retardant materials

The overall prediction of the behavior of the fire-retardant materials that reached flashover before the increase in ignition burner output (e.g., materials #3 and #4) was not accurate. It is hypothesized that

the material properties derived from the bench-scale cone calorimeter and LIFT testing cannot be directly extrapolated to predict full-scale behavior due to the fire-retardants present in these materials.

A possible explanation for this is that when materials are tested in the cone calorimeter, the fire-retardants are able to successfully inhibit the combustion process. The result is an overall reduced rate of heat release, and this behavior is translated to the model prediction when the resulting cone calorimeter curve is provided to the flame spread algorithm as input. It is hypothesized that in the full-scale ISO 9705 tests, the fire-retardants function well after the burner is first ignited by hindering combustion of the lining material. As time passes, the combustion reactions of the lining material flames as well as the burner flames consume a significant portion of the fire-retardants. At this point, the lining material is able to support more rapid combustion.

Figure B5-8 shows the experimental results from materials #3 and #4, indicating potential times where the fire-retardants may be active. Note that there is overlap in the suggested times, as there is a fair degree of uncertainty in the behavior of the fire-retardants. Material #9 is not shown on this graph because the fire-retardants appear to have a more constant effect until the time when the heat release rate of the ignition burner is increased and are overcome, as indicated in Figure B4-7.

This hypothesis was tested by conducting two additional simulations. A cone calorimeter curve from a similar non-fire-retardant material was substituted for the fire-retardant cone calorimeter curve of material #3 and #4 to determine if the effects of the retardants could be removed from the simulation. The cone calorimeter curve for material #8 was substituted for the original material #3 curve because material #8 is a non-fire-retardant polyester based composite and material #3 is a fire-retardant polyester based composite. The substitute for the material #4 cone calorimeter curve came from a composite material found in Jacoby's (Jacoby, 1998) work that was a non-fire-retardant vinylester based composite material (8mm thick, with a ceramic fiberboard backing). The remaining material properties were not changed. A comparison of the fire-retardant and non-fire-retardant cone calorimeter curves used for material #3 and #4 are shown in Figures 5-9 and 5-10. The resulting simulations for material #3 and #4 are presented in Figures 5-11 and 5-12.

The results from the change in cone calorimeter curve for material #3 do not offer much support for the hypothesis. Using the cone curve from material #8 causes material #3 to reach flashover conditions very quickly in a manner similar to that seen with the original baseline for material #8.

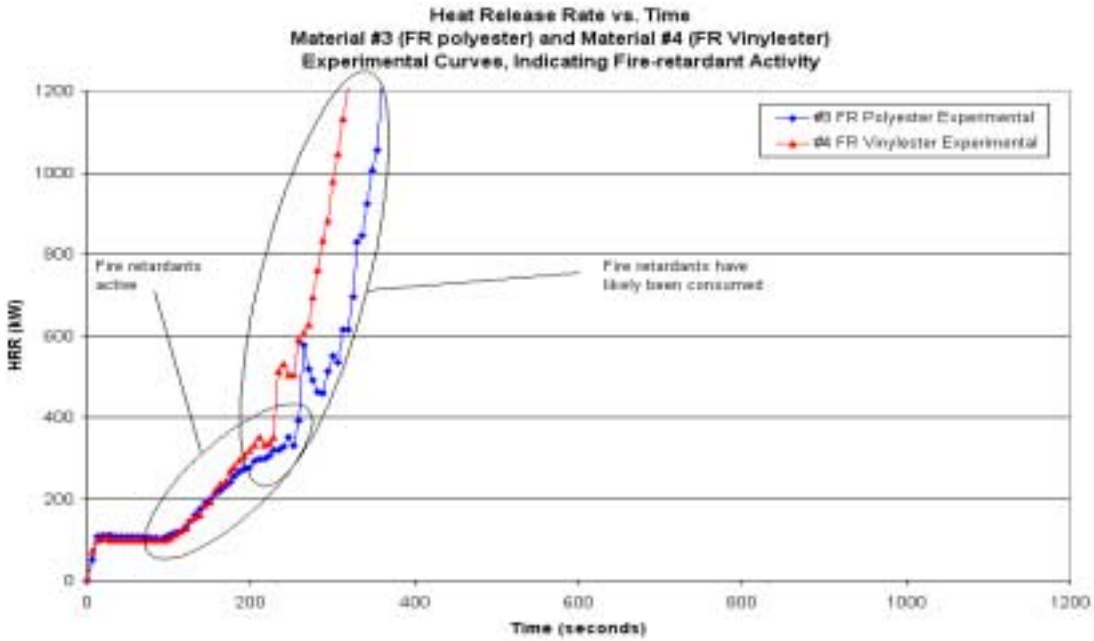

Figure B5-8. – Possible fire-retardant activity for material #3 and #4.

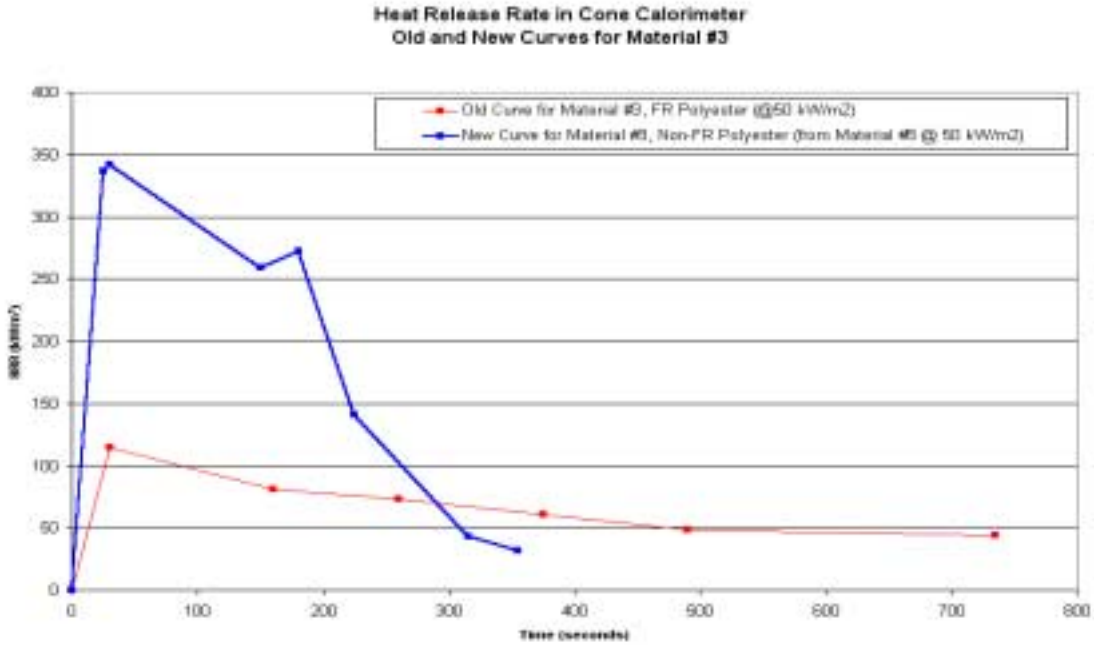

Figure B5-9. – Change of cone calorimeter curve for material #3.

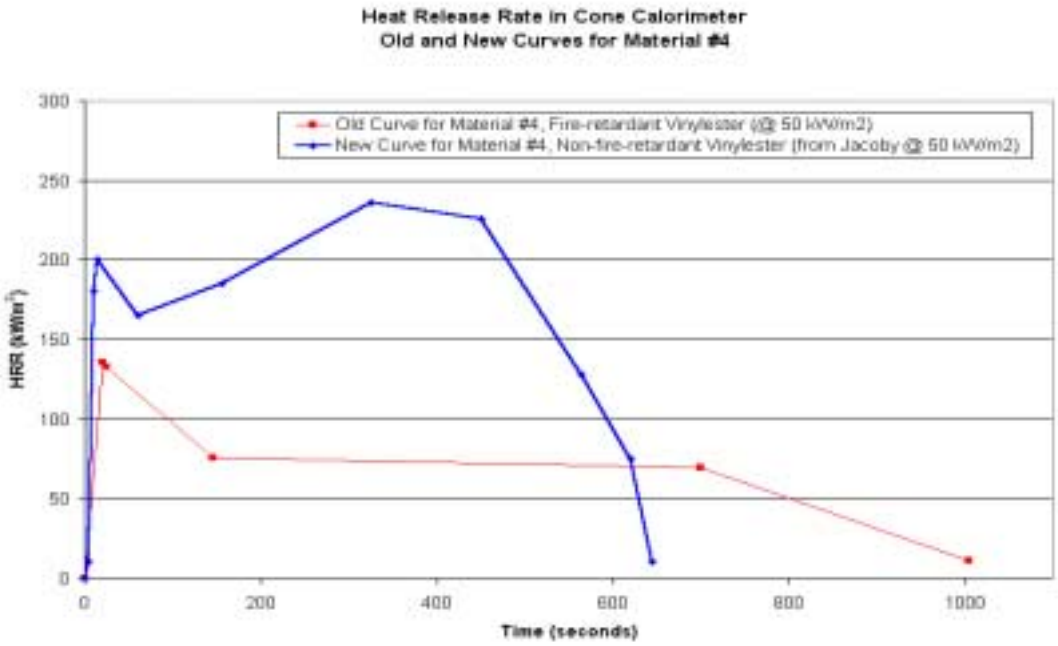

Figure B5-10. – Change of cone calorimeter curve for material #4.

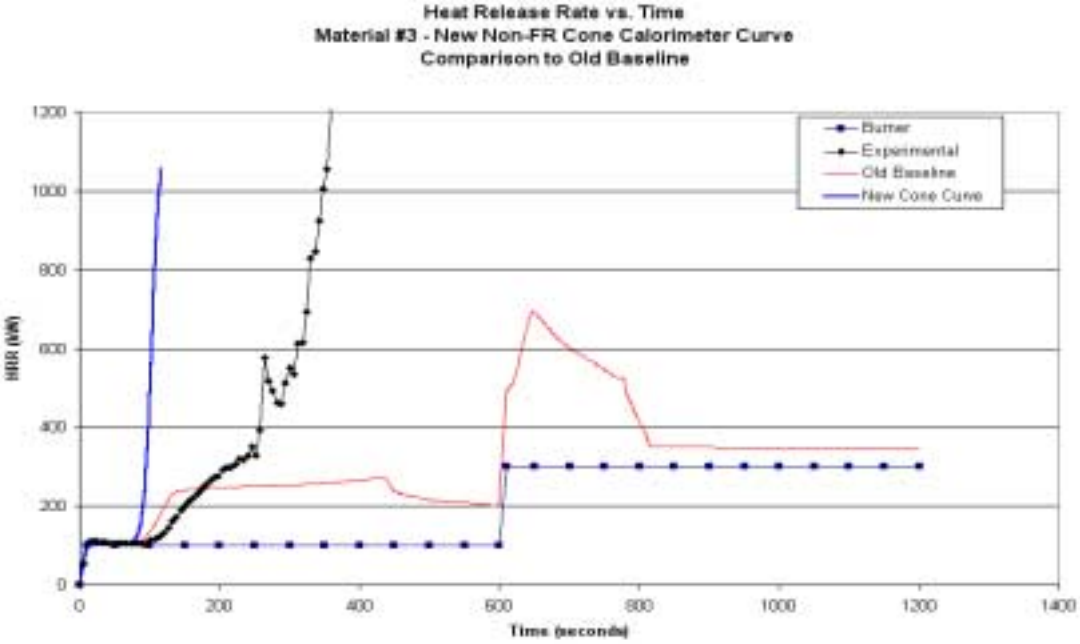

Figure B5-11. – Results from non-FR cone calorimeter curve for material #3.

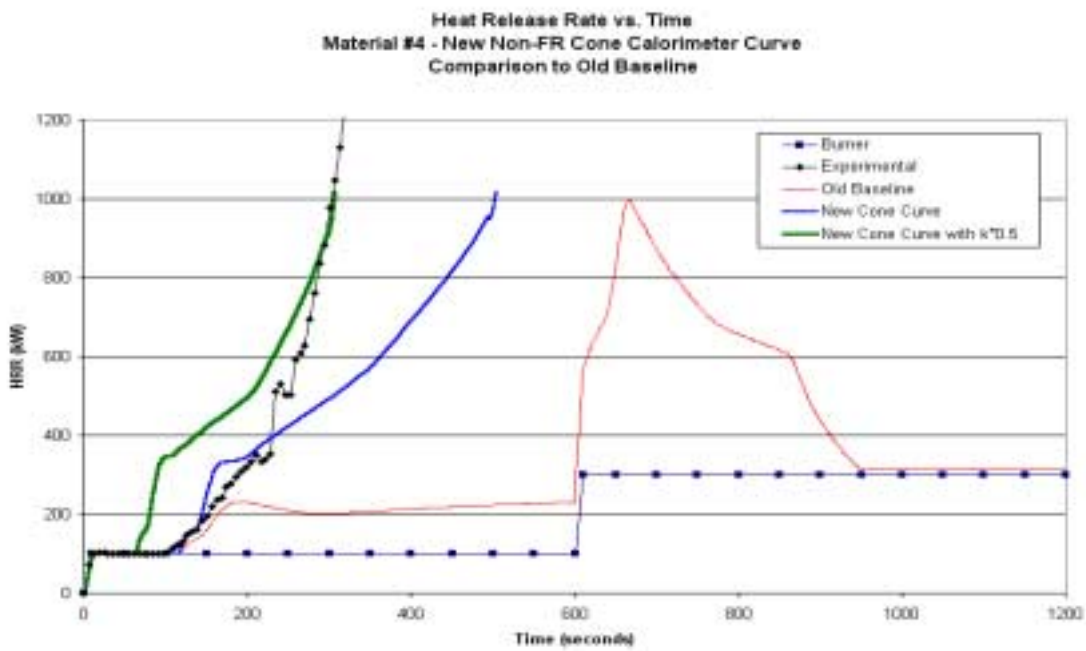

Figure B5-12. - Results from non-FR cone calorimeter curve for material #4.

Switching the cone curve for material #4 shows better results. The heat release rate continues to grow after ignition, but the slope of the continued growth is still shallower than that of the experimental curve. This simulation was conducting using the material properties ($k\rho c_p$, T_{ig}, k, etc.) of the fire-retardant material and the cone calorimeter curve of the non-fire-retardant material. It is possible that the effect of the fire-retardants combined with experimental error or uncertainty from cone calorimeter or LIFT data reduction has produced slightly inaccurate material properties.

For this reason, the thermal conductivity was decreased by a factor of two and an additional simulation was run. As shown in Figure B5-12, the slope of this new curve near flashover matches the experimental curve more closely. Additionally, the predicted time to flashover matches that observed experimentally. The purpose of doing this is to make the case that the fire-retardants contained in these materials may be adversely affecting the accuracy of the simulation. This is most likely the result of a combination of mechanisms, including the skewing of the experimentally derived material properties and the generation of a cone calorimeter curve that cannot be directly extrapolated to predict full-scale behavior due to the presence of fire-retardants. This also illustrates the importance of conducting a sensitivity analysis on material properties.

5.8 Additional variations

In addition to the parameters discussed in the previous sections, the compartment size and ventilation conditions were altered. The temperature of the wall lining material and ambient temperature were also varied. These effects are outlined in the following sections.

5.8.1 Compartment size and ventilation

The size of the compartment was varied by increasing its length and width by a factor of two and three, effectively multiplying the compartment volume by four and nine, respectively. The height was held constant so the flame spread on the ceiling is comparable to the baseline case. The specimen size was also held constant so that the total amount of fuel available for combustion does not change. Simulations were conducted for all nine materials. The results of these simulations show that doubling the length and width of the compartment has almost no effect on the heat release rate. A moderate effect was observed when the length and width of the compartment were tripled. The results for material #3 can be found in Figure B5-13 and are typical of most materials. An exception to this was seen with material #8 which shows almost no variation with compartment size or ventilation conditions. The predicted upper gas layer temperatures for material #3 are shown in Figure B5-14.

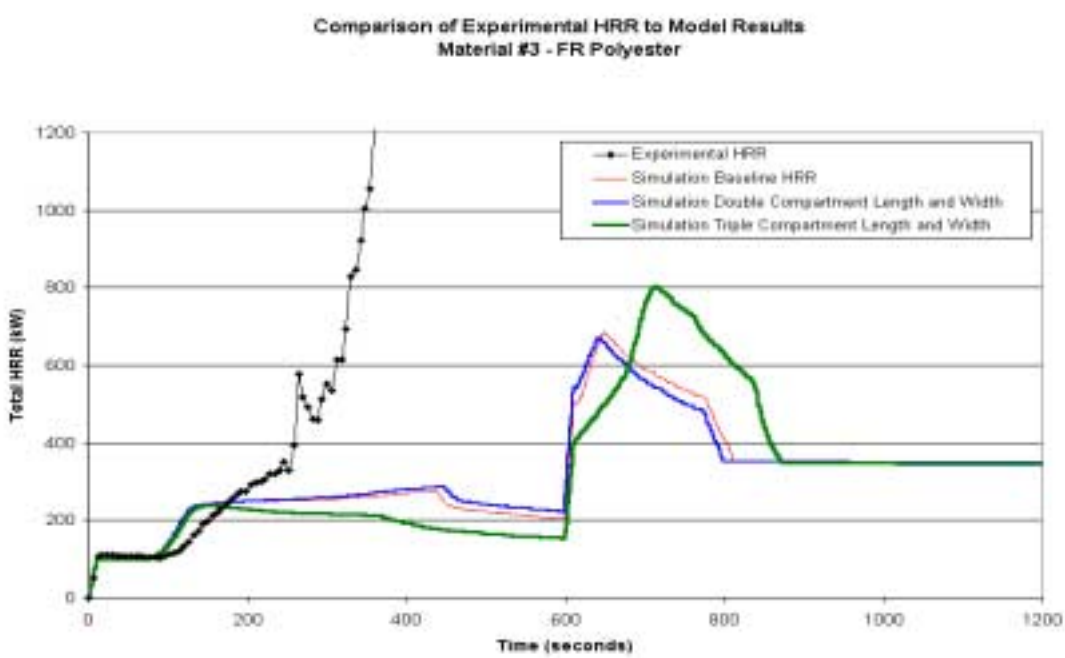

Figure B5-13. – Effect of compartment size on HRR for material #3.

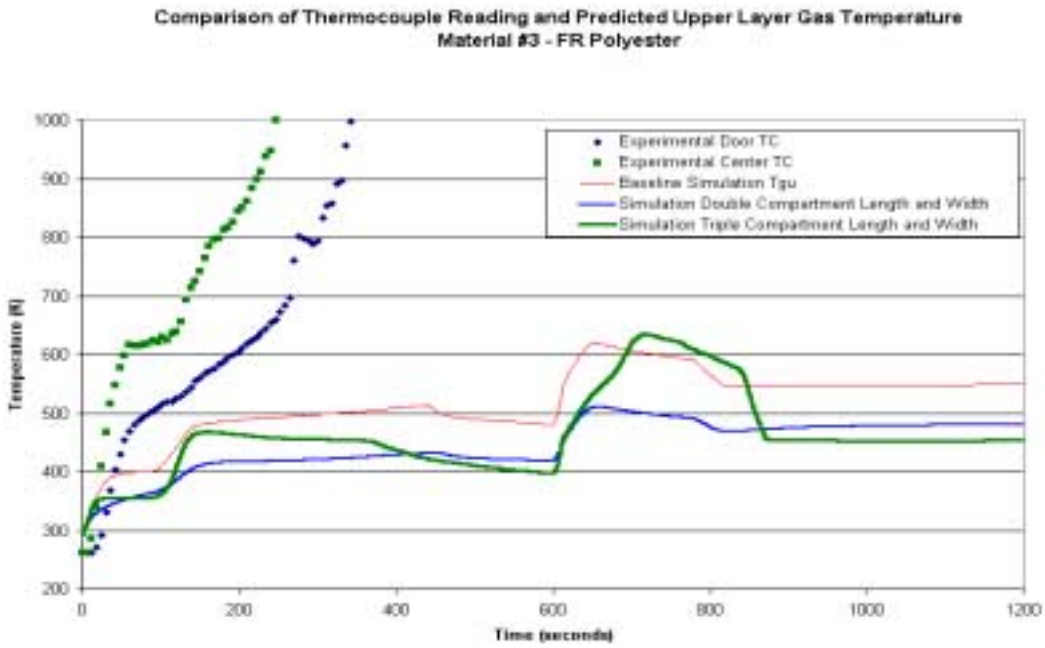

Figure B5-14. – Effect of compartment size on T_{gu} for material #3.

The effect that ventilation has on the model predictions was examined by increasing the size of the ventilation opening from 0.8m by 2.0m to 2.4m by 2.4m. This is analogous to completely opening the swinging walls that form the door in the full-scale test configuration. The simulations showed a cooler upper gas layer and a higher interface height compared to the baseline case. The change in heat release rate for material #9 is shown in Figure B5-15 and its corresponding gas layer temperatures are shown in Figure B5-16.

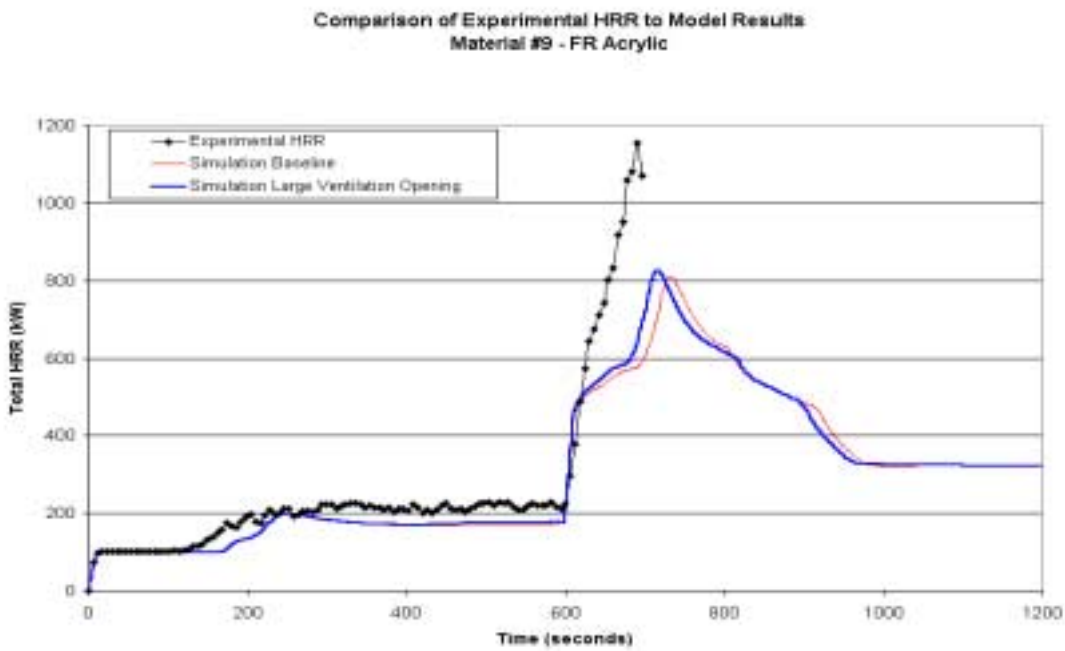

Figure B5-15. – Compartment ventilation effect on HRR for material #9.

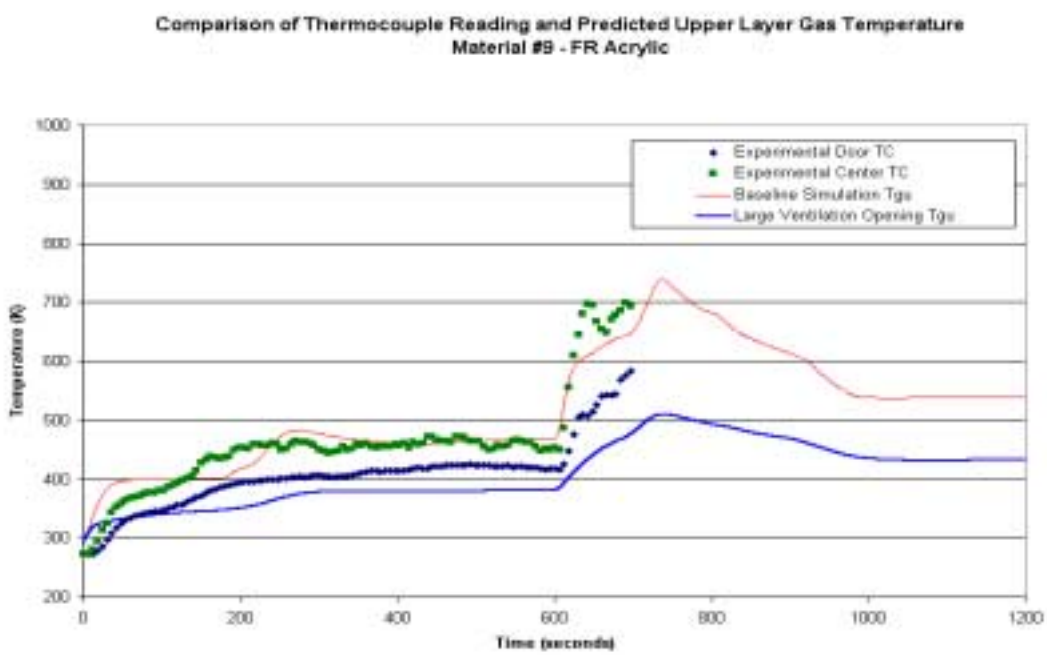

Figure B5-16. – Compartment ventilation effect on T_{gu} for material #9.

5.8.2 Initial temperature

The effect of varying the initial temperature of the wall lining material was also examined. All simulations presented thus far were run with an initial temperature of 293.15K for both the wall temperature and the ambient air temperature. It was expected that there would be little difference

between the results of a simulation with an initial temperature of 293.15K compared to 270K with all other inputs held constant. However, this is not the case as the model exhibits a significant dependence on initial temperature conditions. When the initial temperature is lowered from 293.15 K to 270K, the ignition is delayed by approximately 5 seconds. To validate this behavior, the integral governing the temperature of a semi-infinite solid exposed to a net flux that varies with time given by Carlsaw and Jaeger (Carlsaw, 1959) was numerically integrated using the trapezoidal rule (Bradley, 1995) and Gauss-Seidel iteration (Lay, 1997) for convergence. The delayed ignition at a lowered initial temperature as exhibited by the model is consistent with the results of this integration.

After ignition, the initial fire growth on the material with the reduced initial temperature is significantly more rapid than on the material with the higher initial temperature. Burnout also occurs more rapidly on the material with the lowered initial temperature. This phenomenon is shown in Figures 5-17 and 5-18 for materials #3 and #9.

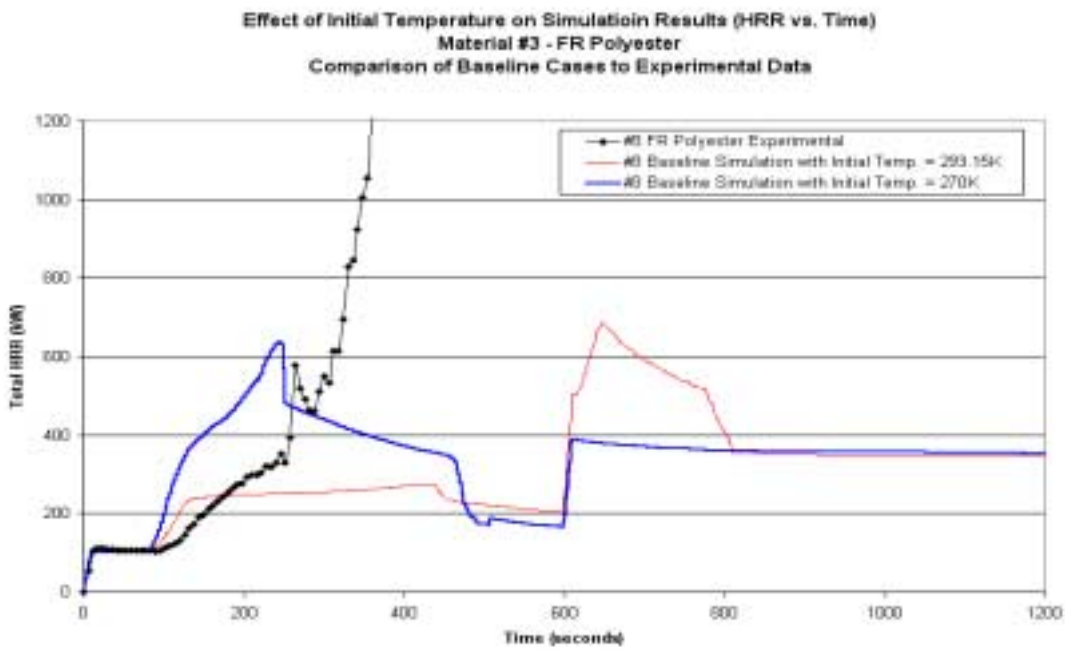

Figure B5-17. – Effect of initial temperature on heat release rate for material #8.

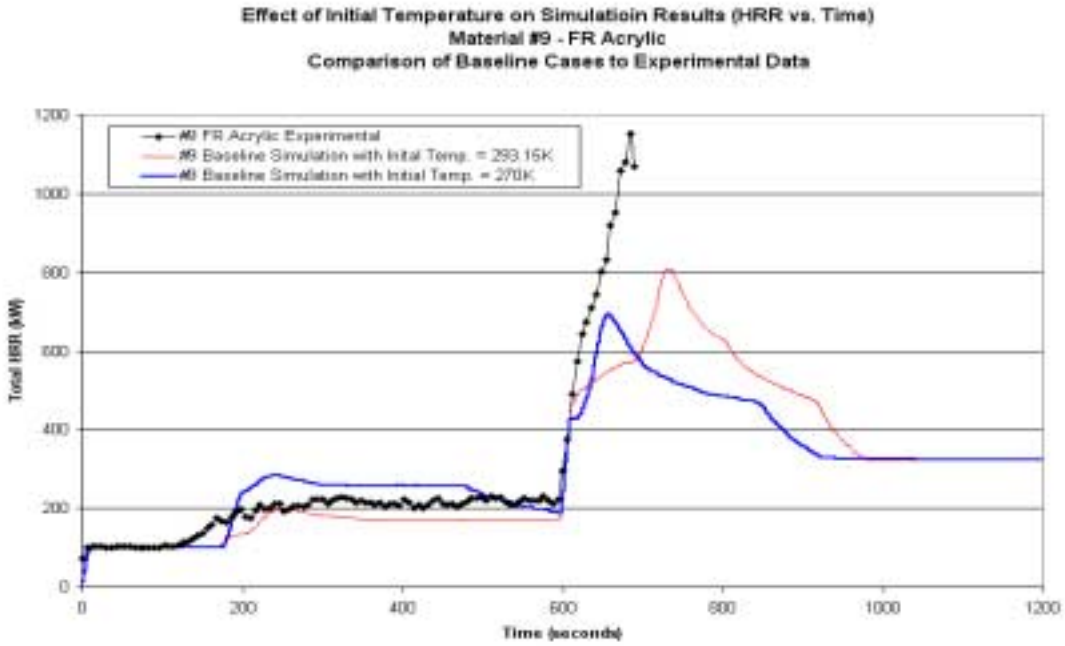

Figure B5-18. – Effect of initial temperature on heat release rate for material #9.

At this time it is known that the lowered initial temperature causes an increase in the overall heat flux distribution to the wall. Figure B5-19 shows the total heat flux to the wall versus distance from the floor at 10 seconds after ignition for material #3. It can be seen that for a distance greater than approximately 0.5 m, the total flux to the wall for an initial temperature of 270K is significantly higher than that with an initial temperature of 293.15K. This is also true for other times and for other materials.

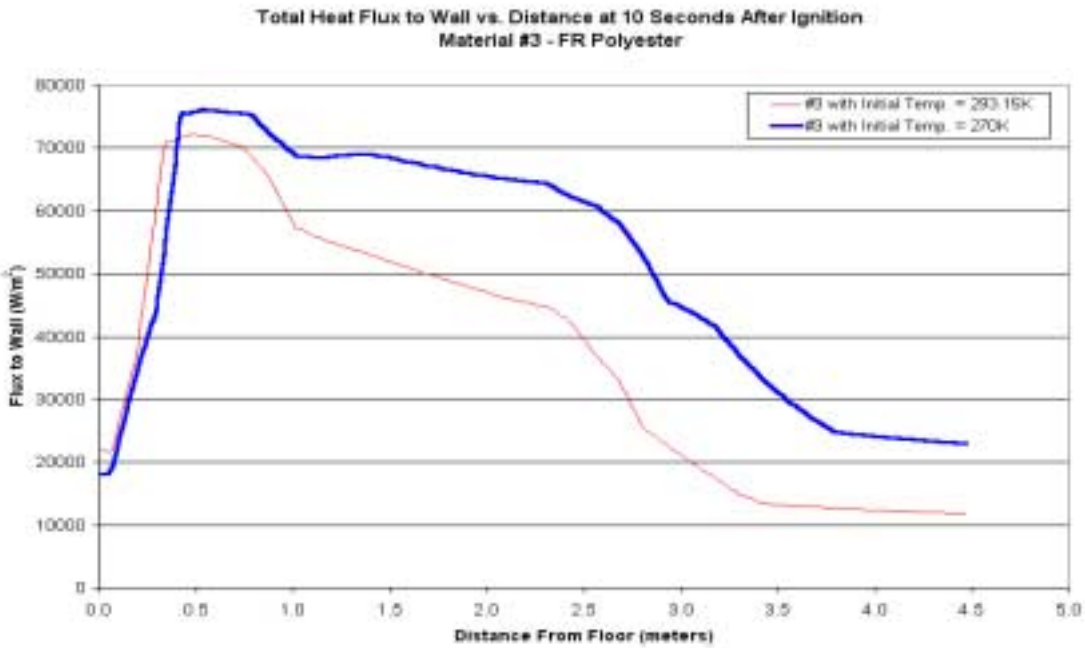

Figure B5-19. – Effect of initial temperature on heat release rate for material #9.

The increased flux to the wall causes an increase in the heat release rate because the mass loss rate of the wall fire is a function the incident flux at each node. The mechanism that is responsible for this increase in heat flux to the wall is unknown at this time. It is possible that this behavior is the result of a programming error or oversight that occurred as part of the algorithm implementation process. It is also possible that the model has been properly coded but the algorithm itself (Mitler, 1993, 1994) contains some particularity that has remained unnoticed to this point and is responsible for this behavior.

It should be noted that the stand-alone program SPREAD (Mitler, 1993) does not exhibit the same dependency on initial temperature that the enhanced CFAST/Mitler implementation does. In fact, a higher initial temperature corresponds to slightly more rapid fire growth in the stand-alone program. However, the changes and additions outlined in Mitler's second paper (Mitler, 1994) (namely radiative transfer between flames on the ceiling and the vertical walls) were never implemented into SPREAD. It is known that the enhanced radiation subroutine described in Section 2.3 is not causing the anomalous behavior because the same phenomenon (i.e., more rapid initial fire growth at a lower initial temperature) is seen when the enhanced radiation subroutine disabled. This same behavior is also observed when the CFAST/Mitler algorithm is run as a line burner against the sidewall. The implication is that this anomalous behavior is related to the model formulation or a coding error, however the exact problem has not been identified at this time.

6.0 CONCLUSIONS

This report has described the development and testing of a corner flame spread algorithm embedded within the zone model CFAST (Peacock, 1993, 1997). This section presents the strengths and weaknesses of the model and makes recommendations for future work.

6.1 Strengths of Model

Certain modules of Mitler's (Mitler, 1993, 1994) algorithm in its current form are particularly powerful. The model is well suited for simulating upward spread on walls. It couples all of the major variables and converges to a solution for the pyrolysis front position at each time step. The entire wall is discretized into elemental strips so that ignition can occur at only one strip, or over a range of strips. The algorithm also has a good pyrolysis submodel because the pyrolysis rate is tracked independently at each ignited element based on a total incident flux at that element and is grounded in bench-scale empirical data. The degree of preheating is also tracked independently at each element. This is possible because the subroutine that calculates the enhanced radiative exchange in the corner allows for a more detailed flux distribution than is feasible with other flame spread models. The algorithm in its current form considers a heat flux that varies with height and calculates the convective and radiative components of this flux separately.

An advantage of the current form of the Mitler flame spread model is that it has the ability to easily track species concentrations in the upper and lower layers because it has been embedded within CFAST. This can be accomplished by specifying the chemical composition of the lining material in the CFAST object database. The zone model then uses the heat release rate of the burning lining material to calculate the species concentrations that develop. This is useful if it ever becomes desirable to use the model to estimate the toxicity conditions during a room corner test.

With respect to the simulations on the nine materials that were discussed in this report, the model seems to perform well with materials that show significant burning, at least initially. Most simulations follow the slope of the experimental heat release rate curve after ignition until initial burnout occurs, at which point the slope is significantly decreased. This is indicative that the flame spread and pyrolysis modules are working well but there may be problems with the portion of the algorithm that governs burnout. It is hypothesized that this is a contributing factor toward the model's tendency to under-predict heat release rate, except for material #8 where the behavior is dominated by the high heat release rate of the cone calorimeter curve.

6.2 Weaknesses of Model

The flamespread model of Mitler (Mitler, 1993, 1994) in its current form does not consider gas phase phenomena. It is based solely on heat transfer in the condensed phase. Seven of the nine materials against which the model was validated were classified as fire-retardant. It is not known what type of fire-retardants was used in the manufacture of these materials; however, it is assumed that these fire-retardants function by hindering combustion in the gas phase. The model is not able to *directly* account for the gas phase effects of these retardants, although these gas phase phenomena are *indirectly* accounted for through the cone calorimeter curves provided to the model as input. One weakness of the model in its current form is that the bench-scale tests may not translate well to full-scale behavior as a result of the fire-retardants acting in the gas phase during combustion in the cone calorimeter. It was previously hypothesized that this is a significant factor contributing toward the model's tendency to under-predict flame spread on fire-retardant materials.

A weakness with this algorithm, and flame spread models in general, is that the experimentally observed shape of the pyrolysis region cannot be described by a simple geometric expression. As a result of this, an over-simplification of the shape of the pyrolysis region is required. The general shape of the pyrolysis region in the model of Mitler (Mitler, 1993, 1994) is shown in Figure B2-1, although it should be noted that this figure depicts more rapid lateral spread in the hot upper gas layer. The shape of the pyrolysis region observed in the video record of the tests conducted by Janssens (Janssens, 1998) is dissimilar to that simulated by the modified flame spread algorithm. The shape of the pyrolysis region is not seen to be discontinuous at the interface, but rather it fans outward toward the ceiling. Additionally, there are three other issues that need to be considered.

#1) The simulations revealed a potential problem with the algorithm's calculation of burnout, especially on the ceiling. Burnout occurred extremely quickly in some cases, detrimentally affecting the simulation results. This effect was even more pronounced on the ceiling. Therefore, the simulation of fire spread across the ceiling is a weakness of the model in its current form.

#2) Once multiple pyrolysis zones exist and they are sufficiently far apart, the validity of the flame height and heat flux calculations is questionable because the algorithm was written to simulate only one pyrolysis zone.

#3) The sensitive dependence on initial temperature conditions is a current weakness of the model. One would expect a slight change in the flamespread behavior to be imparted as a result of a change in the initial temperature of the lining material. However, it was

recently discovered that the model behavior exhibits a significant dependence on the initial temperature conditions.

6.3 Recommendations for Future Work

It is felt that the results of the flame spread model can be improved significantly with additional work. The model development is still in its incipient stages because a considerable portion of the time spent on programming to date has involved the insertion of the algorithm into CFAST and the coding of enhanced radiation network. Several areas have been identified where additional work will likely improve the results of the model considerably. This model, in a more refined version, has the potential to predict room corner test data much more accurately than is indicated by the results presented in this report. Several tasks have been identified that would be beneficial for future research. These are as follows:

(1) Study the effect of fire-retardants and gas-phase phenomena to determine a better way of modeling the complex behavior for which these effects are significant. A possible solution for this problem is to introduce a time-dependent combustion efficiency to describe the changing state of material combustion from the fire-retardant. This is feasible because the model in its current form already utilizes a constant user-specified combustion efficiency.

(2) Compare additional ISO 9705 experimental data to the results predicted by the model for other common non-fire-retardant materials. This would be helpful in further verifying the capabilities of the algorithm. In this project only one such material was simulated, leaving the possibility that other issues concerning “simple” materials may still exist.

(3) Re-examine the manner in which the mass loss rate (and effectively the burn-out rate) is calculated, particularly on the ceiling. Currently, a weighting scheme carried over from the original algorithm is used in the mass loss rate calculations. This scheme was developed for rectangular strips of constant area and may be invalid when used with the circular ceiling strips because their area increases with distance from the corner.

(4) Ensure the validity of the portion of the algorithm that tracks multiple pyrolysis fronts. The algorithm currently calculates several parameters based on the height of a *single* pyrolysis zone. The validity of these calculations (particularly flame height and heat flux to the walls/ceiling) must be examined once multiple pyrolysis zones are established at separate heights.

(5) Review the assumptions made in the use of the heat flux map provided by Dillon (Dillon, 1998). The area of high flux near the ceiling was removed because ignition occurred near the ceiling, while experimental observation places ignition further down on the wall. Experiments designed to determine why sustained ignition does not occur at the area of highest flux would be a good first step in attempting to implement a better heat flux map into the algorithm. Additionally, the validity of translating these two-dimensional heat flux maps to one-dimension requires examination. Using a scheme that tracks a two-dimensional wall temperature and heat flux distribution is a way to incorporate more detail into the model.

(6) Verify the validity of using a flame transmissivity factor to attenuate radiation and ensure that energy is being conserved. The possibility exists that the use of this factor does not conserve energy within the radiation network.

(7) Identify the mechanism that is causing the anomalous behavior with regards to the sensitive dependence on initial temperature conditions. Determine whether this is a fundamental shortcoming of the algorithm itself or the result of a coding error or oversight during the implementation process.

7.0 INPUTS TO THE ALGORITHM

SUMMARY OF BASELINE INPUT VALUES

These data were used as baseline values in the validation of the modified Mitler flame spread algorithm.
Values without a superscript to the right were either reported in Janssens (1998) or derived from cone calorimeter data reported therein.
For superscripted values, see note below.

ALGORITHM BASELINE INPUTS															
Material	Generic Name	T_{ig} K	$T_{s,min}$ K	Φ (kW^2/m^3)	ε †	τ †	k W/m·K	ρ kg/m^3	c_p J/kg·K	$k\rho c_p$ ($kW^2 \cdot s/m^4K^2$)	ΔH_{eff} kJ/g	$\Delta H_c/L_v$ †	L_v kJ/g	Q'' MJ/m^2	δ m
1	FR phenolic	876	788[1]	15.59[2]	0.9[3]	0.5[4]	1.274[5]	1750	1000[6]	2.23	8.22	1.22	6.74	18.12	0.0238
2	Fire restricting material	905	815[1]	15.59[2]	0.9[3]	0.5[4]	6.708[5]	240	1000[6]	1.61	9.63	0.68	14.16	8.08	0.0318
3	FR polyester	671	639	12.13	0.9[3]	0.5[4]	0.782[5]	1650	1000[6]	1.29	11.28	0.75	15.04	35.62	0.0252
4	FR vinylester	671	639	12.32	0.9[3]	0.5[4]	1.221[5]	1630	1000[6]	1.99	13.43	1.26	10.66	49.03	0.0248
5	FR epoxy	681	613[1]	15.59[2]	0.9[3]	0.5[4]	0.958[5]	1910	1000[6]	1.83	8.70	0.18	48.33	12.16	0.0239
6	Coated FR epoxy	791	712[1]	15.59[2]	0.9[3]	0.5[4]	0.534[5]	1910	1000[6]	1.02	8.80	0.24	36.67	12.07	0.0239
7	Textile wall covering	726	653[1]	15.59[2]	0.9[3]	0.5[4]	1.085[5]	1760	1000[6]	1.91	9.08	1.39	6.53	5.80	0.0253[7]
8	Polyester	662	479	19.02	0.9[3]	0.5[4]	0.597[5]	1390	1000[6]	0.83	21.60	2.86	7.55	61.50	0.0241
9	FR modified acrylic	681	569	23.22	0.9[3]	0.5[4]	1.511[5]	1880	1000[6]	2.84	12.28	1.04	11.81	41.16	0.0252

Notes: [1] $T_{s,min}$ was set to $0.9T_{ig}$ when data were not available (not grounded in literature)

[2] Φ was set to the average of materials 3, 4, 8, 9 when data were not available

[3] ε was set to 0.9 as suggested by Grenier (1998)

[4] τ = 0.5 was selected as median value after Karlsson (1992)

[5] k was backed out of reported value of $k\rho c_p$, using c_p = 1000 J/kg·K

[6] c_p was held constant at 1000 J/kg·K as suggested by Grenier (1998)

[7] Data not available. $\therefore \delta$ was set to average thickness of other materials

BASELINE INPUTS FOR MATERIAL #1--FR PHENOLIC

PROP_1?.DAT

MATERIAL PROPERTIES / INPUT PARAMETERS		
Height of bottom of slab above floor	0	m
Material density (ρ)	1750	kg/m^3
Material thickness (δ)	0.0238	m
Material specific heat (c_p)	1000	J/kg·K
Material thermal conductivity (k)	1.274	W/m·K
Material ignition Temperature (T_{ig})	876	K
Material initial uniform temperature	293.15	K
Timestep	0.5	sec
Output interval	1	sec
Simulation length	1200	sec
Specific heat of product gases	1340	J/kg·K
Net heat of complete combustion	1.64E+07	J/kg·K
Efficiency of combustion (χ_A)	0.5	
Radiative fraction (χ_{rad})	0.3	
Material emissivity (ε)	0.9	
Flame transmissivity (τ_{flame})	0.5	
Lateral flame spread parameter (Φ)	15.59	kW^2/m^3
Min. surface temp. for lateral spread ($T_{s,min}$)	788	K
Width of slab (2 x width of shorter wall)	4.8	m
Ceiling present?	1	(yes)
Allow multiple pyrolysis zones?	1	(yes)
Average heat flux from the ceiling	2000	kW/m^2
Paramater p for ceiling/wall arm extensions	1	m^{-1}
Combustible ceiling lining present?	1	(yes)
Corner configuration present?	1	(yes)
Use Complex radiation?	1	(yes)
Use gaslayer calcs. In radiation calcs.?	1	(yes)
Use accurate beam length calculation in radiation calculations?	0	(no)

1_75.MLR

CONE CURVE		
Point #	Time sec	HRR kW/m^2
1	0	0.0
2	5	20.9
3	40	64.0
4	46	69.5
5	60	65.3
6	145	53.0
7	195	44.3
8	310	37.8
9	340	28.2
10	395	23.6
11	410	25.9
12	460	20.5
13	475	22.3
14		
15		
16		
17		
18		
19		
20		
21		
22		
23		
24		
25		
Irrad:	75	kW/m^2

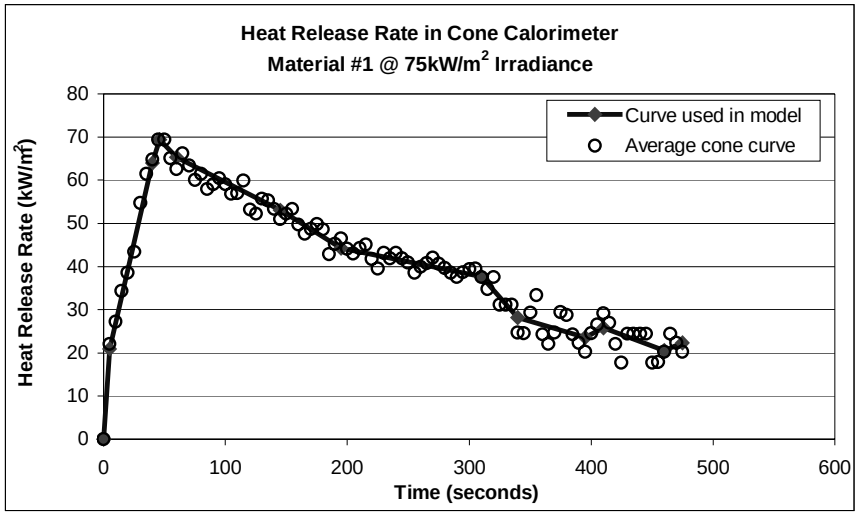

USCG.BRN

BURNER INPUTS		
Burner height above floor	0.152	m
Width of burner side	0.170	m
Use heat flux map?	1	(yes)

ADDITIONAL CONE CALORIMETER CURVES FOR MATERIAL #1--FR PHENOLIC

1_100.MLR

CONE CURVE		
Point #	Time sec	HRR kW/m^2
1	0	0.0
2	5	15.7
3	35	36.7
4	60	67.0
5	80	72.4
6	85	72.4
7	115	68.0
8	350	32.0
9	450	23.0
10	565	17.4
11		
12		
13		
14		
15		
16		
17		
18		
19		
20		
21		
22		
23		
24		
25		
Irrad:	100	kW/m^2

1_50.MLR

CONE CURVE		
Point #	Time sec	HRR kW/m^2
1	0	0.0
2	15	22.3
3	65	29.0
4	85	29.9
5	100	25.7
6	115	18.8
7	140	17.6
8	150	13.7
9	175	14.7
10	225	14.7
11	240	13.8
12		
13		
14		
15		
16		
17		
18		
19		
20		
21		
22		
23		
24		
25		
Irrad:	50	kW/m^2

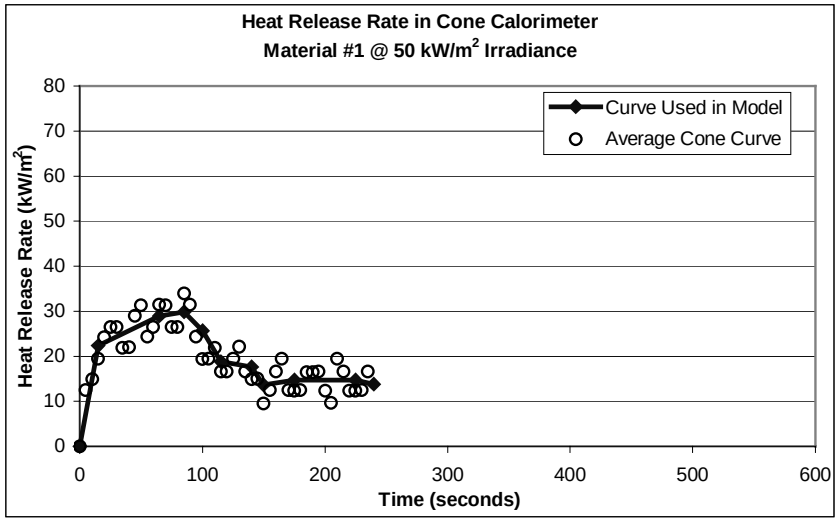

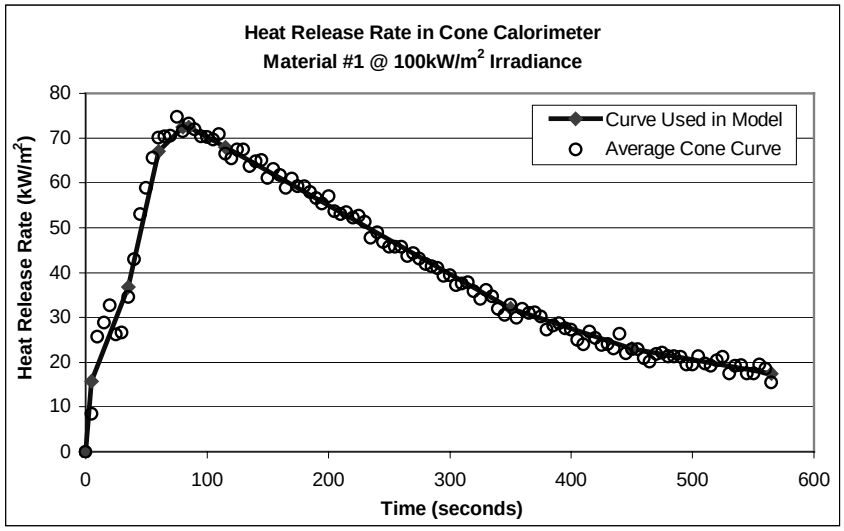

BASELINE INPUTS FOR MATERIAL #2--FIRE RESTRICTING MATERIAL

PROP_2?.DAT

MATERIAL PROPERTIES / INPUT PARAMETERS		
Height of bottom of slab above floor	0	m
Material density (ρ)	240	kg/m^3
Material thickness (δ)	0.0318	m
Material specific heat (c_p)	1000	J/kg·K
Material thermal conductivity (k)	6.708	W/m·K
Material ignition Temperature (T_{ig})	905	K
Material initial uniform temperature	293.15	K
Timestep	0.5	sec
Output interval	1	sec
Simulation length	1200	sec
Specific heat of product gases	1340	J/kg·K
Net heat of complete combustion	1.93E+07	J/kg·K
Efficiency of combustion (χ_A)	0.5	
Radiative fraction (χ_{rad})	0.3	
Material emissivity (ε)	0.9	
Flame transmissivity (τ_{flame})	0.5	
Lateral flame spread parameter (Φ)	15.59	kW^2/m^3
Min. surface temp. for lateral spread ($T_{s,min}$)	815	K
Width of slab (2 x width of shorter wall)	4.8	m
Ceiling present?	1	(yes)
Allow multiple pyrolysis zones?	1	(yes)
Average heat flux from the ceiling	2000	kW/m^2
Paramater p for ceiling/wall arm extensions	1	m^{-1}
Combustible ceiling lining present?	1	(yes)
Corner configuration present?	1	(yes)
Use Complex radiation?	1	(yes)
Use gaslayer calcs. In radiation calcs.?	1	(yes)
Use accurate beam length calculation in radiation calculations?	0	(no)

2_75.MLR

CONE CURVE		
Point #	Time sec	HRR kW/m^2
1	0	0.0
2	15	29.1
3	30	31.6
4	70	29.3
5	80	29.3
6	90	30.9
7	125	27.5
8	175	21.7
9	190	20.4
10	225	21.4
11	250	19.5
12	285	22.6
13	310	21.4
14	340	22.1
15	370	22.2
16	430	22.2
17		
18		
19		
20		
21		
22		
23		
24		
25		
Irrad:	75	kW/m^2

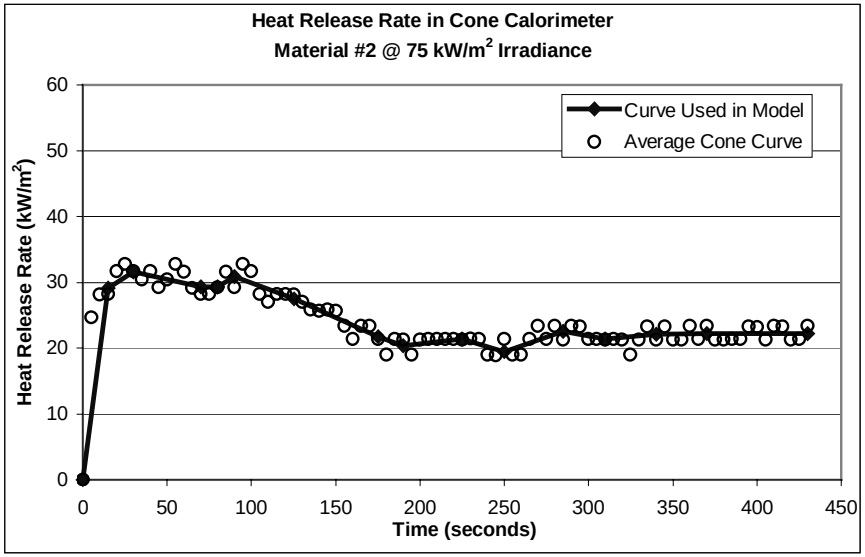

USCG.BRN

BURNER INPUTS		
Burner height above floor	0.152	m
Width of burner side	0.170	m
Use heat flux map?	1	(yes)

ADDITIONAL CONE CALORIMETER CURVES FOR MATERIAL #2--FIRE RESTRICTING MATERIAL

2_100.MLR

CONE CURVE		
Point #	Time sec	HRR kW/m^2
1	0	0.0
2	5	25.1
3	20	43.8
4	25	44.9
5	35	42.9
6	55	45.7
7	160	31.1
8	220	25.0
9	255	23.5
10	280	22.1
11	305	20.0
12		
13		
14		
15		
16		
17		
18		
19		
20		
21		
22		
23		
24		
25		
Irrad:	100 kW/m^2	

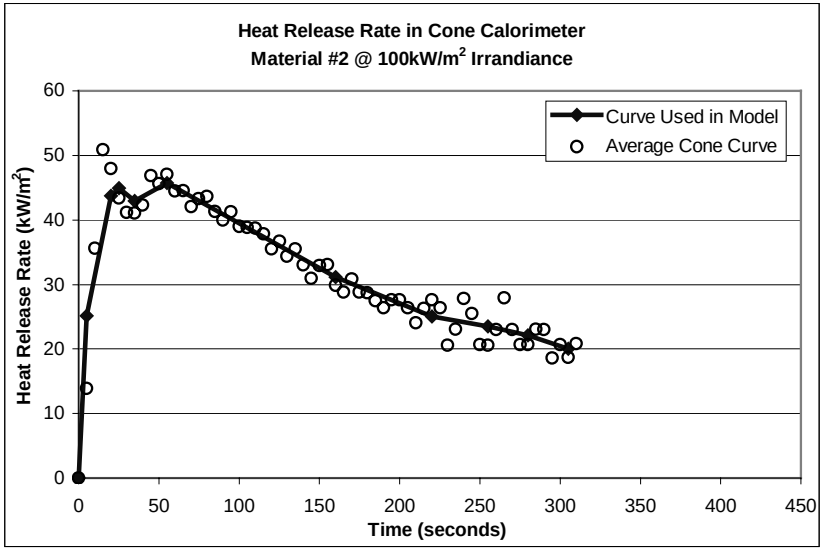

BASELINE INPUTS FOR MATERIAL #3--FR POLYESTER

PROP_3?.DAT

MATERIAL PROPERTIES / INPUT PARAMETERS		
Height of bottom of slab above floor	0	m
Material density (ρ)	1650	kg/m^3
Material thickness (δ)	0.0252	m
Material specific heat (c_p)	1000	J/kg·K
Material thermal conductivity (k)	0.782	W/m·K
Material ignition Temperature (T_{ig})	671	K
Material initial uniform temperature	293.15	K
Timestep	0.5	sec
Output interval	1	sec
Simulation length	1200	sec
Specific heat of product gases	1340	J/kg·K
Net heat of complete combustion	3.25E+07	J/kg·K
Efficiency of combustion (χ_A)	0.347	
Radiative fraction (χ_{rad})	0.476	
Material emissivity (ε)	0.9	
Flame transmissivity (τ_{flame})	0.5	
Lateral flame spread parameter (Φ)	12.13	kW^2/m^3
Min. surface temp. for lateral spread ($T_{s,min}$)	639	K
Width of slab (2 x width of shorter wall)	4.8	m
Ceiling present?	1	(yes)
Allow multiple pyrolysis zones?	1	(yes)
Average heat flux from the ceiling	2000	kW/m^2
Paramater p for ceiling/wall arm extensions	1	m^{-1}
Combustible ceiling lining present?	1	(yes)
Corner configuration present?	1	(yes)
Use Complex radiation?	1	(yes)
Use gaslayer calcs. In radiation calcs.?	1	(yes)
Use accurate beam length calculation in radiation calculations?	0	(no)

3_50.MLR

CONE CURVE		
Point #	Time sec	HRR kW/m^2
1	0	0.0
2	30	114.9
3	160	81.1
4	260	73.5
5	375	60.4
6	490	48.1
7	735	43.8
8		
9		
10		
11		
12		
13		
14		
15		
16		
17		
18		
19		
20		
21		
22		
23		
24		
25		
Irrad:	50	kW/m^2

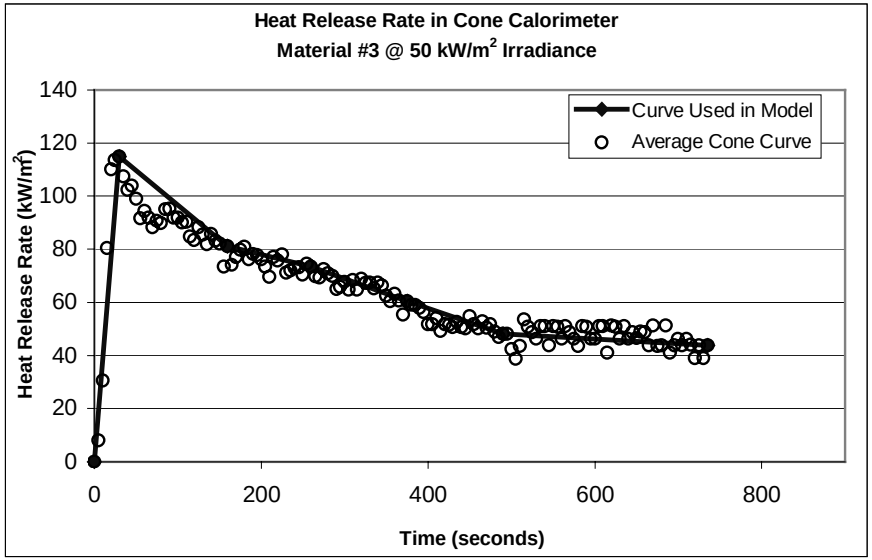

USCG.BRN

BURNER INPUTS		
Burner height above floor	0.152	m
Width of burner side	0.170	m
Use heat flux map?	1	(yes)

ADDITIONAL CONE CALORIMETER CURVES FOR MATERIAL #3--FR POLYESTER

3_75.MLR

CONE CURVE		
Point #	Time sec	HRR kW/m^2
1	0	0
2	10	7.35
3	25	129.75
4	30	133.75
5	75	105
6	155	97.5
7	215	87.1
8	375	79.95
9	485	53.8
10	650	30
11	820	9
12		
13		
14		
15		
16		
17		
18		
19		
20		
21		
22		
23		
24		
25		
Irrad:	75	kW/m^2

3_25.MLR

CONE CURVE		
Point #	Time sec	HRR kW/m^2
1	0	0
2	5	17.1
3	40	93.1
4	70	84.54
5	100	52.72
6	115	54
7	140	45.52
8	155	51.2
9	165	51.12
10	210	42.44
11	230	43.94
12	255	34
13		
14		
15		
16		
17		
18		
19		
20		
21		
22		
23		
24		
25		
Irrad:	25	kW/m^2

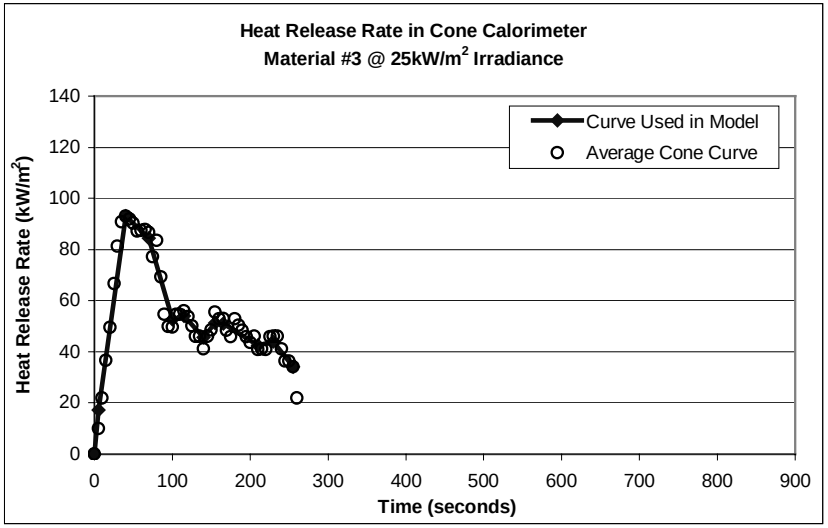

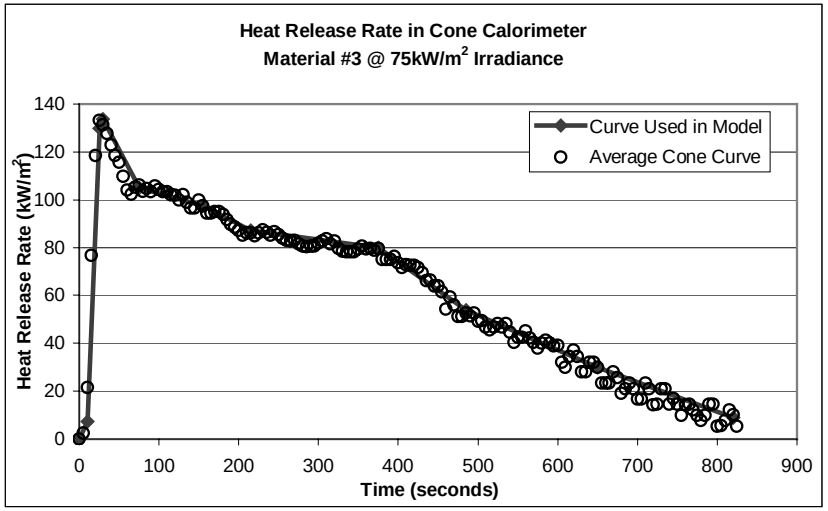

BASELINE INPUTS FOR MATERIAL #4--FR VINYLESTER

PROP_4?.DAT

MATERIAL PROPERTIES / INPUT PARAMETERS		
Height of bottom of slab above floor	0	m
Material density (ρ)	1630	kg/m^3
Material thickness (δ)	0.0248	m
Material specific heat (c_p)	1000	J/kg·K
Material thermal conductivity (k)	1.221	W/m·K
Material ignition Temperature (T_{ig})	671	K
Material initial uniform temperature	293.15	K
Timestep	0.5	sec
Output interval	1	sec
Simulation length	1200	sec
Specific heat of product gases	1340	J/kg·K
Net heat of complete combustion	2.69E+07	J/kg·K
Efficiency of combustion (χ_A)	0.5	
Radiative fraction (χ_{rad})	0.3	
Material emissivity (ε)	0.9	
Flame transmissivity (τ_{flame})	0.5	
Lateral flame spread parameter (Φ)	12.315	kW^2/m^3
Min. surface temp. for lateral spread ($T_{s,min}$)	639	K
Width of slab (2 x width of shorter wall)	4.8	m
Ceiling present?	1	(yes)
Allow multiple pyrolysis zones?	1	(yes)
Average heat flux from the ceiling	2000	kW/m^2
Paramater p for ceiling/wall arm extensions	1	m^{-1}
Combustible ceiling lining present?	1	(yes)
Corner configuration present?	1	(yes)
Use Complex radiation?	1	(yes)
Use gaslayer calcs. In radiation calcs.?	1	(yes)
Use accurate beam length calculation in radiation calculations?	0	(no)

4_50.MLR

CONE CURVE		
Point #	Time sec	HRR kW/m^2
1	0	0.0
2	20	135.3
3	25	132.7
4	145	75.7
5	700	69.3
6	1005	10.8
7		
8		
9		
10		
11		
12		
13		
14		
15		
16		
17		
18		
19		
20		
21		
22		
23		
24		
25		
Irrad:	50	kW/m^2

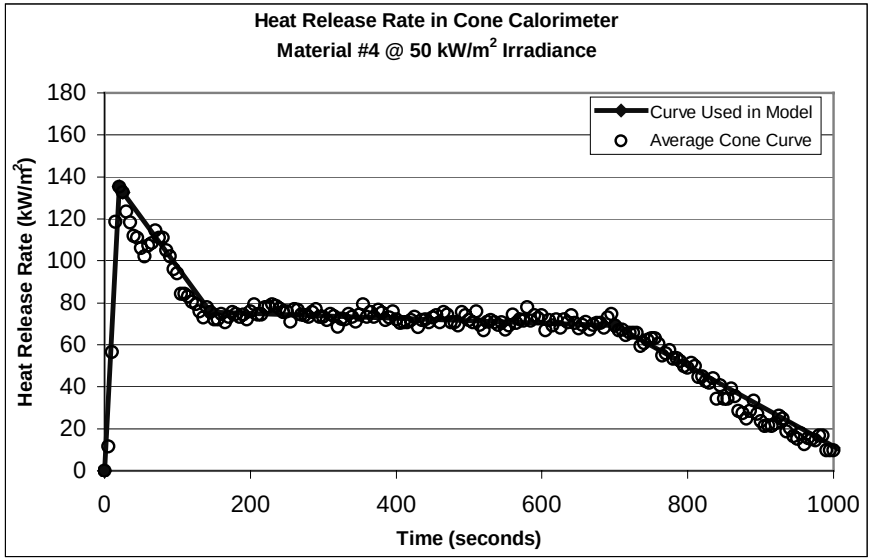

USCG.BRN

BURNER INPUTS		
Burner height above floor	0.152	m
Width of burner side	0.170	m
Use heat flux map?	1	(yes)

ADDITIONAL CONE CALORIMETER CURVES FOR MATERIAL #4--FR VINYLESTER

4_75.MLR

CONE CURVE		
Point #	Time sec	HRR kW/m^2
1	0	0
2	5	2.2
3	25	158.05
4	95	120.4
5	150	117
6	230	98
7	405	92.65
8	540	66.75
9	845	17.45
10	855	13.35
11		
12		
13		
14		
15		
16		
17		
18		
19		
20		
21		
22		
23		
24		
25		
Irrad:	75	kW/m^2

4_25.MLR

CONE CURVE		
Point #	Time sec	HRR kW/m^2
1	0	0
2	5	3.7
3	25	93.5
4	30	99.95
5	75	83.7
6	100	76.15
7	145	64.5
8	165	64.6
9	250	57
10	260	28.3
11		
12		
13		
14		
15		
16		
17		
18		
19		
20		
21		
22		
23		
24		
25		
Irrad:	25	kW/m^2

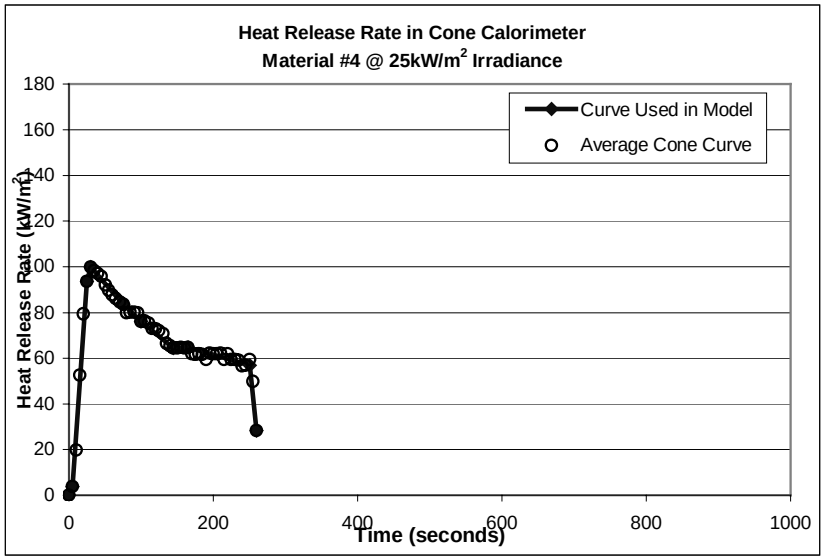

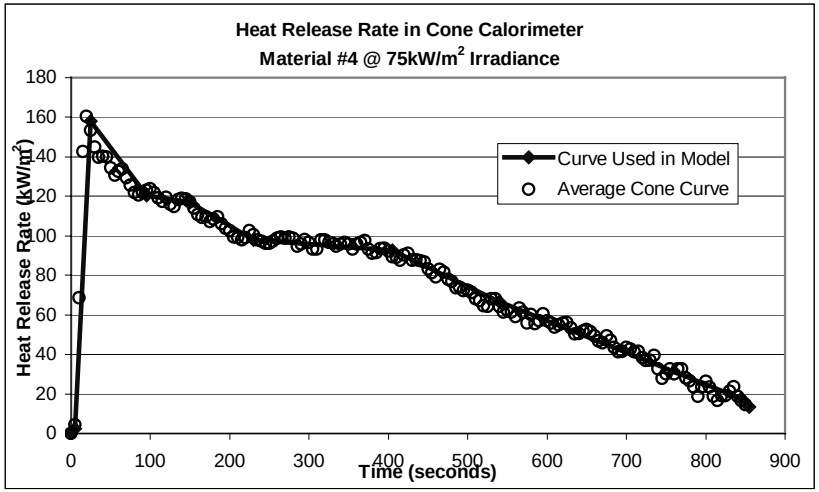

BASELINE INPUTS FOR MATERIAL #5--FR EPOXY

PROP_5?.DAT

MATERIAL PROPERTIES / INPUT PARAMETERS		
Height of bottom of slab above floor	0	m
Material density (ρ)	1910	kg/m^3
Material thickness (δ)	0.0239	m
Material specific heat (c_p)	1000	J/kg·K
Material thermal conductivity (k)	0.958	W/m·K
Material ignition Temperature (T_{ig})	681	K
Material initial uniform temperature	293.15	K
Timestep	0.5	sec
Output interval	1	sec
Simulation length	1200	sec
Specific heat of product gases	1340	J/kg·K
Net heat of complete combustion	1.74E+07	J/kg·K
Efficiency of combustion (χ_A)	0.5	
Radiative fraction (χ_{rad})	0.3	
Material emissivity (ε)	0.9	
Flame transmissivity (τ_{flame})	0.5	
Lateral flame spread parameter (Φ)	15.59	kW^2/m^3
Min. surface temp. for lateral spread ($T_{s,min}$)	613	K
Width of slab (2 x width of shorter wall)	4.8	m
Ceiling present?	1	(yes)
Allow multiple pyrolysis zones?	1	(yes)
Average heat flux from the ceiling	2000	kW/m^2
Paramater p for ceiling/wall arm extensions	1	m^{-1}
Combustible ceiling lining present?	1	(yes)
Corner configuration present?	1	(yes)
Use Complex radiation?	1	(yes)
Use gaslayer calcs. In radiation calcs.?	1	(yes)
Use accurate beam length calculation in radiation calculations?	0	(no)

5_75.MLR

CONE CURVE		
Point #	Time sec	HRR kW/m^2
1	0	0.0
2	5	10.8
3	15	76.6
4	25	81.4
5	35	83.0
6	47.5	62.5
7	62.5	60.0
8	80	47.0
9	120	52.0
10	155	48.0
11	200	48.0
12	265	42.8
13	355	21.2
14	395	16.5
15	472.5	14.6
16		
17		
18		
19		
20		
21		
22		
23		
24		
25		
Irrad:	75	kW/m^2

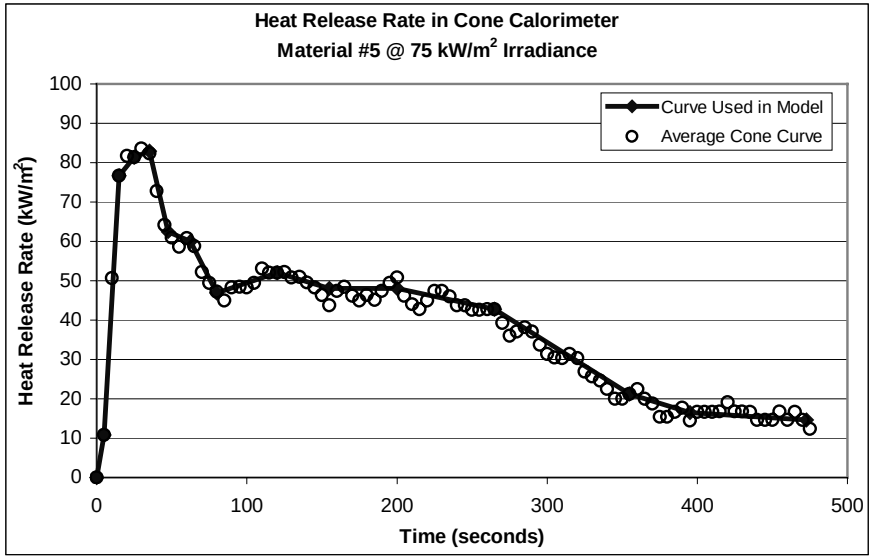

USCG.BRN

BURNER INPUTS		
Burner height above floor	0.152	m
Width of burner side	0.170	m
Use heat flux map?	1	(yes)

ADDITIONAL CONE CALORIMETER CURVES FOR MATERIAL #5--FR EPOXY

5_100.MLR

CONE CURVE		
Point #	Time sec	HRR kW/m^2
1	0	0.0
2	10	47.9
3	15	91.1
4	40	73.1
5	70	43.6
6	140	37.0
7	195	41.5
8	295	27.7
9	330	19.0
10	425	14.3
11		
12		
13		
14		
15		
16		
17		
18		
19		
20		
21		
22		
23		
24		
25		
Irrad:	100	kW/m^2

5_50.MLR

CONE CURVE		
Point #	Time sec	HRR kW/m^2
1	0	0.0
2	5	27.0
3	17.5	50.0
4	45	67.0
5	60	55.7
6	70	44.1
7	85	38.3
8	115	43.2
9	130	34.9
10		
11		
12		
13		
14		
15		
16		
17		
18		
19		
20		
21		
22		
23		
24		
25		
Irrad:	50	kW/m^2

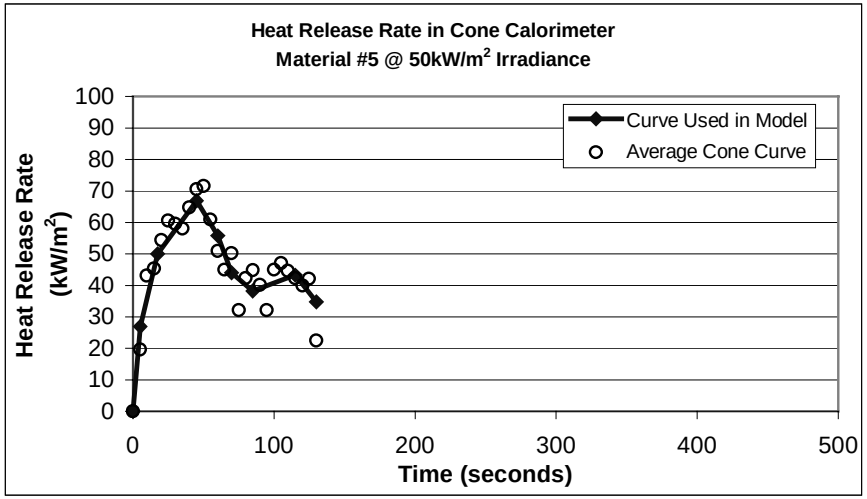

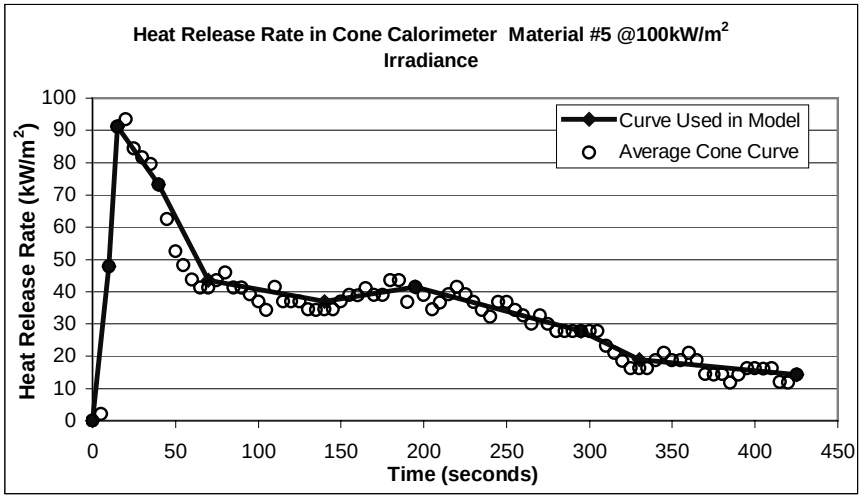

BASELINE INPUTS FOR MATERIAL #6--COATED FR EPOXY

PROP_6?.DAT

MATERIAL PROPERTIES / INPUT PARAMETERS		
Height of bottom of slab above floor	0	m
Material density (ρ)	1910	kg/m^3
Material thickness (δ)	0.0239	m
Material specific heat (c_p)	1000	J/kg·K
Material thermal conductivity (k)	0.534	W/m·K
Material ignition Temperature (T_{ig})	791	K
Material initial uniform temperature	293.15	K
Timestep	0.5	sec
Output interval	1	sec
Simulation length	1200	sec
Specific heat of product gases	1340	J/kg·K
Net heat of complete combustion	1.76E+07	J/kg·K
Efficiency of combustion (χ_A)	0.5	
Radiative fraction (χ_{rad})	0.3	
Material emissivity (ε)	0.9	
Flame transmissivity (τ_{flame})	0.5	
Lateral flame spread parameter (Φ)	15.59	kW^2/m^3
Min. surface temp. for lateral spread ($T_{s,min}$)	712	K
Width of slab (2 x width of shorter wall)	4.8	m
Ceiling present?	1	(yes)
Allow multiple pyrolysis zones?	1	(yes)
Average heat flux from the ceiling	2000	kW/m^2
Paramater p for ceiling/wall arm extensions	1	m^{-1}
Combustible ceiling lining present?	1	(yes)
Corner configuration present?	1	(yes)
Use Complex radiation?	1	(yes)
Use gaslayer calcs. In radiation calcs.?	1	(yes)
Use accurate beam length calculation in radiation calculations?	0	(no)

6_75.MLR

CONE CURVE		
Point #	Time sec	HRR kW/m^2
1	0	0
2	30	24.5
3	50	9.4
4	100	12.6
5	130	15.9
6	165	12.3
7	215	15.8
8	250	14.2
9	290	25.2
10	345	70.8
11	400	77.2
12	435	75.9
13	525	35.0
14	675	23.7
15	750	23.0
16	760	20.9
17		
18		
19		
20		
21		
22		
23		
24		
25		
Irrad:	75	kW/m^2

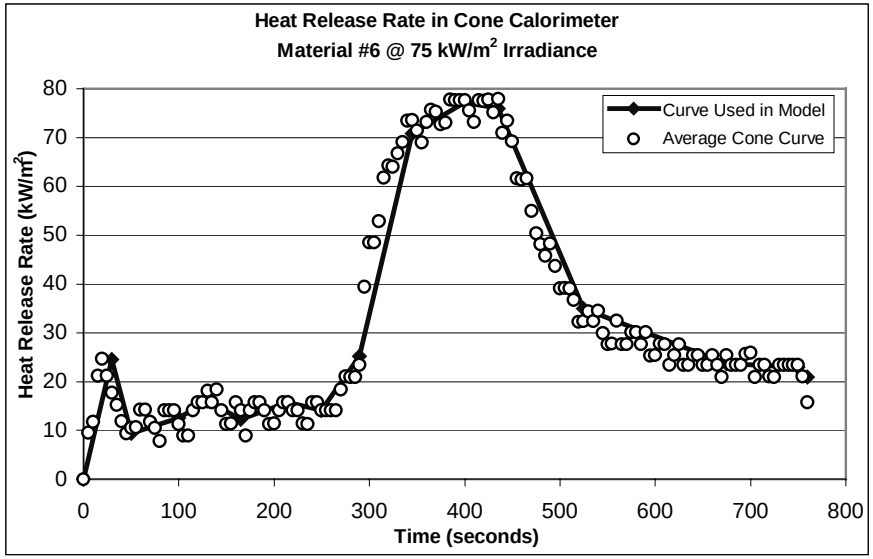

USCG.BRN

BURNER INPUTS		
Burner height above floor	0.152	m
Width of burner side	0.170	m
Use heat flux map?	1	(yes)

ADDITIONAL CONE CALORIMETER CURVES FOR MATERIAL #6--COATED FR EPOXY

6_100.MLR

CONE CURVE		
Point #	Time sec	HRR kW/m^2
1	0	0
2	5	17.8
3	15	51.0
4	55	14.2
5	70	11.4
6	95	17.2
7	150	18.4
8	180	42.3
9	200	40.0
10	270	52.7
11	290	49.0
12	320	31.3
13		
14		
15		
16		
17		
18		
19		
20		
21		
22		
23		
24		
25		
Irrad:	100	kW/m^2

6_50.MLR

CONE CURVE		
Point #	Time sec	HRR kW/m^2
1	0	0
2	10	19.2
3	20	41.0
4	35	9.5
5	47	7.0
6		
7		
8		
9		
10		
11		
12		
13		
14		
15		
16		
17		
18		
19		
20		
21		
22		
23		
24		
25		
Irrad:	50	kW/m^2

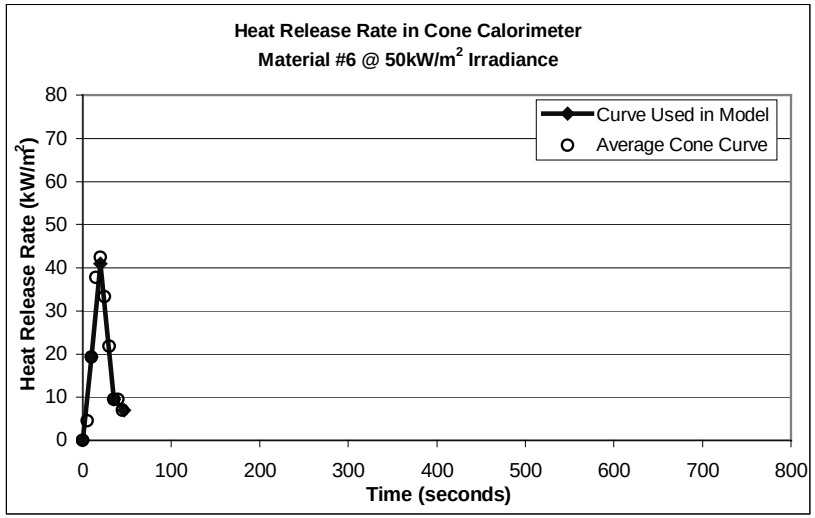

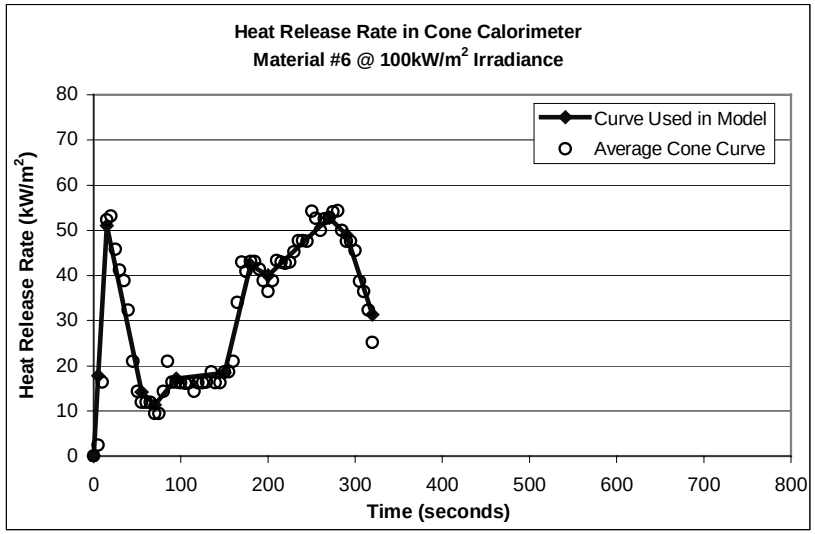

BASELINE INPUTS FOR MATERIAL #7--TEXTILE WALL COVERING

PROP_7?.DAT

MATERIAL PROPERTIES / INPUT PARAMETERS		
Height of bottom of slab above floor	0	m
Material density (ρ)	1760	kg/m^3
Material thickness (δ)	0.0253	m
Material specific heat (c_p)	1000	J/kg·K
Material thermal conductivity (k)	1.085	W/m·K
Material ignition Temperature (T_{ig})	726	K
Material initial uniform temperature	293.15	K
Timestep	0.5	sec
Output interval	1	sec
Simulation length	1200	sec
Specific heat of product gases	1340	J/kg·K
Net heat of complete combustion	1.82E+07	J/kg·K
Efficiency of combustion (χ_A)	0.5	
Radiative fraction (χ_{rad})	0.3	
Material emissivity (ε)	0.9	
Flame transmissivity (τ_{flame})	0.5	
Lateral flame spread parameter (Φ)	15.59	kW^2/m^3
Min. surface temp. for lateral spread ($T_{s,min}$)	653	K
Width of slab (2 x width of shorter wall)	4.8	m
Ceiling present?	1	(yes)
Allow multiple pyrolysis zones?	1	(yes)
Average heat flux from the ceiling	2000	kW/m^2
Paramater p for ceiling/wall arm extensions	1	m^{-1}
Combustible ceiling lining present?	1	(yes)
Corner configuration present?	1	(yes)
Use Complex radiation?	1	(yes)
Use gaslayer calcs. In radiation calcs.?	1	(yes)
Use accurate beam length calculation in radiation calculations?	0	(no)

7_50.MLR

CONE CURVE		
Point #	Time sec	HRR kW/m^2
1	0	0
2	5	8.9
3	30	34.0
4	55	41.0
5	72.5	30.0
6	80	37.3
7	102.5	65.5
8	130	32.0
9	145	10.0
10	160	0.0
11		
12		
13		
14		
15		
16		
17		
18		
19		
20		
21		
22		
23		
24		
25		
Irrad:	50	kW/m^2

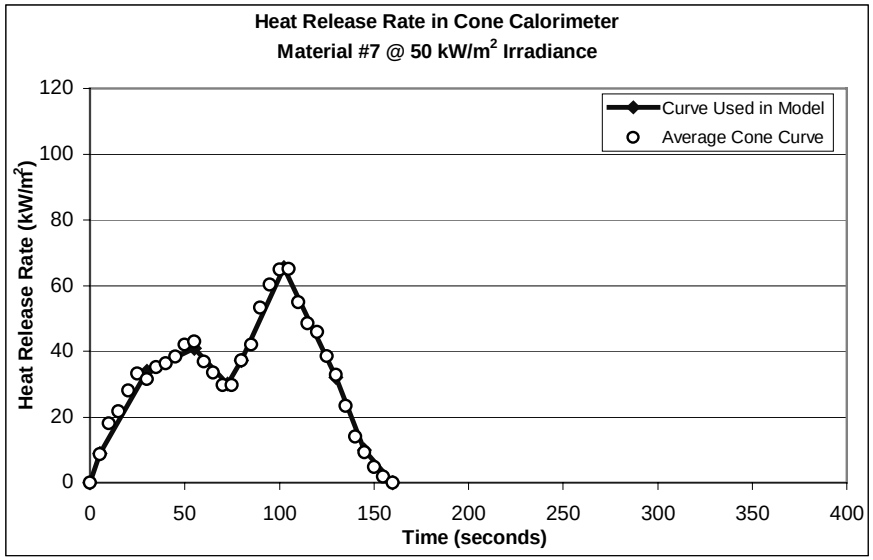

USCG.BRN

BURNER INPUTS		
Burner height above floor	0.152	m
Width of burner side	0.170	m
Use heat flux map?	1	(yes)

ADDITIONAL CONE CALORIMETER CURVES FOR MATERIAL #7--TEXTILE WALL COVERING

7_75.MLR

CONE CURVE		
Point #	Time sec	HRR kW/m^2
1	0	0
2	25	72.7
3	35	76.0
4	45	104.0
5	83	22.5
6	125	22.5
7	170	8.4
8		
9		
10		
11		
12		
13		
14		
15		
16		
17		
18		
19		
20		
21		
22		
23		
24		
25		
Irrad:	75	kW/m^2

7_25.MLR

CONE CURVE		
Point #	Time sec	HRR kW/m^2
1	0	0
2	60	30.0
3	90	33.0
4	145	28.2
5	235	11.0
6	305	9.9
7	335	2.2
8		
9		
10		
11		
12		
13		
14		
15		
16		
17		
18		
19		
20		
21		
22		
23		
24		
25		
Irrad:	25	kW/m^2

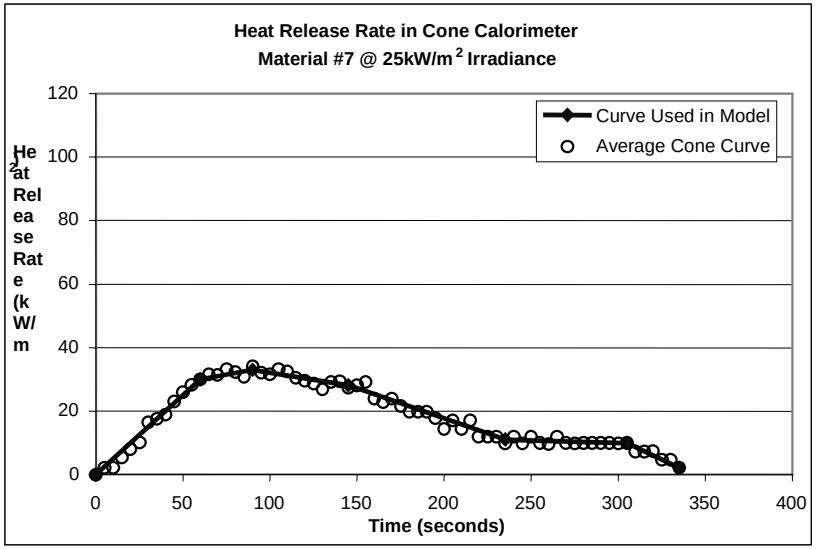

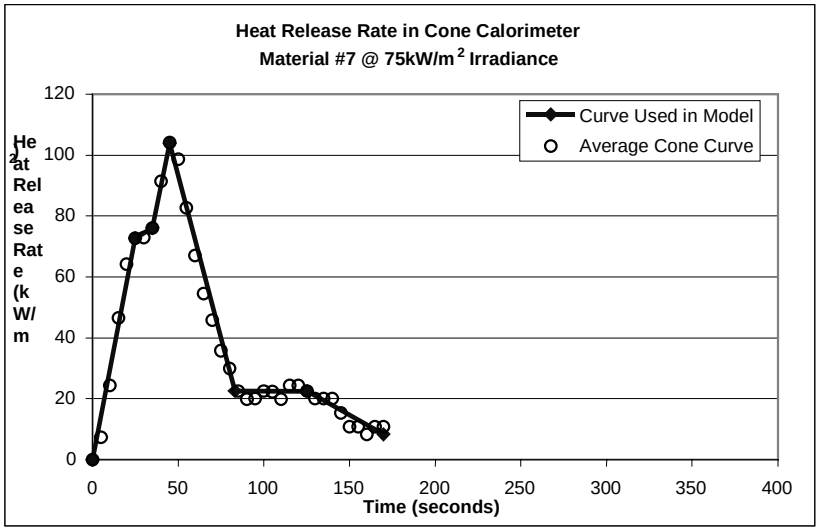

BASELINE INPUTS FOR MATERIAL #8--POLYESTER

PROP_8?.DAT

MATERIAL PROPERTIES / INPUT PARAMETERS		
Height of bottom of slab above floor	0	m
Material density (ρ)	1390	kg/m^3
Material thickness (δ)	0.0241	m
Material specific heat (c_p)	1000	J/kg·K
Material thermal conductivity (k)	0.597	W/m·K
Material ignition Temperature (T_{ig})	662	K
Material initial uniform temperature	293.15	K
Timestep	0.5	sec
Output interval	1	sec
Simulation length	1200	sec
Specific heat of product gases	1340	J/kg·K
Net heat of complete combustion	3.25E+07	J/kg·K
Efficiency of combustion (χ_A)	0.665	
Radiative fraction (χ_{rad})	0.476	
Material emissivity (ε)	0.9	
Flame transmissivity (τ_{flame})	0.5	
Lateral flame spread parameter (Φ)	19.02	kW^2/m^3
Min. surface temp. for lateral spread ($T_{s,min}$)	479	K
Width of slab (2 x width of shorter wall)	4.8	m
Ceiling present?	1	(yes)
Allow multiple pyrolysis zones?	1	(yes)
Average heat flux from the ceiling	2000	kW/m^2
Paramater p for ceiling/wall arm extensions	1	m^{-1}
Combustible ceiling lining present?	1	(yes)
Corner configuration present?	1	(yes)
Use Complex radiation?	1	(yes)
Use gaslayer calcs. In radiation calcs.?	1	(yes)
Use accurate beam length calculation in radiation calculations?	0	(no)

8_50.MLR

CONE CURVE		
Point #	Time sec	HRR kW/m^2
1	0	0
2	25	336.7
3	30	341.8
4	150	259.4
5	180	272.0
6	225	140.7
7	315	43.4
8	355	32.1
9		
10		
11		
12		
13		
14		
15		
16		
17		
18		
19		
20		
21		
22		
23		
24		
25		
Irrad:	50	kW/m^2

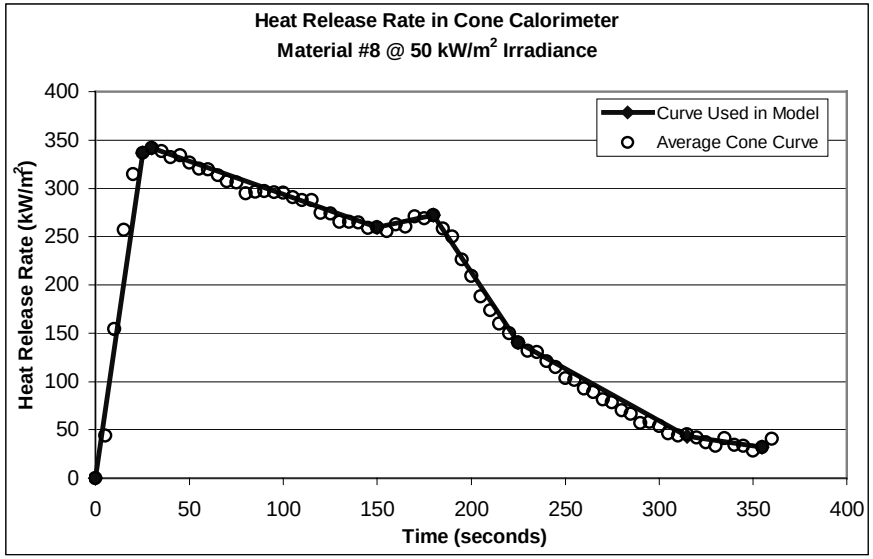

USCG.BRN

BURNER INPUTS		
Burner height above floor	0.152	m
Width of burner side	0.170	m
Use heat flux map?	1	(yes)

ADDITIONAL CONE CALORIMETER CURVES FOR MATERIAL #8--POLYESTER

8_75.MLR

CONE CURVE		
Point #	Time sec	HRR kW/m^2
1	0	0
2	5	12.35
3	25	407.3
4	30	424
5	40	423.5
6	75	357.1
7	105	324.45
8	125	341.85
9	130	330.1
10	165	105.45
11	190	49.25
12	230	26.35
13	340	1.45
14		
15		
16		
17		
18		
19		
20		
21		
22		
23		
24		
25		
Irrad:	75	kW/m^2

8_25.MLR

CONE CURVE		
Point #	Time sec	HRR kW/m^2
1	0	0
2	5	3.65
3	25	299
4	50	227.45
5	75	205.8
6	100	203.45
7	120	212.75
8	140	200.75
9	175	190.9
10	235	93.5
11	290	74.15
12	400	55.45
13	500	26.95
14	505	18.3
15	620	8.9
16		
17		
18		
19		
20		
21		
22		
23		
24		
25		
Irrad:	25	kW/m^2

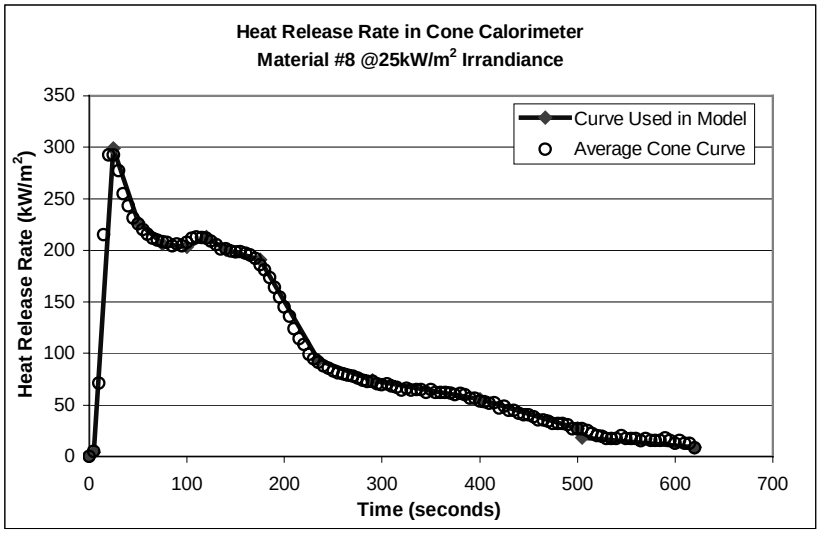

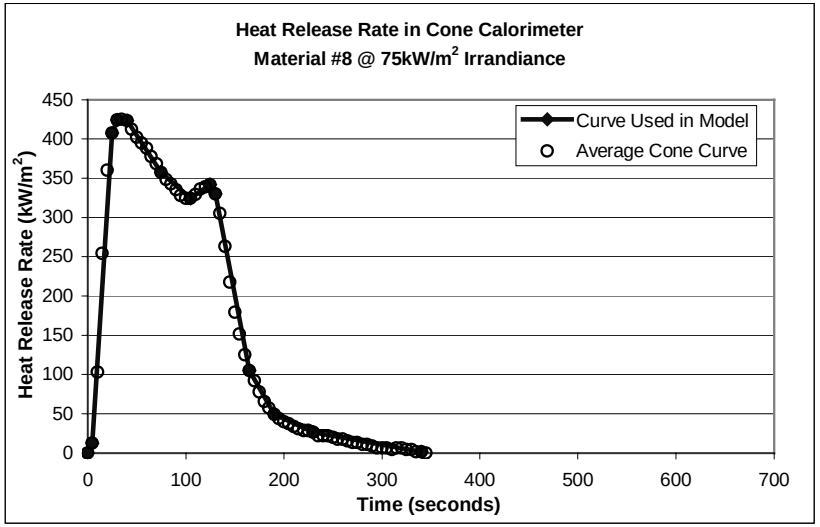

BASELINE INPUTS FOR MATERIAL #9--FR MODIFIED ACRYLIC

PROP_9?.DAT

MATERIAL PROPERTIES / INPUT PARAMETERS		
Height of bottom of slab above floor	0	m
Material density (ρ)	1880	kg/m^3
Material thickness (δ)	0.0252	m
Material specific heat (c_p)	1000	J/kg·K
Material thermal conductivity (k)	1.511	W/m·K
Material ignition Temperature (T_{ig})	681	K
Material initial uniform temperature	293.15	K
Timestep	0.5	sec
Output interval	1	sec
Simulation length	1200	sec
Specific heat of product gases	1340	J/kg·K
Net heat of complete combustion	2.52E+07	J/kg·K
Efficiency of combustion (χ_A)	0.489	
Radiative fraction (χ_{rad})	0.314	
Material emissivity (ε)	0.9	
Flame transmissivity (τ_{flame})	0.5	
Lateral flame spread parameter (Φ)	23.22	kW^2/m^3
Min. surface temp. for lateral spread ($T_{s,min}$)	569	K
Width of slab (2 x width of shorter wall)	4.8	m
Ceiling present?	1	(yes)
Allow multiple pyrolysis zones?	1	(yes)
Average heat flux from the ceiling	2000	kW/m^2
Paramater p for ceiling/wall arm extensions	1	m^{-1}
Combustible ceiling lining present?	1	(yes)
Corner configuration present?	1	(yes)
Use Complex radiation?	1	(yes)
Use gaslayer calcs. In radiation calcs.?	1	(yes)
Use accurate beam length calculation in radiation calculations?	0	(no)

9_50.MLR

CONE CURVE		
Point #	Time sec	HRR kW/m^2
1	0	0
2	5	1.8
3	12	56.0
4	18	98.3
5	28	128.5
6	79	75.6
7	155	59.9
8	550	41.6
9	645	40.3
10	1070	18.0
11		
12		
13		
14		
15		
16		
17		
18		
19		
20		
21		
22		
23		
24		
25		
Irrad:	50	kW/m^2

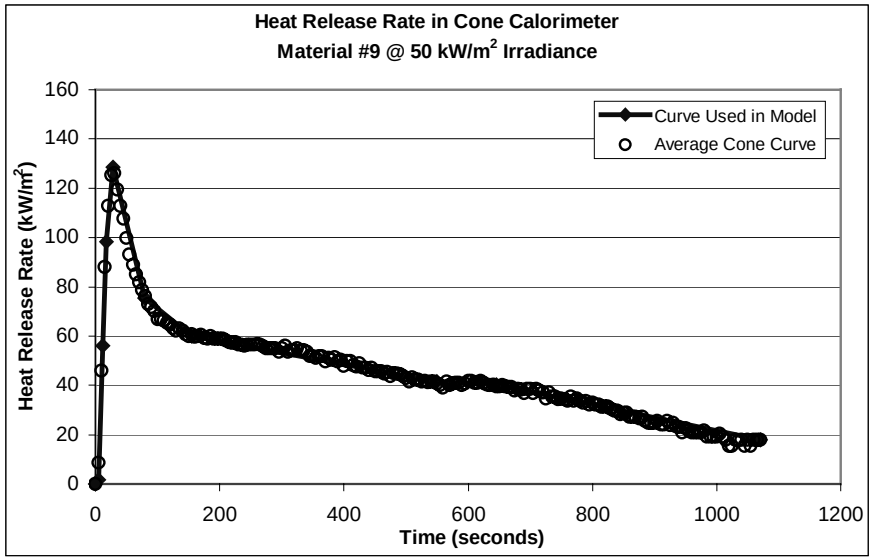

USCG.BRN

BURNER INPUTS		
Burner height above floor	0.152	m
Width of burner side	0.170	m
Use heat flux map?	1	(yes)

ADDITIONAL CONE CALORIMETER CURVES FOR MATERIAL #9--FR MODIFIED ACRYLIC

9_75.MLR

CONE CURVE		
Point #	Time sec	HRR kW/m^2
1	0	0
2	20	145.33
3	25	152.03
4	30	145.83
5	65	102.43
6	125	69.667
7	280	64.2
8	405	51.033
9	655	43.433
10	1010	21.8
11	1150	18.5
12		
13		
14		
15		
16		
17		
18		
19		
20		
21		
22		
23		
24		
25		
Irrad:	75	kW/m^2

9_25.MLR

CONE CURVE		
Point #	Time sec	HRR kW/m^2
1	0	0
2	10	22.7
3	30	98.7
4	115	60
5	205	33.5
6	270	24.3
7	350	18.85
8	355	18.75
9	440	17.5
10	775	21.6
11		
12		
13		
14		
15		
16		
17		
18		
19		
20		
21		
22		
23		
24		
25		
Irrad:	25	kW/m^2

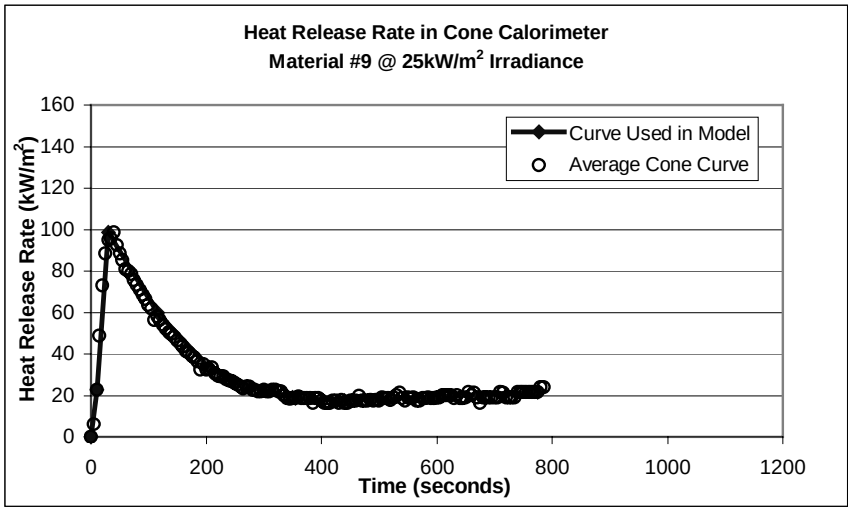

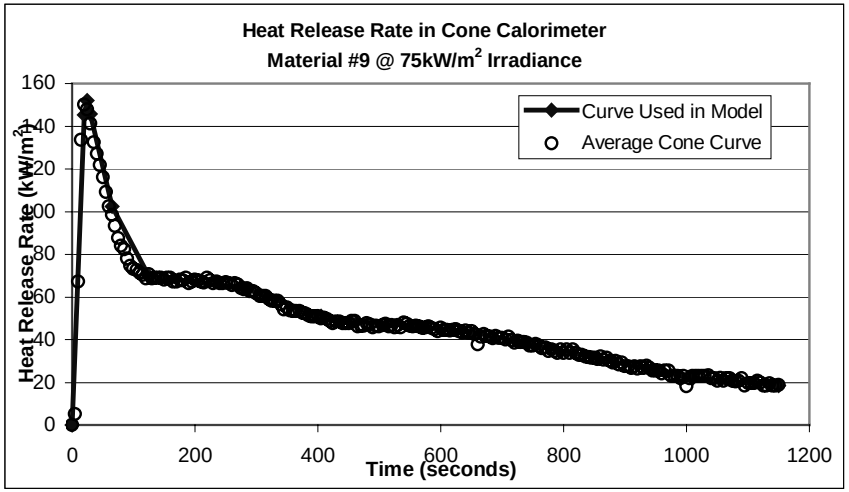

[This page has been left blank intentionally.]

[This page has been left blank intentionally.]

8.0 BASELINE HRR RESULTS

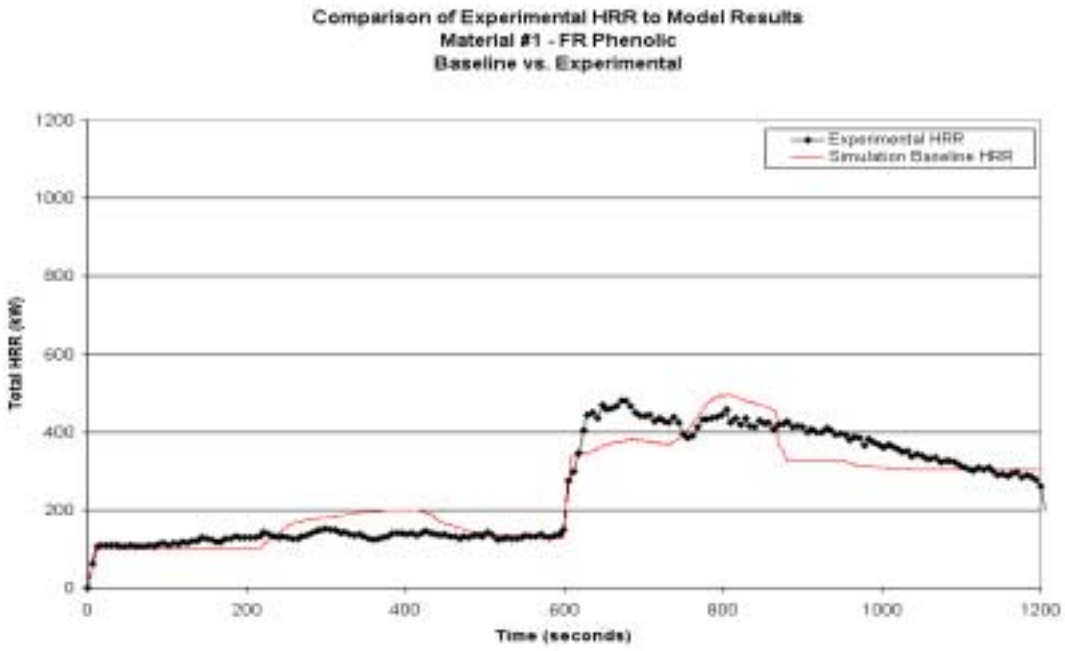

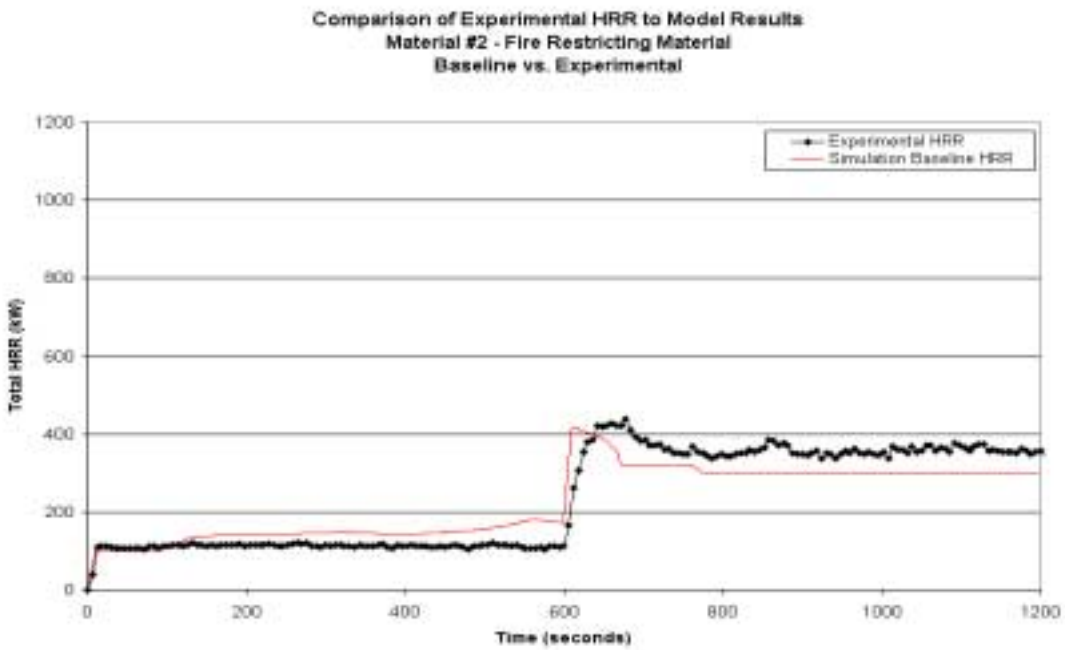

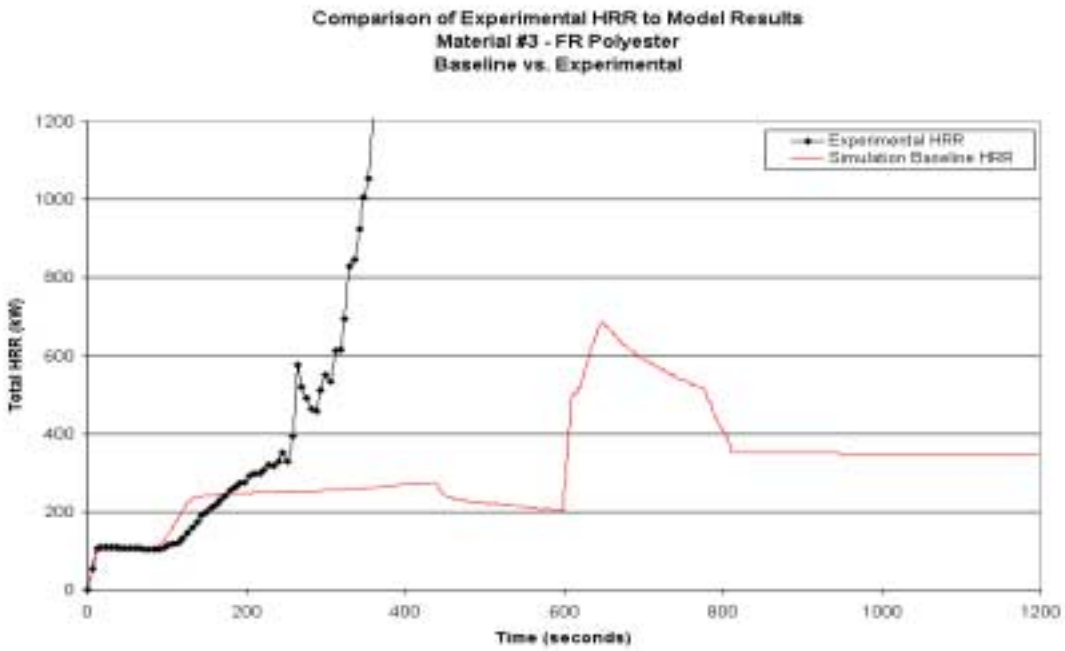
Comparison of Experimental HRR to Model Results
Material #3 - FR Polyester
Baseline vs. Experimental
Experimental HRR
Simulation Baseline HRR
Total HRR (kW)
Time (seconds)
0
200
400
600
800
1000
1200

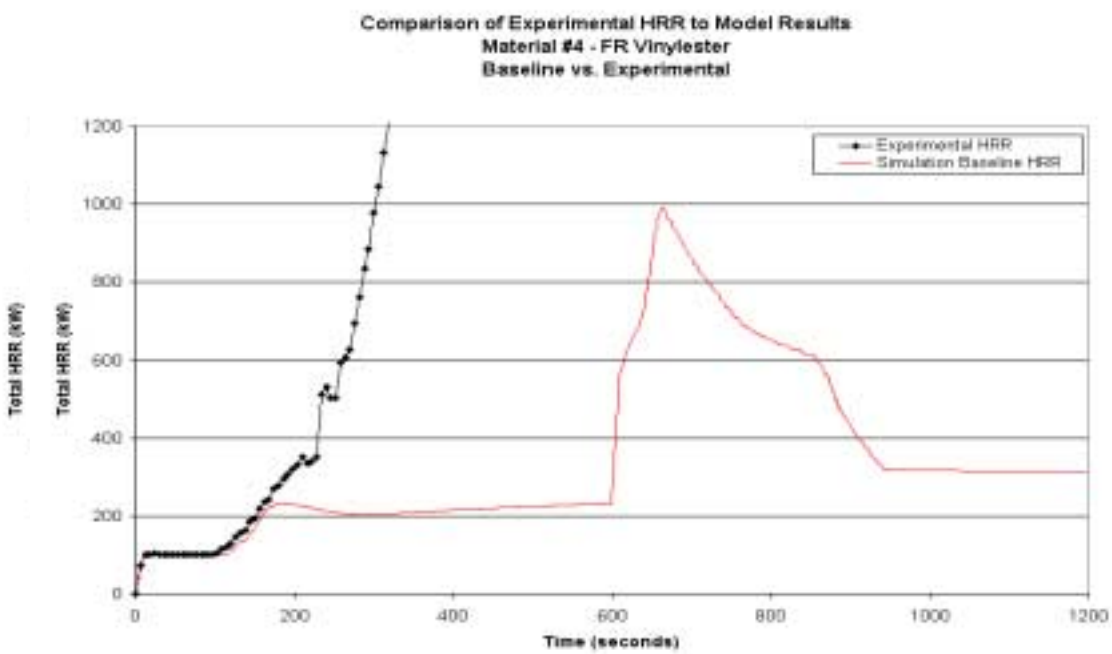
Comparison of Experimental HRR to Model Results
Material #4 - FR Vinylester
Baseline vs. Experimental
Experimental HRR
Simulation Baseline HRR
Total HRR (kW)
Total HRR (kW)
Time (seconds)
0
200
400
600
800
1000
1200

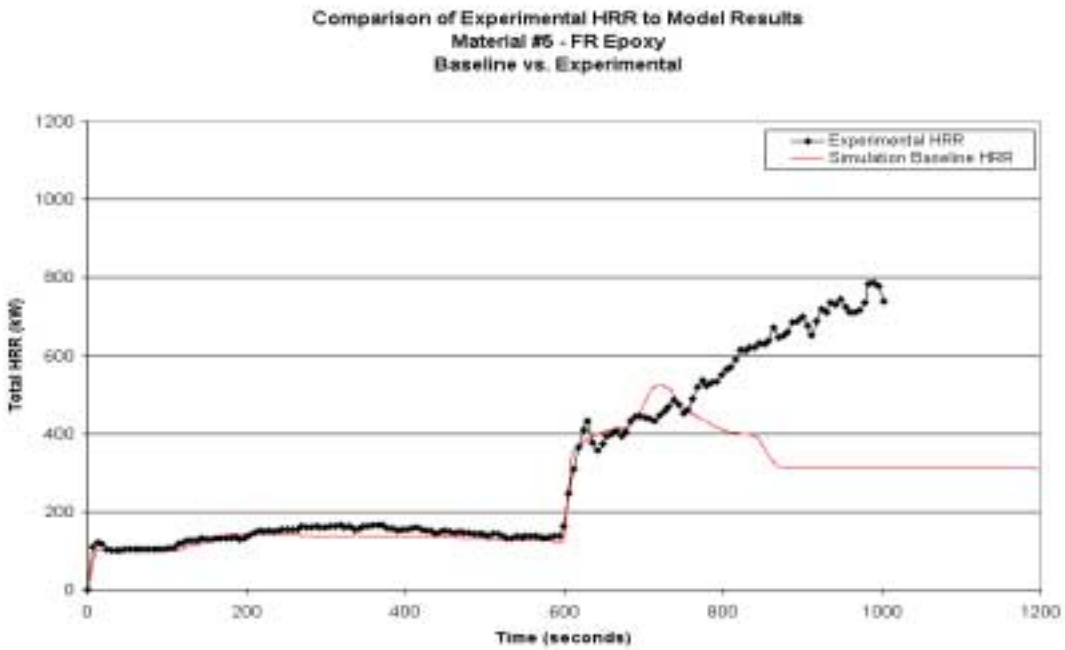
Comparison of Experimental HRR to Model Results
Material #5 - FR Epoxy
Baseline vs. Experimental
Experimental HRR
Simulation Baseline HRR
Total HRR (kW)
Time (seconds)
0
200
400
600
800
1000
1200

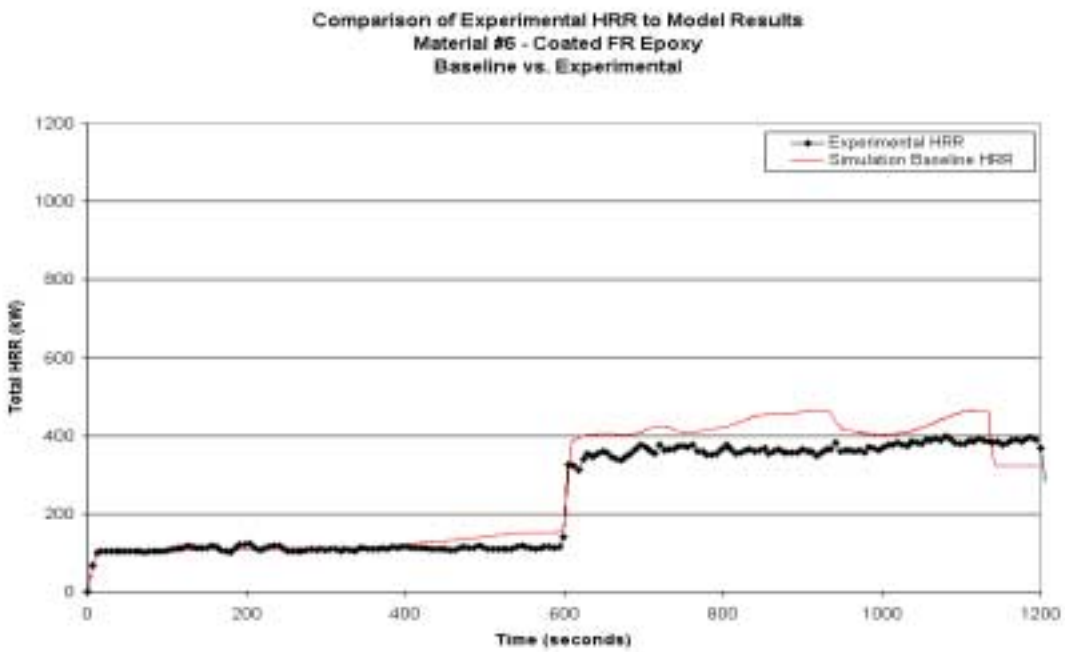
Comparison of Experimental HRR to Model Results
Material #6 - Coated FR Epoxy
Baseline vs. Experimental
Experimental HRR
Simulation Baseline HRR
Total HRR (kW)
Time (seconds)
0
200
400
600
800
1000
1200

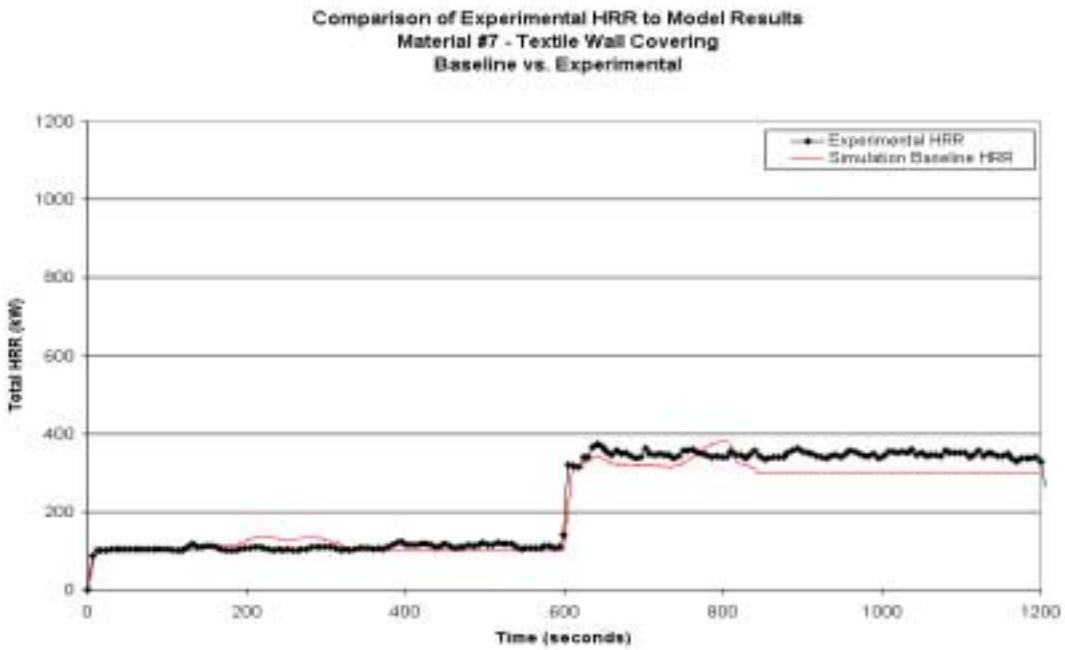
Comparison of Experimental HRR to Model Results
Material #7 - Textile Wall Covering
Baseline vs. Experimental
Experimental HRR
Simulation Baseline HRR
Total HRR (kW)
Time (seconds)
0
200
400
600
800
1000
1200

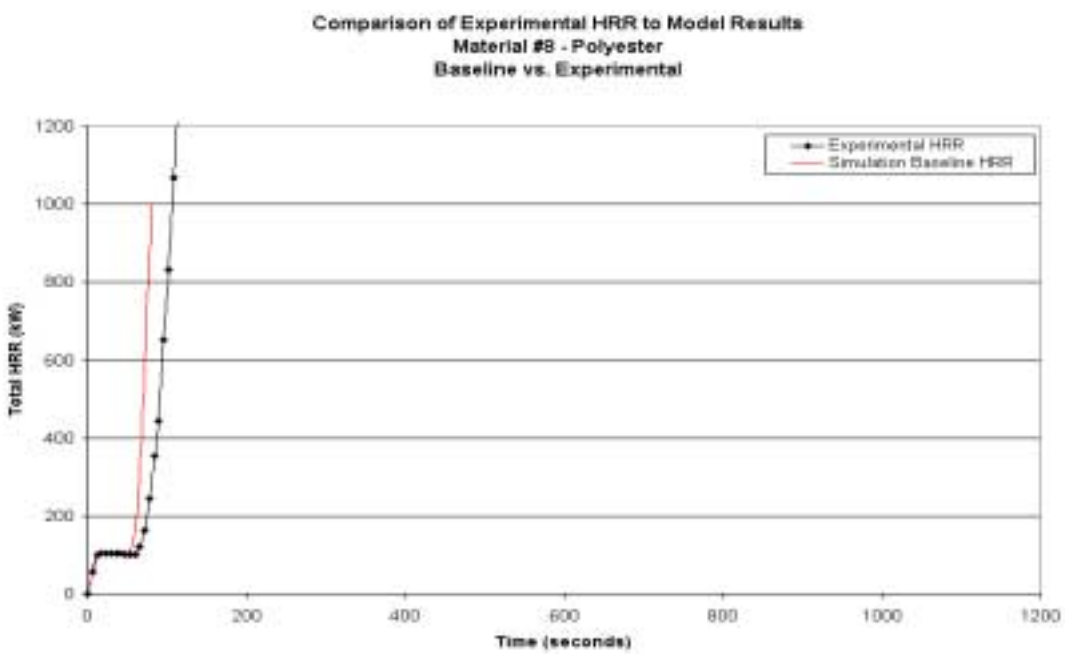
Comparison of Experimental HRR to Model Results
Material #8 - Polyester
Baseline vs. Experimental
Experimental HRR
Simulation Baseline HRR
Total HRR (kW)
Time (seconds)
0
200
400
600
800
1000
1200

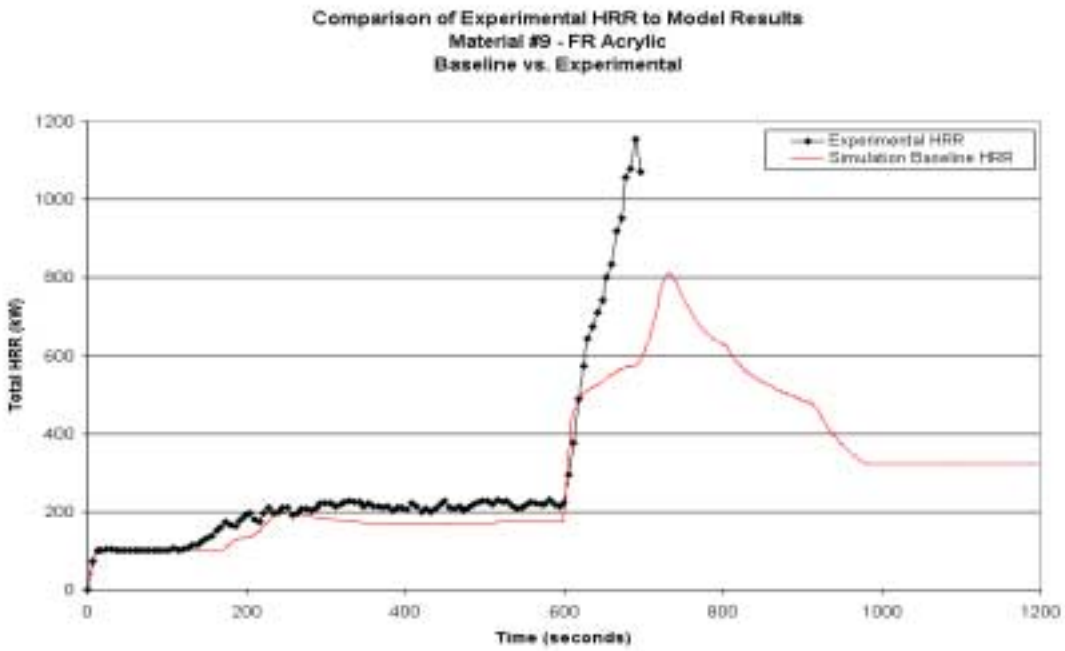
Comparison of Experimental HRR to Model Results
Material #9 - FR Acrylic
Baseline vs. Experimental
Experimental HRR
Simulation Baseline HRR
Total HRR (kW)
Time (seconds)
0
200
400
600
800
1000
1200

9.0 BASELINE UPPER LAYER GAS TEMPERATURE RESULTS

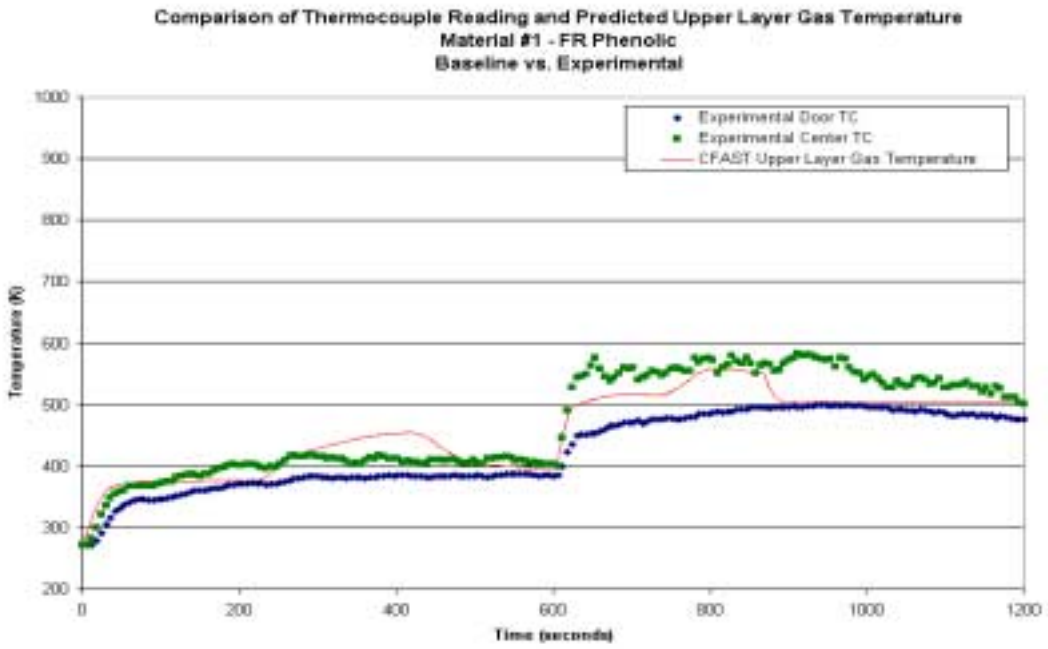

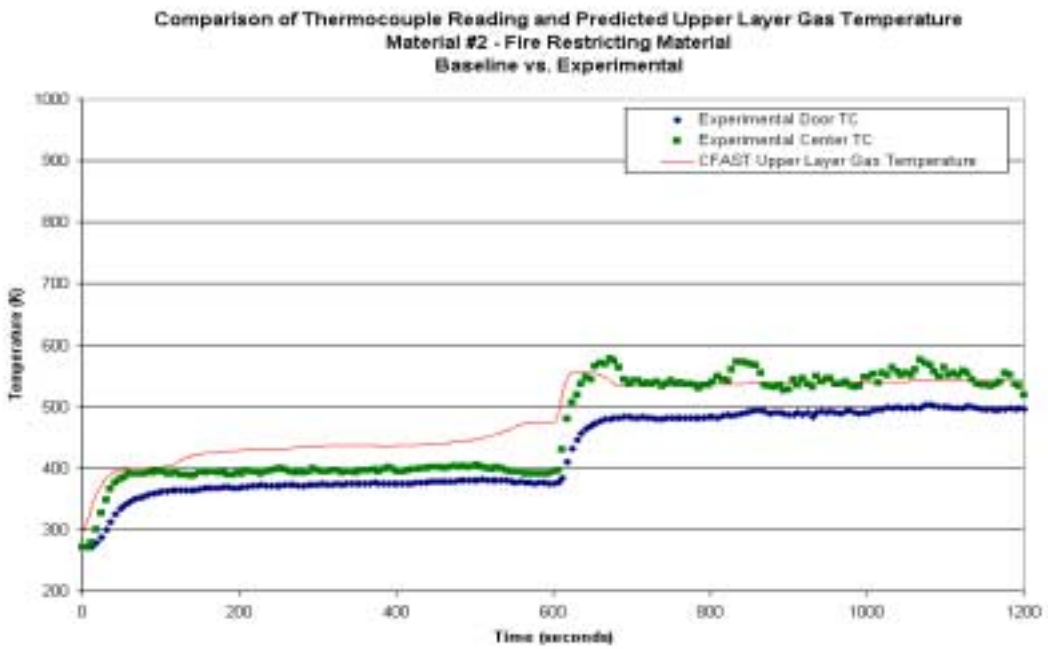

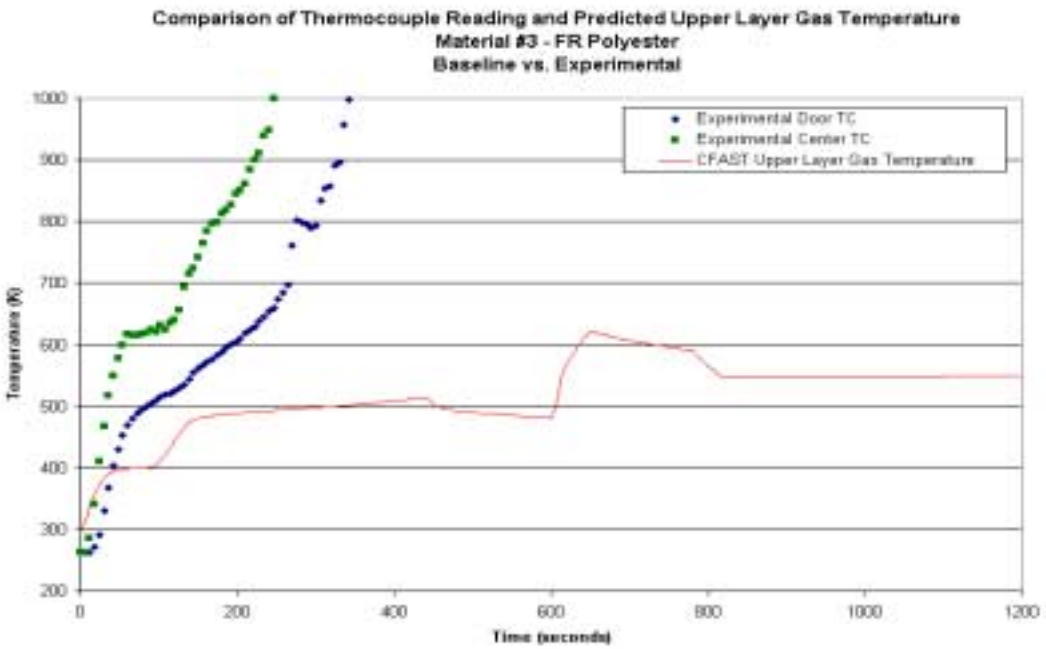
Comparison of Thermocouple Reading and Predicted Upper Layer Gas Temperature
Material #3 - FR Polyester
Baseline vs. Experimental
Experimental Door TC
Experimental Center TC
CFAST Upper Layer Gas Temperature
Temperature (K)
Time (seconds)
1000
900
800
700
600
500
400
300
200
0
200
400
600
800
1000
1200

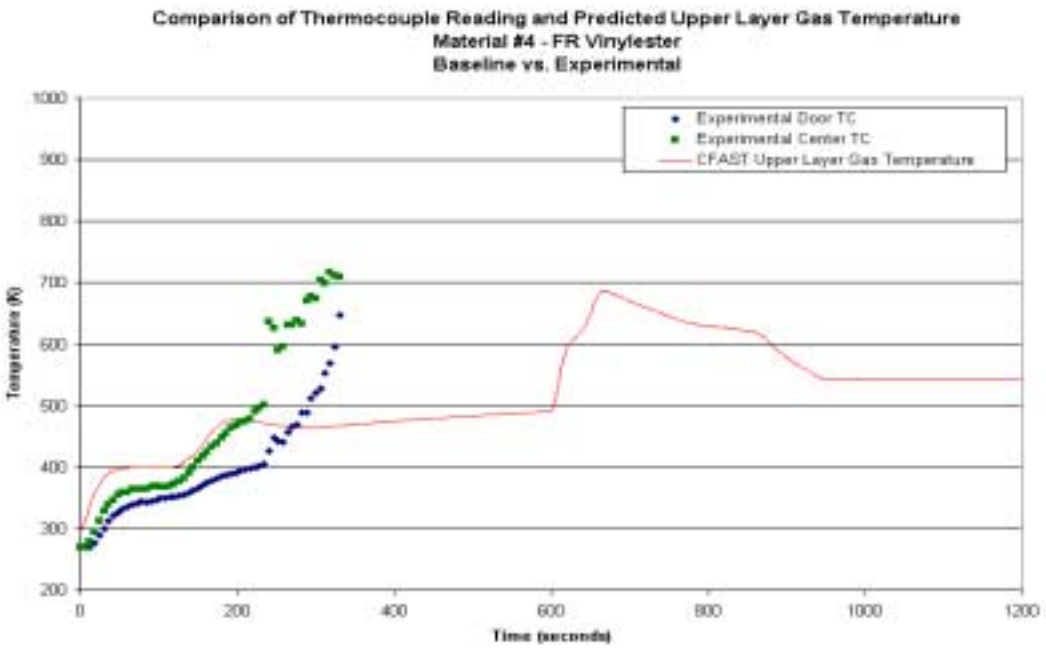
Comparison of Thermocouple Reading and Predicted Upper Layer Gas Temperature
Material #4 - FR Vinylester
Baseline vs. Experimental
Experimental Door TC
Experimental Center TC
CFAST Upper Layer Gas Temperature
Temperature (K)
Time (seconds)
1000
900
800
700
600
500
400
300
200
0
200
400
600
800
1000
1200

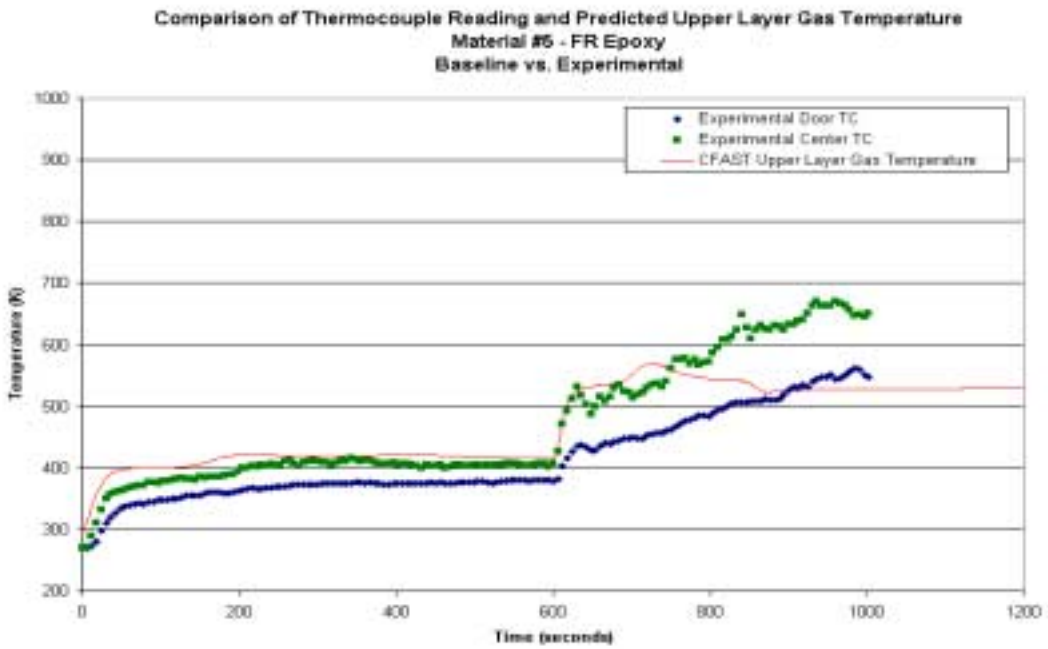
Comparison of Thermocouple Reading and Predicted Upper Layer Gas Temperature
Material #5 - FR Epoxy
Baseline vs. Experimental
Experimental Door TC
Experimental Center TC
CFAST Upper Layer Gas Temperature
Temperature (K)
Time (seconds)
1000
900
800
700
600
500
400
300
200
0
200
400
600
800
1000
1200

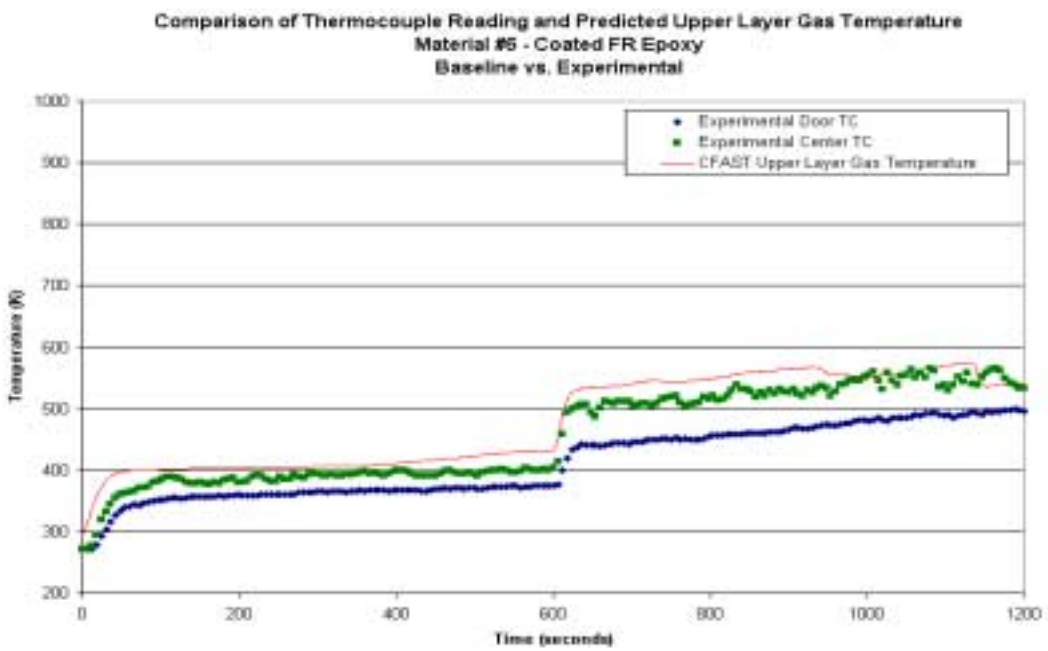
Comparison of Thermocouple Reading and Predicted Upper Layer Gas Temperature
Material #5 - Coated FR Epoxy
Baseline vs. Experimental
Experimental Door TC
Experimental Center TC
CFAST Upper Layer Gas Temperature
Temperature (K)
Time (seconds)
1000
900
800
700
600
500
400
300
200
0
200
400
600
800
1000
1200

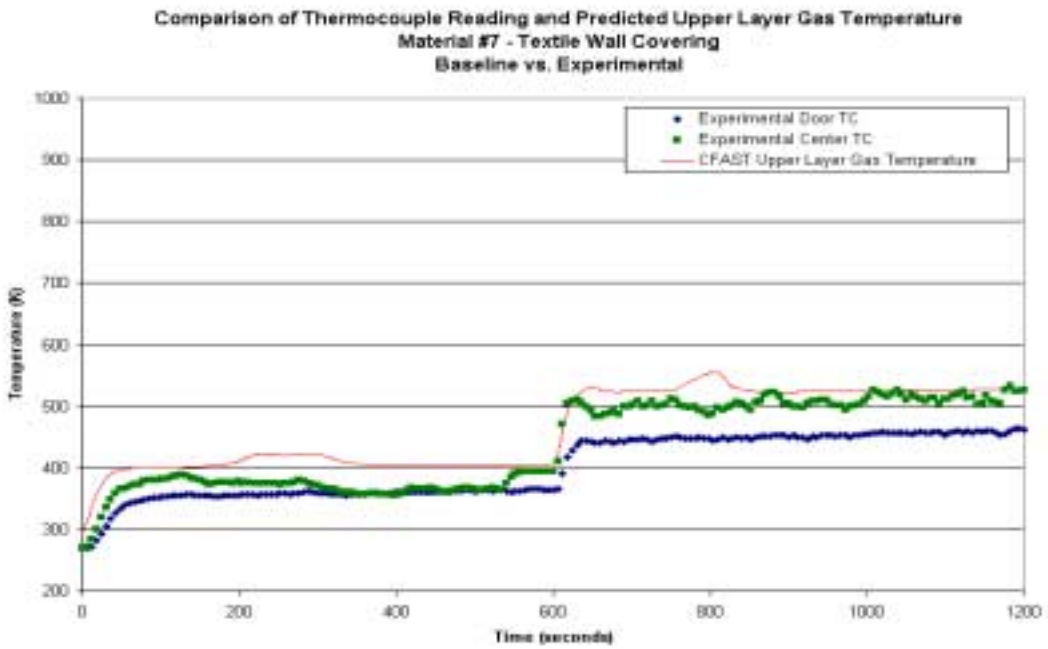
Comparison of Thermocouple Reading and Predicted Upper Layer Gas Temperature
Material #7 - Textile Wall Covering
Baseline vs. Experimental
Experimental Door TC
Experimental Center TC
CFAST Upper Layer Gas Temperature
Temperature (K)
Time (seconds)
1000
900
800
700
600
500
400
300
200
0
200
400
600
800
1000
1200

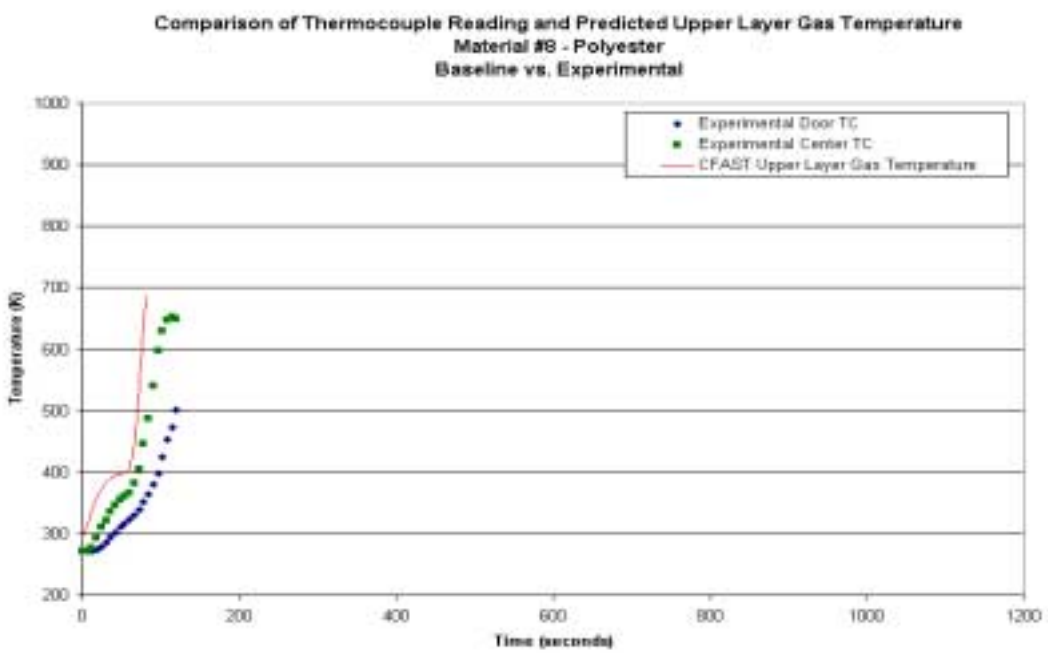
Comparison of Thermocouple Reading and Predicted Upper Layer Gas Temperature
Material #8 - Polyester
Baseline vs. Experimental
Experimental Door TC
Experimental Center TC
CFAST Upper Layer Gas Temperature
Temperature (K)
Time (seconds)
1000
900
800
700
600
500
400
300
200
0
200
400
600
800
1000
1200

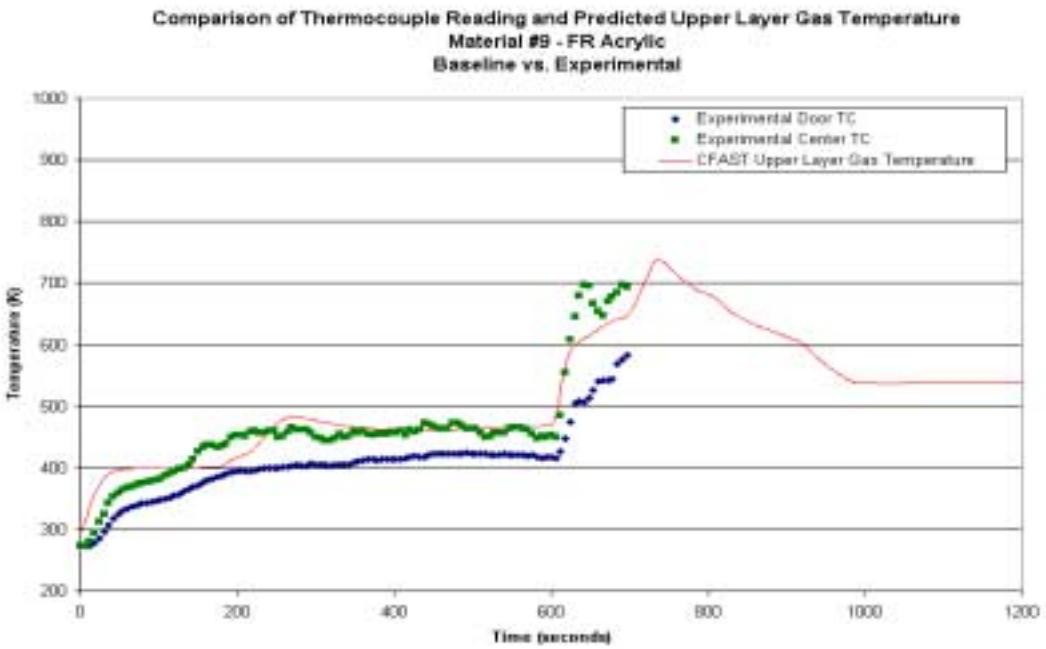
Comparison of Thermocouple Reading and Predicted Upper Layer Gas Temperature
Material #9 - FR Acrylic
Baseline vs. Experimental
Experimental Door TC
Experimental Center TC
CFAST Upper Layer Gas Temperature
Temperature (K)
Time (seconds)
1000
900
800
700
600
500
400
300
200
0
200
400
600
800
1000
1200

10.0 BASELINE SMOKE PRODUCTION RATE RESULTS

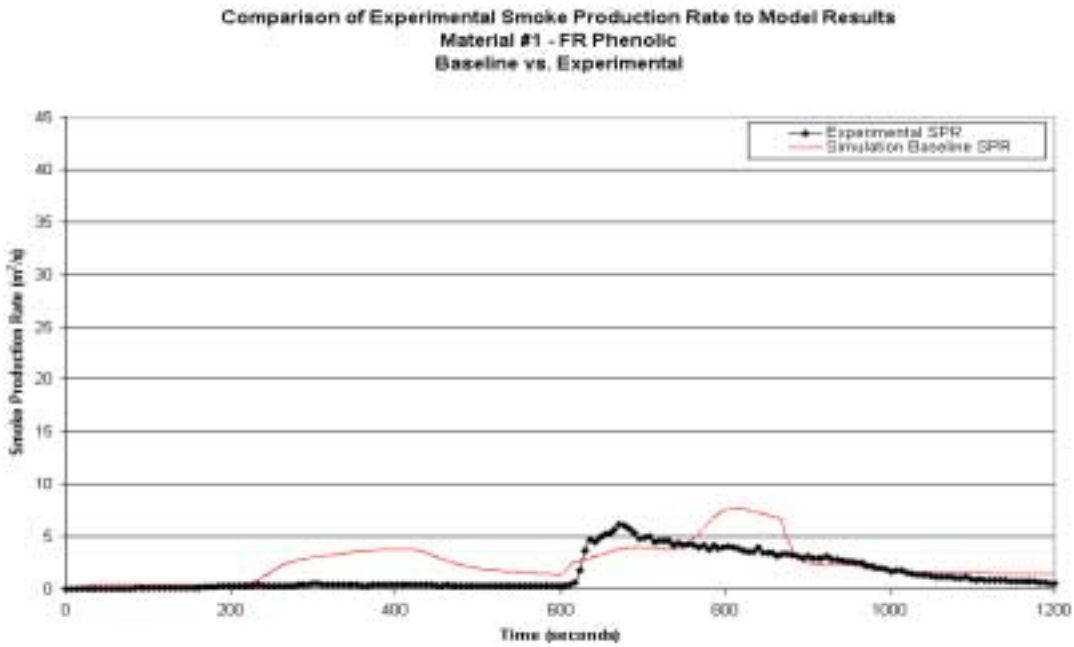

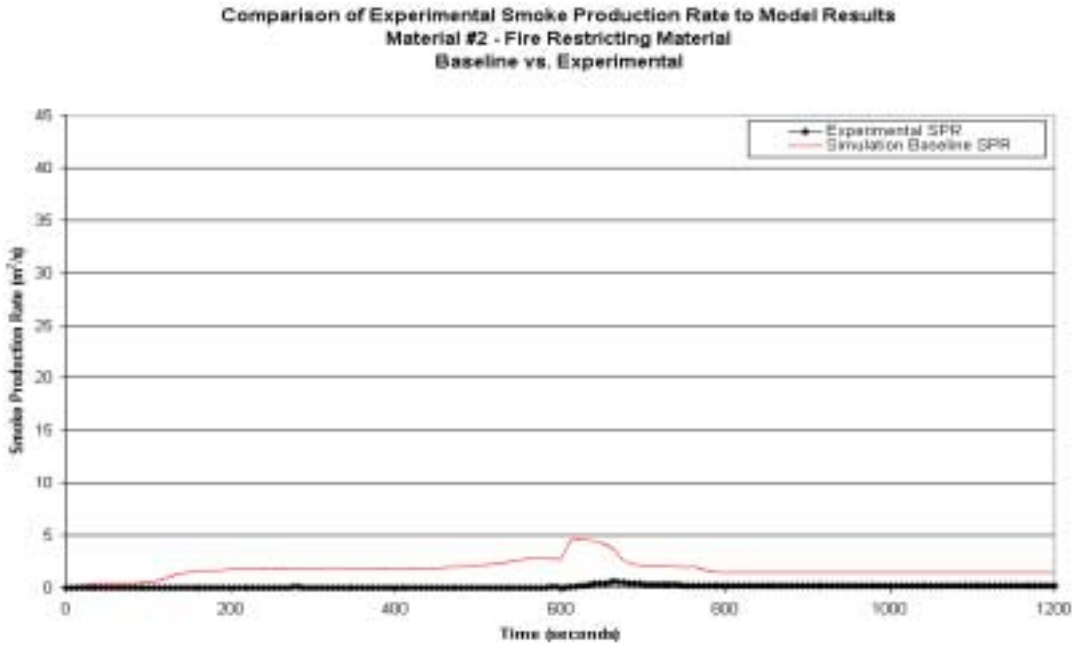

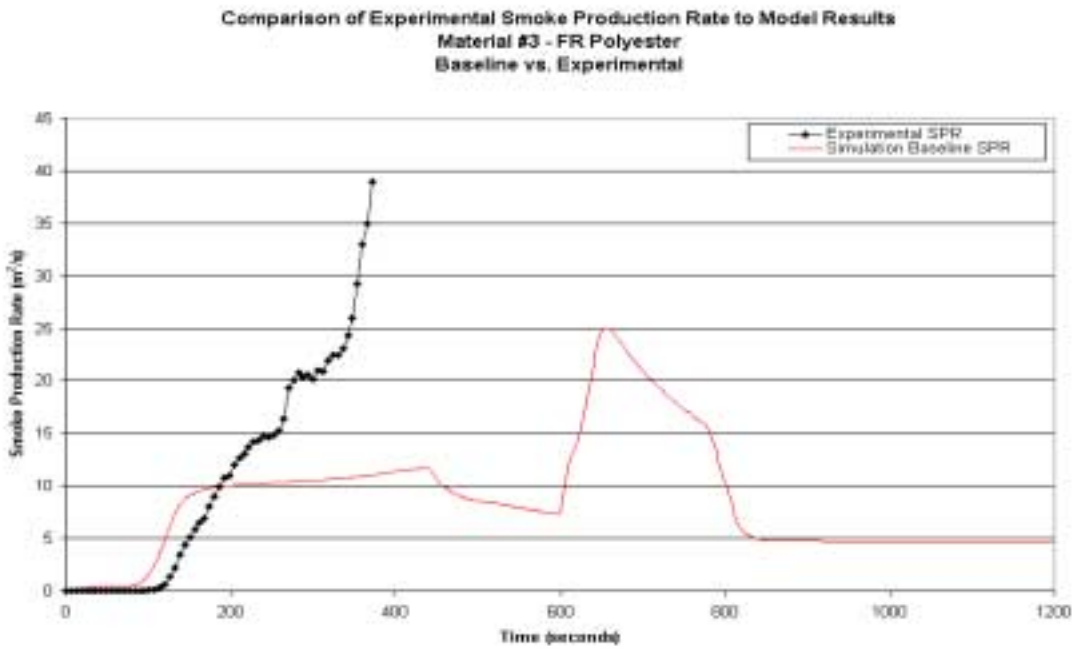
Comparison of Experimental Smoke Production Rate to Model Results
Material #3 - FR Polyester
Baseline vs. Experimental
Experimental SPR
Simulation Baseline SPR
Smoke Production Rate (m²/s)
Time (seconds)
0
5
10
15
20
25
30
35
40
45
0
200
400
600
800
1000
1200

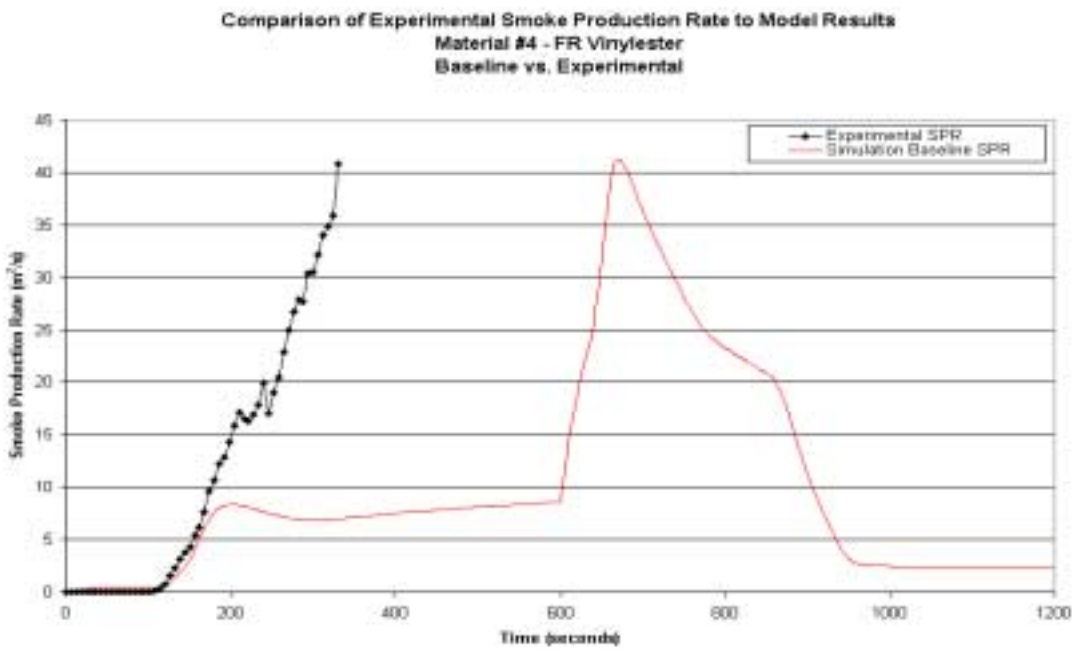
Comparison of Experimental Smoke Production Rate to Model Results
Material #4 - FR Vinylester
Baseline vs. Experimental
Experimental SPR
Simulation Baseline SPR
Smoke Production Rate (m²/s)
Time (seconds)
0
5
10
15
20
25
30
35
40
45
0
200
400
600
800
1000
1200

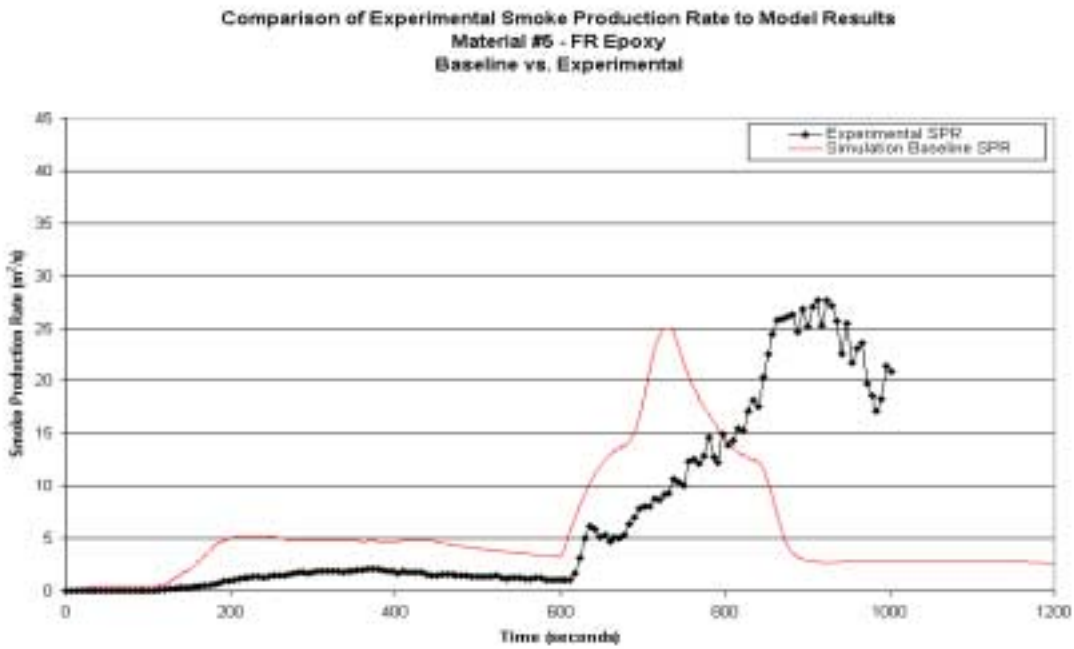
Comparison of Experimental Smoke Production Rate to Model Results
Material #5 - FR Epoxy
Baseline vs. Experimental
Experimental SPR
Simulation Baseline SPR
Smoke Production Rate (m²/s)
Time (seconds)
0
5
10
15
20
25
30
35
40
45
0
200
400
600
800
1000
1200

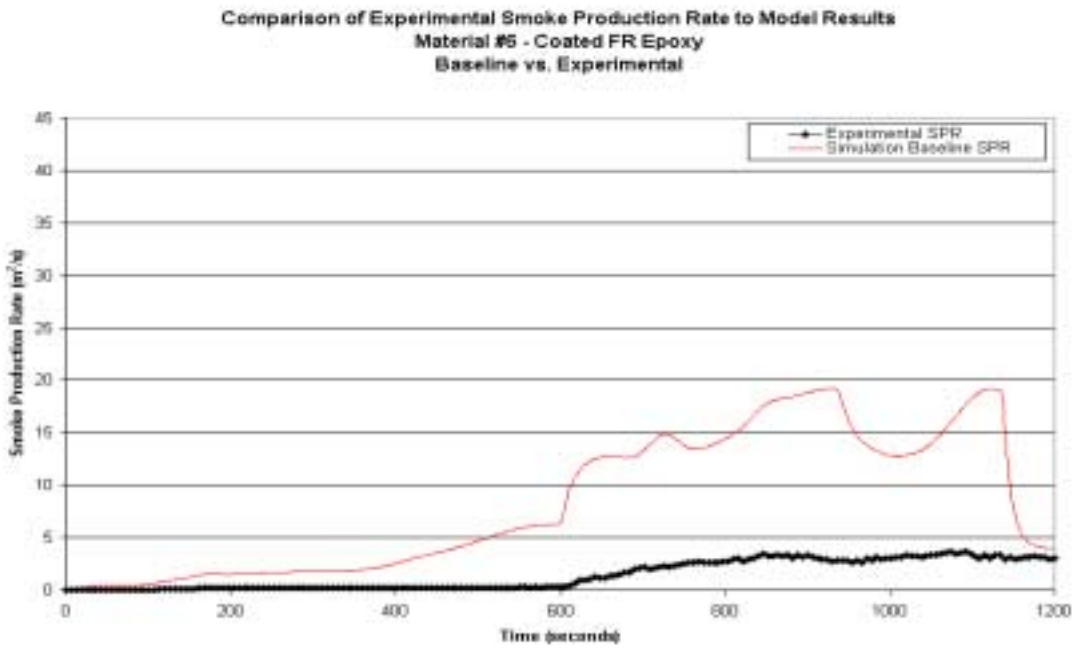
Comparison of Experimental Smoke Production Rate to Model Results
Material #5 - Coated FR Epoxy
Baseline vs. Experimental
Experimental SPR
Simulation Baseline SPR
Smoke Production Rate (m²/s)
Time (seconds)
0
5
10
15
20
25
30
35
40
45
0
200
400
600
800
1000
1200

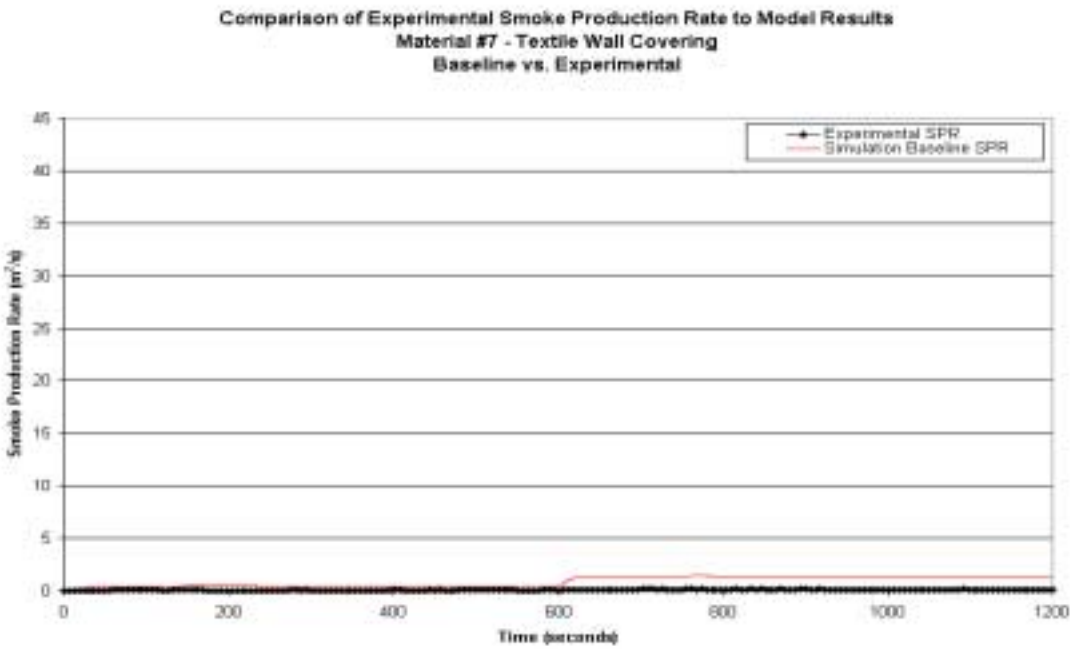
Comparison of Experimental Smoke Production Rate to Model Results
Material #7 - Textile Wall Covering
Baseline vs. Experimental
Experimental SPR
Simulation Baseline SPR
Smoke Production Rate (m²/s)
Time (seconds)
0
5
10
15
20
25
30
35
40
45
0
200
400
600
800
1000
1200

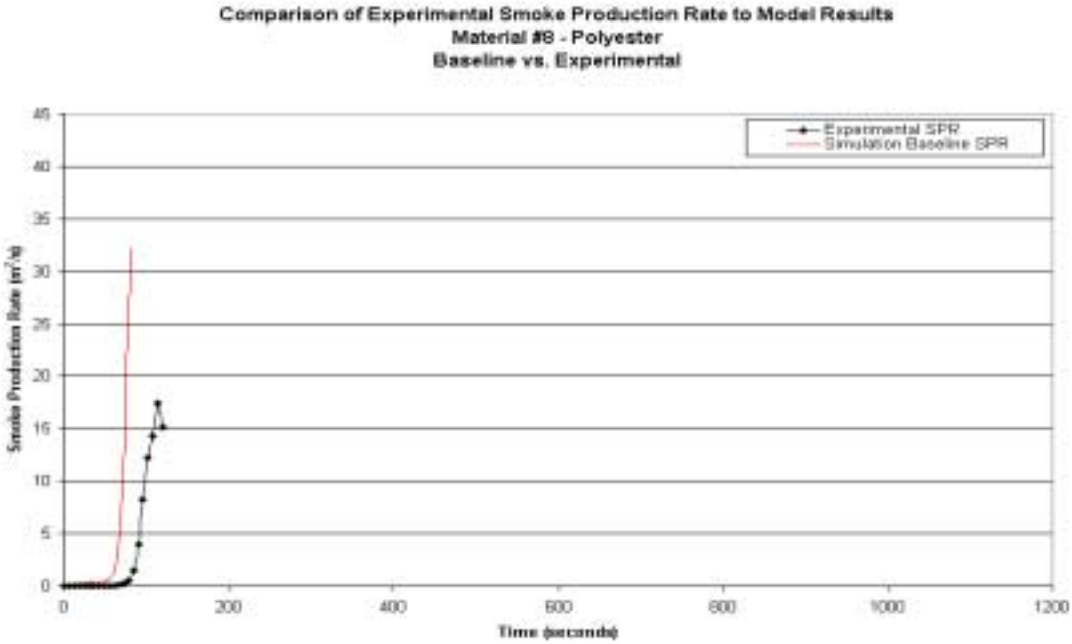
Comparison of Experimental Smoke Production Rate to Model Results
Material #8 - Polyester
Baseline vs. Experimental
Experimental SPR
Simulation Baseline SPR
Smoke Production Rate (m²/s)
Time (seconds)
0
5
10
15
20
25
30
35
40
45
0
200
400
600
800
1000
1200

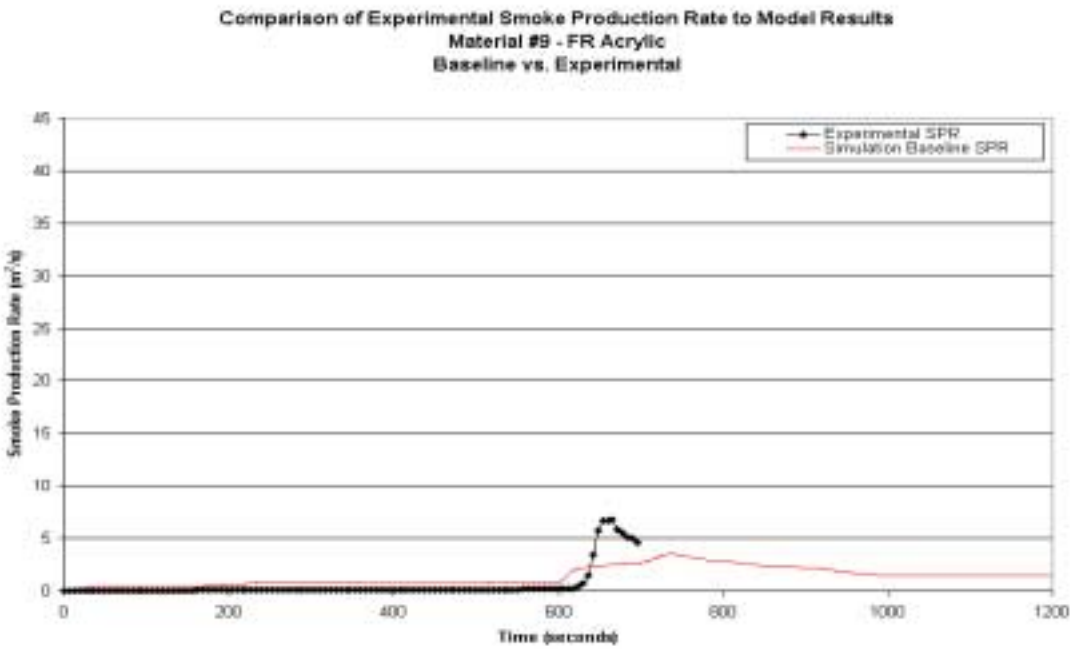
Comparison of Experimental Smoke Production Rate to Model Results
Material #9 - FR Acrylic
Baseline vs. Experimental
Experimental SPR
Simulation Baseline SPR
Smoke Production Rate (m²/s)
Time (seconds)
0
5
10
15
20
25
30
35
40
45
0
200
400
600
800
1000
1200

11.0 BASELINE FLOOR HEAT FLUX RESULTS

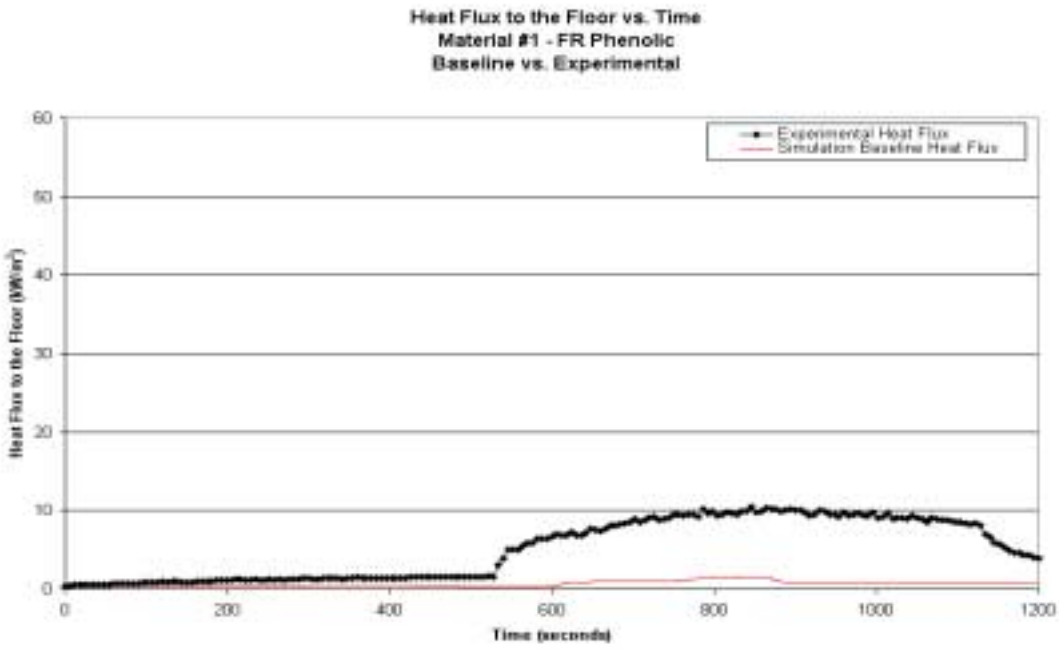

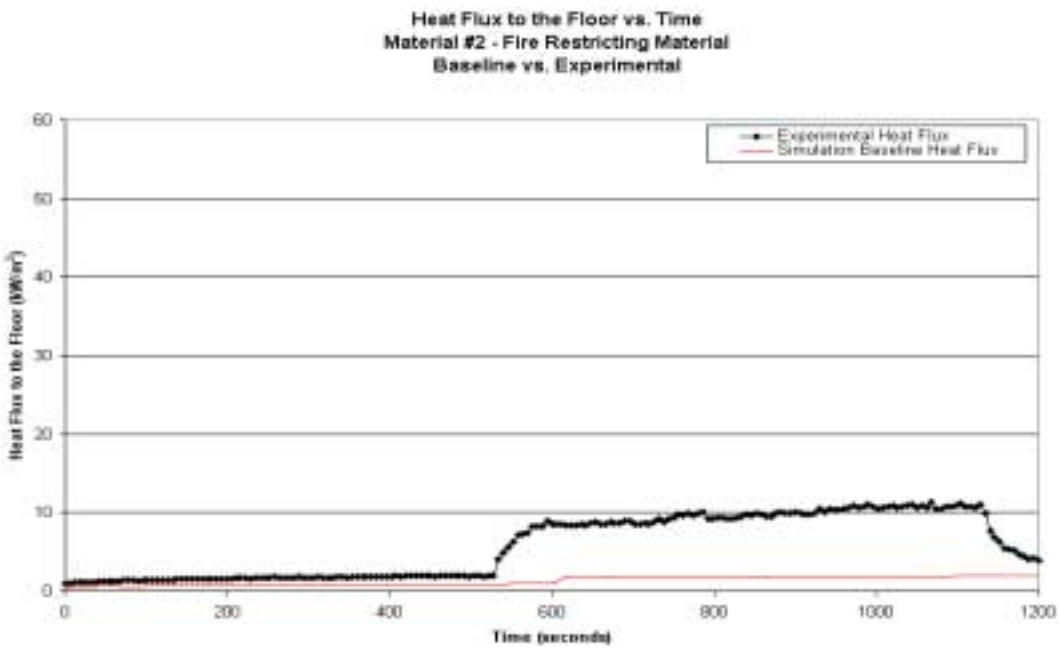

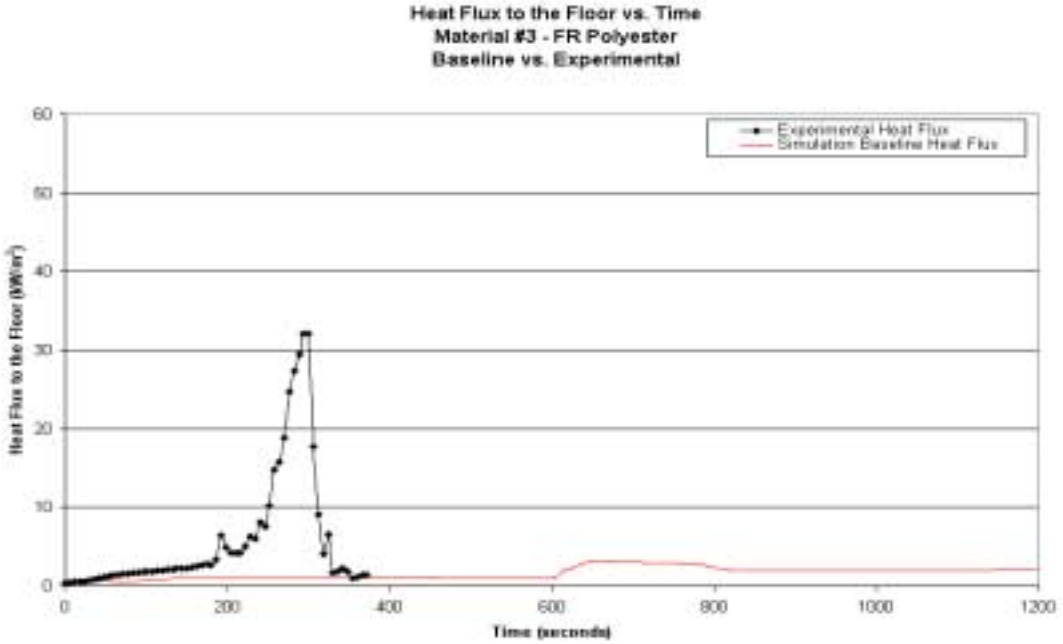
Heat Flux to the Floor vs. Time
Material #3 - FR Polyester
Baseline vs. Experimental
Experimental Heat Flux
Simulation Baseline Heat Flux
Heat Flux to the Floor (kW/m²)
Time (seconds)
0
10
20
30
40
50
60
0
200
400
600
800
1000
1200

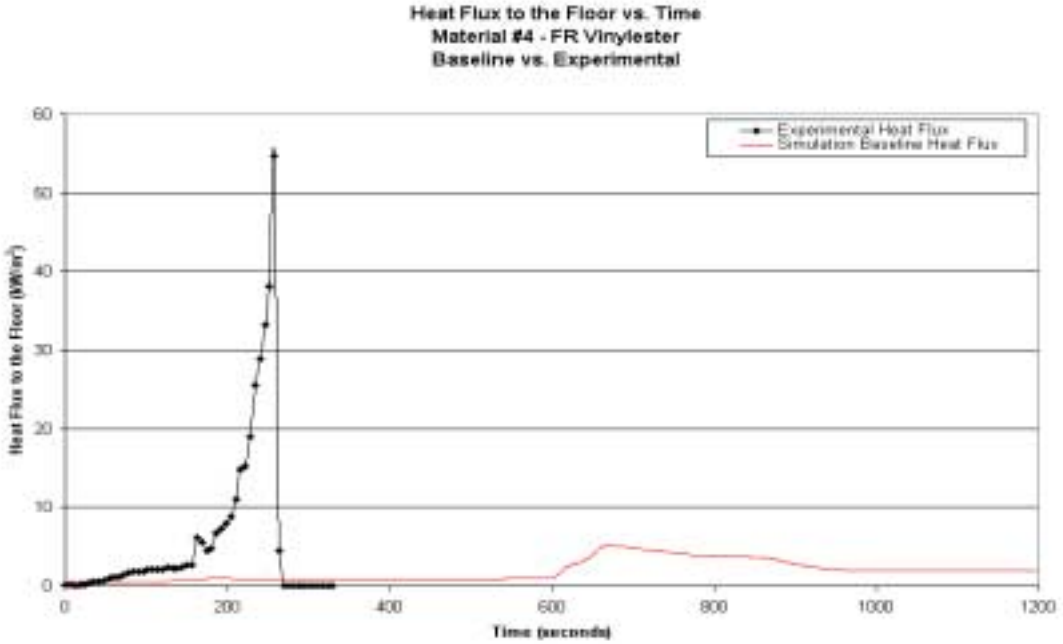
Heat Flux to the Floor vs. Time
Material #4 - FR Vinylester
Baseline vs. Experimental
Experimental Heat Flux
Simulation Baseline Heat Flux
Heat Flux to the Floor (kW/m²)
Time (seconds)
0
10
20
30
40
50
60
0
200
400
600
800
1000
1200

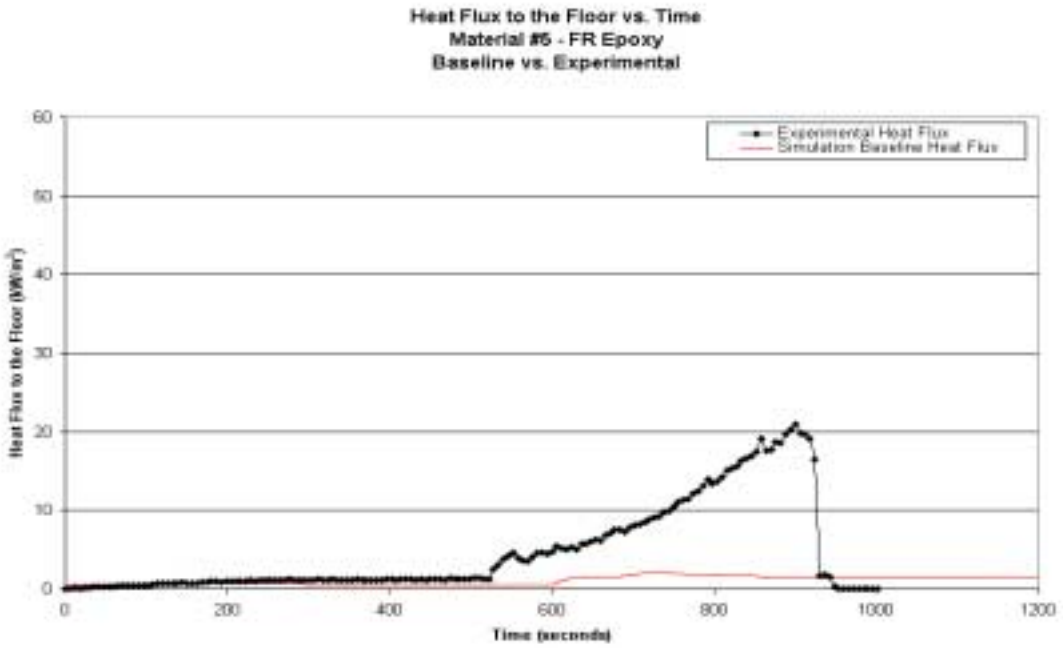
Heat Flux to the Floor vs. Time
Material #5 - FR Epoxy
Baseline vs. Experimental
Experimental Heat Flux
Simulation Baseline Heat Flux
Heat Flux to the Floor (kW/m²)
Time (seconds)
0
10
20
30
40
50
60
0
200
400
600
800
1000
1200

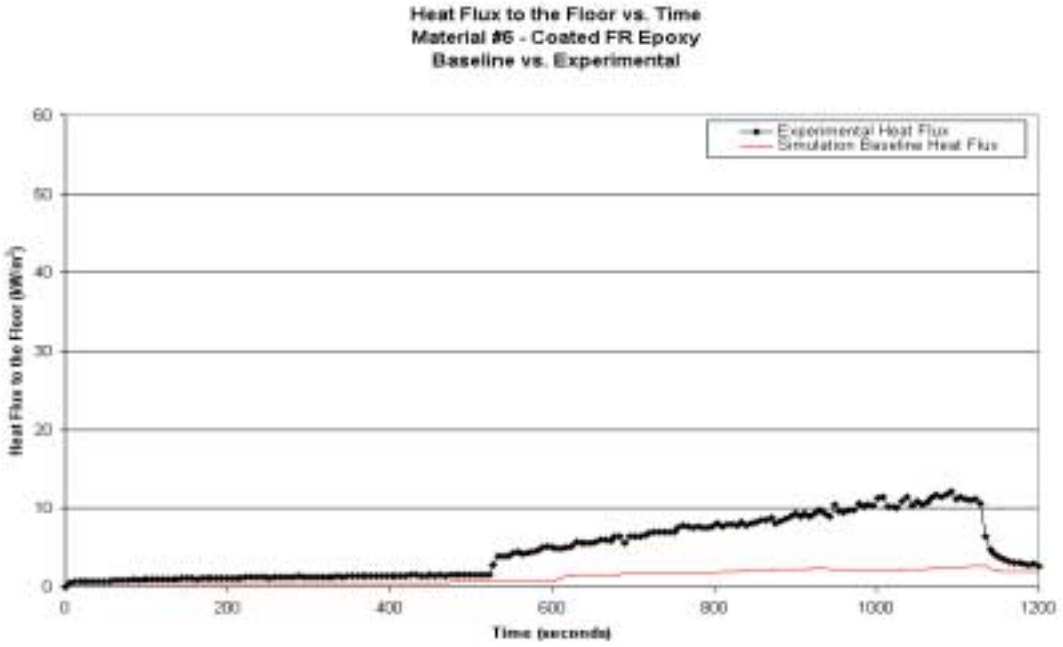
Heat Flux to the Floor vs. Time
Material #6 - Coated FR Epoxy
Baseline vs. Experimental
Experimental Heat Flux
Simulation Baseline Heat Flux
Heat Flux to the Floor (kW/m²)
Time (seconds)
0
10
20
30
40
50
60
0
200
400
600
800
1000
1200

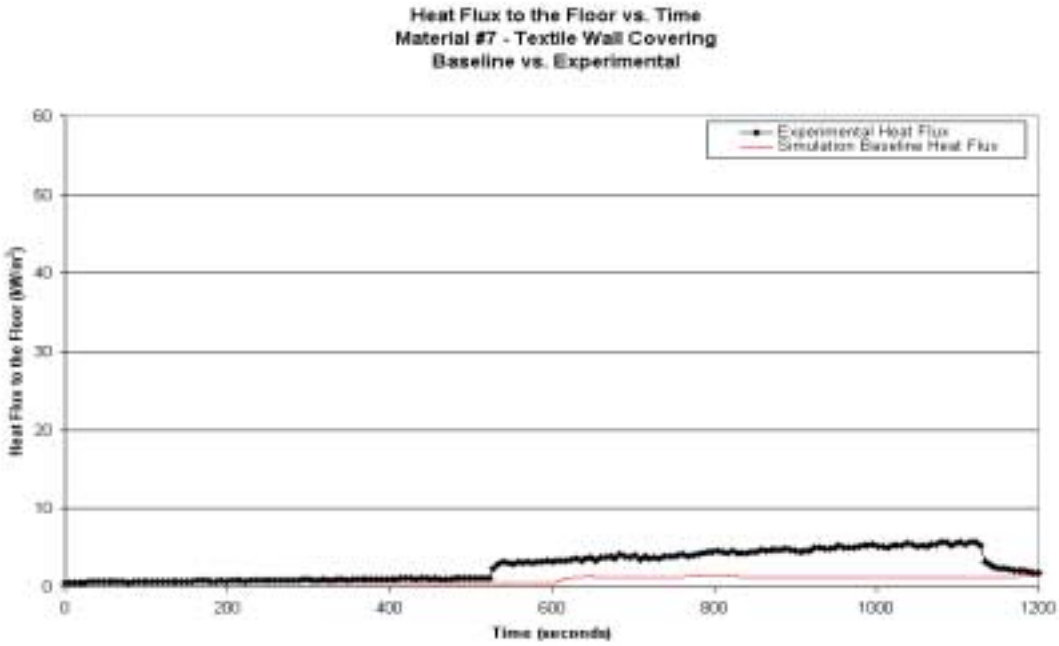
Heat Flux to the Floor vs. Time
Material #7 - Textile Wall Covering
Baseline vs. Experimental
Experimental Heat Flux
Simulation Baseline Heat Flux
Heat Flux to the Floor (kW/m²)
Time (seconds)
0
10
20
30
40
50
60
0
200
400
600
800
1000
1200

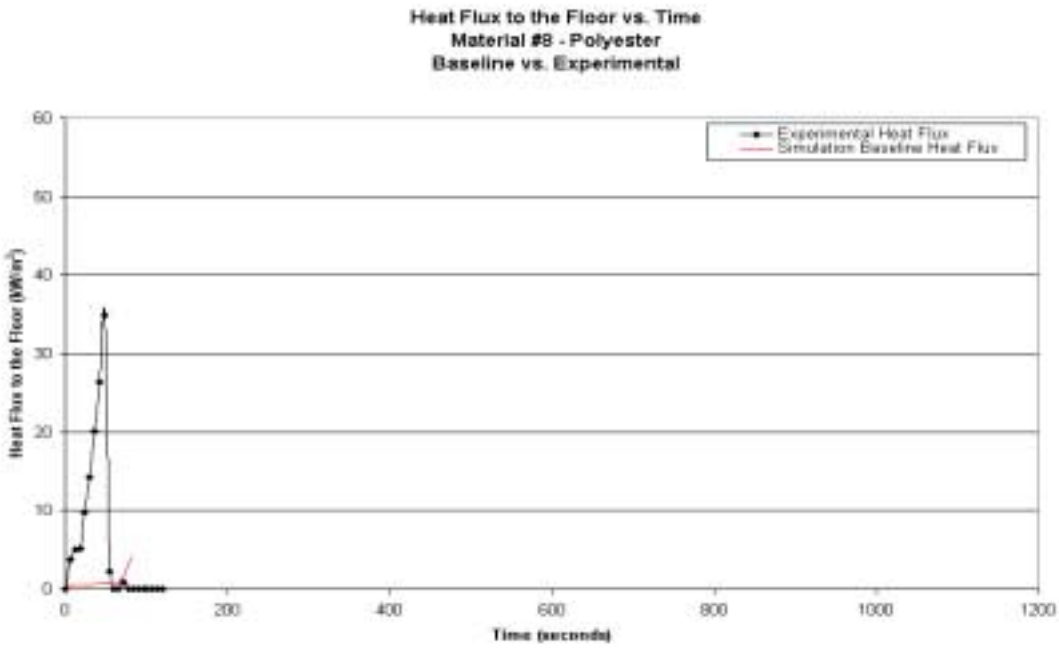
Heat Flux to the Floor vs. Time
Material #8 - Polyester
Baseline vs. Experimental
Experimental Heat Flux
Simulation Baseline Heat Flux
Heat Flux to the Floor (kW/m²)
Time (seconds)
0
10
20
30
40
50
60
0
200
400
600
800
1000
1200

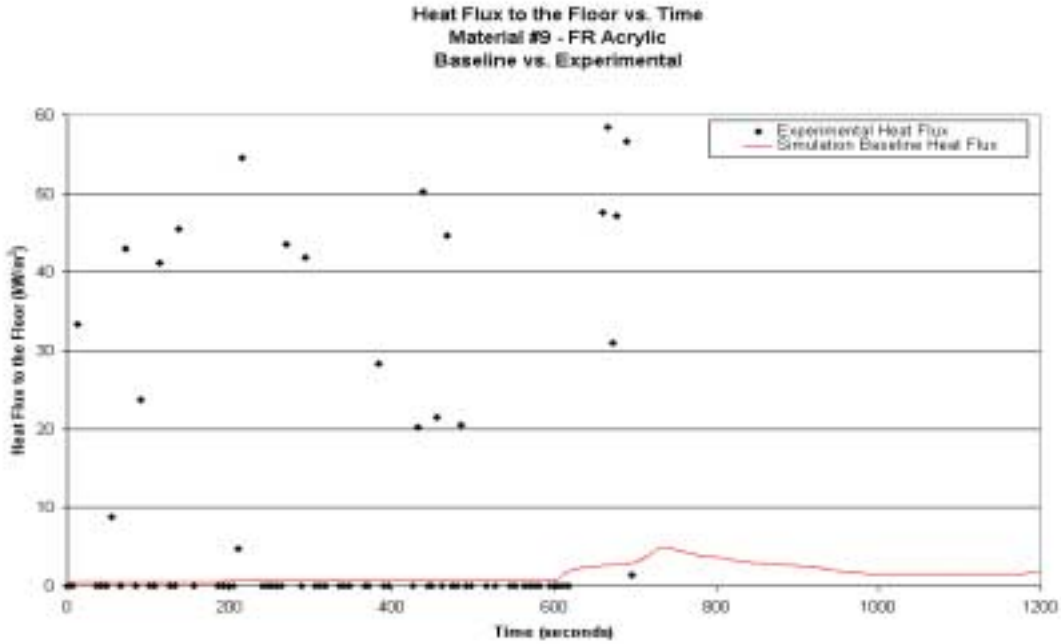
Heat Flux to the Floor vs. Time
Material #9 - FR Acrylic
Baseline vs. Experimental
Experimental Heat Flux
Simulation Baseline Heat Flux
Heat Flux to the Floor (kW/m²)
Time (seconds)
0
10
20
30
40
50
60
0
200
400
600
800
1000
1200

12.0 REFERENCES

American Society for Testing and Materials. Standard Test Method for Determining Material Ignition and Flame Spread Properties. ASTM E-1321-97a. American Society for Testing and Materials: West Conshohocken, PA. 1997.

Bradley, G. L., and K. J. Smith. Calculus. Prentice Hall: Upper Saddle River, NJ. 1995. pp. 303-304.

Carlsaw, H. S., and J. C. Jaeger. Conduction of Heat in Solids. Oxford University Press: Oxford. 1959. pp. 76.

Dillon, S. E. Analysis of the ISO 9705 Room/Corner Test: Simulations, Correlations, and Heat Flux Measurements. NIST-GCR-98-756. U.S. Dept. of Commerce. National Institute of Standards and Technology: Gaithersburg, MD. 1998.

Drysdale, Dougal. An Introduction to Fire Dynamics. 2nd ed. John Wiley and Sons: Chichester, England. 1999.

Grenier, A.T., N. A. Dembsey, and J. R. Barnett. "Fire Characteristics of Cored Composite Materials for Marine Use." *Fire Safety Journal*. V.30. 1998. pp. 137-159.

Hasemi, Y. and T. Tokunaga. "Some Experimental Aspects of Turbulent Diffusion Flames and Buoyant Plumes from Fire Sources Against a Wall and in a Corner of Walls." *Combustion Science and Technology*. V.40. 1984. pp. 1-17.

International Maritime Organization. FTP Code: International Code for Application of Fire Test Procedures (Resolution MSC.61(67)). "Resolution A.653(16) – Recommendation on Improved Fire Test Procedures for Surface Flammability of Bulkhead, Ceiling and Surface Finish Materials (1989)." International Maritime Organization: London. 1998.

International Organization for Standardization. International Standard ISO 5660: Fire Tests – Reaction to Fire – Part 1: Rate of Heat Release from Building Products (Cone Calorimeter Method). Reference number ISO 5660-1:1993. International Organization for Standardization: Geneva, Switzerland. 1993.

International Organization for Standardization. International Standard ISO 9705: Fire Tests – Full-scale room test for surface products. Reference number ISO 9705:1993(E). International Organization for Standardization: Geneva, Switzerland. 1993.

Jacoby, D. Ignition Characteristics of Marine Cored Composites: Effect of Skin Thickness and Core Composition. Worcester Polytechnic Institute: Worcester, MA. 1998.

Janssens, M.L., A. Garabedian, and W. Gray. Establishment of international Standards Organization (ISO) 5660 Acceptance Criteria for Fire Restricting Materials Used on High Speed Craft. U.S. Dept. of Transportation. U.S. Coast Guard. Marine Safety and Environmental Protection (G-M): Washington, DC. 1998.

Karlsson, Björn. Modeling Fire Growth on Combustible Lining Material in Enclosures. Lund University: Sweden, 1992.

Lay, D. Linear Algebra and its Applications. Addison-Wesley: New York. 1997. pp. 145-147.

Mitler, Henri E. and Kenneth D. Steckler. SPREAD – a Model of Flame Spread on Vertical Surfaces. NISTIR 5619. U.S. Dept. of Commerce. National Institute of Standards and Technology: Gaithersburg, MD. Written 1993, Issued 1995.

Mitler, Henri E. An Algorithm to Describe the Spread of a Wall Fire Under a Ceiling. NISTIR 5547. U.S. Dept. of Commerce. National Institute of Standards and Technology: Gaithersburg, MD. 1994.

Peacock, R. D., G. P. Forney, P. A. Reneke, R. M. Portier, and W. W. Jones. CFAST, the Consolidated Model of Fire Growth and Smoke Transport. NIST Technical Note 1299. U.S. Department of Commerce, National Institute of Standards and Technology: Gaithersburg, MD. 1993.

Peacock, R. D., P. A. Reneke, W. W. Jones, R. W. Bukowski, and G. P. Forney. A User's Guide for FAST: Engineering Tools for Estimating Fire Growth and Smoke Transport. NIST Special Publication 921. U.S. Department of Commerce, National Institute of Standards and Technology: Gaithersburg, MD. 1997.

Quintiere, James, G. "A Simulation Model for Fire Growth on Materials Subject to a Room-Corner Test." *Fire Safety Journal.* V.20. 1993. pp. 313-339.

Satterfield, D.B., and J.R. Barnett. User's Guide for WPI/Fire Version 2: Compartment Fire Model. Worcester Polytechnic Institute: Worcester, MA. 1990.

Tewarson, A. SFPE Handbook of Fire Protection Engineering. 2nd ed. "Generation of Heat and Chemical Compounds in Fires." National Fire Protection Association: Quincy, MA. 1995.

Tien, C.L., K.Y. Lee, and A.J. Stretton. SFPE Handbook of Fire Protection Engineering. 2nd ed. "Radiation Heat Transfer." National Fire Protection Association: Quincy, MA. 1995.

Wright, M. T. Flame Spread on Composite Materials for use in High Speed Craft. Worcester Polytechnic Institute: Worcester, MA. 1999.

APPENDIX C

HUGHES ASSOCIATES, INC./U.S. NAVY CORNER FLAME SPREAD MODEL AND COMPARISON WITH USCG ISO 9705 TEST RESULTS

Written by

Sean Hunt
Brian Lattimer
Craig Beyler
Hughes Associates, Inc.
3610 Commerce Drive, Suite 718

November, 1999

CONTENTS

Page

1.0 OVERVIEW C-4

2.0 SUMMARY OF NEW FLAME SPREAD MODEL CALCULATIONS C-5

2.1 Overview of the Corner Flame Spread Model Calculations C-5

2.2 Heat Flux Correlations C-6

2.2.1 Area Source Fire Scenario C-6

2.2.2 Line Source Fire Scenario C-10

2.3 Opposed Flow Flame Spread C-11

2.4 Hot Layer Effects C-12

2.5 Heat of Gasification C-14

3.0 MODEL VALIDATION C-19

3.1 Validation Test 1: Vinyl Ester (40 % Resin) in ISO 9705 Room C-20

3.2 Validation Test 2: Vinyl Ester (30 % Resin) in Full Scale Open Corner Test C-21

3.3 Validation Test 3: Phenolic Resin Composite in ISO 9705 Room C-21

3.4 Validation Test 4: Plywood in Full Scale Open Corner Test C-27

3.5 Evaluation of the Effect of the Hot Layer C-27

4.0 MODEL RESULTS C-30

4.1 Material Properties C-30

4.2 Heat Release Rate Comparisons C-32

4.3 Hot Layer Temperature Comparisons C-32

4.4 Heat Flux to the Floor C-51

4.5 Smoke Production Rate C-51

5.0 SENSITIVITY ANALYSIS C-70

5.1 Solution Convergence C-70

5.2 Material Properties C-73

5.2.1 Substrate Thickness C-73

5.2.2 Composite Thickness C-74

5.2.3 Percent Mass Burned C-74

5.2.4 LIFT Thermal Inertia C-74

5.2.5 LIFT Flame Heating Parameter C-83

5.2.6 Minimum Temperature for Flame Spread C-83

5.2.7 Heat of Gasification C-83

5.2.8 Critical Heat Flux C-89

5.2.9 Ignition Time C-89

5.2.10 Lateral Flame Spread Velocity C-89
5.2.11 Cone Calorimeter Heat Release Rate C-97
5.3 Room Dimensions C-97

6.0 SUMMARY C-104
6.1 Calculation Results C-104
6.2 Model Sensitivity C-107

7.0 REFERENCES C-109

1.0 OVERVIEW

The current version of the flame spread model is an expanded and improved version of the earlier vertical wall flame spread model [Williams *et al.*, 1997, Beyler *et al.*, 1997]. Additional features include two dimensional flame spread, area source fire exposures, corner/ceiling configurations, and hot layer effects. The model retains the ability to calculate flame spread on vertical walls that are not influenced by a corner or ceiling. All new features incorporated into the current flame spread model are summarized in this report. A model verification section is also included. The model results when used to predict the USCG ISO 9705 full-scale room fire tests are presented and compared with the test data. The ISO 9705 room fire tests were performed on a variety of composite materials for the U. S. Coast Guard. The reader is referred to Williams *et al.* [1997] and Beyler *et al.* [1997] for details regarding the mechanics of previously incorporated features.

The flame spread model retains the element and node concept and the surface-heating algorithm that was part of the original version. A node has a specific coordinate relative to the base of the corner and an element is a region bounded by four nodes, one at each corner. This version of the flame spread model divides the corner-ceiling configuration into uniformly spaced horizontal and vertical nodes. Symmetry requires that the ceiling be square and that it be discretized in the same way as the horizontal wall dimension. The flame spread model calculates the temperature and burning condition at each element. The documentation for the original flame spread model explains in detail how the elements and nodes are treated and the specifics of the surface heating equations [Williams *et al.*, 1997]. The focus of this document is to present the new features of the model and the results of the model predictions of the USCG ISO 9705 tests.

This study was motivated by the need to evaluate the performance of composite materials. A means of predicting the heat release rate and the flame spread potential of materials with known properties was sought. A computer flame spread model seemed ideally suited for this goal, offering the ability to calculate conditions on an elemental basis where simple hand calculations fall short. The corner version of the flame-spread model was developed for the U. S. Navy to predict the performance of composite materials in an open corner test configuration [Lattimer *et al.*, 1999]. When this code was adapted for use with the U. S. Coast Guard ISO 9705 tests, it was apparent that the effect of the hot layer had to be included. Hence, an expanded version of the corner flame spread model was developed.

2.0 SUMMARY OF NEW FLAME SPREAD MODEL CALCULATIONS

2.1 Overview of the Corner Flame Spread Model Calculations

The corner flame spread model uses a two-dimensional flame spread algorithm to calculate the total heat release rate of a corner fire as a function of time. The model assumes that the corner is symmetrical such that each wall segment is the same size and the ceiling is square. The fire source, which can either be a line fire or an area fire, must always be located in the corner. Figure 2-1 shows the corner configuration after the wall and ceiling have ignited for an area source fire and Figure 2-2 shows the same corner configuration for a line burner source fire.

Three distinct burning regions were identified in corner fires during the full-scale open corner fire tests [Lattimer *et al.*, 1999]. These regions, also shown in Figures 2-1 and 2-2, are (1) the area on the wall ignited by the fire source, (2) the ceiling, and (3) the upper part of the wall ignited by the ceiling jet. Heat flux correlations were obtained from the full-scale open corner fire test data for each of the three regions. The heat flux correlations generally depend on the type of source fire, the target position relative to the heat source, and the total heat release rate of the source fire and the walls.

Two of the three regions support lateral flame spread in the model. The portion of the wall ignited by the source fire laterally spreads away from the corner and the portion of the wall ignited by the ceiling jet laterally spreads downward. The ceiling is not assumed to support lateral flame spread in this model. The only mechanism that a ceiling element can ignite is by surface heating in response to the incident heat flux.

An entirely new feature to the flame spread program is the ability to calculate the heat transfer to the wall and ceiling from a hot gas layer. This is particularly useful for predicting flame spread in small compartments. When reviewing the ISO 9705 test data, it was concluded that the hot gas layer has a significant effect on the flame spread and total heat release rate in the compartment. The current method for predicting the hot layer temperature used by the flame spread model is based on an empirical correlation that was modified for a corner configuration.

An important task of the flame spread model is to keep track of the corner fire burning stage. There are three possible burning stages during the corner fire burning process, though all three do not need to be experienced in any given simulation. The stages are a means for addressing the appropriate heat release rate to use in the heat flux functions. The stages depend on which portions of the wall and

ceiling are burning or are burned out, and on the status of the source fire. The first stage assumes that there is a source fire and that the wall heat release rate can be added to the source heat release rate when evaluating the flame height. Normally the first stage describes the initial burning in the corner. The second stage occurs when either (1) the source is shut off or (2) the wall and ceiling have burned out beyond the area exposed by the source fire. This stage separates the source heat release rate from the wall heat release rate when calculating the flame height. The third stage occurs when the ceiling has spread beyond the wall fire and has burned out in the area where the wall fire is located. This stage separates the source and/or wall heat release rate from the ceiling heat release rate and calculates the flame height/lengths separately. The next sections describe the heat flux correlations assuming that the corner is burning under the first stage criteria. The discussion is readily extended to the second and third stage burning conditions. The model automatically determines which stage to use at each time step. In most cases, the first stage will persist until the end of the simulation.

2.2 Heat Flux Correlations

The heat flux incident on a cell determines when a cell will ignite and how much heat will be released from that cell once ignition occurs. Empirical correlations are used by the model to determine the heat flux incident on each cell in the simulation at each time step. Due to the three-dimensional nature of the corner fire, several heat flux correlations are necessary to describe the heat fluxes on the wall and the ceiling. As previously described, three distinct regions were assumed in a corner fire: the walls, the ceiling, and the wall-ceiling boundary. One or more heat flux correlations is necessary for each of these regions to accurately describe the thermal environment. The type of fire in the corner also has an impact on the heat fluxes in the corner. Two types of source fire scenarios are currently included in the model: the area source fire and the line source fire. The model treatment of both situations is described in this section.

2.2.1 Area Source Fire Scenario

2.2.1.1 Walls

Initially during the fire before the walls ignite, the incident heat flux to the walls is dependent only the area source fire. The incident heat flux to the wall from an area source fire located in the corner was found to vary with the target elevation above the source fire base and the lateral distance from the corner. The peak heat flux was determined to be a function of the source diameter and is given by the following equation [Lattimer *et al.*, 1999]:

$$\dot{q}''_{peak} = 120\,(1 - \exp(-4\,D)) \tag{2-1}$$

where $\dot{q}_{peak}''$ is the peak heat flux in the corner (kW/m^2) and D is the diameter of the source (m) for square or rectangular source fires the length of the side facing the wall should be used for the diameter. The peak heat flux occurs in the corner where the two walls join. The peak heat flux varies with elevation above the base of the source fire according to the following equations [Lattimer *et al.*, 1999]:

$$\begin{aligned}
&\dot{q}''_{max}(y) = \dot{q}''_{peak} && \frac{y}{L_{f,tip}} \le 0.40 \\
&\dot{q}''_{max}(y) = \dot{q}''_{peak} - 4\left(\frac{y}{L_{f,tip}} - \frac{2}{5}\right)\left(\dot{q}''_{peak} - 30\right) && 0.4 < \frac{y}{L_{f,tip}} < 0.65 \\
&\dot{q}''_{max}(y) = 7.2\left(\frac{y}{L_{f,tip}}\right)^{-10/3} && \frac{y}{L_{f,tip}} \ge 0.65
\end{aligned} \tag{2-2}$$

where $\dot{q}_{max}''(y)$ is the maximum heat flux from an area source fire to the corner where the two walls meet (kW/m^2), y is the target elevation above the base of the source fire (m), and $L_{f,tip}$ is the flame tip length measured from the fire base (m).

The flame tip length is a function of the dynamic diameter of the fire, *d(t)*, which is defined in this context as the width of burning wall 0.9 m above the base of the source fire. The flame spread at this elevation was measured in the tests and was the assumed diameter when correlating the data. If this width is less than the diameter of the source fire, then the source fire diameter is used. The flame length for an area source was determined using:

$$L_{f,tip} = 5.9\,d(t)\,\dot{Q}_d^{*\,1/2} \tag{2-3}$$

where *d(t)* is the dynamic diameter (m) and $\dot{Q}_d^*$ is a dimensionless heat release rate parameter. The dimensionless heat release rate parameter is calculated using the following equation:

$$\dot{Q}_d^* = \frac{\dot{Q}(t)}{1090\,d(t)^{5/2}} \tag{2-4}$$

where $\dot{Q}(t)$ is the total heat release rate of the source fire and the walls. Note that the heat release from the ceiling is excluded from the flame length calculation. This was done because all of the heat flux correlations were developed with fires located below the ceiling.

The horizontal heat flux distribution from the source was found to be a function of the distance from the corner and the maximum vertical heat flux distribution:

$$\dot{q}''(x,y) = \dot{q}''_{max}(y)\exp(-7.5\,x^2) \tag{2-5}$$

where $\dot{q}''(x,y)$ is the horizontal and vertical heat flux distribution on the wall (kW/m^2) and x is the distance from the corner (m). This relation was applied at all values of x.

As material in the corner ignites, the heat flux to the surface becomes some combination of the heat fluxes generated by the area source fire and those generated by the wall fire. Flat wall fires have been shown to produce heat fluxes similar to those produced by line fires against a flat wall [Quintiere *et al.*, 1986]. This is attributed to the flames produced in both cases being relatively thin flames that buoyantly rise up the surface. For the corner configuration, the flames from burning walls were assumed to produce heat flux levels similar to those measured with an "L" shaped line burner in the corner.

Cells that ignite between the corner and the edge of the burner had an incident flux that was equal to either result from Equation 2-3 or an incident flux of 50 kW/m^2, whichever is larger. The 50 kW/m^2 was determined from an average of the heat fluxes measured over the width of the flaming region in the "L" shaped burner tests. The 50 kW/m^2 minimum heat flux was applied because in some cases the correlation may underpredict the heat flux to the wall as it is a best-fit function. Because 50kW/m^2 was the measured average in this region, this limit was placed on the correlation. Attempts to use the line burner correlation instead of the prescribed minimum heat flux resulted in poor predictions. It is not clear why this occurs at this time.

As cells begin to ignite outside of the burner, the wall fire is assumed to have a horizontal heat flux distribution,

$$q(x,y) = 60\exp[-1.0\,(x/d(t))^2], \tag{2-6}$$

where $d(t)$ is the distance between the corner and the horizontal flaming pyrolysis front. This relation is a simplified version of the horizontal relation developed from the "L" line burner tests. When cells are

burning outside the edge of the burner, the heat flux incident upon burning cells outside the burner is taken as the highest of the three values: 50 kW/m^2, the result from Equation 2-5 , or the result from Equation 2-6. For cells that are not ignited but the wall is ignited outside of the burner edge, the incident heat flux is either the result from Equation 2-5 or the result from Equation 2-6, whichever is largest. This approach allows the model to decide when the wall fire begins to dominate the preheating process.

2.2.1.2 Wall-Ceiling Boundary

The heat flux along the wall-ceiling boundary is physically due to the hot ceiling jet traveling out from the corner. As a result, the heat flux decays with distance from the corner as follows:

$$\dot{q}_c''(x) = 120 \qquad \left(\frac{x+H}{L_{f,tip}}\right) \le 0.52$$

$$\dot{q}_c''(x) = 13.0\left(\frac{x+H}{L_{f,tip}}\right)^{-3.5} \qquad \left(\frac{x+H}{L_{f,tip}}\right) > 0.52 \tag{2-7}$$

This relation is applied along the wall-ceiling boundary outside of the burning region on the wall. Along this region, the heat flux was assumed to be constant over the depth of the ceiling jet, which was taken to be $\delta = 0.1\,H$ [Alpert, 1975]. Cells over the ceiling jet depth that have ignited were assumed to have an incident heat flux of either the result in Equation 2-7 or 30 kW/m^2, whichever is greater. Refer to Section 2.2.1.1 for a discussion of correlation limits such as this.

After the cells within the ceiling jet ignite, cells below the ceiling jet begin getting preheated. The heat flux distribution below the ceiling jet is described through the following relation:

$$q''(y) = 30\exp\{-12[(H-y)-d_c(t)]\} \tag{2-8}$$

where $d_{cj}(t)$ is distance between the wall-ceiling boundary flame front and the ceiling. This relation is based on results from the “L” shaped burner tests.

2.2.1.3 Ceiling

The heat flux distribution on the ceiling was found to be a function of the radial distance from the corner. This was found to be the case whether or not the ceiling was burning. The following equations describe the heat flux distribution on the ceiling:

$$\dot{q}_c''(r) = 120 \qquad \left(\frac{r+H}{L_{f,tip}}\right) \le 0.52$$

$$\dot{q}_c''(r) = 13.0\left(\frac{r+H}{L_{f,tip}}\right)^{-3.5} \qquad \left(\frac{r+H}{L_{f,tip}}\right) > 0.52 \tag{2-9}$$

where $\dot{q}_c''(r)$ is the incident heat flux on the ceiling (kW/m^2) at a distance r (m) from the corner, H is the height of the ceiling above the floor (m), and $L_{f,tip}$ is the height of the flame tip (m) calculated using Equations 2-3 and 2-4. This is the same correlation used in the wall-ceiling boundary region, except the x is replaced with r. The radial coordinate of each ceiling element is calculated from the Cartesian coordinate of the element center:

$$r = \sqrt{x_c^2 + z_c^2} \tag{2-10}$$

where x_c is the x-coordinate of the element center relative to the corner (m) and z_c is the z-coordinate of the element center relative to the corner (m).

Burning ceilings have been shown to produce heat fluxes of 20 kW/m^2 [Hasemi et al, 1995]. For this reason, ignited cells on the ceiling have a heat flux of either that determined in Equation 2-9 or 20 kW/m^2, whichever is greater. Refer to Section 2.2.1.1 for a discussion on correlation limits such as this.

2.2.2 Line Source Fire Scenario

The line source fire scenario is treated very similar to that of the area source fire scenario with the exception of the conditions produced by the line source fire itself. As previously described, line fire sources result in flat, thin flames that buoyantly rise along a surface. Line fires against a flat wall have been shown to result in lower heat fluxes compared with those produced by the area fire sources in a similar configuration [Quintiere et al, 1986; Back *et al.*, 1994]. This effect is believed to be due to line fires producing thinner flames than area fires [Quintiere *et al.*, 1992]. Results from tests performed in this study and elsewhere [Kokkala, 1993; Hasemi *et al*, 1996] have shown that “L” shaped line fires placed in a corner produce lower heat fluxes than area fires.

The peak heat flux to the wall surface is a function of the elevation above the base of the source only and is not a function of the source heat release rate or the width of the base. The following equation describes the maximum heat flux to the wall in the corner:

$$q''_{\max} = 70 \qquad \frac{y}{L_{f,tip}} \le 0.5$$

$$q''_{max} = 10.0\left(\frac{y}{L_{f,tip}}\right)^{-2.8} \qquad \frac{y}{L_{f,tip}} > 0.5 \qquad (2\text{-}11)$$

where y is the target elevation above the base of the source fire (m) and $L_{f,tip}$ is the flame tip length (m). The flame tip was determined using Equations 2-3 and 2-4, which are the same equations used in the area source fire scenario. The horizontal heat flux distribution is given by the following equation:

$$\dot{q}''(x,y) = \dot{q}''_{max}(y)\exp[-1.0(x/d)^2] \qquad (2\text{-}12)$$

where all terms have been defined. Once the wall begins to ignite, the heat flux to the wall is determined using the same procedures used in the area source fire scenario, except the horizontal heat flux distribution for the area source fire is replaced by the one for the line source fire given in Equation 2-12.

The heat flux to the wall ceiling boundary and the ceiling were determined in the noncombustible boundary testing to be insensitive to the type of source fire in the corner. As a result, the model uses the same procedures outlined in the area source fire section to determine the heat fluxes in these regions with a line source fire in the corner.

2.3 Opposed Flow Flame Spread

Opposed flow flame spread is the mechanism by which flame spreads laterally along the wall from the corner and down the wall below the ceiling. The opposed flow spread velocity has been shown to be a function of the thermal properties, flame spread properties, and the surface temperature of the elements that are adjacent to a burning zone [Quintiere and Harkleroad, 1985]. Thermal and flame spread properties for a material are determined from the LIFT apparatus using the procedure outlined in ASTM E1321 [1997]. To model the opposed flow flame spread, flame front spread velocity is calculated using the following relation [Quintiere and Harkleroad, 1985]:

$$v(i,j,t) = \frac{\Phi}{(k\rho c)_L (T_{ig} - T_s)^2} \qquad (2\text{-}13)$$

where $v(i,j,t)$ is the lateral flame spread velocity across element i,j at time t (m/s), Φ is the flame heating parameter measured in the LIFT apparatus (kW^2/m^3), $k\Delta c$ is the effective thermal inertia and is also measured in the LIFT

apparatus (kW^2-s/m^4-K^2), T_{ig} is the material ignition temperature (K), and T_s is the surface temperature (K). If T_s is less than the minimum temperature for lateral flame spread, $T_{s,min}$, determined in the LIFT apparatus, then no opposed flow flame spread is calculated.

The three opposed flow flame material properties, Φ, $k\Delta c$, $T_{s,min}$, collectively define how quickly a material will propagate flame either laterally or downward. Materials that have a flame heating parameter, Φ, equal to 0 kW^2/m^3 do not spread flame laterally or downward, while materials with a large flame heating parameter tend to rapidly spread flame laterally or downward. Materials that spread flame slowly typically have a minimum flame spread temperature close to their ignition temperature. In other words, these materials need to be heated to nearly their ignition temperature before opposed flow flame spread is even possible. The LIFT $k\Delta c$ value is derived from the surface heat loss coefficient at the ignition temperature and the ignition time data [Quintiere and Harkleroad, 1985]. It is important to note that this $k\Delta c$ parameter used for opposed flow flame spread is different from the $k\Delta c$ parameter used in the surface-heating algorithm, and the two parameters are not interchangeable. Consequently, the model requires input of both $k\Delta c$ values.

Opposed flow flame spread is implemented after the wall has ignited. In the wall region, opposed flow flame spread calculations are performed on cells horizontally adjacent to an ignited cell. In the wall-ceiling interface region, opposed flow flamespread calculations are performed on cells vertically adjacent to an ignited cell. Elements outside of the burning region can either be ignited from surface heating or through the opposed flow flame spread. The maximum ignition time of an adjacent element is calculated using the opposed flow flame spread algorithm using the flame spread velocity and the dimensions of the element. This ignition time is stored and updated after each time step. If the element has not ignited and the maximum ignition time has been reached, then the element is ignited and the surface temperature raised to the ignition temperature. If a particular element happens to be adjacent to both regions, the shortest element dimension determines which direction the flame spread occurs.

2.4 Hot Layer Effects

The effect of the hot layer on the heating and subsequent ignition of the wall and ceiling materials was found to be very significant after reviewing the USCG ISO 9705 fire test data. This effect was most pronounced when the hot gas layer temperature exceeded the minimum flame spread temperature, $T_{s,min}$. If the hot gas layer temperature exceeded the ignition temperature of the wall and ceiling materials then flashover was found to be imminent. As a direct result of these findings, it was apparent that an accurate prediction of the hot layer temperature is a critical aspect of the flame spread model.

The most readily integrated approach to calculating the hot gas layer temperature in a compartment is the method of McCaffrey, Quintiere, and Harkleroad (the MQH Method) [McCaffrey *et al.*, 1981]. The MQH method is an empirical relation that uses dimensionless variables to correlate the average hot gas layer temperature in a compartment. The MQH calculation assumes that the hot gas layer temperature is calculated using the following equation:

$$T_r\ (t) = 1.63\ T_\infty \left(\frac{\dot{Q}\ (t)}{c_p\ \rho_\infty\ A_o\ \sqrt{g\ H_o}} \right)^{2/3} \left(\frac{h_k\ \ A_T}{c_p\ \rho_\infty\ A_o\ \sqrt{g\ H_o}} \right)^{-1/3} + T_\infty \qquad (2\text{-}14)$$

where $T_r(t)$ is the room temperature (K) at time t (s), T_4 is the initial/ambient room temperature (K), c_p is the heat capacity of air (1.0 kJ/kg), ρ_4 is the density of air at ambient temperature (1.2 kg/m^3), A_o is the total area of the openings (m^2), g is the acceleration of gravity (9.8 m/s^2), H_o is the height of the opening (m), h_k is the effective heat transfer coefficient (kW/m^2-K), and A_T is the total wall and ceiling surface area of the compartment (m^2).

The effective heat transfer coefficient can be calculated from the following equations [McCaffrey *et al.*, 1981]:

$$h_k = \sqrt{\frac{k\ \rho\ c_p}{t}} \qquad (2\text{-}15)$$

where k is the wall boundary thermal conductivity (kW/m-K), ρ is the wall boundary density (kW/m^3), c_p is the wall heat capacity (kJ/kg-K). If there is more than one wall material, as is the case when a composite is attached to a substrate, then a weighted average should be used for the thermal conductivity, density, and heat capacity. The weighted average can be found using the following equation:

$$TP_{avg} = \frac{1}{\delta} \bullet \sum_{i=1}^{n} \delta_i\, TP_i \qquad (2\text{-}16)$$

where TP is the thermal property, i is the ith material, ∗ is the wall thickness, (m), and n is the total number of materials.

Karlsson and Magnusson [1991] have modified the MQH method to account for corner effects. They found that using a connection factor of 1.34 resulted in better temperature predictions for smoke layers. This approach is used in one flame speed model.

2.5 Heat of Gasification

The flame-spread model requires an effective heat of gasification to determine the mass loss rate per unit area from an ignited cell. An average effective heat of gasification was developed using cone calorimeter data at three different irradiance levels where ignition occurred.

The procedure for determining the average effective heat of gasification was similar to that proposed in Quintiere [1993]. Heat of gasification was defined through the following relation:

$$\Delta h_g = \frac{\dot{q}''_{net}}{\dot{m}''} \tag{2-19}$$

where Δh_g is the heat of gasification (kJ/kg), $\dot{q}_{net}''$ is the heat flux to the surface of the material (kW/m^2), and $\dot{m}''$ is the mass loss rate per unit surface area (kg/m^2). The heat of gasification was used in the model to determine the heat released by the material. As such, the mass loss rate per unit area was determined using the following equation:

$$\dot{m}'' = \frac{\dot{Q}''}{\Delta H_c} \tag{2-20}$$

where $\dot{Q}''$ is the test average heat release rate per unit area (kW/m^2) and ΔH_c is the effective heat of combustion (kJ/kg). The net heat flux to the surface of a material burning in a cone calorimeter test was determined from a heat balance at the material surface:

$$\dot{q}''_{net} = \dot{q}''_{imp} + \dot{q}''_f - \dot{q}''_{loss} \tag{2-21}$$

where $\dot{q}''_{imp}$ is the imposed irradiance from the cone heater (kW/m^2), $\dot{q}''_f$ is the heat flux from the flame to the target surface (kW/m^2), and $\dot{q}''_{loss}$ is the heat loss from the target surface (kW/m^2). Heat losses are due to both convection and radiation and were calculated using the following equation [Quintiere and Harkleroad, 1985]:

$$\dot{q}_{loss}'' = h_c(T_{ig} - T_\infty) + \varepsilon\sigma(T_{ig}^4 - T_\infty^4) \tag{2-22}$$

where h_c is the convective heat transfer coefficient (0.015 kW/m^2-K), ε is the surface emissivity (0.95), σ is the Stefan-Boltzman constant (5.67E-11 kW/m^2-K^4), T_{ig} is the ignition temperature, and T_4 is the

ambient temperature (298 K). Because the ignition temperature is known, the heat losses from the surface could be calculated. Inserting Equations 2-20 and 2-21 into Equation 2-19 results in the following relation:

$$\dot{q}''_{imp} - \dot{q}''_{loss} = \Delta h_g \left(\frac{\dot{Q}''}{\Delta H_c}\right) - \dot{q}''_f \qquad (2\text{-}23)$$

where all terms have been defined. By using the cone calorimeter data at different irradiance levels, a plot of ($\dot{q}''_{imp} - \dot{q}''_{loss}$) versus $\dot{Q}''/\Delta H_c$ can be generated that should yield a straight line. The slope of this line is the average effective heat of gasification and the *y*-intercept is the negative of the flame heat flux.

The results of using this approach to calculate the average effective heat of gasification for the materials in this study are shown in Table 2-2. For most of the composites, this analysis resulted in flame heat flux values much higher than expected for the small-scale apparatus, where flame heat flux are expected to range from 20-30 kW/m^2. In addition, the analysis resulted in a negative average effective heat of gasification and a negative flame heat flux for the FR Epoxy. To determine whether these inconsistent values were due to the calculation method, a variety of other more common materials were evaluated.

Cone calorimeter and ignition data for a variety of common plastics were taken from Hirschler [1992] and Tewarson [1995]. The data for the plywood was taken from Lattimer *et al.*, [1999]. The data and the calculated average heat of gasification are also shown in Table 2-2. The average effective heat of gasification ranged between 2.0 and 4.6 MJ/kg and the flame heat flux ranged between 17 and 31 kW/m^2. The flame heat flux values for these materials are in the expected range, verifying that the approach used to determine the heat of gasification is appropriate.

The reason for the high flame heat flux values calculated for the composite materials is not known. An overestimate in the flame heat flux value results in an average effective heat of gasification that is higher than expected, making the results less conservative. More conservative values for the average effective heat of gasification of the composite materials were determined by assuming the flame heat flux is 20 kW/m^2, which is the average flame heat flux determined for the plastics and wood in Table 2-2. The results of the data analysis with the flame heat flux set to 20 kW/m^2 are shown in Table 2-3. The heat of gasification was determined to range between 4.2 and 20.5 MJ/kg. These heat of gasification values determined with a flame heat flux of 20 kW/m^2 were used in flame spread model calculations presented in this analysis.

Table 2-2. Data Needed to Determine the Heat of Gasification Using the Best-Fit Method.

Material	T_{ig} (K)	ΔH_c (MJ/kg)	Cone Test Average $\dot{Q}''$ (kW/m^2)				$\dot{q}_f''$ (kW/m^2)	Δh_g (MJ/kg)
			25	50	75	100		
U. S. Coast Guard Materials								
1-FR Phenolic	876	8.22	N.I.	29	49	54	17	10.4
2-Fire-Restricting[1]	905	9.63	N.I.	N.I.	24	35	24	21.9
3-FR Polyester	657	11.26	61	80	100	--	68	14.4
4-FR Vinyl Ester	650	13.4	80	90	120	--	76	15.5
5-FR Epoxy	726	8.7	N.I.	53	50	42	-256	-37.0
6-Coated FR Epoxy[2]	916	7.67	N.I.	N.I.	30	35	121	38.4
7-Textile Wall Covering	756	9.08	22	45	50	--	35	14.3
8-Polyester	610	21.6	225	300	390	--	62	17.5
9- FR Acrylic	658	12.33	50	70	85	--	62	17.5
Other Materials								
Plywood[4]	630	11.74	87	135	21	--	21	4.7
PMMA[3]	598	24.23	380	660	880	--	31	2.4
Polypropylene[3]	658	42.6	550	766	1,283	--	29	2.8
Polyethylene[3]	598	43.4	385	36	1,260	--	17	2.5
Nylon[3]	598	27.9	369	629	1,113	--	19	1.9

[1]Phenolic-resin-impregnate glass fiber core with malamine facing, overall thickness 0.0118 m
[2]Water based intumescent coating 0.5 mm thick
[3]Cone data from Hirschler [1992] and ignition data from Tewarson [1995]
[4]Cone and ignition data from Lattimer *et al.*, [1999]
N.I. - No ignition

Table 2-3. Calculated Heat of Gasification Assuming Flame Heat Flux of 20 kW/m^2.

Material	T_{ig} (K)	$\dot{q}_f''$ (kW/m^2)	Δh_g (MJ/kg)
1-FR Phenolic	876	20	11.0
2-Fire Restricting Material[1]	905	20	20.5
3-FR Polyester	657	20	8.0
4-FR Vinyl Ester	650	20	7.9
5-FR Epoxy	726	20	12.9
6-Coated FR Epoxy[2]	916	20	14.5
7-Textile Wall Covering	756	20	11.0
8-Polyester	610	20	4.2
9-FR Modified Acrylic	658	20	10.2

[1]Phenolic-resin-impregnate glass fiber core with malamine facing, overall thickness 0.0118 m
[2]Water based intumescent coating 0.5 mm thick

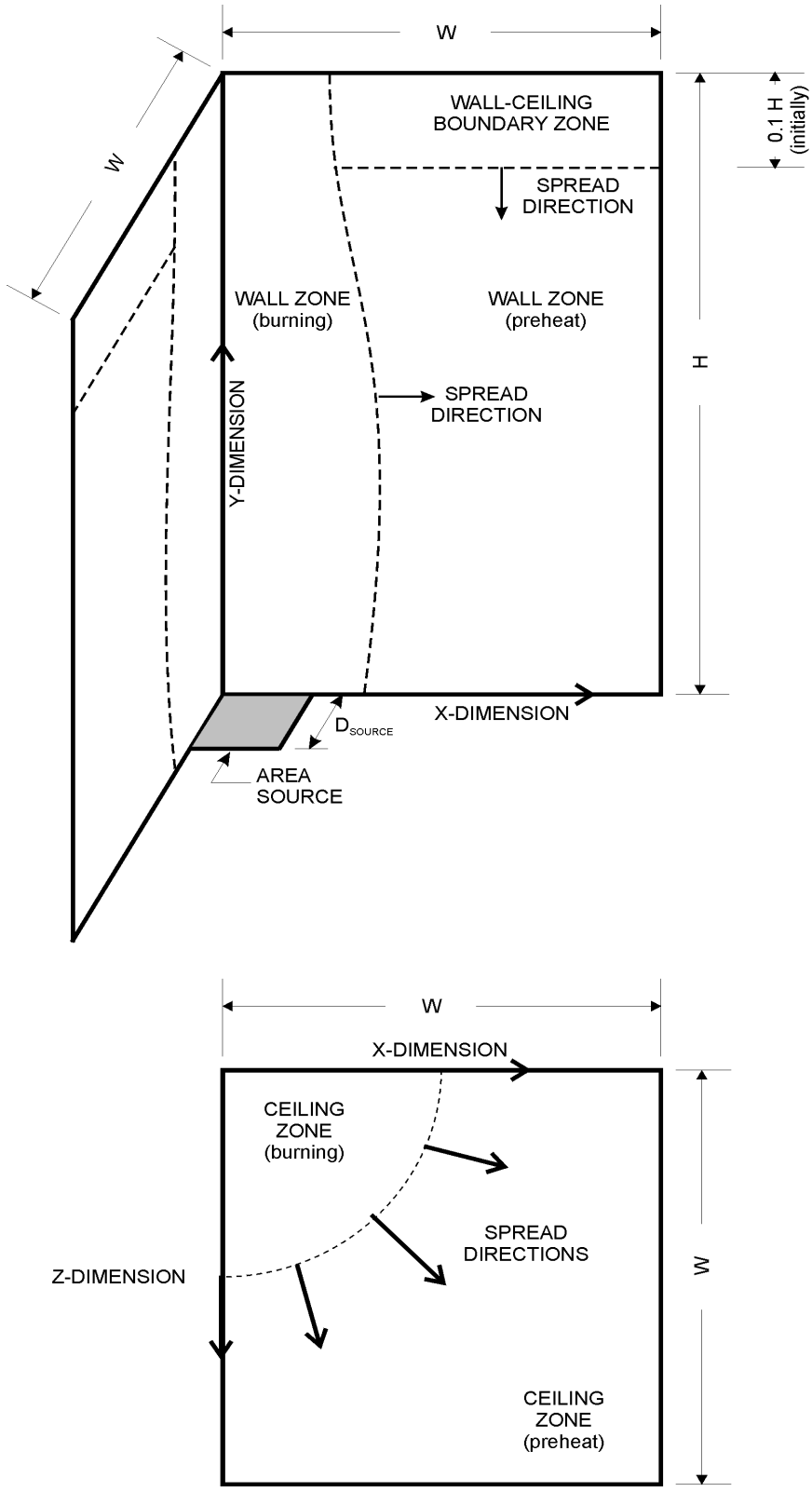

Figure 2.1. Corner Configuration with Area Source Fire.

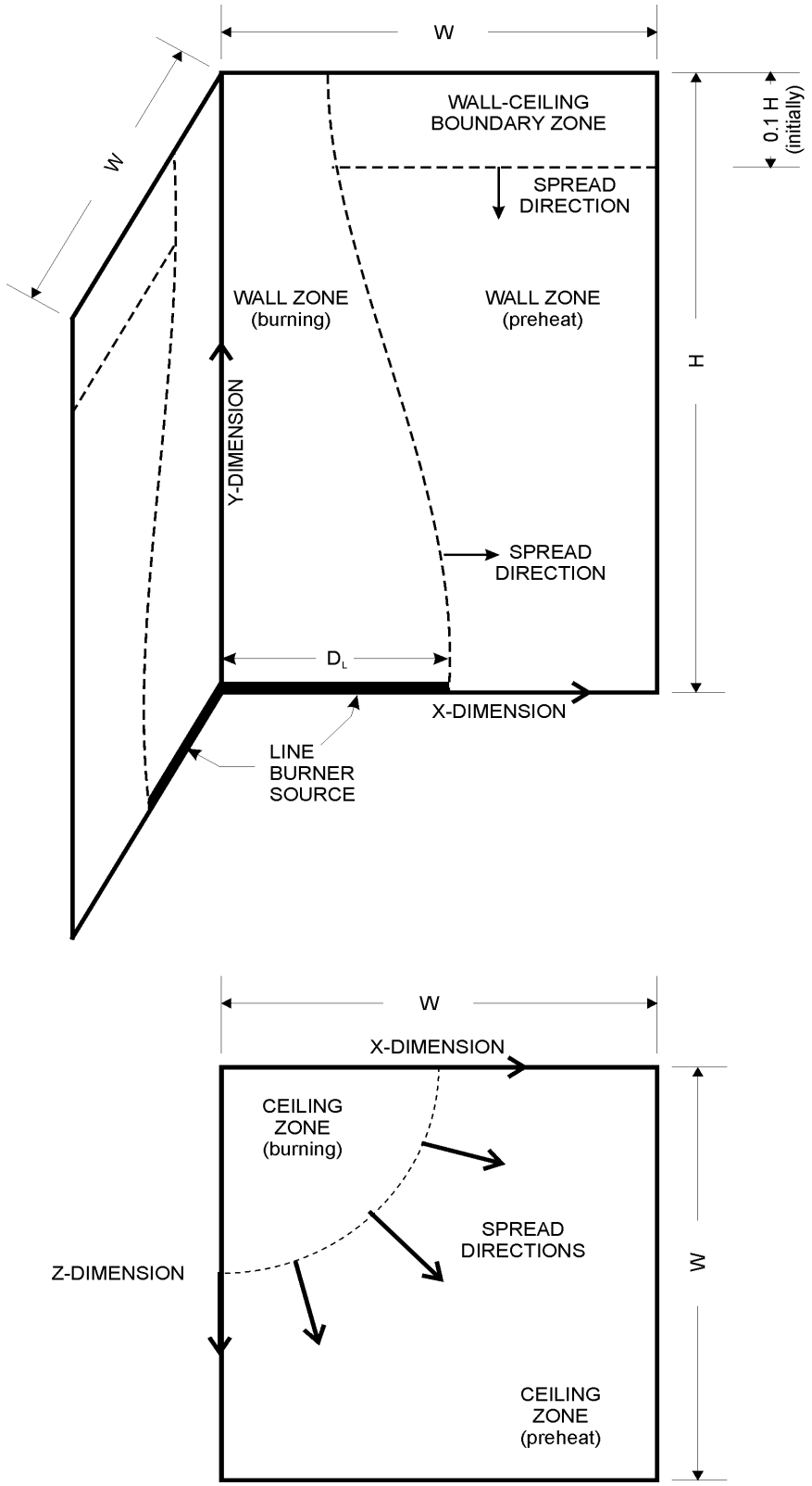

Figure 2.2. Corner Configuration with Line Burner Source Fire.

3.0 MODEL VALIDATION

The flame spread model predictions have been compared to full-scale fire test data to validate the calculation algorithms. Both ISO 9705 room fire test data and open corner fire test data were used in the program validation process. Three materials were used in the validation process: fire retardant phenolic composite [Janssens *et al.*, 1998]; vinyl ester composite with thirty and forty percent resin [Lattimer *et al.*, 1999]; and Douglas fir plywood [Lattimer *et al.*, 1999]. These materials were selected because the material properties represented a range of flame spread potential. Also, to show the effects of the hot gas layer, the ISO 9705 fire tests were modeled using the modified MQH correlation. The predicted heat release rate and the temperature of the hot gas layer, when applicable, were compared to measured test data.

The thermal properties of the three materials are shown in Table 3-1 and the flame-spread properties are shown in Table 3-2. Plywood and the thirty- percent resin vinyl ester are not listed in Table 3-1 because they were not tested in the ISO 9705 room and were therefore not influenced by a hot gas layer. The substrate is listed in Table 3-1 because it has a significant impact on the heat loss through the compartment boundaries. Two different types of vinyl ester were used each with slightly different flame spread properties. The material with the greatest flame spread potential was the plywood, followed by the vinyl ester, and then the fire retardant phenolic resin. The minimum flame spread temperature for the forty-percent vinyl ester was assumed to be 50K less than the ignition temperature because the reported value was greater than the ignition temperature. A flame spread temperature 50K less than the ignition temperature is the minimum observed among the materials that had a flame spread parameter greater than zero and is consistent with the value for the thirty-percent vinyl ester.

Table 3-1. Thermal Material Properties Used to Calculate Hot Layer Temperature.

Material	Thickness (m)	Density (kg/m^3)	Conductivity (kW/m-K)	Heat Capacity (kJ/kg-K)
F.R. Phenolic	0.0038	1,750	0.00035	1.35
Vinyl Ester (30% Res)	0.0048	1,630	0.00035	1.26
Calcium Silicate (Substrate)	0.02	700	0.00011	1.1

Table 3-2. Flame Spread Properties of Materials Used for Model Validation.

Material Property	Material			
	Vinyl Ester (40% Resin)[1]	Vinyl Ester (30% Resin)[1]	Fire Retardant Phenolic[2]	Plywood[1]
Ignition Temp (K)	643	675	876	623
$T_{s,\,min}$ (K)	593[3]	630	876	448
Φ (kW/m^3)	6.26	1.8	0	9.85
$k\Delta c$ (LIFT) (kW^2-s/m^4-K^2)	1.89	2.77	N/A	0.84
$k\Delta c$ (Cone) (kW^2-s/m^4-K^2)	0.624	0.456	0.284	0.766
Fraction Burned	0.36	0.3	0.3	0.82
Thickness	0.0048	0.0125	0.0038	0.0092
Density (kg/m^3)	1,630	1,920	1,750	770
ΔH_c (kJ/kg)	13,430	10,740	8,200	11,740
Latent Heat of Vaporization (MJ/kg)	7.94	7.05	10.9	4.65

[1]Lattimer *et al.*, [1999]
[2]Janssens *et al.*, [1998]
[3]$T_{s,min}$ was assumed to be 50 K less than the ignition temperature

3.1 Validation Test 1: Vinyl Ester (40 % Resin) in ISO 9705 Room

The first validation comparison used the test data from the vinyl ester test in the ISO 9705 compartment [Lattimer *et al.*, 1999]. The ISO 9705 room is 2.4-m long, 3.6-m wide, and 2.4 m high. There is a single opening that is 0.8 m wide and 2.0 m tall. The vinyl ester was attached to a calcium silicate board substrate material that was 0.02 m thick. The source fire was a 0.17-m by 17-m area burner. The heat release rate of the source fire was 100 kW for the first ten minutes and then 300 kW for the last ten minutes, as prescribed by ISO 9705 [1990] and Resolution MSC.40(64) [1994]. The goal of these tests was to determine if the composite material lining the walls and ceiling could cause flashover in the space. Because this test was conducted in a compartment, the hot gas layer was an important aspect of the test.

Figure 3-1 shows the predicted and actual heat release rate for this test configuration. The actual heat release rate and the predicted heat release rate suggest that flashover occurred before 400 seconds.

The model predicted a more gradual rise in the heat release rate until about 350 seconds, at which time a rapid growth in heat release occurred and flashover occurred. This rapid heat release rate increase corresponds to the time the hot layer exceeded the ignition temperature of the vinyl ester lining the walls and ceiling. When the hot gas layer exceeds the ignition temperature of the lining material, ignition of all exposed surfaces is imminent and rapid. The actual test data showed a faster heat release rate growth and a flashover time at about 300 seconds. Comparison of the hot layer temperatures shows good agreement up to about 250 seconds, about the time that flashover occurred in the ISO 9705 compartment. Although the model predictions for this fire and material are not unacceptable, it is expected that they could be improved if the flame-spread data were regenerated. The minimum temperature for flame spread had to be assumed, as noted in Table 3-2, because a value that was greater than the ignition temperature was reported. As will be seen in the sensitivity analysis, the results can deviate considerably as the uncertainty in the flamespread properties increases.

3.2 Validation Test 2: Vinyl Ester (30 % Resin) in Full Scale Open Corner Test

A different vinyl ester material was tested in an open corner configuration [Lattimer *et al.*, 1999]. This vinyl ester had less resin that the material tested in the ISO compartment, but otherwise had similar material properties. The open corner test does not result in a hot layer build-up, thus it is possible to assess the impact of the hot layer on the fire development by comparing these results with those presented in Section 3-1. The open corner used in this test was 1.83 m wide and 2.28 m tall. The ceiling was 1.83 m by 1.83 m.

Figure 3-3 shows the predicted and actual heat release rate for this test. The open corner tests do not produce a hot layer thus this feature was turned off in the model. The actual and predicted heat release rate are in agreement for this test.

3.3 Validation Test 3: Phenolic Resin Composite in ISO 9705 Room

This fire test was conducted with a fire retardant phenolic resin composite in the ISO 9705 room [Lattimer *et al.*, 1999]. The dimensions of the room and opening as well as the size of the opening were described in Section 3.1. This material was selected for validation because it did not result in flashover despite the fact that hot layer was present in the space. Figure 3-4 shows the actual and predicted heat release rate and Figure 3-5 shows the actual and predicted hot gas layer temperature. In both cases the agreement between the actual and predicted data is excellent. The temperature predictions are within 50 K of the actual temperature readings for the entire 20-minute period.

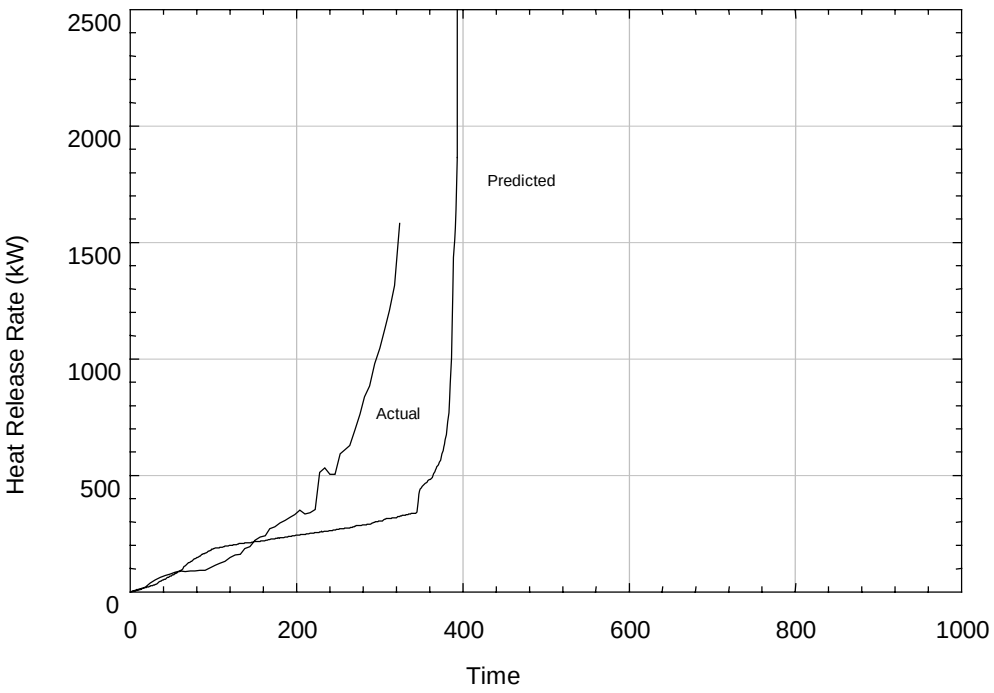

Figure 3-1. Predicted and Actual Heat Release Rate for Vinyl Ester (40 % Resin) ISO 9705 Fire Test

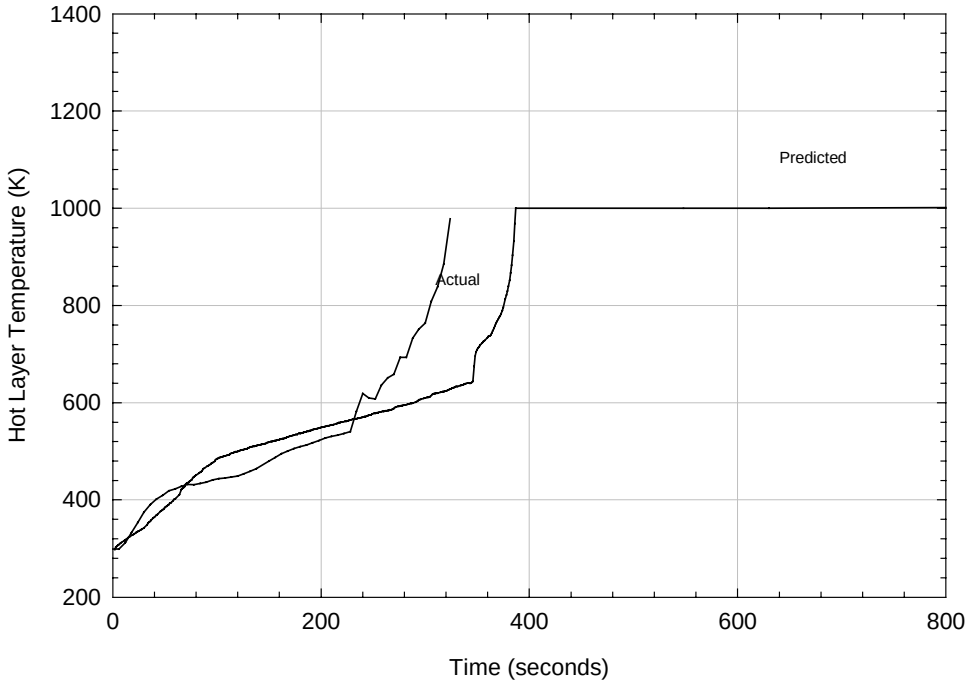

Figure 3-2. Predicted and Actual Smoke Layer Temperature for Vinyl Ester ISO 9705 Fire Test

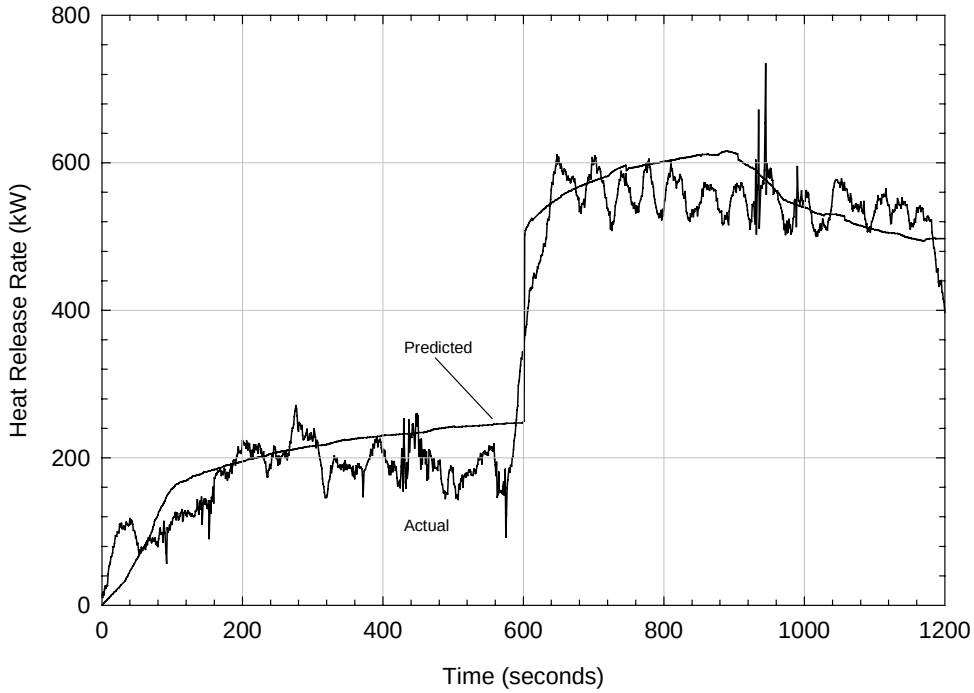

Figure 3-3. Predicted and Actual Heat Release Rate for Vinyl Ester Open Corner Test

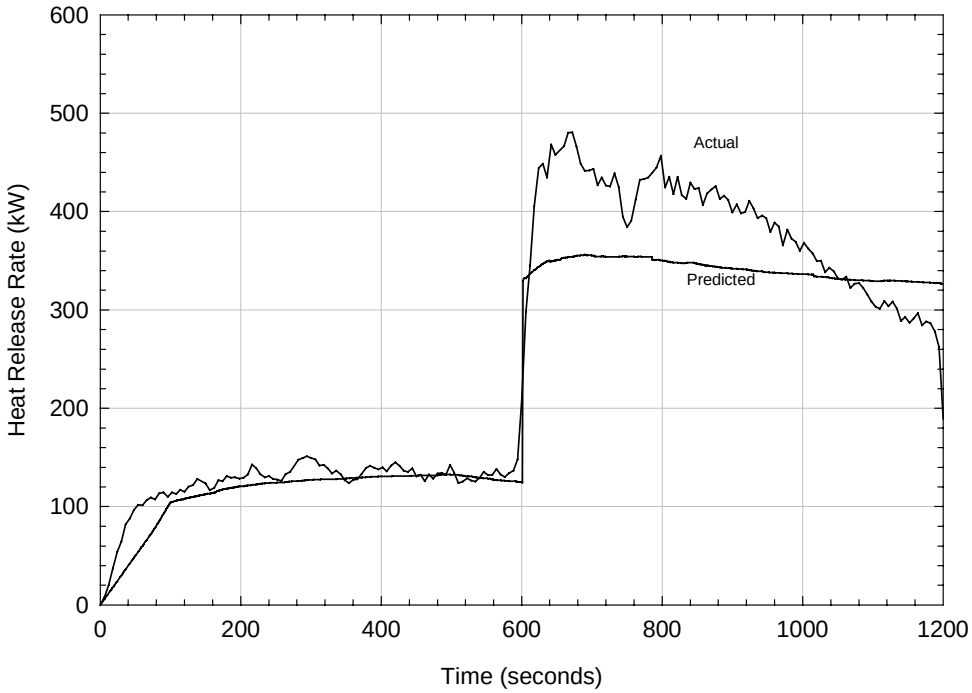

Figure 3-4. Predicted and Actual Heat Release Rate for Fire Retardant Phenolic Resin Composite ISO 9705 Fire Test

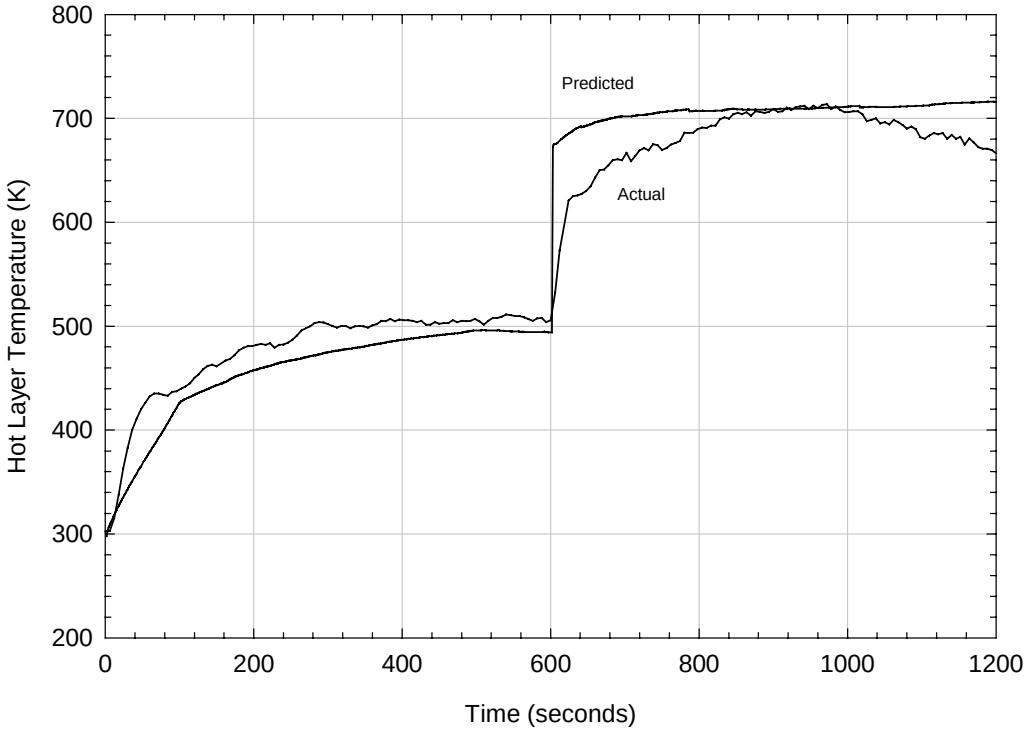

Figure 3-5. Predicted and Actual Smoke Layer Temperature for Fire Retardant Phenolic Resin Composite ISO 9705 Fire Test

3.4 Validation Test 4: Plywood in Full Scale Open Corner Test

The final validation comparison was done using the plywood test data from the open corner fire test [Lattimer *et al.*, 1999]. No hot layer effects were present. Figure 3-6 shows the predicted and actual heat release rate for this test configuration. The heat release rate predictions are in good agreement up until about 10 minutes, when the source fire heat release rate increases. At this point, the model under-predicts the heat release rate by about twenty-percent. This may be due to the plywood detaching from the ceiling and igniting the wall. This type of phenomena leads to a rapid increase in the heat release rate as is evidenced by Figure 3-6 and cannot be predicted in the flamespread model.

3.5 Evaluation of the Effect of the Hot Layer

The true effect of the hot gas layer was evaluated by modeling the forty percent resin vinyl ester material tested in the ISO 9705 room without a hot layer. This has been done and is shown in Figure 3-7. It can be seen that the vinyl ester material does not readily burn and would not lead to flashover conditions if there were no hot layer. However, if the effects of the hot layer are included, this material can lead to flashover within eight minutes.

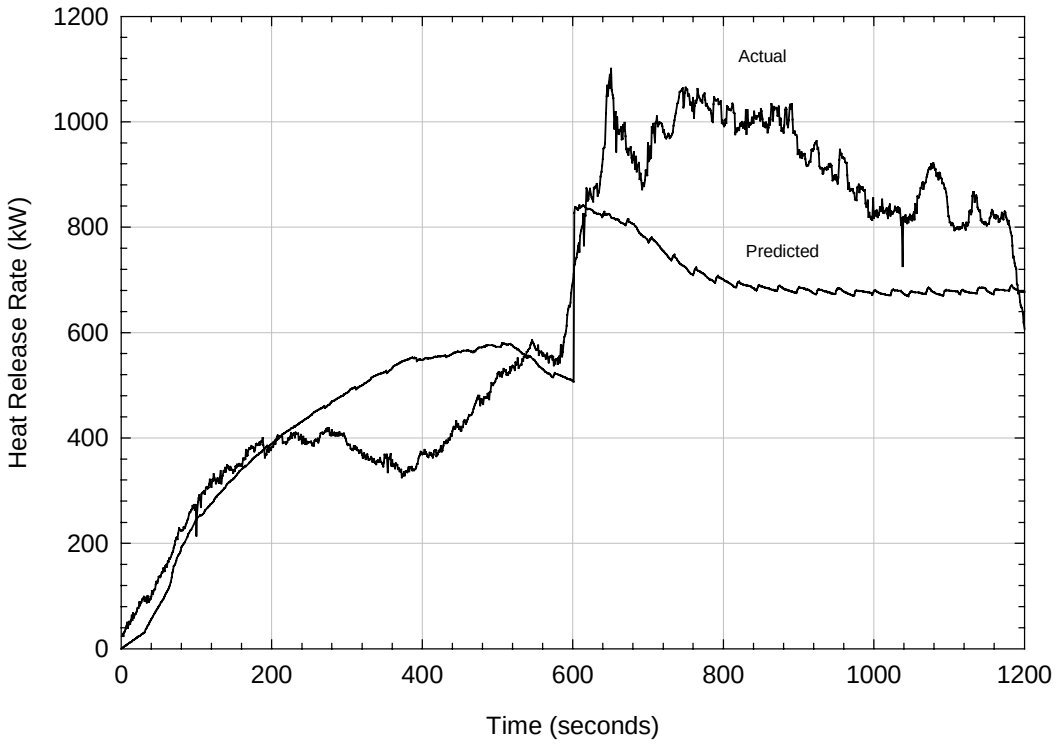

Figure 3-6. Predicted and Actual Heat Release Rate of Plywood Open Corner Fire Test

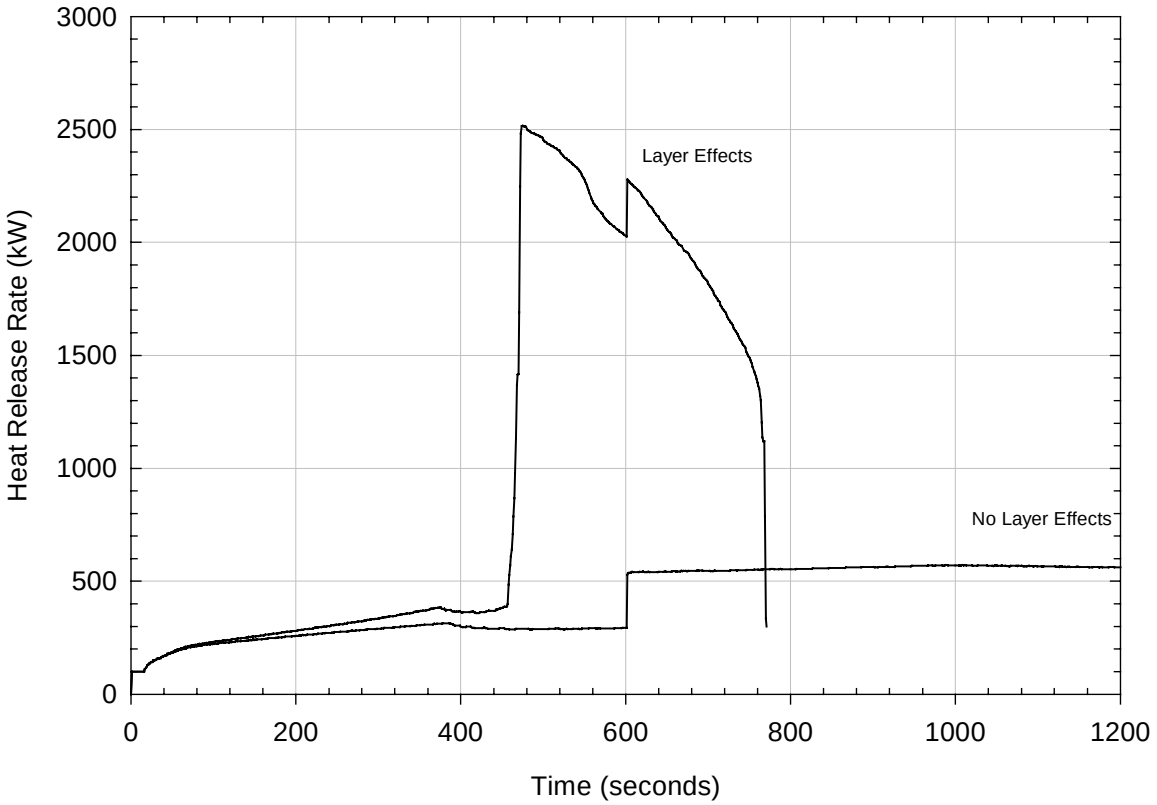

Figure 3-7. Comparison of Predicted Vinyl Ester (40 % Resin) Heat Release Rates: Layer and No Layer Calculations

4.0 MODEL RESULTS

The flamespread model was used to calculate the heat release rate, compartment temperature, smoke production rate, and floor heat flux in the nine ISO 9705 fire tests. The heat release rate and temperature data were compared directly to the measured fire test data and are presented in Sections 4.2 and 4.3, respectively. The smoke production rate and the floor heat flux, both of which were calculated from the fire test data, are presented in Section 4.4 and 4.5, respectively. Each ISO 9705 fire test used a different wall lining material. The source fire was a 0.17 m^2 area burner. The heat release rate was 100 kW for the first ten minutes and was increased to 300 kW for the next ten minutes, as specified in the IMO Resolution [Resolution MSV.41(64), 1994].

4.1 Material Properties

The flame-spread properties for the nine test materials are shown in Tables 4-1a, 4-1b, and 4-1c. There is some overlap between these tables and Table 3-1. The information is repeated in this section for completeness. Five of the material listed the tables do not spread fire laterally. The only means that these materials are predicted to ignite in the flame spread model is when the incident heat flux raises the surface temperature to the ignition temperature.

Table 4-1a. Flame Spread Properties of Materials 1-3 Tested in ISO 9705 Room.

Material Property	Material		
	Fire Retardant Phenolic	**Fire Restricting Material**	**Fire Retardant Polyester**
Test/Material Number	1	2	3
Ignition Temp (K)	876	905	648
$T_{s,\,min}$ (K)	876	905	598
M (kW/m^3)	0	0	19.5
$k\Delta c$ (LIFT) (kW^2 –s/m^4-K^2)	N/A[1]	N/A[1]	1.65
$k\Delta c$ (CONE) (kW^2 –s/m^4-K^2)	0.77	0.6	0.9
Fraction Burned	0.3	0.37	0.33
Thickness (m)	0.0038	0.0118	0.0052
Density (kg/m^3)	1,750	240	1,650
$)H_c$ (kJ/kg)	8,200	9.630	11,280
Latent Heat of Vaporization (MJ/kg)	10.9	20.5	7.97

[1]Not available; material did not ignite

Table 4-1b. Flame Spread Properties of Materials 4 - 6 Tested in ISO 9705 Room.

Material Property	Material		
	Vinyl Ester (40% Resin)	**Fire Retardant Epoxy**	**Fire Retardant Epoxy (Coated)**
Teat/Material Number	4	5	6
Ignition Temp (K)	643	726	916
$T_{s,\,min}$ (K)	593[1]	726	916
Φ (kW/m^3)	6.26	0	0
$k\rho c$ (LIFT) (kW^2-s/m^4-K^2)	1.89	1.73	8.0
$k\rho c$ (Cone) (kW^2-s/m^4-K^2)	1.16	2.0	1.5
Fraction Burned	0.36	0.19	0.17
Thickness (m)	0.0048	0.0039	0.0039
Density (kg/m^3)	1,630	1,910	1,910
ΔH_c (kJ/kg)	13,430	8,700	7,670
Latent Heat of Vaporization (MJ/kg)	7.94	12.88	14.4

[1]$T_{s,min}$ was assumed to be 50 K less than the ignition temperature

Table 4-1c. Flame Spread Properties of Materials 7 – 9 Tested in ISO 9705 Room.

Material Property	Material		
	Textile Wall Covering	**Polyester**	**Fire Retardant Acrylic**
Test/Material Number	7	8	9
Ignition Temp (K)	756	610	631
$T_{s,\,min}$ (K)	756	507	580
Φ (kW/m^3)	0	19.1	32.8
$k\rho c$ (LIFT) (kW^2-s/m^4-K^2)	0.27	0.74	1.72
$k\rho c$ (Cone) (kW^2-s/m^4-K^2)	0.68	0.65	2.0
Fraction Burned	0.08[1]	0.58	0.34
Thickness (m)	0.0064[1]	0.0041	00052
Density (kg/m^3)	1,760	1,390	1,880
ΔH_c (kJ/kg)	,080	21,600	12,280
Latent Heat of Vaporization (MJ/kg)	11.02	4.23	10.08

[1] Includes backing material

The thermal material properties for the nine test materials are shown in Table 4-2. The density and thickness are also listed in Tables 4-1a through 4-1c because they are also used in the flamespread calculation.

Table 4-2. Thermal Properties of Materials Tested in ISO 9705 Room.

Material Number	Thickness (m)	Density (kg/m^3)	Conductivity[1] (kW/m-K)	Heat Capacity[1] (kJ/kg-K)
1	0.0038	1,750	0.00035	1.35
2	0.0118	240	0.00043	1.0
3	0.0052	1,650	0.00035	1.26
4	0.0048	1,630	0.00035	1.26
5	0.0039	1,910	0.00045	1.1
6	0.0039	1,910	0.00045	1.1
7[2]	0.0064	1,760	0.00069	0.84
8	0.0041	1,390	0.0001	1.26
9	0.0052	1,880	0.00045	1.1
Substrate	0.02	700	0.00011	1.1

[1] Conductivity and heat capacity properties obtained from Laramee [1987]
[2] Includes backing material

4.2 Heat Release Rate Comparisons

Figures 4-1 through 4-9 show the calculated and predicted heat release rate for all nine-test materials. The results can be grouped into three categories: those materials that caused flashover conditions in the room during the 100 kW source fire exposure, those that caused flashover during the 300 kW source fire exposure, and those that did not result in flashover at all. The flame-spread model predicted the heat release rate most satisfactorily in seven of the nine cases. These seven simulations included materials from each of the three groups listed above.

4.3 Hot Layer Temperature Comparisons

The actual and predicted hot gas layer temperatures for the nine test materials are shown in Figures 4-10 through 4-18. The average ceiling jet layer temperature data and the hot layer temperature measured at the door are shown in the figures. The average ceiling jet temperature is not representative of the hot layer temperature. It was assumed then that the hot gas temperatures measured near the door would be more representatives of the average hot layer temperature in the compartment. When the hot layer temperature calculation was implemented in the flame spread model, it was intended that the predicted temperatures match the temperatures measured at the door.

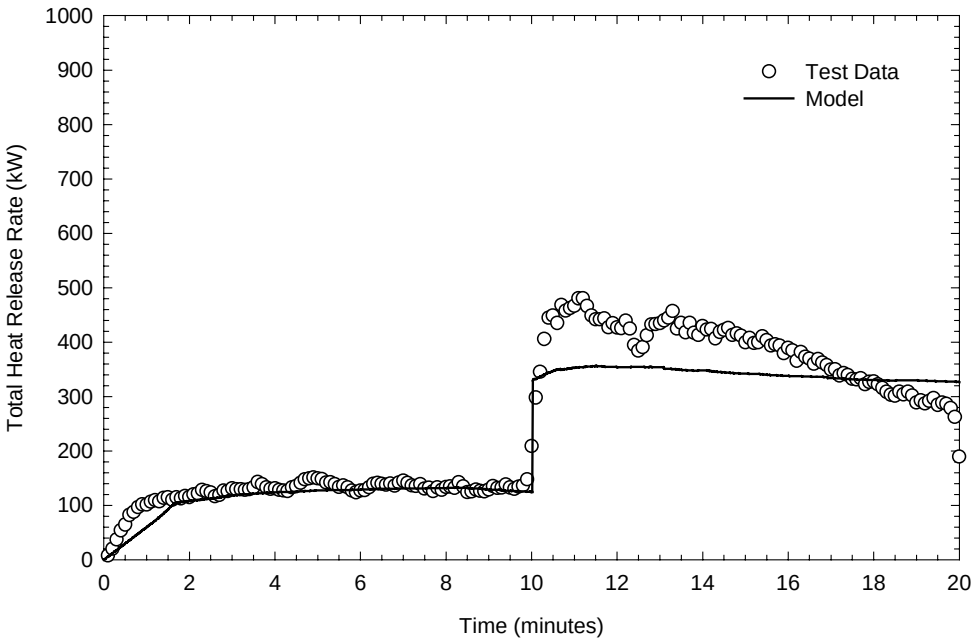

Figure 4-1. Actual and Predicted Heat Release Rate for Material # 1

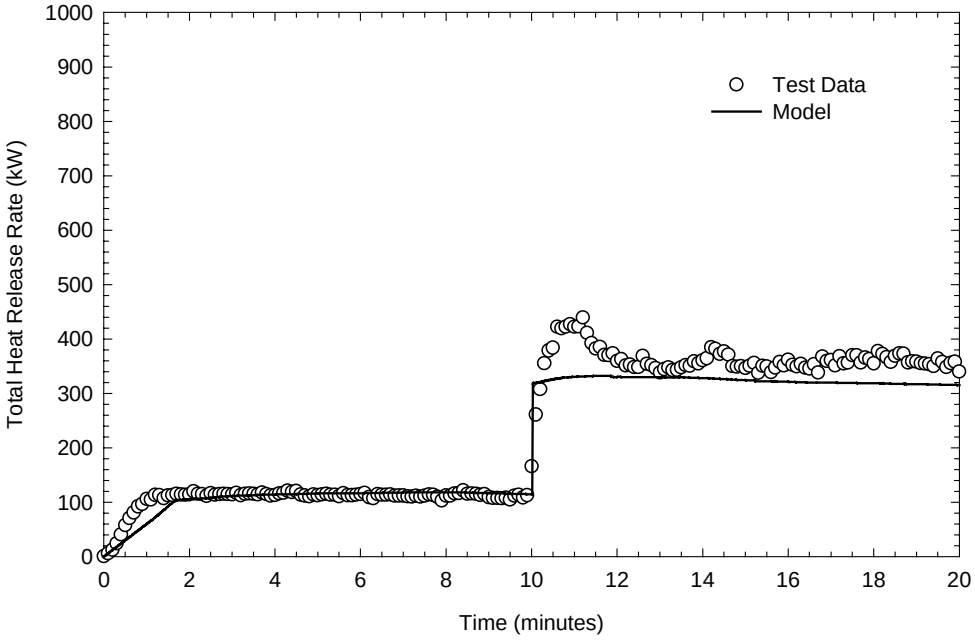

Figure 4-2. Actual and Predicted Heat Release Rate for Material # 2

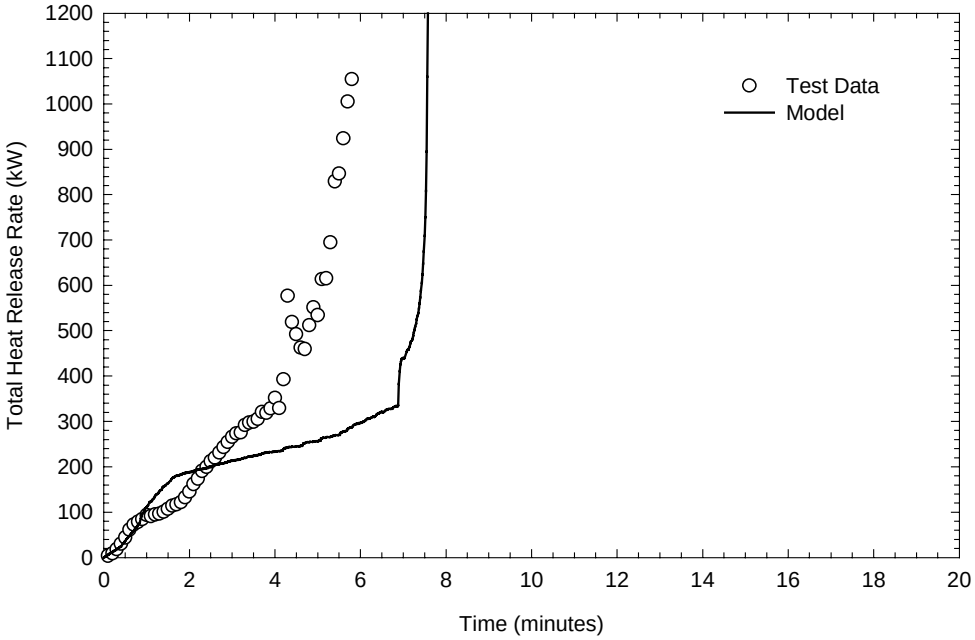

Figure 4-3. Actual and Predicted Heat Release Rate for Material # 3.

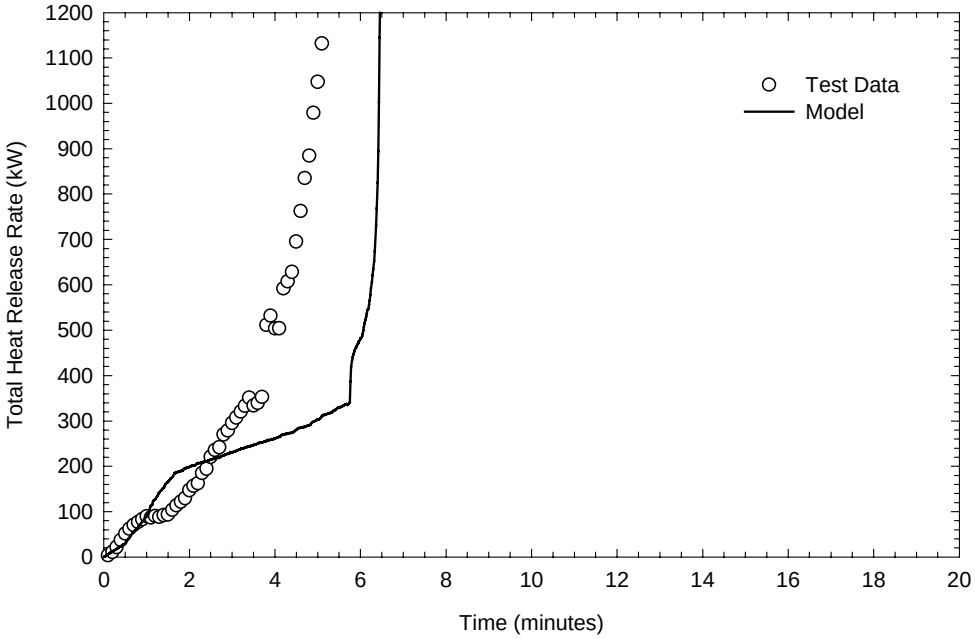

Figure 4-4. Actual and Predicted Heat Release Rate for Material # 4

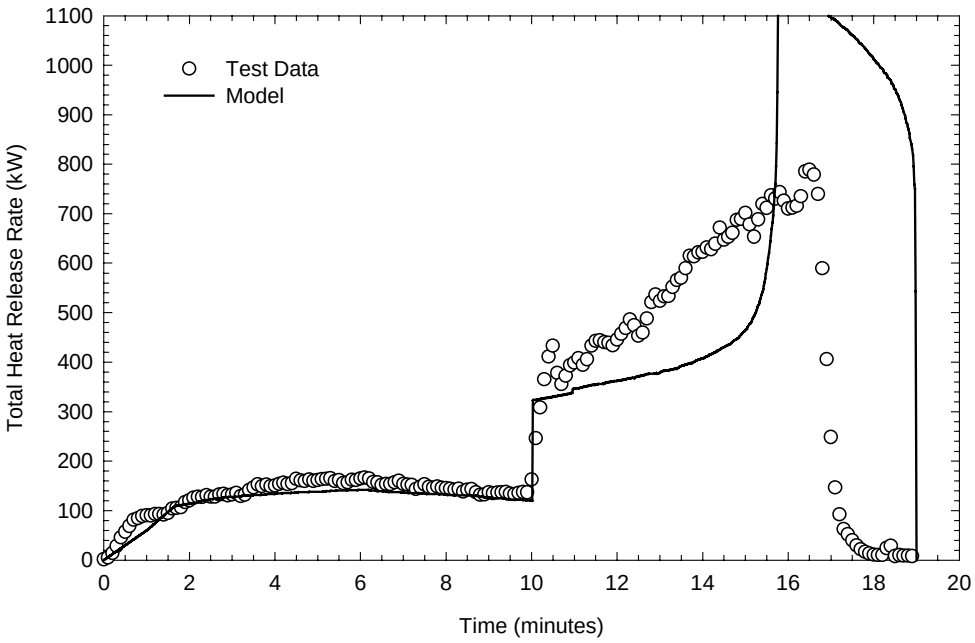

Figure 4-5. Actual and Predicted Heat Release Rate for Material # 5

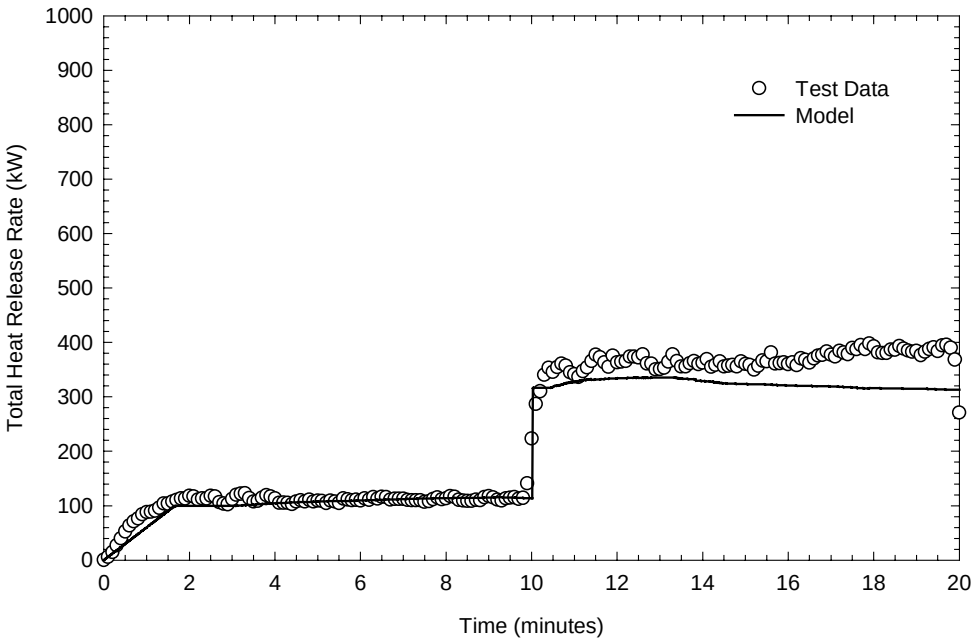

Figure 4-6. Actual and Predicted Heat Release Rate for Material # 6

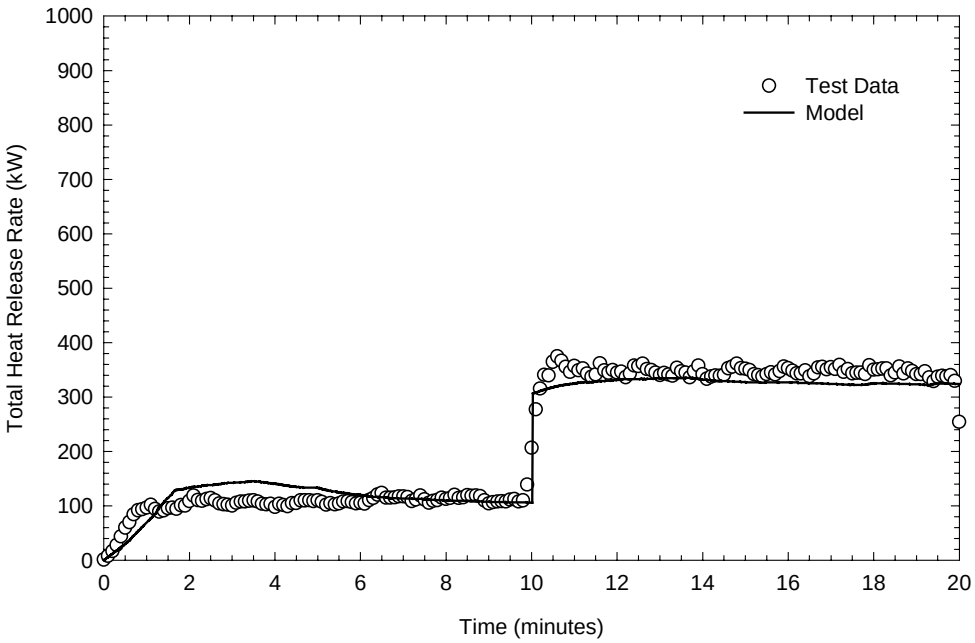

Figure 4-7. Actual and Predicted Heat Release Rate for Material # 7

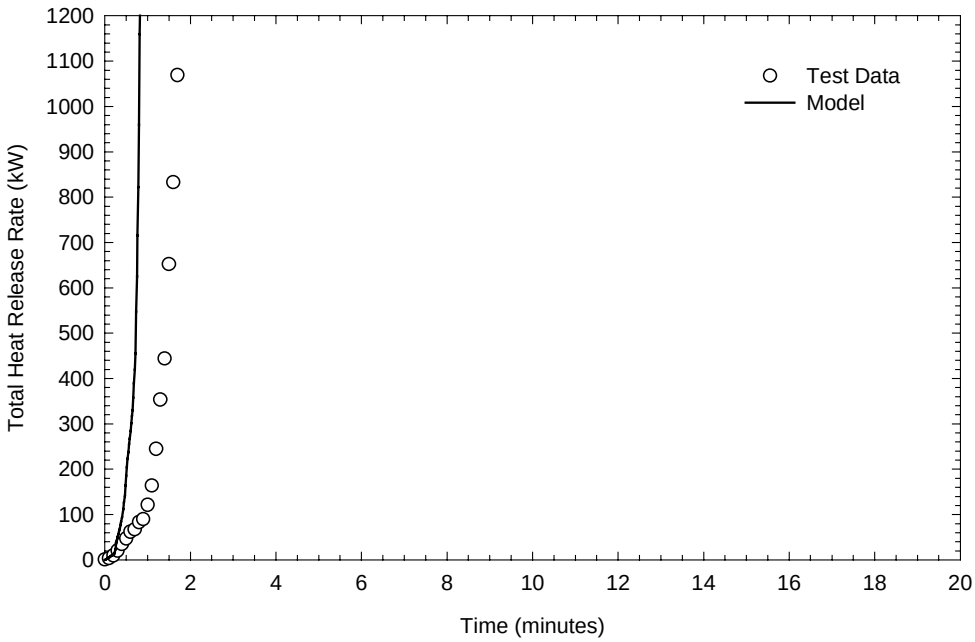

Figure 4-8. Actual and Predicted Heat Release Rate for Matierial # 8

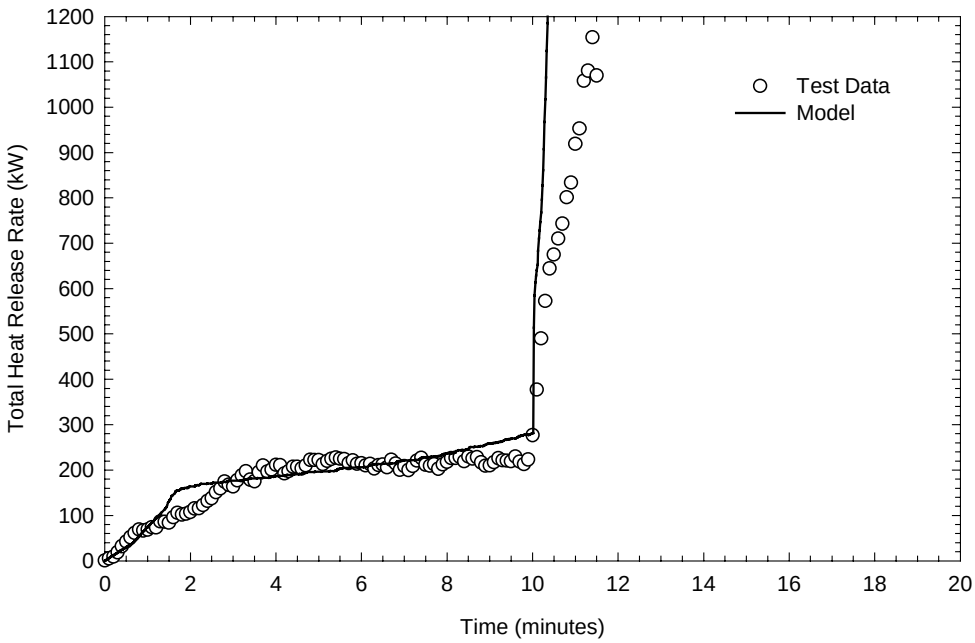

Figure 4-9. Actual and Predicted Heat Release Rate for Material # 9

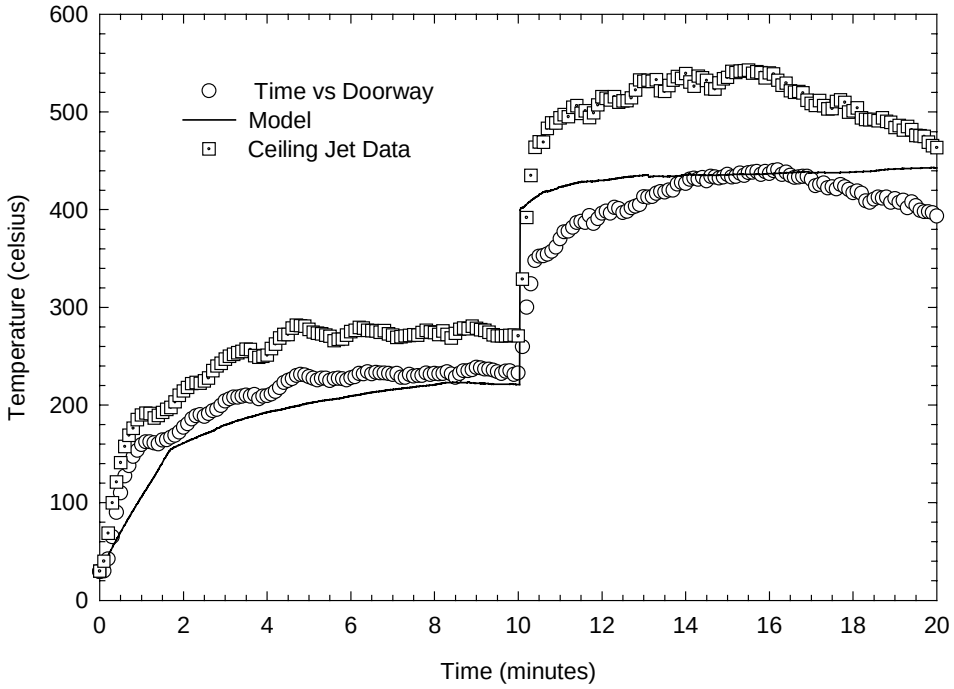

Figure 4-10. Actual and Predicted Hot Layer Temperatures for Material # 1

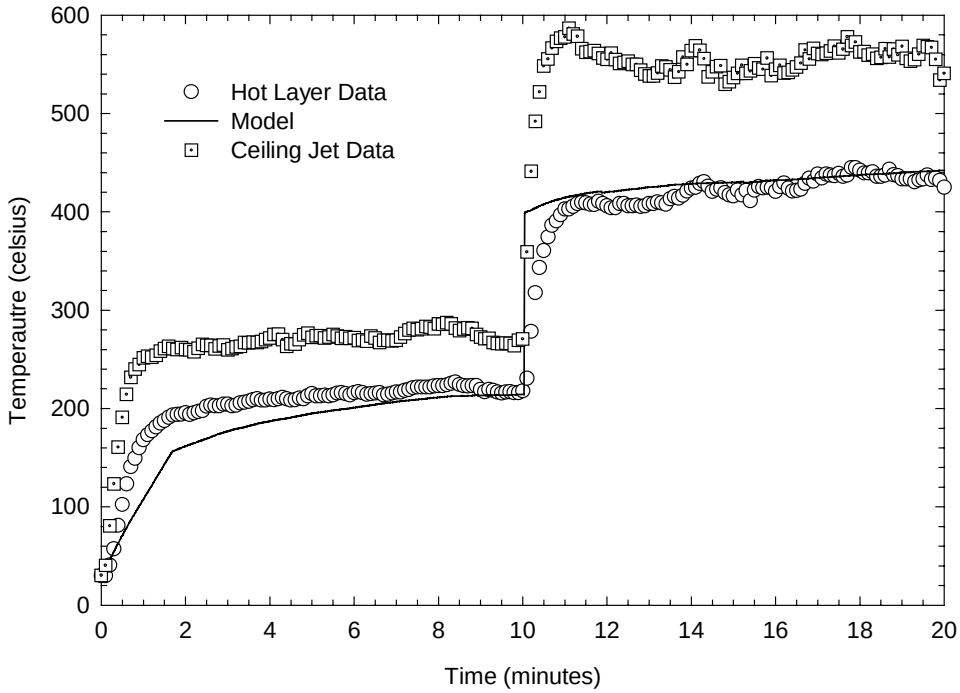

Figure 4-11. Actual and Predicted Hot Layer Temperature for Material # 2

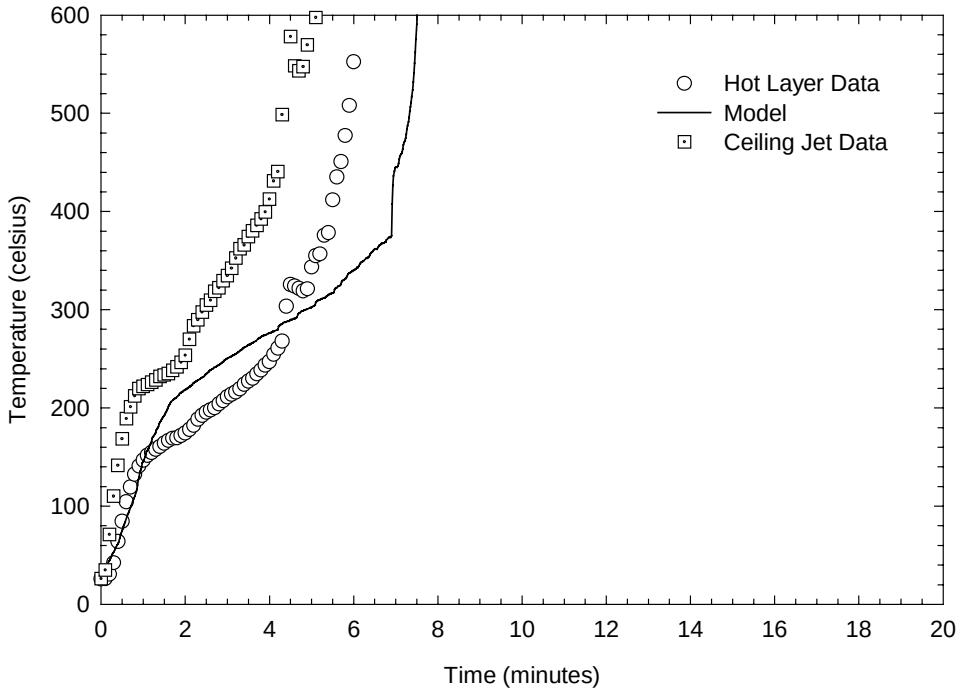

Figure 4-12. Actual and Predicted Hot Layer Temperature for Material # 3

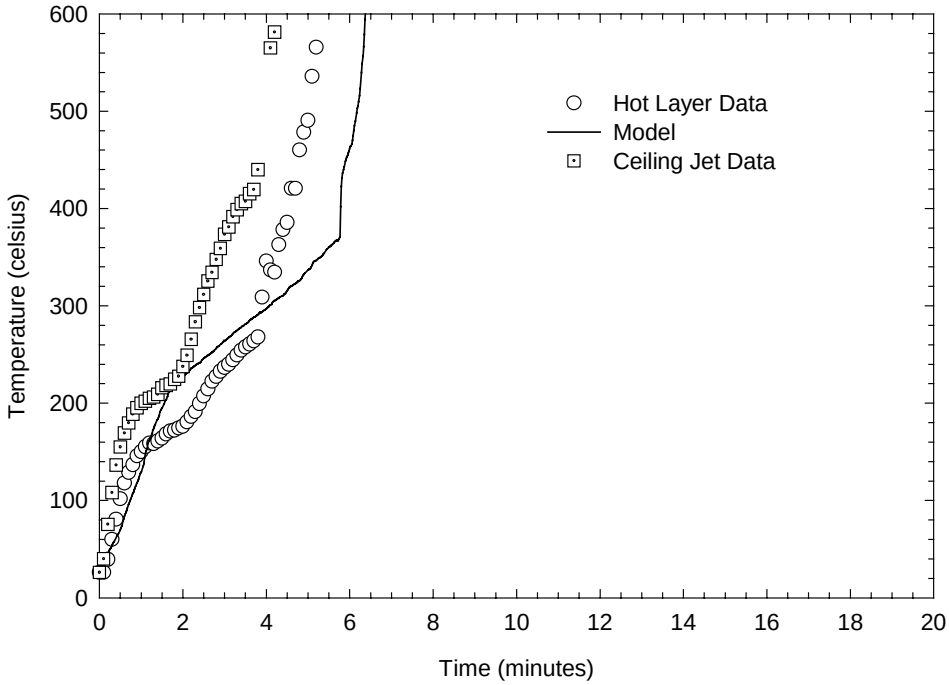

Figure 4-13. Actual and Predicted Hot Layer Temperatures for Material # 4

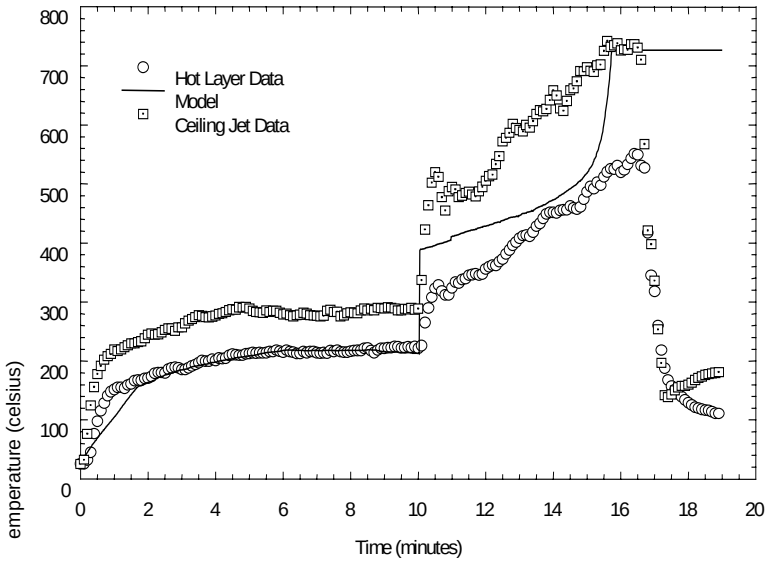

Figure 4-14. Actual and Predicted Hot Layer Temperatures for Material # 5

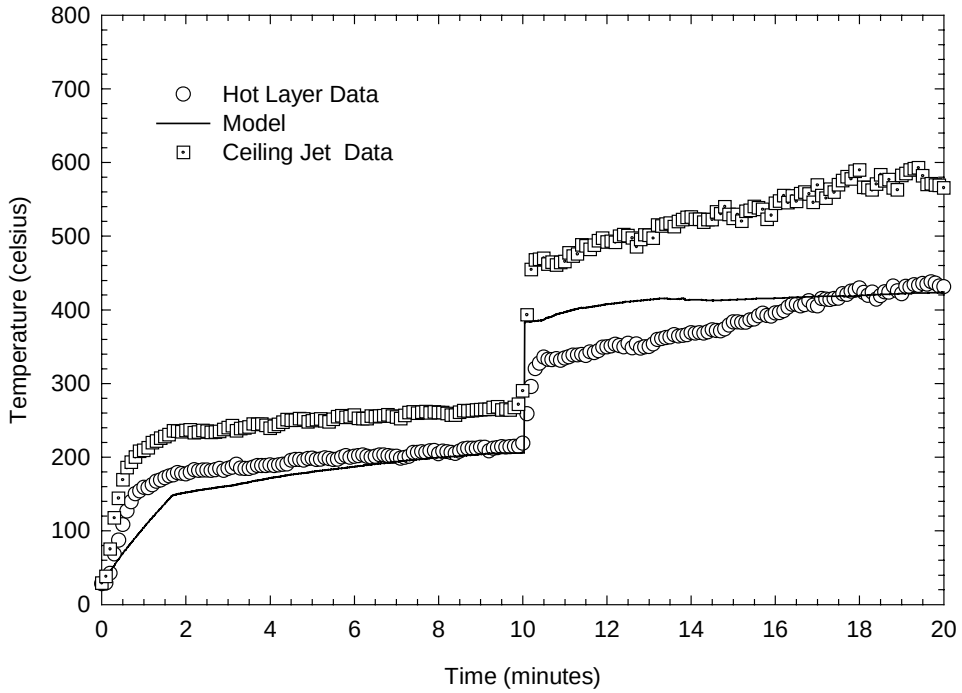

Figure 4-15. Actual and Predicted Hot Layer Temperatures for Material # 6

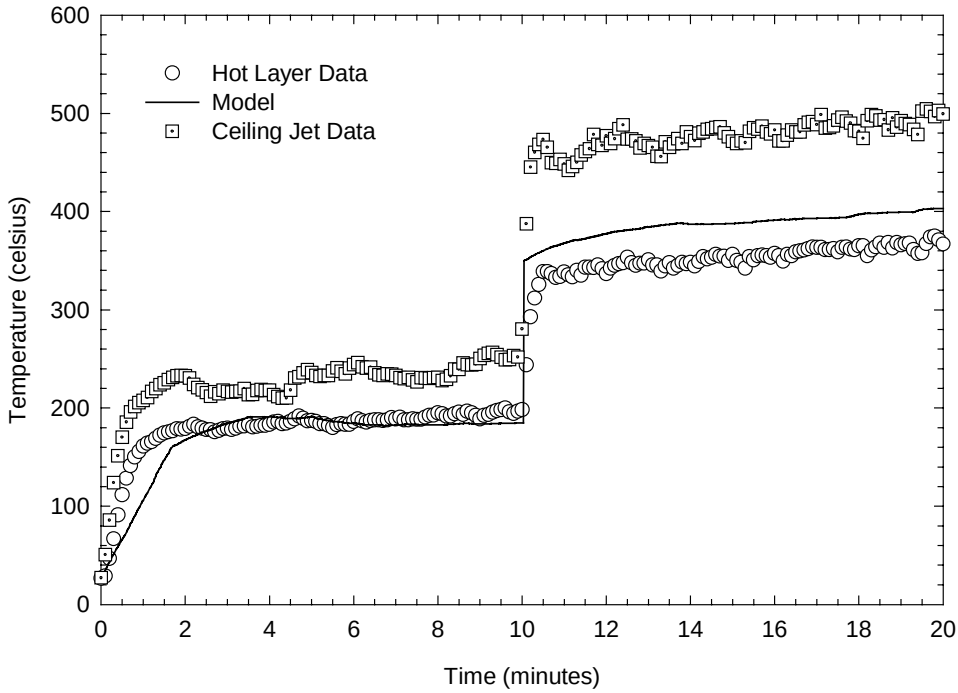

Figure 4-16. Actual and Predicted Hot Layer Temperatures for Material # 7

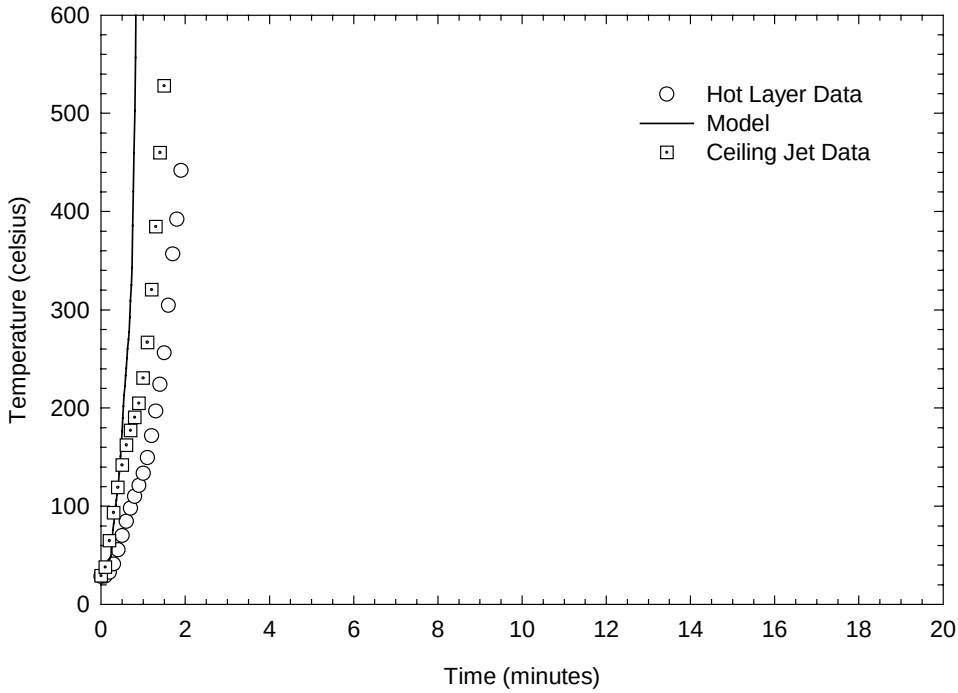

Figure 4-17. Acutal and Predicted Hot Layer Temperatures for Material # 8

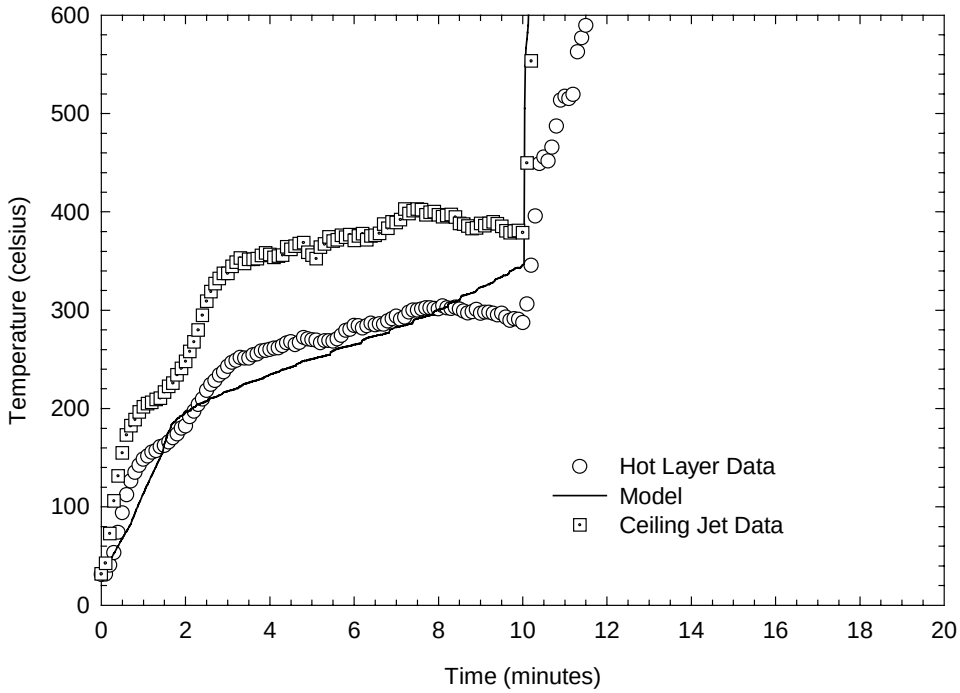

Figure 4-18. Actual and Predicted Hot Layer Temperatures for Material # 9

4.4 Heat Flux to the Floor

The heat flux to the floor of the ISO 9705 compartment was computed from the hot layer data using the following equation:

$$\dot{q}'' = \sigma T_L^4 \tag{4-1}$$

where $\dot{q}''$ is the heat flux to the floor (kW/m^2) and T_L is the temperature of the hot layer (K). Figures 4-19 through 4-27 show the predicted floor heat flux as a function of time for each of the nine test materials.

The comparisons of the predicted and measured heat fluxes are consistent with the comparisons of the predicted and measured hot layer temperatures as would be expected from Equation 4-1. As such the heat flux prediction errors are directly traceable to the temperature prediction errors. This indicates that the assumption that the layer is optically thick is not contributing significantly to the heat flux prediction errors. It is apparent in Figure 4-27 that the radiometer was not functioning properly for Test #9.

4.5 Smoke Production Rate

The smoke production rate was calculated using the following equation:

$$SPR = \sigma_f \ \dot{m}_f = \sigma_f \ \frac{\left(\dot{Q}(t) - \dot{Q}_s(t)\right)}{\Delta H_c} \tag{4-2}$$

where SPR is the smoke production rate (m^2/s), Φ_f is the specific extinction area as measured in the cone calorimeter and is the average of all tests (m^2/kg), $\dot{m}_f$ is the total mass loss rate of the wall and ceiling materials (kg/s);) H_c is the heat of combustion as measured in the cone calorimeter and averaged over all tests (kJ/kg), $\dot{Q}(t)$ is the total calculated heat release rate (kW) at time t (s), and $\dot{Q}_s(t)$ is the heat release rate of the source fire (kW) at time t.

Figures 4-28 through 4-36 show the calculated smoke production rate as a function of time for all nine test materials. The predicted smoke production rate correlated well for only four tests, seen in Figures 4-30, 4-31, 4-32, and 4-33. It is not known why the predicted results do not correlate well for the other five test materials.

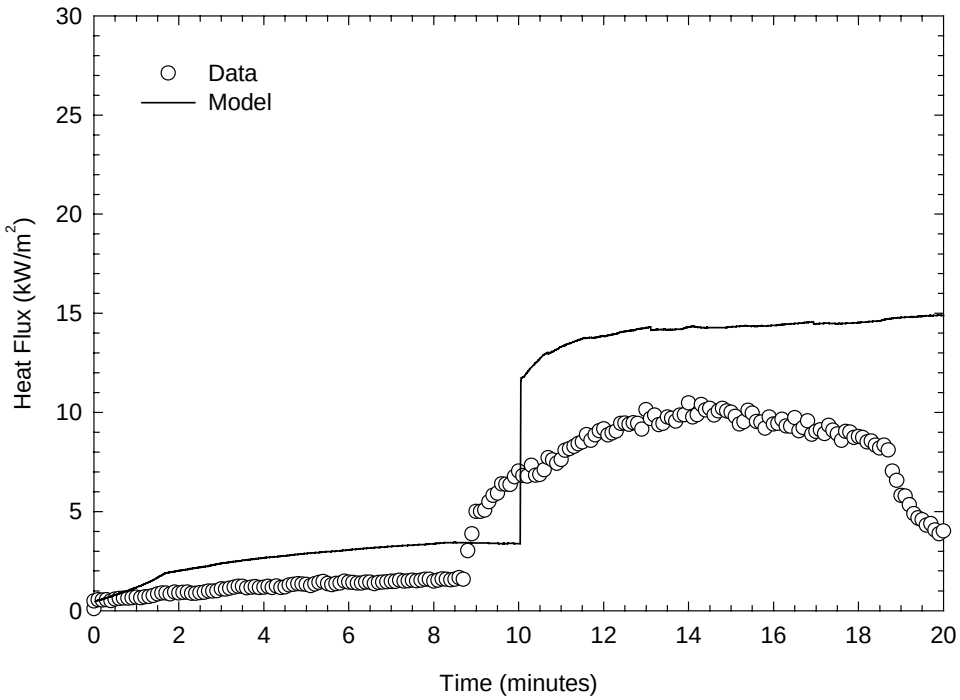

Figure 4-19. Actual and Predicted Heat Flux for Material #1

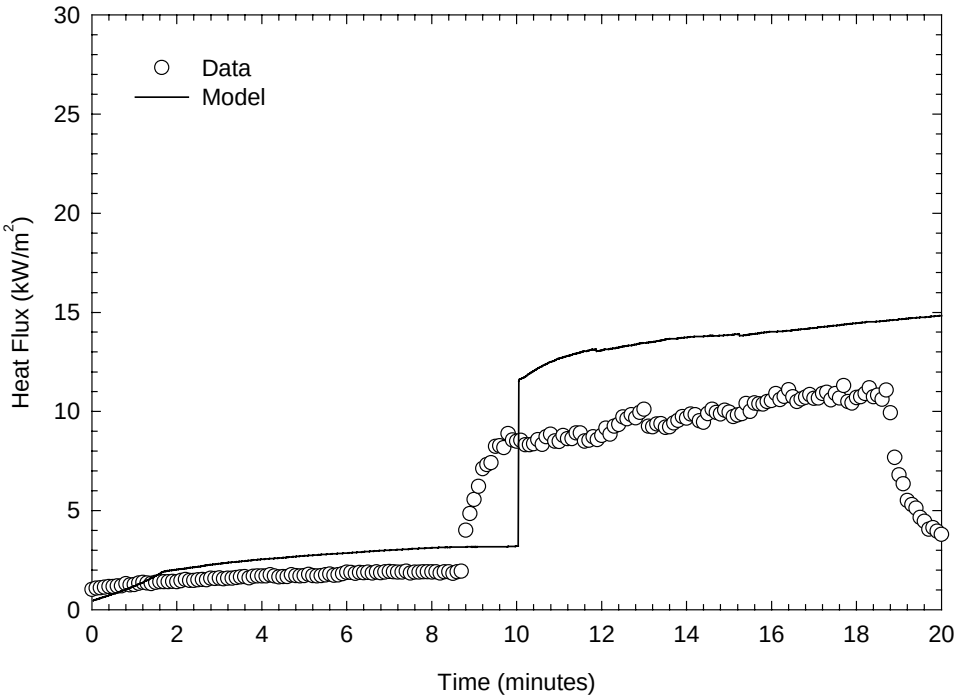

Figure 4-20. Actual and Predicted Heat Flux for Material #2

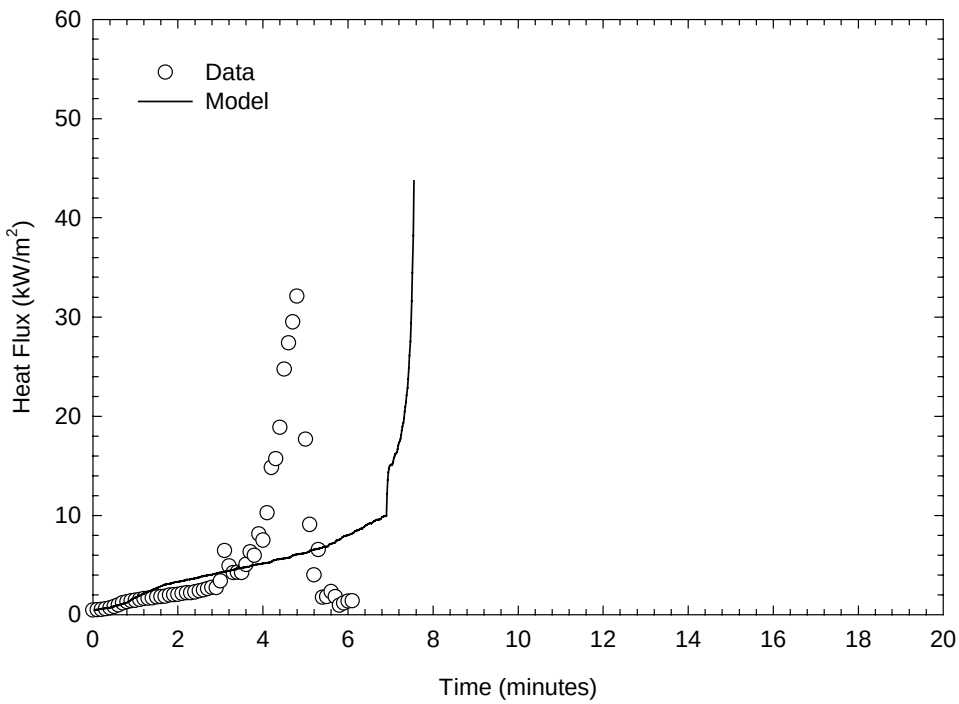

Figure 4-21. Actual and Predicted Heat Flux for Material #3

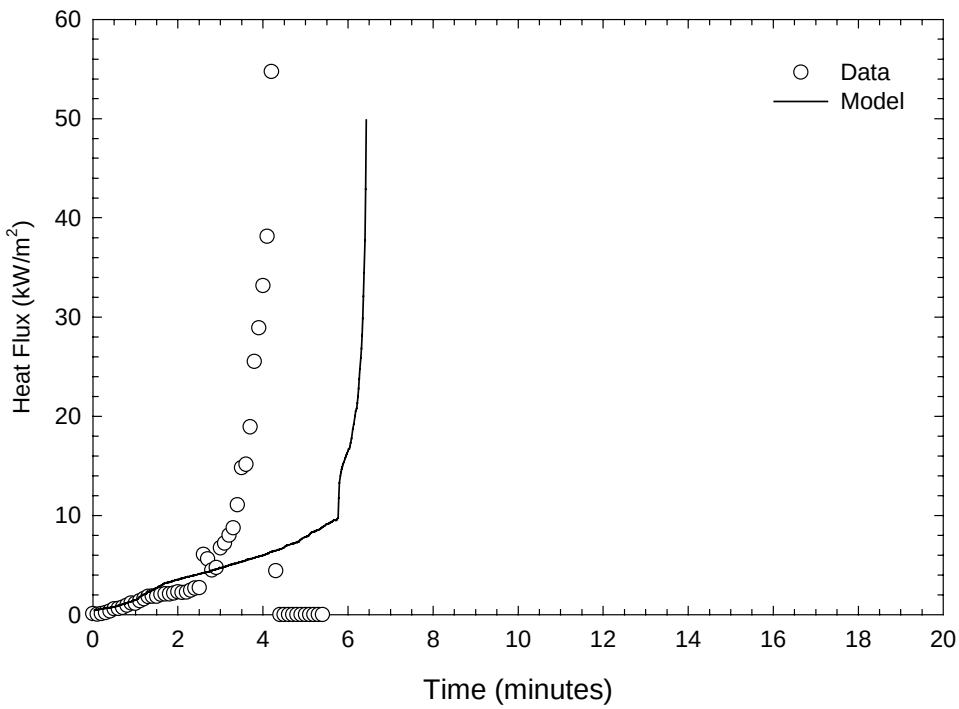

Figure 4-22. Actual and Predicted Heat Flux for Material #4

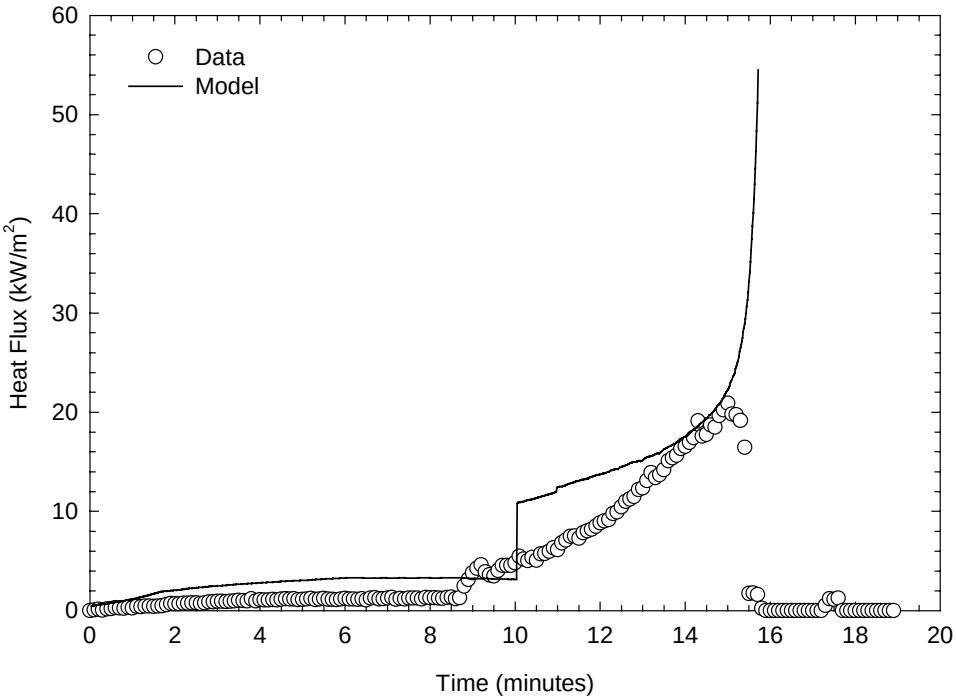

Figure 4-23. Actual and Predicted Heat Flux for Material #5

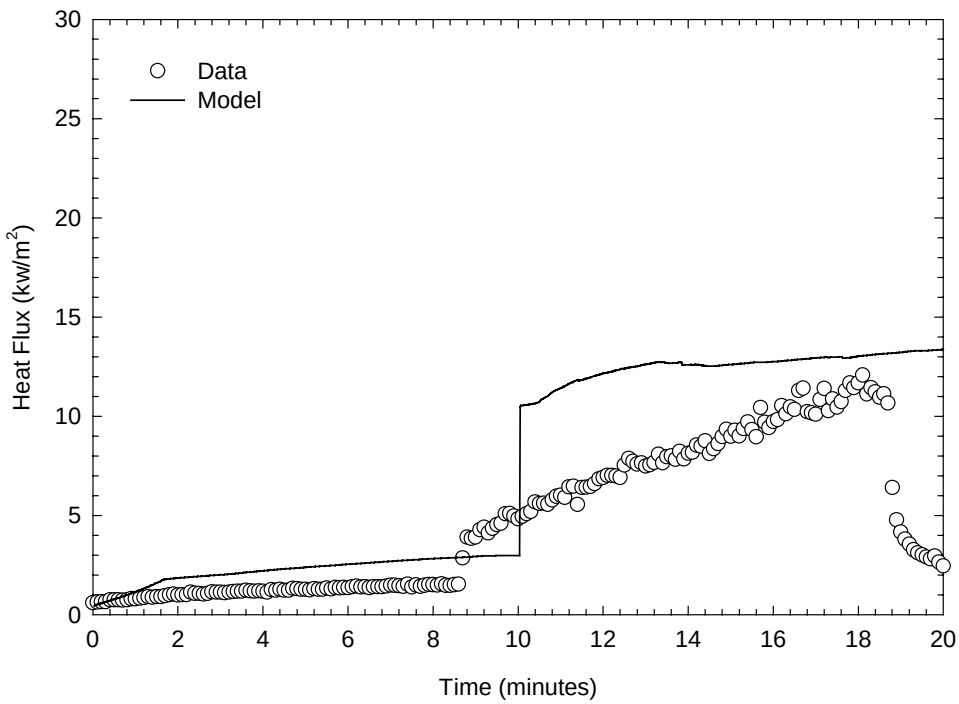

Figure 4-24. Actual and Predicted Heat flux for Material #6

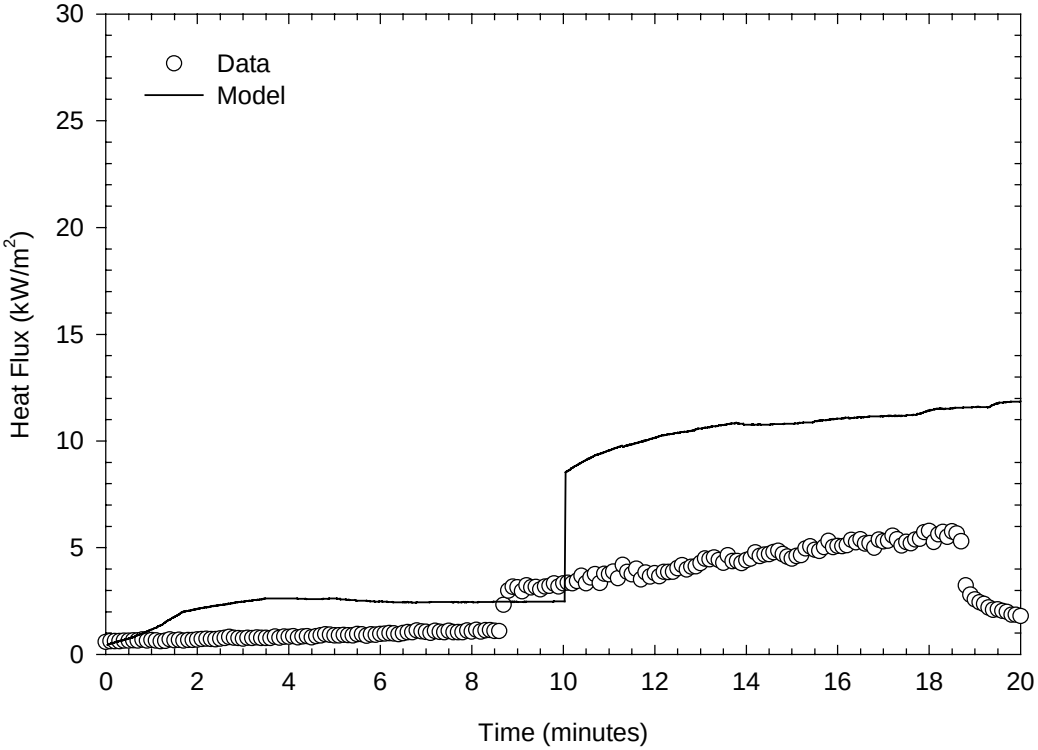

Figure 4-25. Actual and Predicted Heat Flux for Material #7

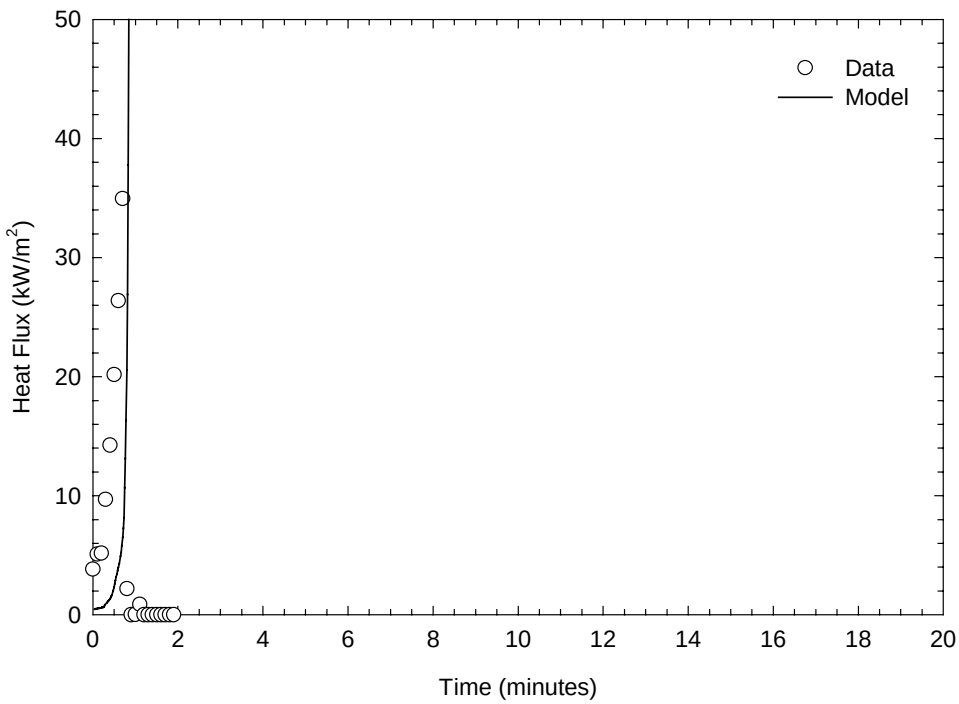

Figure 4-26. Actual and Predicted Heat Flux for Material #8

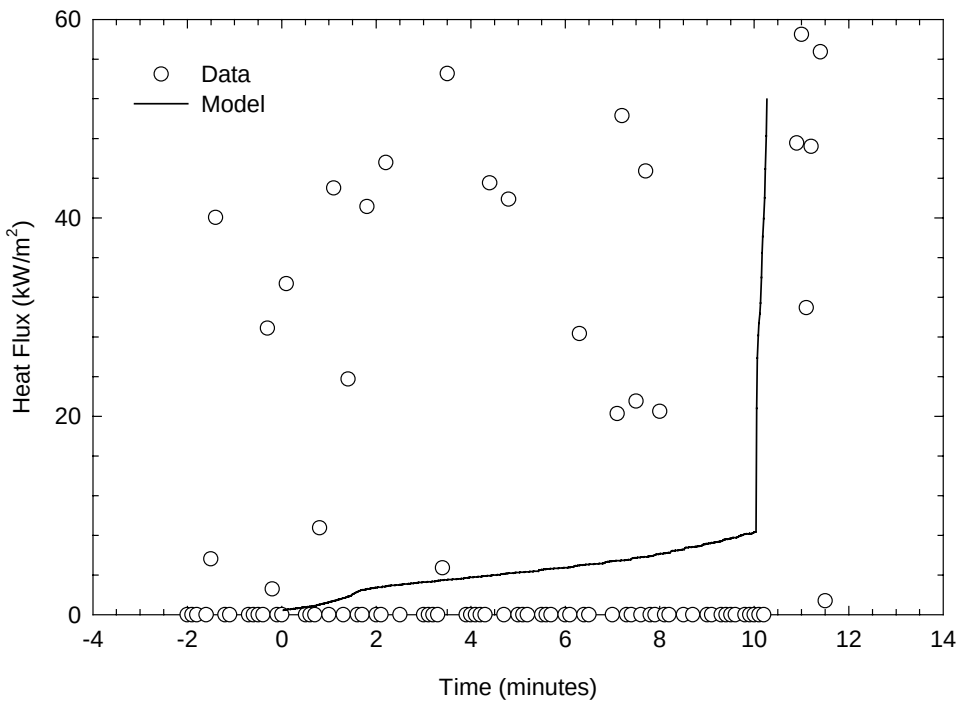

Figure 4-27. Actual and Predicted Heat Flux for Material #9

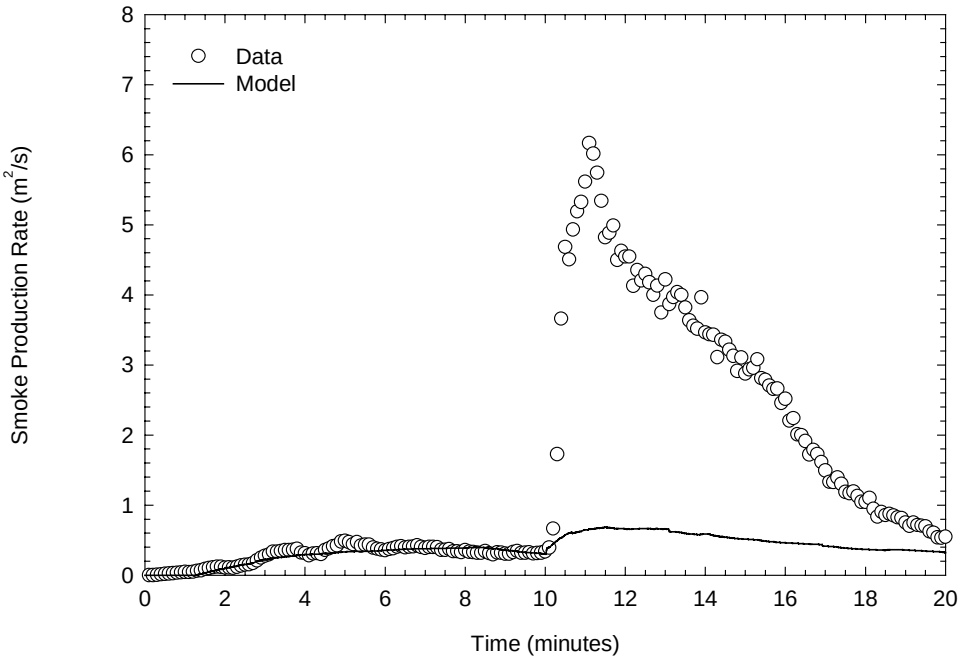

Figure 4-28. Actual and Predicted Smoke Production Rate for Material #1

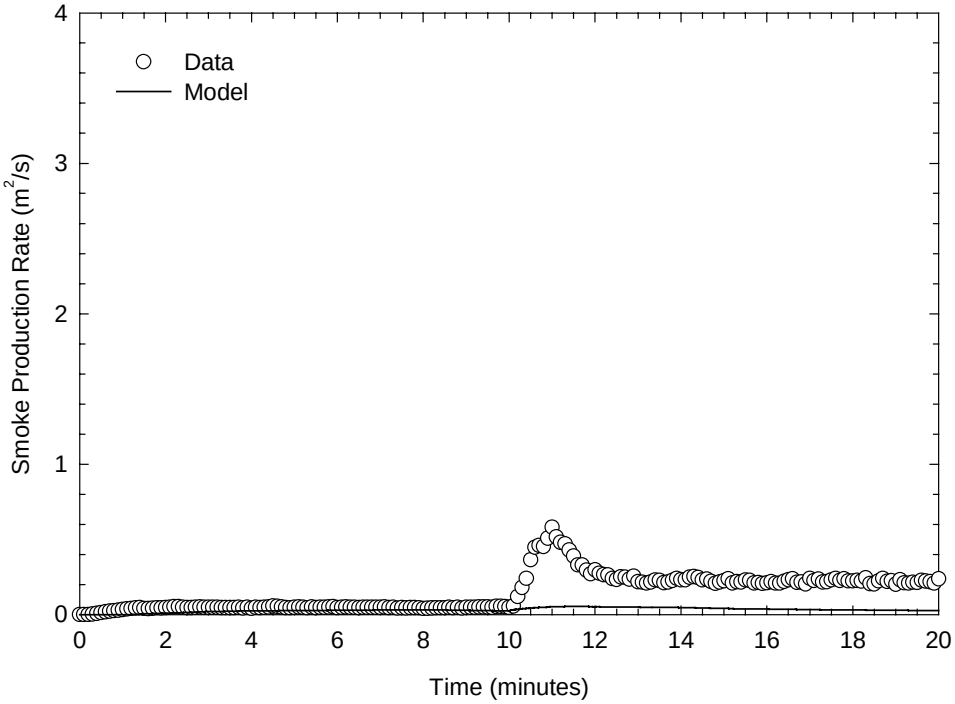

Figure 4-29. Actual and Predicted Smoke Production Rate for Material #2

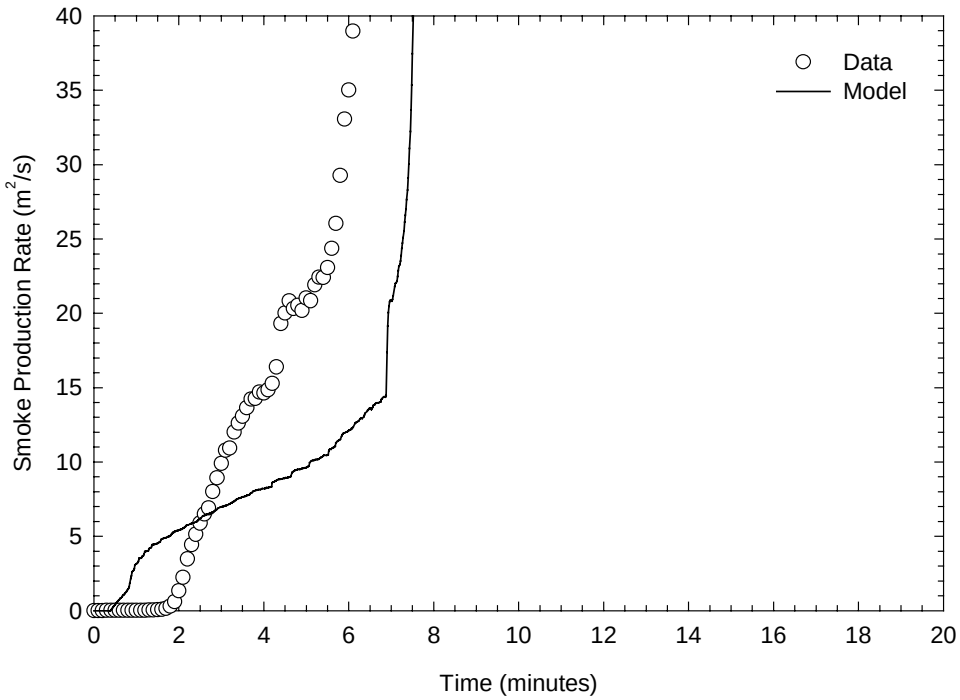

Figure 4-30. Actual and Predicted Smoke Production Rate for Material #3

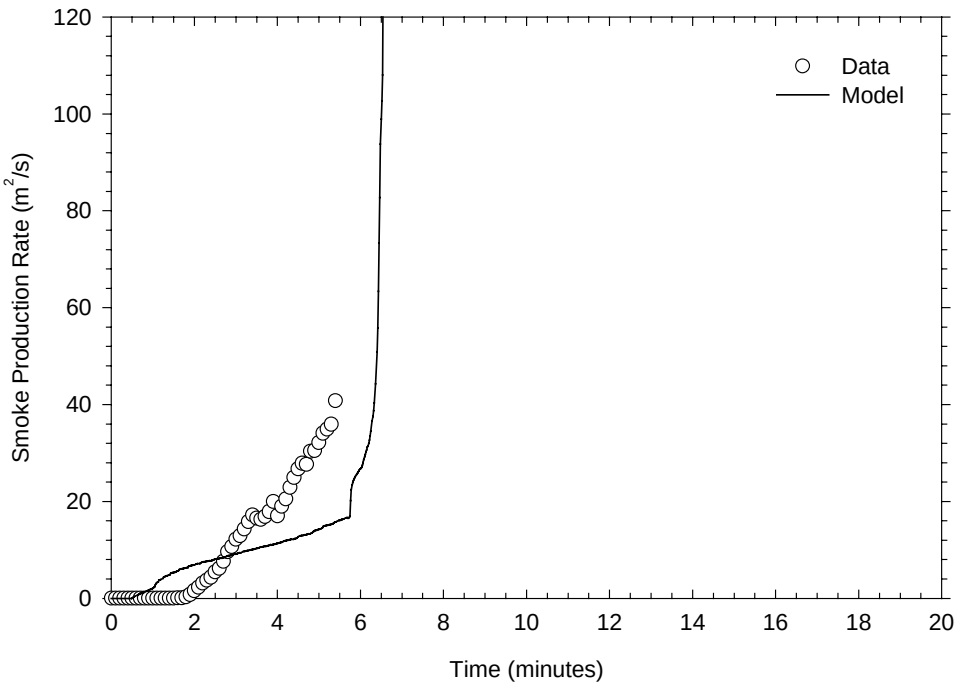

Figure 4-31. Actual and Predicted Smoke Production Rate for Material #4

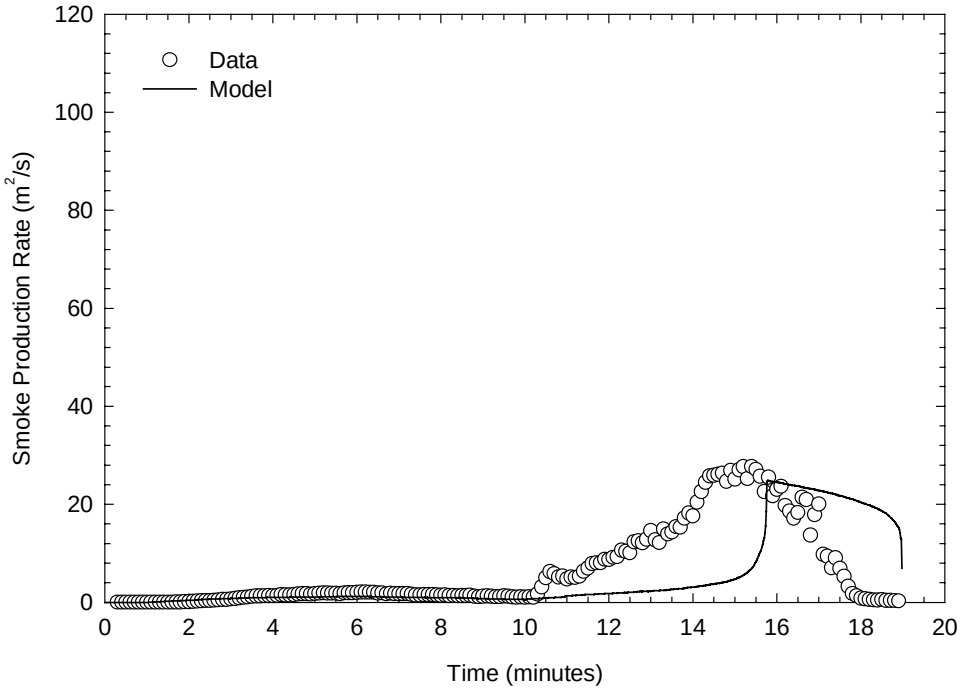

Figure 4-32. Actual and Predicted Smoke Production Rate for Material #5

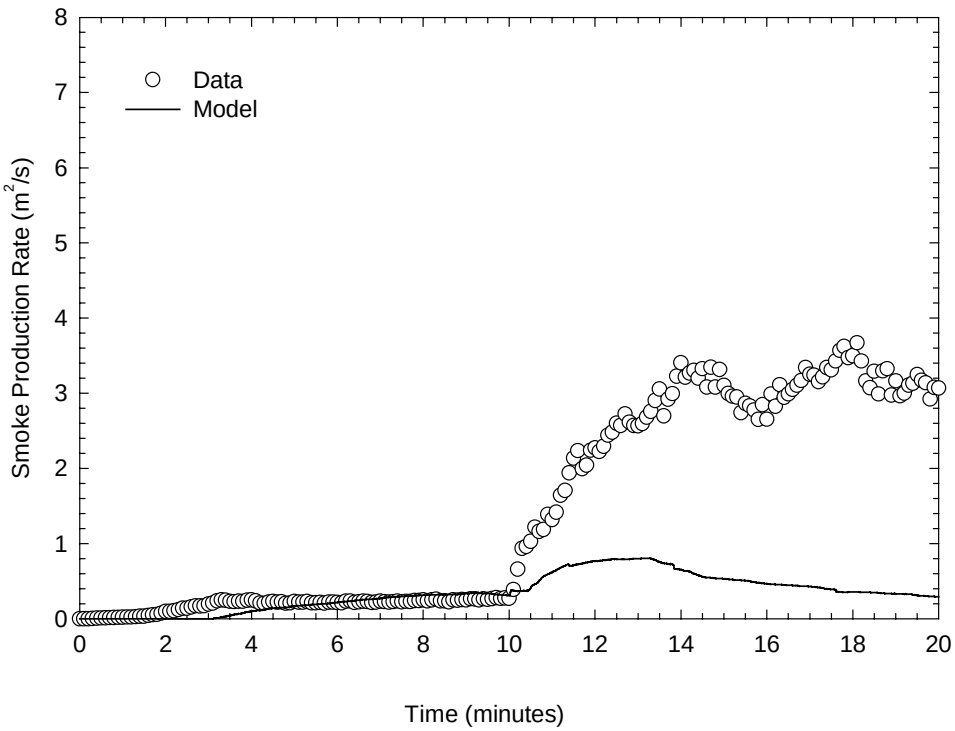

Figure 4-33. Actual and Predicted Smoke Production Rate for Material #6

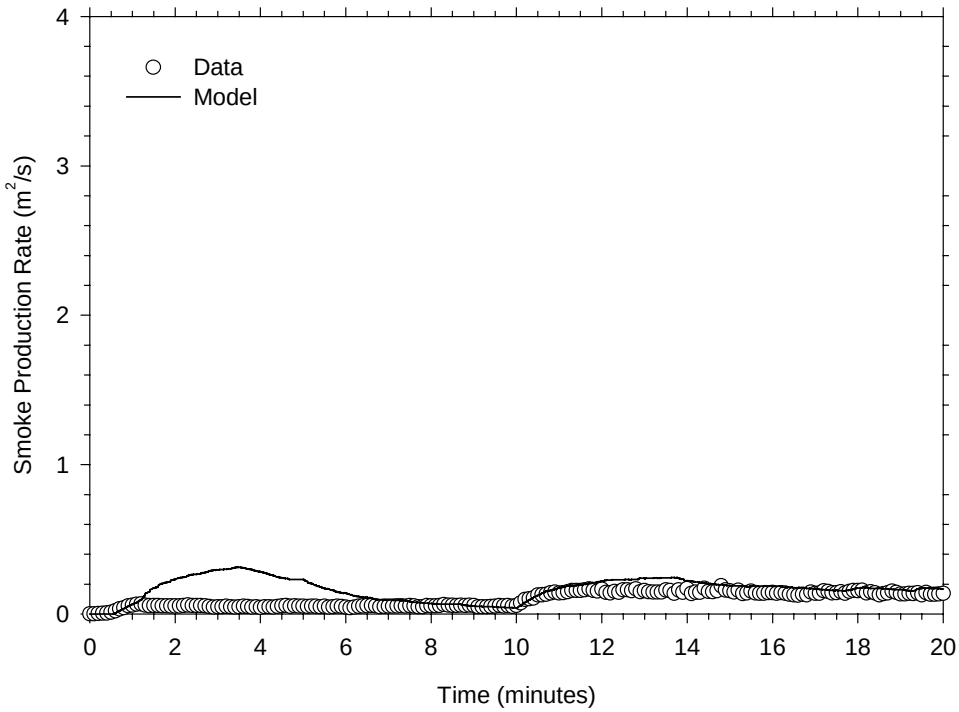

Figure 4-34. Actual and Predicted Smoke Production Rate for Material #7

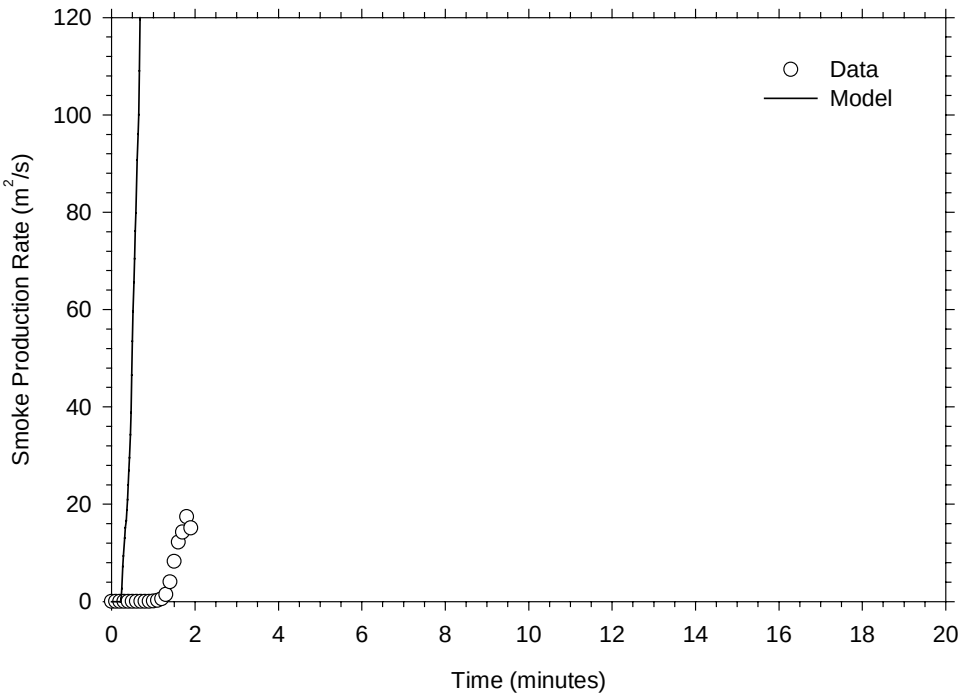

Figure 4-35. Actual and Predicted Smoke Production Rate for Material #8

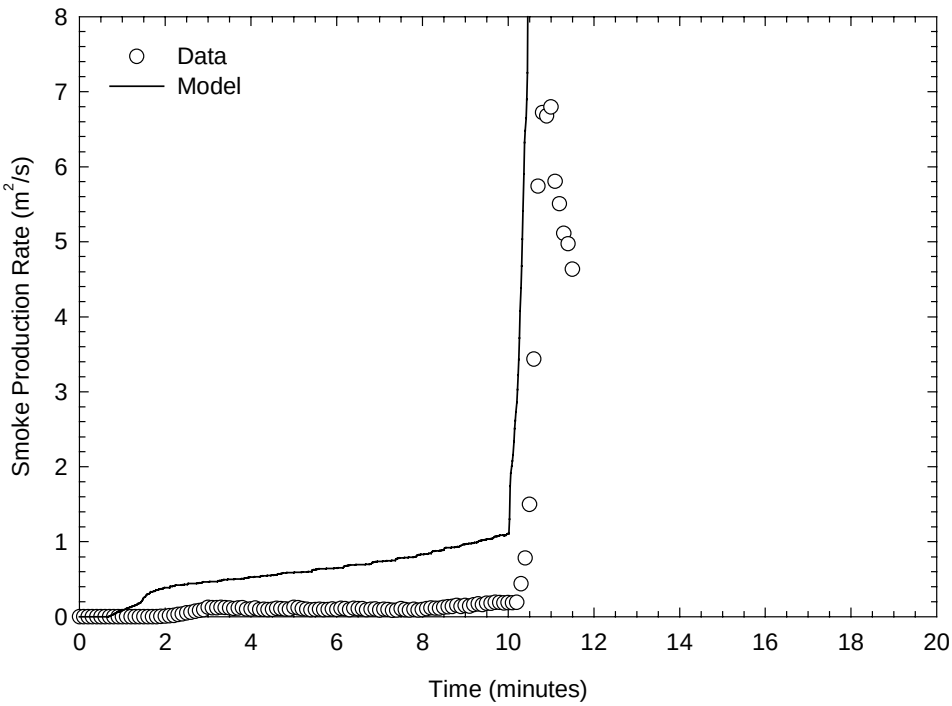

Figure 4-36. Actual and Predicted Smoke Production Rate for Material #9

5.0 SENSITIVITY ANALYSIS

The sensitivity of the model flame spread predictions to the potential uncertainty in the material properties was investigated. Solution convergence was also established by changing the time step and element size and comparing the results. This section describes the uncertainty in the material properties and presents the results of a systematic variation of these parameters on the predictions of the model. This information is needed to highlight the most significant material properties that impact the model results. In addition to the material properties and solution convergence, the effect of the compartment dimensions and the opening area were evaluated. This was done to show how the layer temperature and possibly the performance of a composite material can change with room size.

5.1 Solution Convergence

The solution convergence was investigated by varying the number of elements used on the wall and ceiling and by varying the time step. Note that symmetry requires the ceiling have the same number of elements in the X and Z directions. Figure 5-1 shows the effect of the number of nodes on the model predictions for the fire retardant polyester (Material 3) tested in the ISO 9705 room. Several conclusions can be drawn from this figure. First, the model is less sensitive to the number of vertical (Y) elements as it is to the number of horizontal (X) elements. This is not unexpected, because a coarse horizontal mesh could impede the lateral flame spread. Vertical flame spread is influenced more by the size of the source fire. If the source fire were small, then the model could be more sensitive to the number of vertical elements. It can also be concluded from Figure 5-1 that the 100x100 mesh sized used to predict the ISO 9705 corner fires was sufficient. A finer wall mesh (230x230) resulted in a slightly shifted heat release rate curve after six minutes. The additional computation time for such a fine mesh is clearly not justified.

Figure 5-2 shows the effect of the time step size on the predictions for Material 3. The time step was varied from 0.1 second to 10 seconds. The time step used in this analysis was 1.0 second. Time steps greater than 2 seconds were not expected to result in reliable predictions because the temperature rise of heated elements is too rapid for the differential equation solver over this amount of time. Figure 5-2 shows that a 5 and 10-second time step result in completely different predictions. However, a 0.1 and 1 second time step are nearly the same. It could be concluded from this that a 1-second time step was sufficiently small for this type of exposure.

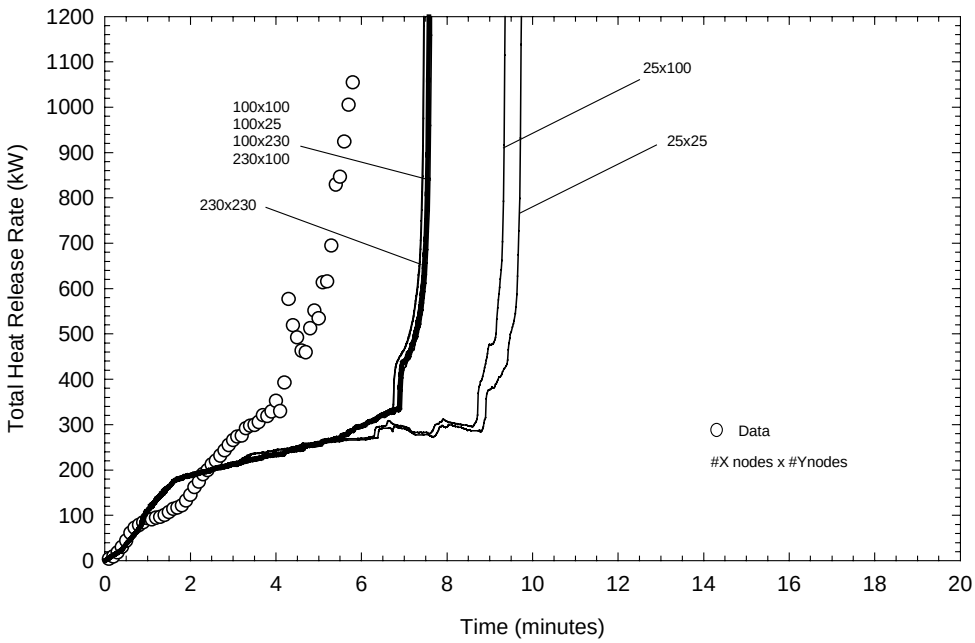

Figure 5-1. Effect of the Number of X and Y Nodes on the Model Predictions for Material # 3.

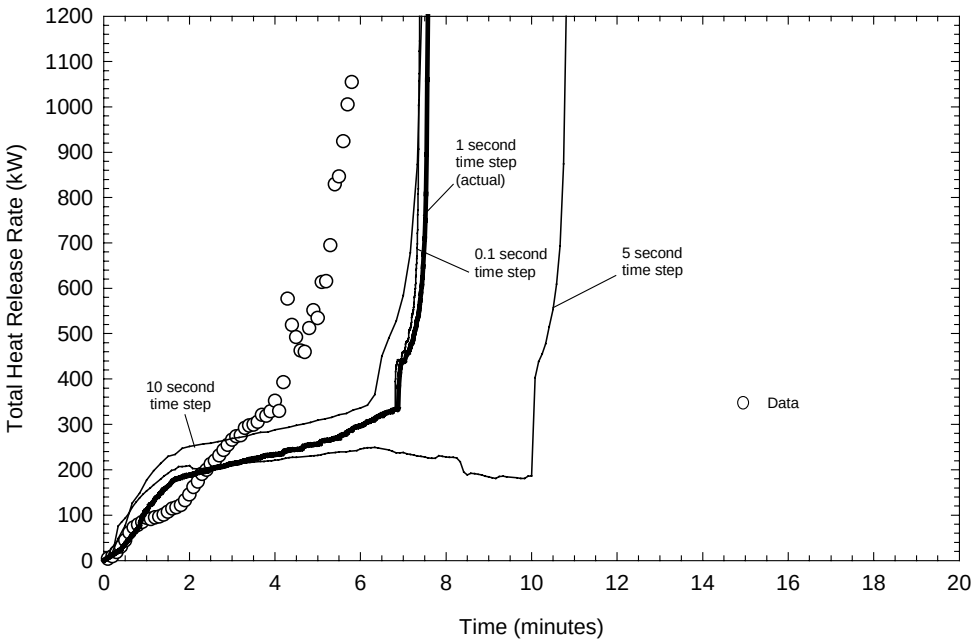

Figure 5-2. Effect of the Time Step Size on Model Predictions for Material # 3.

5.2 Material Properties

The sensitivity of the model predictions to the uncertainty in the material properties was evaluated estimating what the potential range of values for a specific material property could be, then running the model with the maximum and minimum value in this range. Two different types of materials were used to assess the impact of a specific material property. One material that was used caused the ISO 9705 room to reach flashover when exposed to the 100 kW fire source (Material 3) and the other material caused the room to reach flashover only when exposed to the 300 kW fire source (Material 9).

Some properties were found to have little of no impact on the model predictions. These properties are:

1. Heat of combustion of the composite material;
2. The density of the substrate material;
3. The thermal conductivity of the substrate material;
4. The thermal conductivity of the composite material; and
5. The heat capacity of the substrate material;

The substrate refers to the 0.02-m thick calcium silicone wall boards that the nine composite materials were attached to during the ISO 9705 tests.

5.2.1 Substrate Thickness

The effect of the substrate thickness on the model predictions is shown in Figures 5-3 and 5-4. The actual thickness of the substrate in the fire tests was 20 mm for both materials. The thickness was arbitrarily varied from 10 mm to 30 mm to test the sensitivity of the results to this parameter. Figure 5-3 shows that the predicted time to flashover changes from about six minutes for a 10-mm thick substrate to about 9 minutes for a 30-mm thick substrate. Conversely, the substrate thickness has no appreciable effect on Material #9, as evidenced by Figure 5-4. Because the thickness of Materials #3 and #9 are the same, the difference likely is a result of a change in the effective thermal properties of the wall.

5.2.2 Composite Thickness

The effect of the composite thickness on the model predictions is shown in Figures 5-5 and 5-6. The actual composite thickness was 5.2 mm for both Material #3 and Material #9. The thickness was arbitrarily varied from 2.6 mm to 10.4 mm. Figures 5-5 and 5-6 show that the impact of the composite thickness was more pronounced with Material #3, as was the case with the substrate thickness. The composite thickness will have an impact on the heat loss to the wall, which will in turn influence the hot layer temperature. The composite thickness will also determine the fire duration, though that is not an issue with Materials #3 and #9.

5.2.3 Percent Mass Burned

The effect of the percent mass burned on the model predictions is shown in Figures 5-7 and 5-8. The range of values for the percent mass burned were obtained from the maximum and minimum values measured in the cone calorimeter for each material. The average percent mass lost for Material #3 was 33%; the minimum was 10 and the maximum was 50%. The average percent mass lost for material #3 was 34%; the minimum was 18 and the maximum was 51%. The percent mass influences the burning duration. Figure 5-7 shows that this has more of an impact on the results for Material #3 than Material #9. Other factors contribute to the burning duration and may reduce the overall effect on the heat release rate predictions for Material #9.

5.2.4 LIFT Thermal Inertia

The effect of the LIFT thermal inertia ($k\rho c$) on the model predictions is shown in Figures 5-9 and 5-10. The results obtained by using the minimum or maximum reported value in one data set were compared to the results obtained using the actual value. The actual value for Material #3 is 1.65 kW^2-s/m^4-K^2 and the minimum reported value was 1.54 kW^2-s/m^4-K^2. The actual value for Material #9 is 1.72 kW^2-s/m^4-K^2 and the maximum reported value was 1.89 kW^2-s/m^4-K^2. Figures 5-9 and 5-10 show that this parameter does not have a significant influence on the model predictions. The results were included in this section to demonstrate the difference between the LIFT thermal inertia and the cone calorimeter thermal inertia.

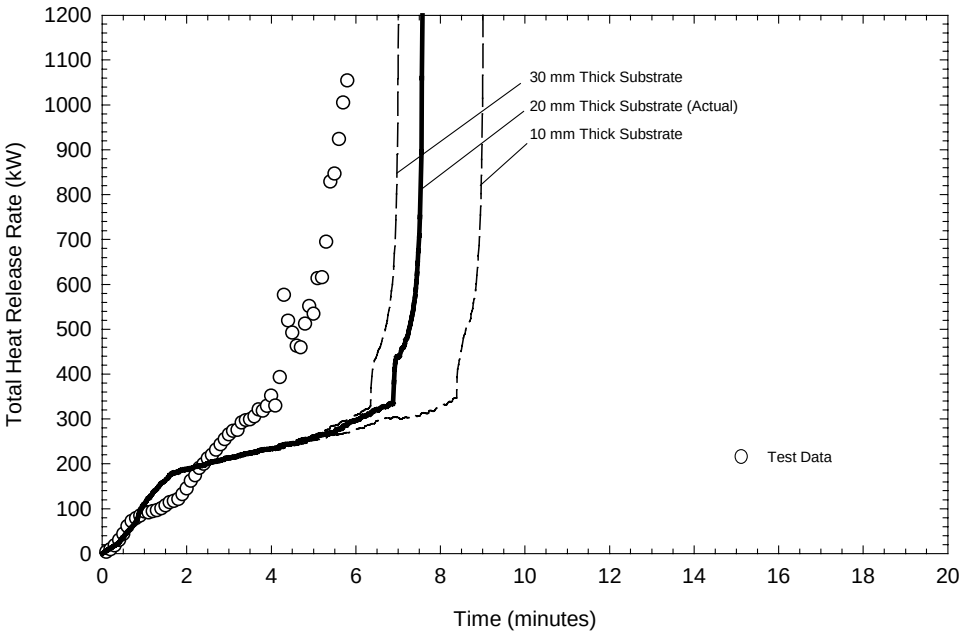

Figure 5-3. Effect of the Substrate Thickness on the Model Predictions for Material # 3.

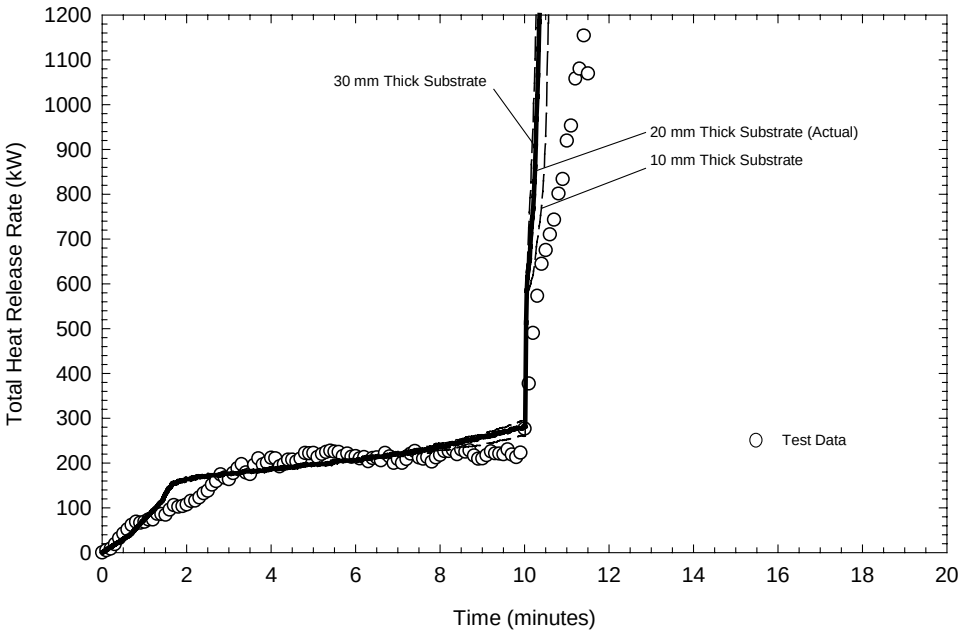

Figure 5-4. Effect of Substrate Thickness on the Model Predictions for Material # 9

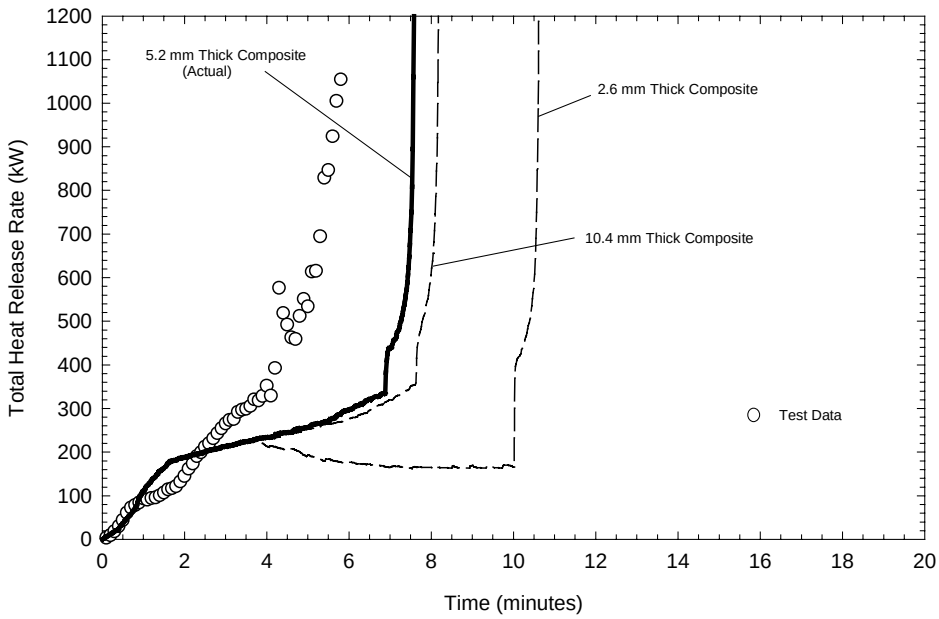

Figure 5-5. Effect of the Composite Thickness on the Model Predictions for Material # 3.

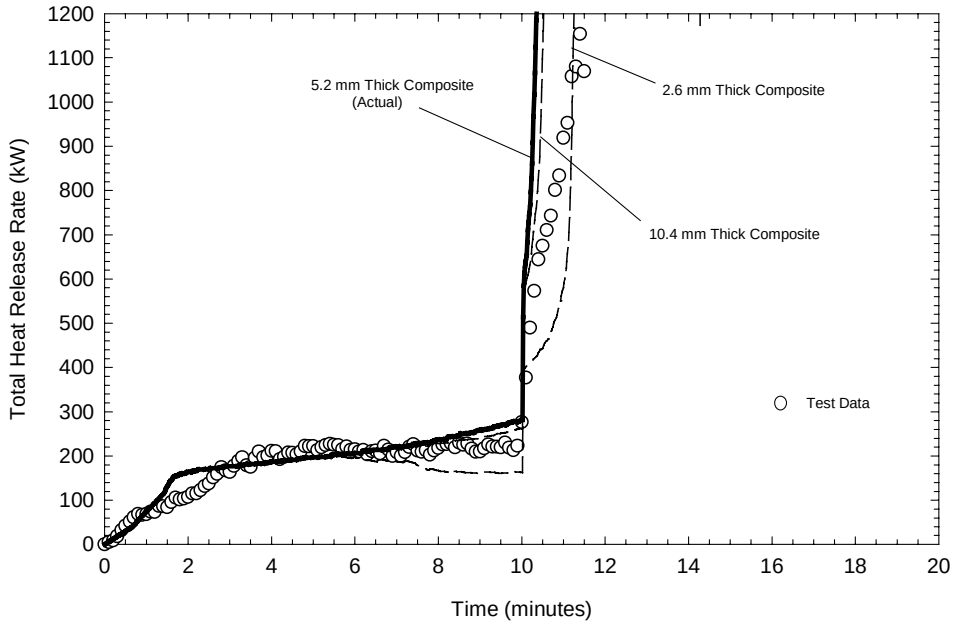

Figure 5-6. Effect of the Composite Thickness on the Model Predictions for Material # 9

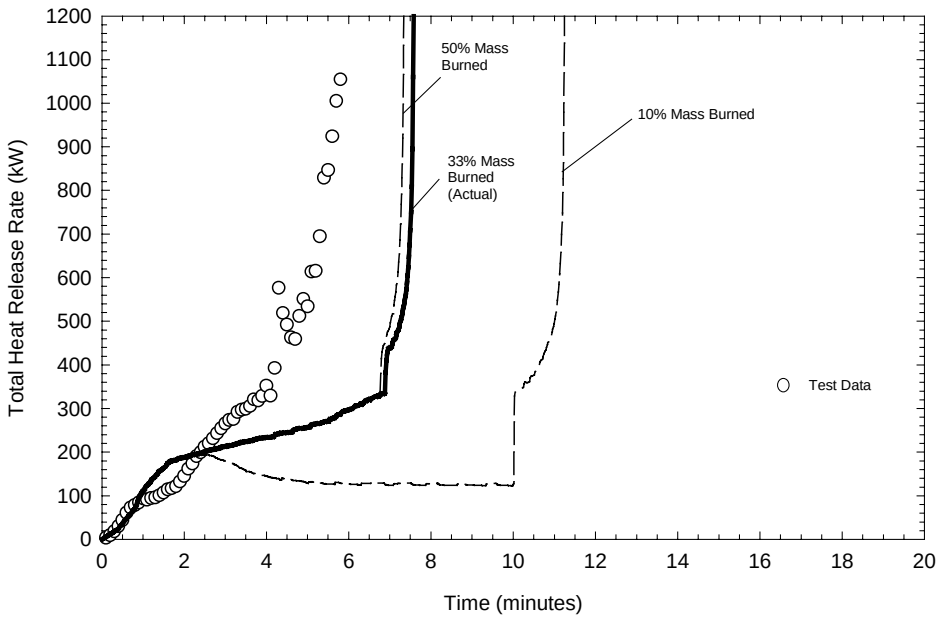

Figure 5-7. Effect of the Percent Mass Burned on the Model Predictions for Material # 3.

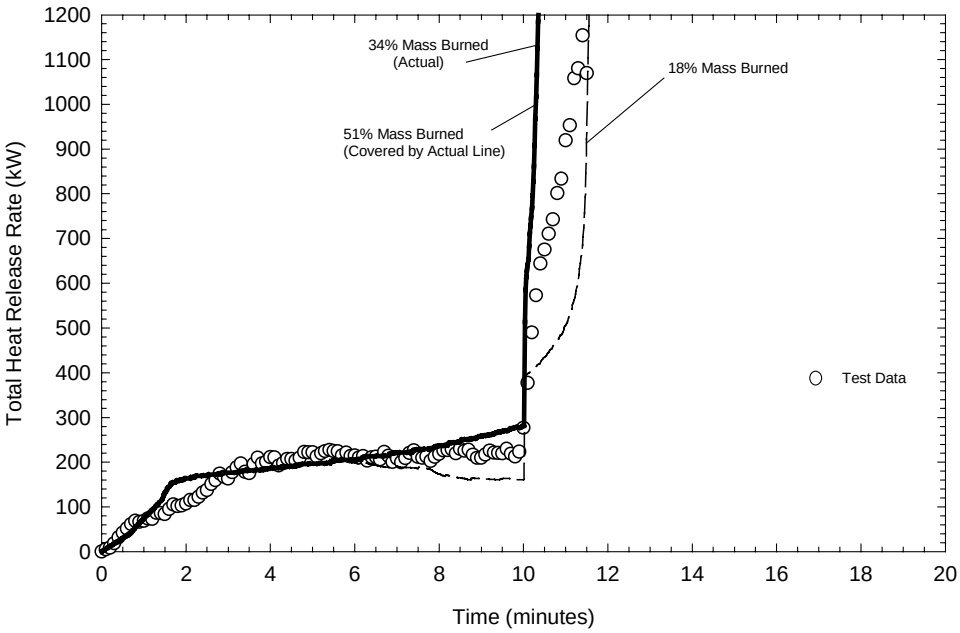

Figure 5-8. Effect of the Percent Mass Burned on the Model Predictions for Material # 9

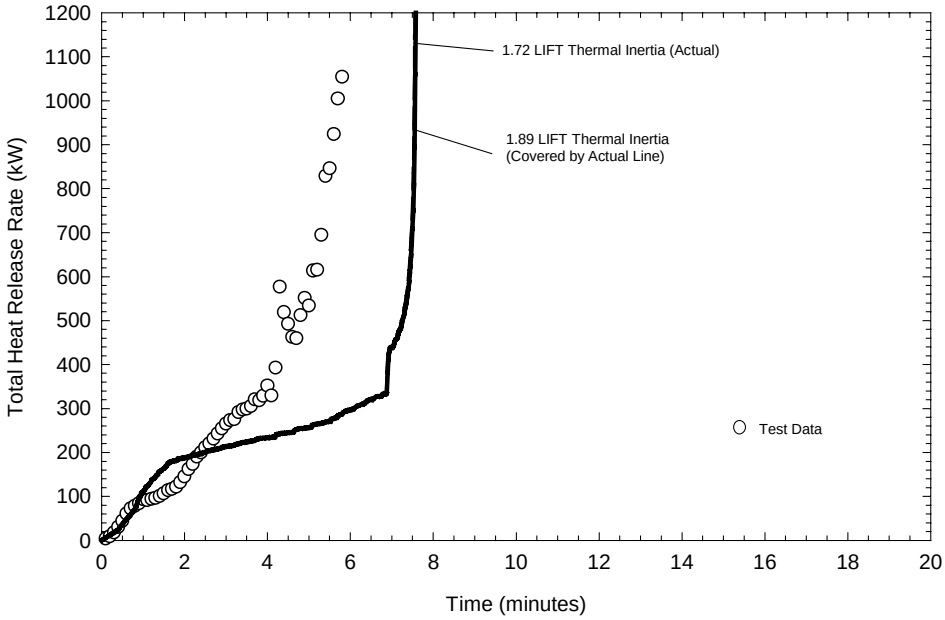

Figure 5-9. Effect of the LIFT Thermal Inertia on the Model Predictions for Material # 3.

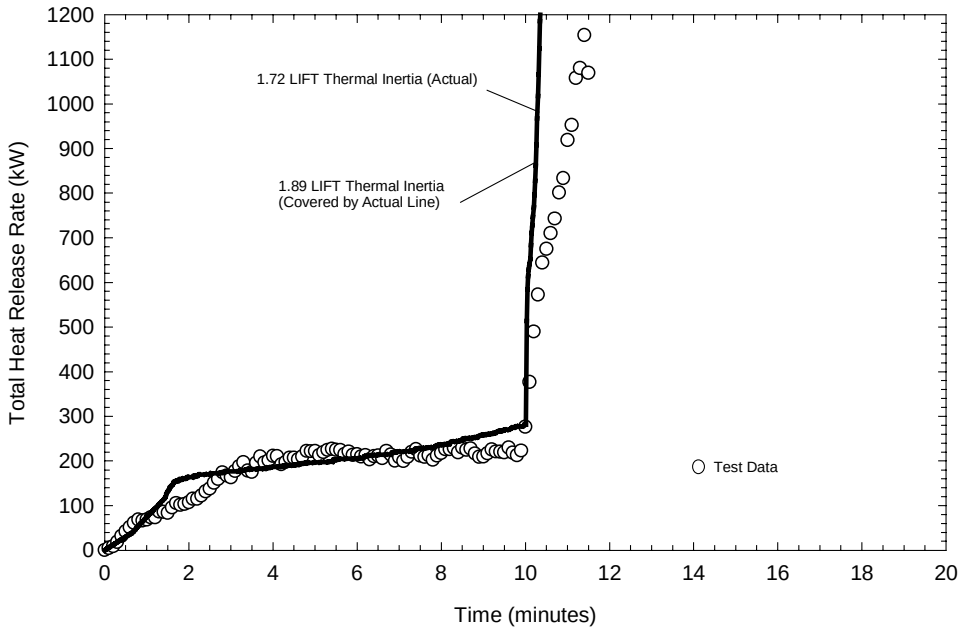

Figure 5-10. Effect of the LIFT Thermal Inertia on the Model Predictions for Material # 9

5.2.5 LIFT Flame Heating Parameter

The effect of the LIFT flame heating parameter on the model predictions is shown in Figures 5-11 and 5-12. The maximum flame heating parameter value was obtained by using a best-fit line from one test. The minimum value was obtained by using a best-fit line through one test also. The range for the flame heating parameter was extended for Material #3 by using the critical heat flux to obtain a best-fit line. This was assumed to be a typical error when determining this material property and resulted in an extremely low value, which effectively would shut off lateral flame spread in the model.

Figures 5-11 and 5-12 show that the results are relatively insensitive to the flame heating parameter, except for the erroneously low value used with material #3. This means that the results are more sensitive to the presence or absence of lateral flame spread than the actual flame spread velocity.

5.2.6 Minimum Temperature for Flame Spread

The effect of the LIFT flame heating parameter on the model predictions is shown in Figures 5-13 and 5-14. The range of values for the minimum flame spread temperature were based on the potential error in determining the location where the flame spread stopped on the test sample. The actual minimum flame spread temperature for Material #3 is 580 K and the maximum value using this approach is 646 K. The actual minimum flame spread temperature for Material #9 is 598 K and the maximum value is 630 K. Figure 5-13 and 5-14 show that Material #3 is more sensitive to this parameter than Material #9.

5.2.7 Heat of Gasification

The effect of the heat of gasification is shown in Figures 5-15 and 5-16. The maximum and minimum values were obtained by using the highest and lowest critical heat flux, heat of combustion, and heat release rate values among all the tests. Table 5-1 summarizes the maximum, minimum, and actual values used for this parameter evaluation.

Table 5-1. Summary of Values.

Material	**Heat of Combustion (kJ/kg)**			**Heat of Gasification (kJ/kg)**		
	Actual	**Maximum**	**Minimum**	**Actual**	**Maximum**	**Minimum**
3	11,280	14,280	8,280	12,280	15,280	9,280
9	8,000	18,700	3,920	10,240	22.900	3,720

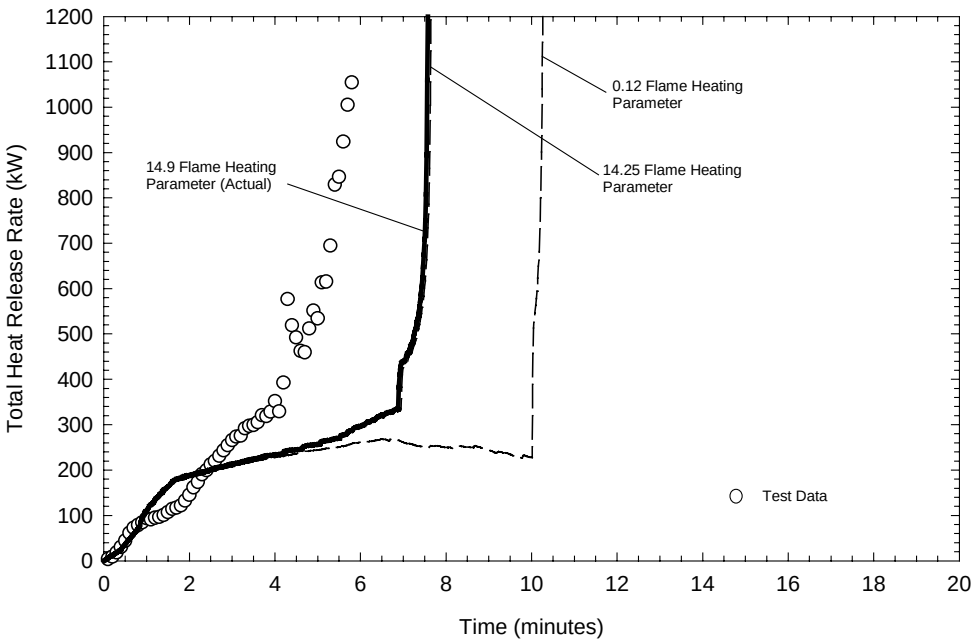

Figure 5-11. Effect of the Flame Heating Parameter on the Model Predictions for Material # 3.

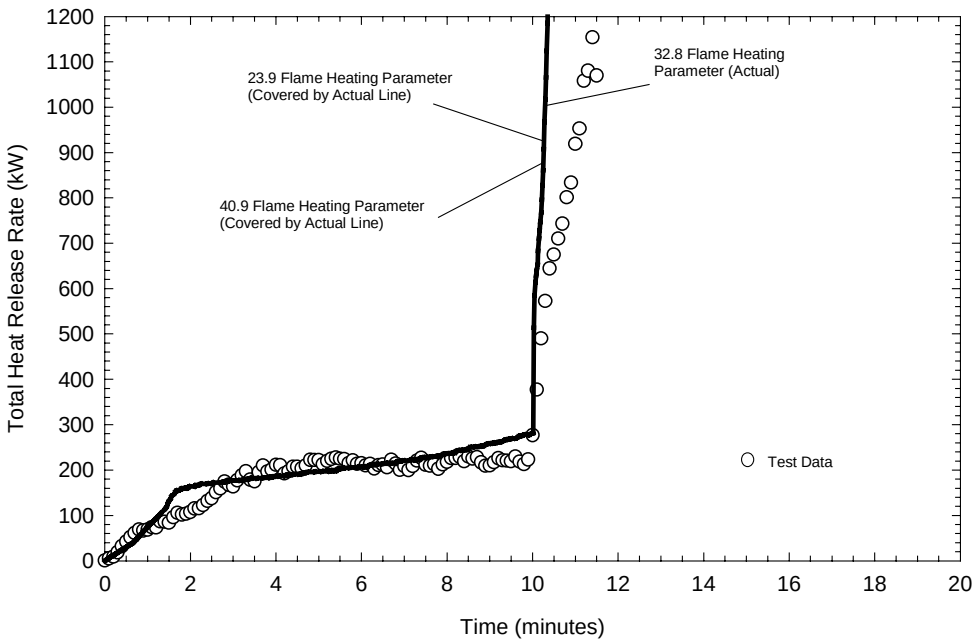

Figure 5-12. Effect of the LIFT Flame Heating Parameter on the Model Predictions for Material # 9

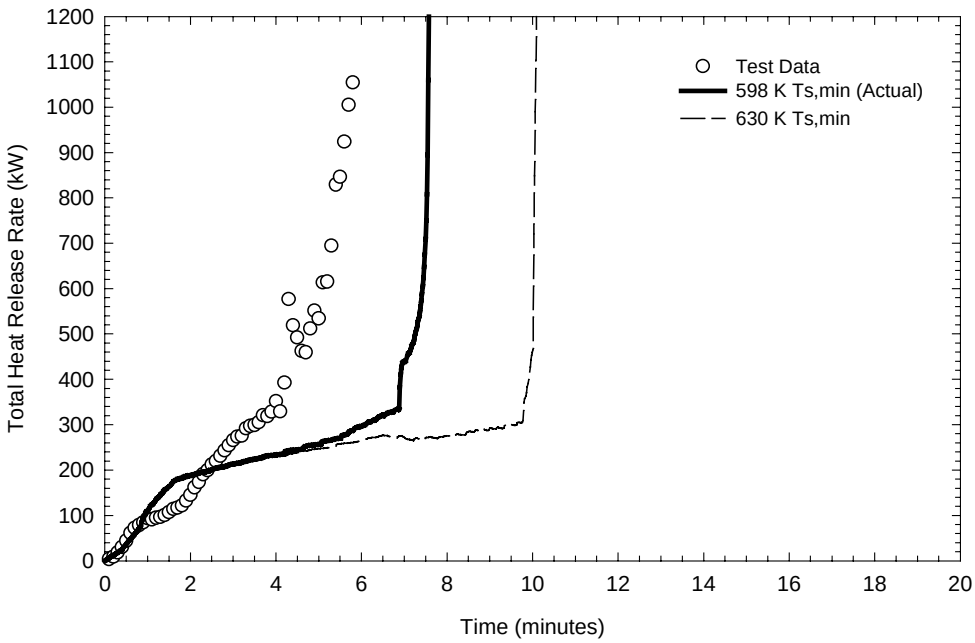

Figure 5-13. Effect of the Minimum Flame Spread Temperature on the Model Predictions for Material # 3.

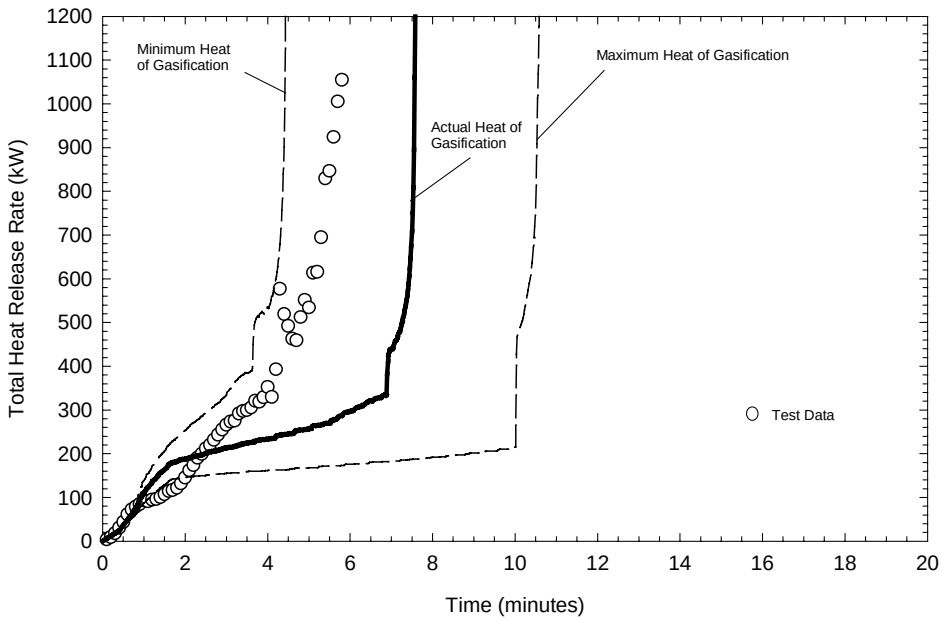

Figure 5-15. Effect of the Heat of Gasification on the Model Predictions for Material # 3.

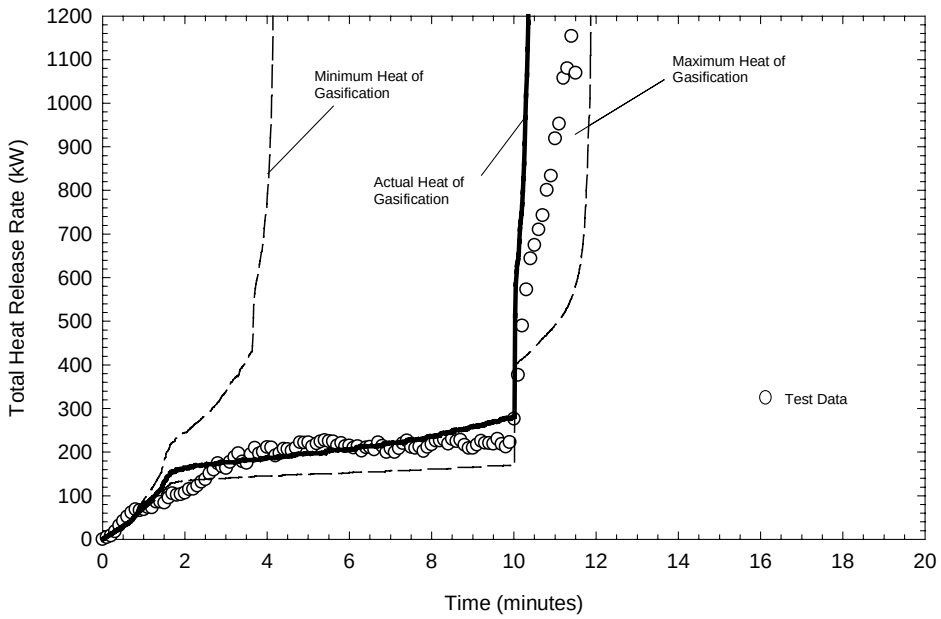

Figure 5-16. Effect of the Heat of Gasification on the Model Predictions for Material # 9

The results show that the heat of gasification has a significant impact on the results. This is easily understood considering the mass loss rate and the heat release rate all are a function of this parameter.

5.2.8 Critical Heat Flux

The effect of the critical heat flux is shown in Figures 5-17 and 5-18. ASTM E1321 requires that the accuracy of the reported value be within 2 kW/m^2. The reported critical heat flux for Material #3 is 14.9 kW/m^2. The maximum expected value is therefore 16.9 kW/m^2. The reported critical heat flux for Material #9 is 15.7 kW/m^2 and the expected maximum value is 17.7 kW/m^2. Figures 5-17 and 5-18 show that Material #3 is more sensitive to the critical heat flux than Material #9.

5.2.9 Ignition Time

The effect of the ignition time is shown in Figures 5-19 and 5-20. The range of values for this parameter were obtained using the Reproducibility equation determined from the Inter-laboratory trials as listed in ASTM E1321 [1997]:

$$R = 7.4 + 0.22t_{ig} \tag{5-1}$$

where R is the range (s) and t_{ig} is the ignition time (s). Equation 5-1 is applied to the measured ignition time at all heat flux levels measured in the cone calorimeter. The ignition time is actually entered into the corner flame spread model by varying the cone thermal conductivity, ignition temperature, and the heat of gasification. Figures 5-19 and 5-20 show that Material #3 is more sensitive to the ignition time than Material #9, which is nearly insensitive to this parameter.

5.2.10 Lateral Flame Spread Velocity

The effect of the lateral flame spread velocity on the model predictions is shown in Figures 5-21 and 5-22. The flamespread velocity was minimized and maximized by taking the maximum or minimum of all the parameters that contribute to the flame spread velocity. These include the LIFT thermal inertia, the LIFT flame heating parameter, and the minimum temperature for flame spread. The effect of each of these parameters has already been investigated and the ranges have already been presented. The flame spread velocity parameter changes them all at once. Figures 5-21 and 5-22 shows that both Material #3 and Material #9 are sensitive to the flame spread velocity.

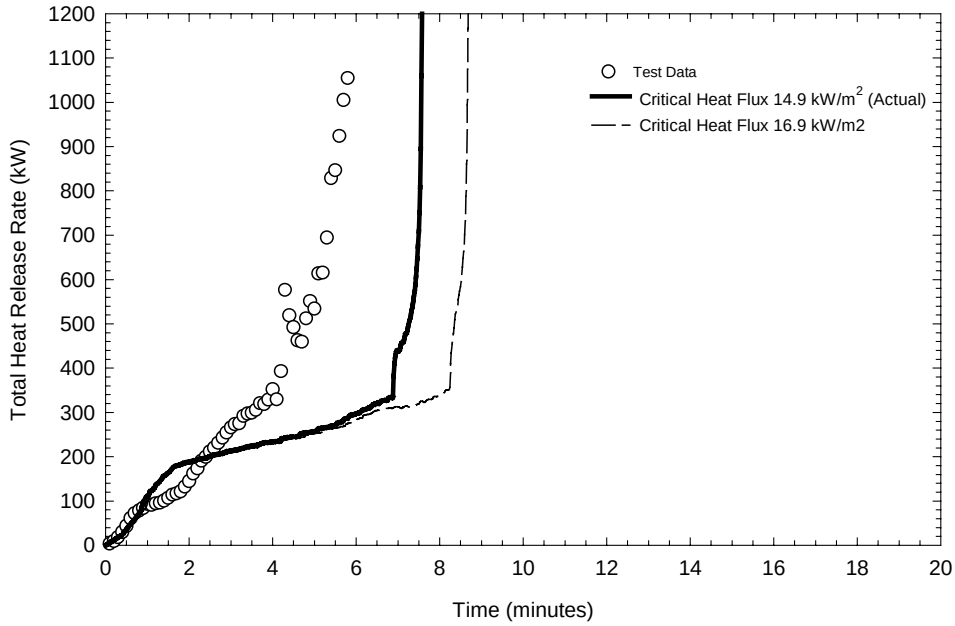

Figure 5-17. Effect of the Critical Heat Flux on the Model Predictions for Material # 3.

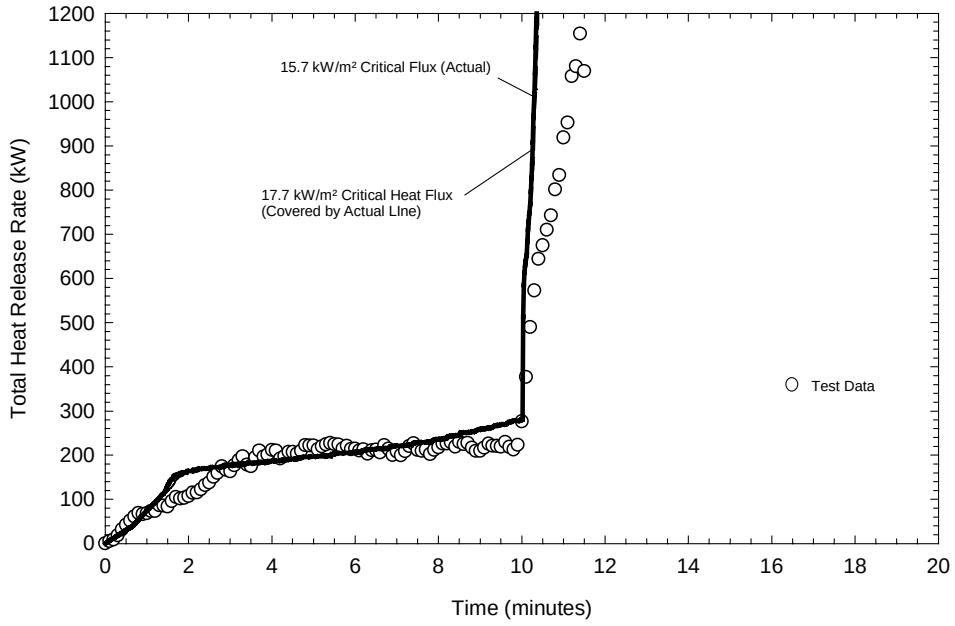

Figure 5-18. Effect of the Critical Heat Flux on the Model Predictions for Material # 9

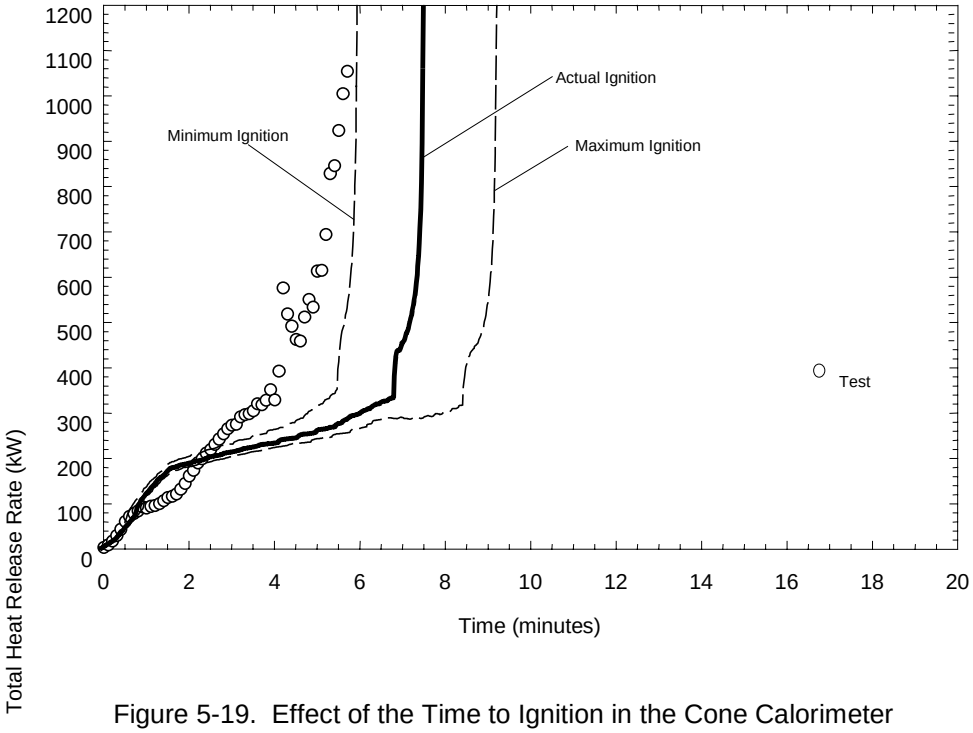

Figure 5-19. Effect of the Time to Ignition in the Cone Calorimeter Model Predictions for Material

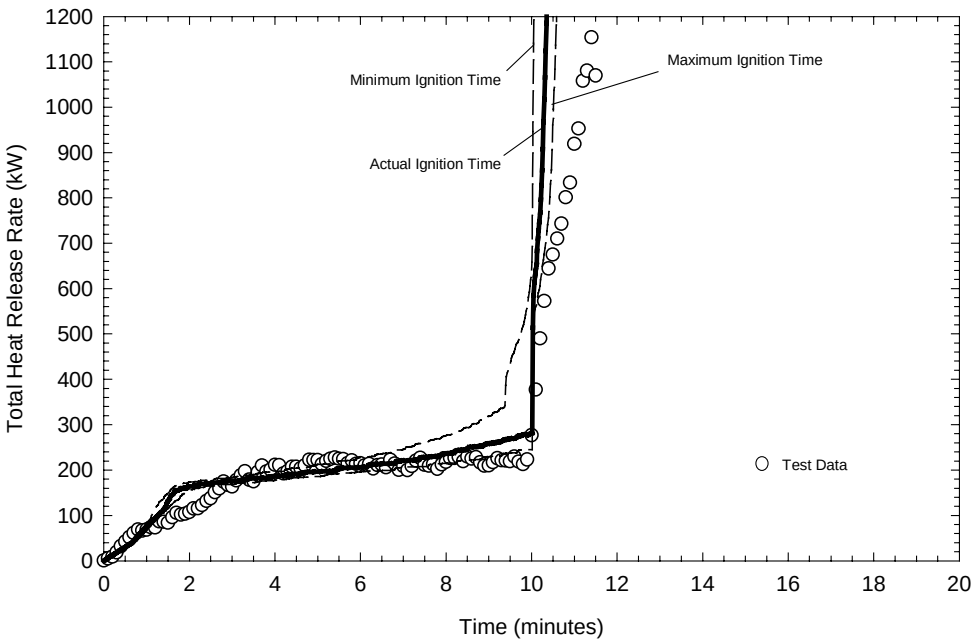

Figure 5-20. Effect of the Cone Calorimeter Time to Ignition on the Model Predictions for Material # 9

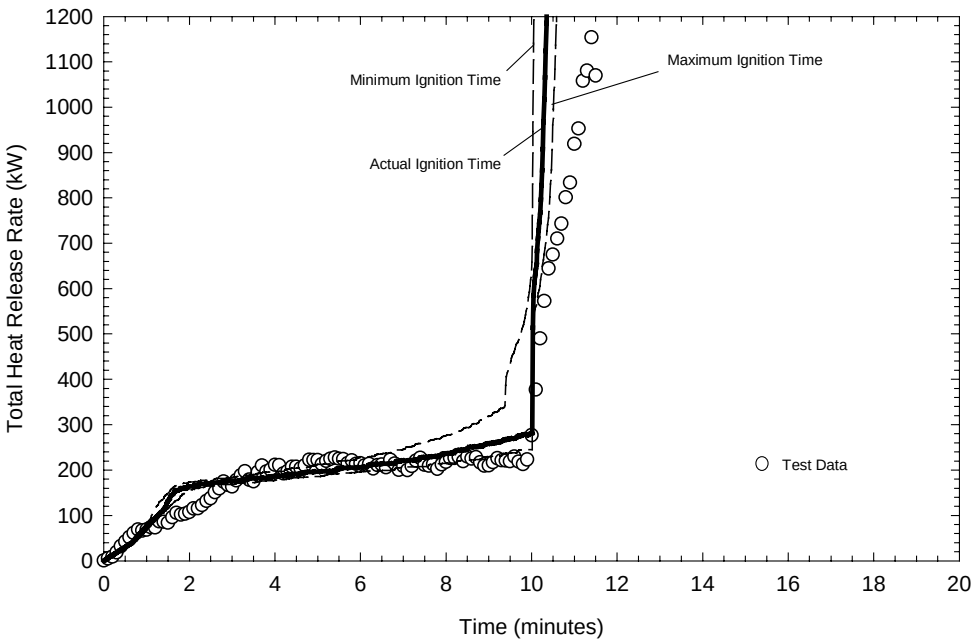

Figure 5-20. Effect of the Cone Calorimeter Time to Ignition on the Model Predictions for Material # 9

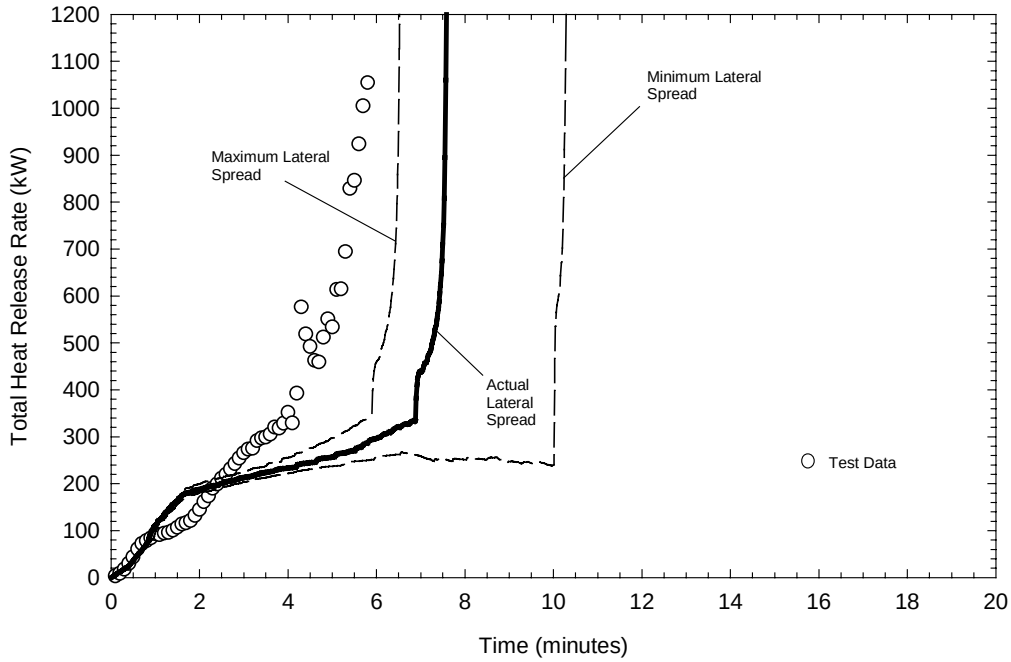

Figure 5-21. Effect of the Lateral Flame Spread on the Model Predictions for Material # 3.

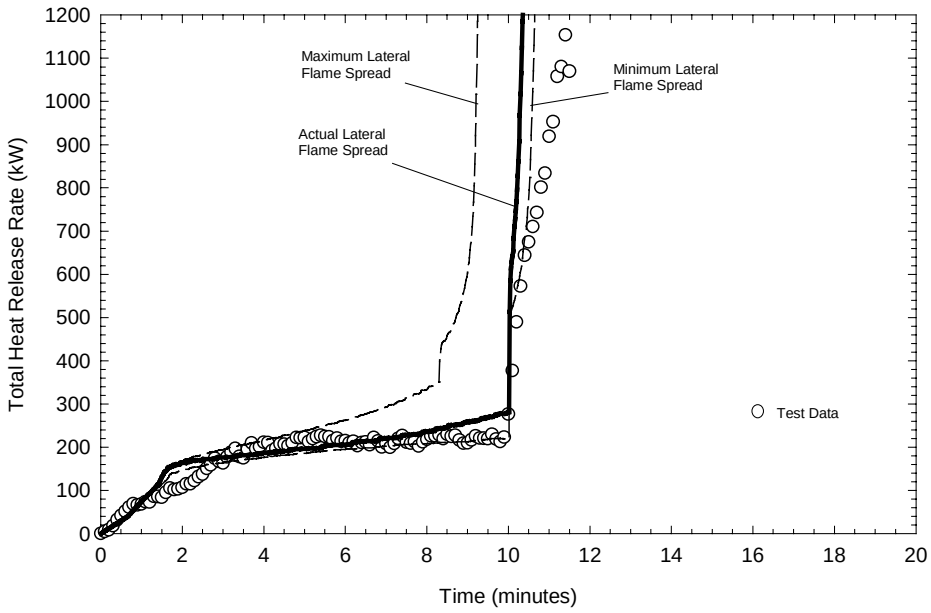

Figure 5-22. Effect of the Lateral Flame Spread on the Model Predictions for Material # 9

5.2.11 Cone Calorimeter Heat Release Rate

The effect of the heat release rate on the predictions of the model are shown in Figures 5-23 and 5-24. The range of values for the heat release rate was obtained using the Reproducibility equation from the Inter-laboratory trials as listed in ASTM E1321:

$$R = 25.5 + 0.151\dot{Q}'' \tag{5-2}$$

where R is the heat release rate range (kW/m^2) and $\dot{Q}''$ is the measured heat release rate per unit area at a given exposure flux (kW/m^2). Figures 5-23 and 5-24 show that both materials are very sensitive to this parameter.

5.3 Room Dimensions

The sensitivity of the model to the dimensions of the room and the area of the vent opening was performed to show the effect of the hot layer. Changing the room size will cause the hot layer to increase or decrease, thereby exposing the boundaries to different temperatures. Figure 5-25 shows the effect of increasing the room floor area on the heat release rate predictions and Figure 5-26 shows the corresponding hot layer temperatures. It is interesting to note that increasing the room area causes the material to flashover after the source increases to 300 kW.

Figure 5-27 shows the effect of increasing the vent width on the heat release rate predictions. Figure 5-28 shows the corresponding hot layer temperature. Because increasing the vent width increases the area and outflow, the hot layer cools, and the effect is analogous to increasing the floor area.

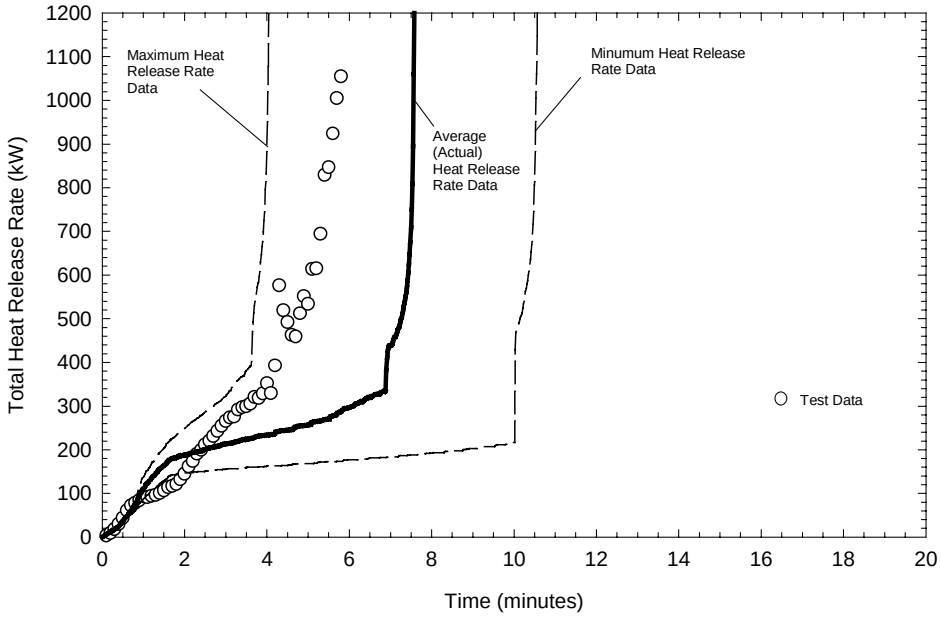

Figure 5-23. Effect of the Heat Release Rates on the Model Predictions for Material # 3.

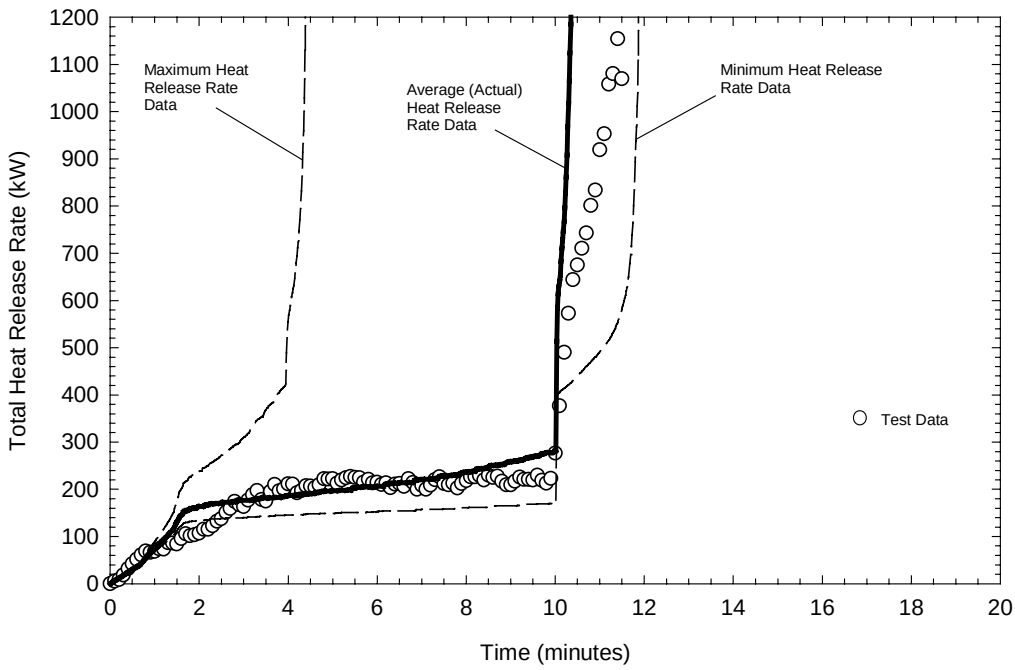

Figure 5-24. Effect of the Heat Release Rates on the Model Predictions for Material # 9

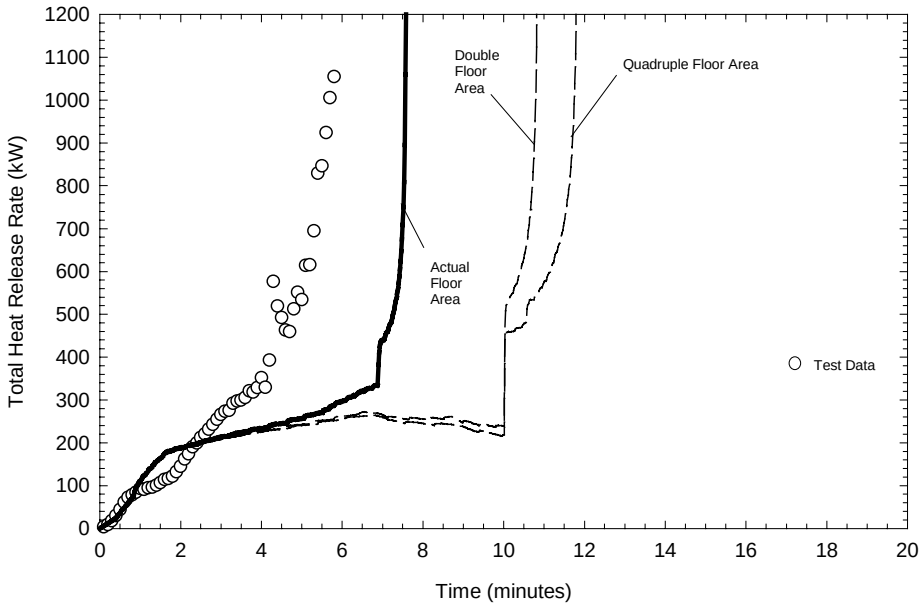

Figure 5-25. Effect of the Compartment Floor Area on the Model Predictions for Material # 3

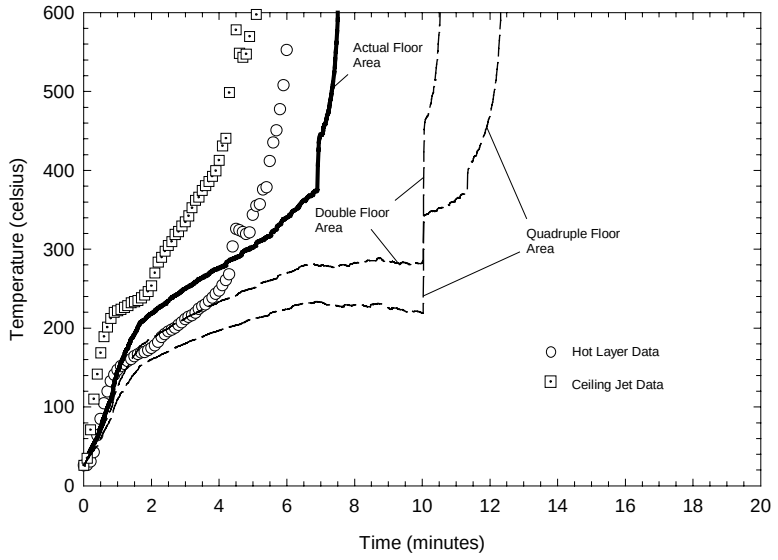

Figure 5-26. Effect of Compartment Floor area on the Model Predictions for Material # 3

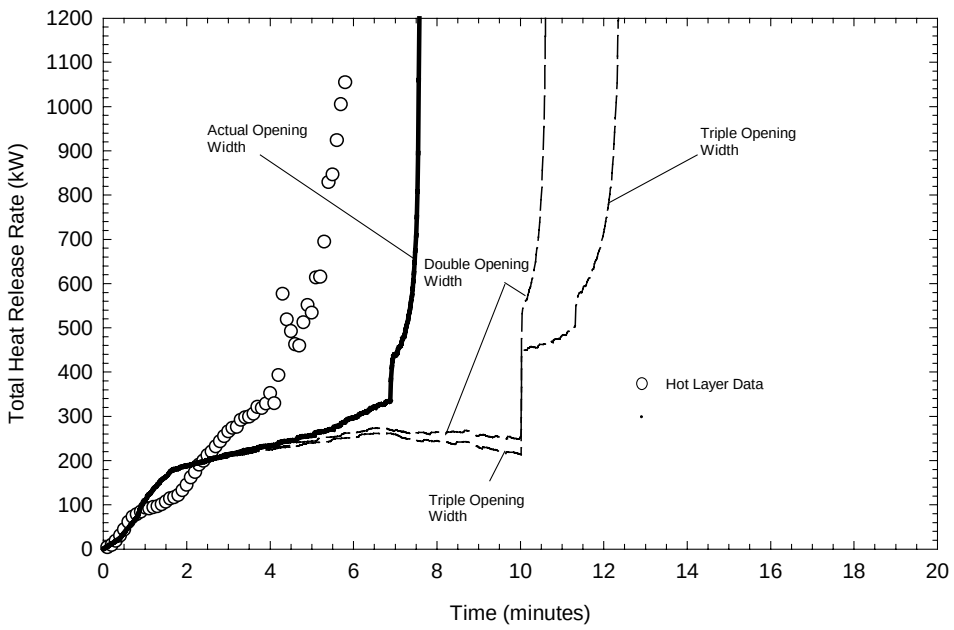

Figure 5-27. Effect of the Opening Width on the Model Predictions for Material # 3

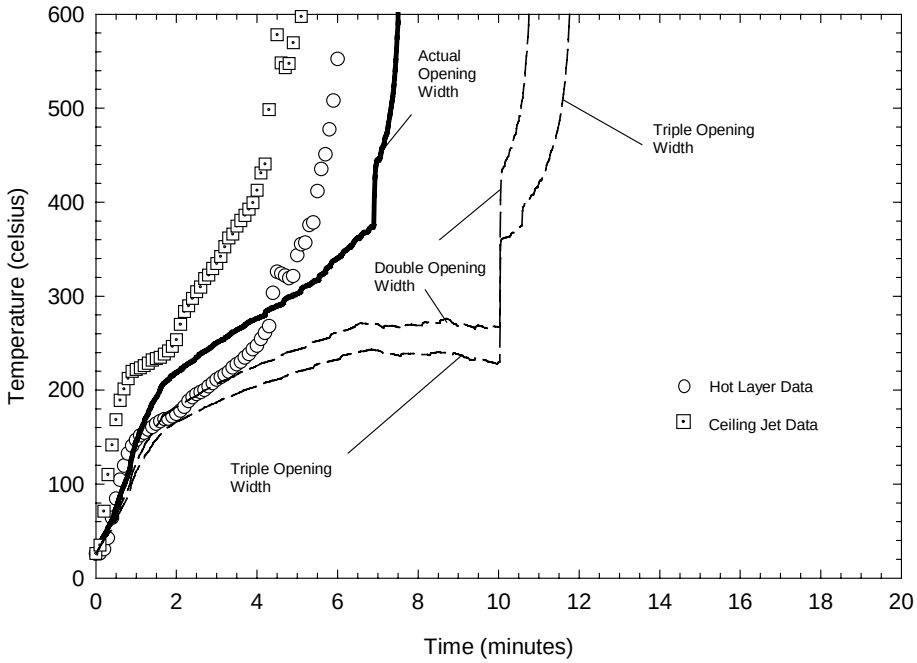

Figure 5-28. Effect of the Opening Width on the Model Predictions for Material # 3

6.0 SUMMARY

The room/corner flame spread model was developed to evaluate the performance of composite materials under actual installation configurations. The model is an extension of a previously developed flame spread program that calculated the flame spread on vertical walls. The room/corner model retains the element and node concepts as well as the surface heating algorithms. New features include lateral flame spread, corner heat flux correlations, hot gas layer effects, area source fires, and a new means of calculating the heat of gasification.

Full-scale fire tests of combustible materials in room/corners revealed that there are three distinct burning regions in a corner. These regions are the wall, the ceiling, and the wall-ceiling boundary. Heating and flame spread in each of these regions is calculated in the flame spread model using heat flux correlations specifically developed for each region. Both area source fires and line burner source fires can be modeled.

The effect of the hot gas layer was found to have a significant impact on the flame spread by pre-heating the compartment boundary materials. Consequently, the effects of the hot layer were included in the corner flame spread model using the Method of McCaffery, Quintiere, and Harkleroad [McCaffrey *et al.*, 1981] modified for corner configurations [Karlsson and Magnusson, 1991].

The room/corner flame spread model requires material property data that is obtained from the Cone Calorimeter data and from the LIFT apparatus. These properties include the material thermal inertia, the ignition temperature of the material, the flame heating parameter, the heat of gasification, and the minimum flame spread temperature. The thermal inertia obtained from the Cone Calorimeter data is calculated using the heating algorithm in the flame spread model and is a best-fit value to the ignition data. Other input parameters include the thermal material properties of the boundary materials for use with the hot layer temperature calculation, the dimensions of the compartment, and the dimensions of the compartment opening.

6.1 Calculation Results

The calculation results of the flame spread model were compared to the full-scale test data for nine composite materials tested in the ISO 9705 Test. The model performance was evaluated by comparing the time to flashover heat release rate, hot layer temperature, smoke production rate, and floor heat flux predictions. The results are summarized in Table 6-1 time to flashover for the heat release rate, layer temperature, and smoke production rate. The test data was averaged over thirty seconds for peak

heat release rate and sixty seconds for bench smoke production rate, sliding intervals to reduce noise. The model predictions were not averaged.

Table 6-1 shows that the model predicts the flashover time well. Flashover was not predicted for Materials 1, 2, 6, and 7, consistent with test observations. The predicted time to Shaded regions indicate tests that were terminated due to severe fire conditions. As such, the peak heat release rate and smoke production rate comparisons are invalidated by the test termination. Average heat and smoke release rates are averaged up to the time of predicted flashover to be consistent with the tests. *Material No. 7 (textile wall covering) fell off the wall during the Room/Corner test. Flashover for Materials 3, 4, 5, 8, and 9 was within two minutes of the measured time to flashover in all cases.

The peak heat release rate predictions are also shown in Table 6-1, but may not be a good parameter to assess the flame spread model performance for materials that resulted in flashover. This is because these tests were terminated before the intended twenty-minute test period due to the severity of the fire. Hence, the experimental data corresponds to the period just before the test was terminated, whereas the model results reflect the peak heat release under the assumption that the test were run to completion. Tests that resulted in flashover are shaded in Table 6-1. Predicted peak heat release rates for materials that did not flashover are 25-35 percent of the measured values.

Table 6-1. Summary of ISO Room/Corner Test Results and HAI/U.S. Navy Room/Corner Model Results for the USCG High Speed Craft Bulkhead Lining and Ceiling Materials.

USCG High Speed Craft Materials	Time to Flashover t_{fo} 1 MW (500 °C)		ISO 9705 Room/Corner Test Full-Scale Heat Release Rate		Predicted Heat Release Rate from Room/Corner Model		ISO 9705 Room/Corner Test Full-Scale Smoke Production Rate		Predicted Smoke Production Rate from Room/Corner Model	
	ISO 9705 Room/ Corner Test (min)	Room/ Corner Model (min)	Peak 30 sec Average (kW)	Net Average (kW)	Peak (kW)	Net Average (kW)	Peak 60 sec Average (m^2/sec)	Net Average (m^2/sec)	Peak (m^2/sec)	Net Average (m^2/sec)
1-FR phenolic	∞	∞	159	62	56	31	5.40	1.5	0.68	0.38
2- Fire restricting Material	∞	∞	129	31	33	18	0.48	0.15	0.05	0.03
3-FR polyester	5.7 (5.5)	7.5 (7.3)	677	191	2300	140	21.7	10	59	9.1
4-FR vinylester	5.1 (5.0)	6.5 (6.2)	463	190	2990	150	32.0	9	13	11
5-FR epoxy	16.5 (15.2)	15.7 (17.7)	421	115	867	54	26.50	6.5	18	1.6
6-Coated FR epoxy	∞	∞	134	28	36	15	3.50	1.5	0.8	0.3
7-Textile wall covering*	∞	∞	131	17	45	23	0.16	0.1	0.31	0.17
8-Polyester	1.7 (1.5) 441 °C	0.8 (0.8)	568	170	10780	130	4.0	2.3	313	57
9-FR modified acrylic	11.2 (11.5)	10.3 (10.0)	542	109	119	102	3.80	0.4	4.4	0.64
IMO Critera (Resolution MSC.40 (64)			≤500 kW	≤100 kW	≤500 kW	≤100 kW	≤8.3 m^2/s	≤1.4 m^2/s	≤8.3 m^2/s	≤1.4 m^2/s

The average heat release rates for the model shown in Table 6-1 were averaged only up to the time of flashover, such that this is a better indicator of the model performance. Overall, the preflashover heat release rates compare well with the test data. Predicted average heat release rates are 50-90 percent of the measured values.

Smoke production is generally under-predicted in the room/corner flame spread model. The model predicted the smoke production to be 10-25 percent of the measured value for three of the four tests that did not result in flashover. The model over-predicted the smoke production for Material 7. Although the reason for this is not know, material was observed to fall off during the test, possibly reducing the experimentally observed smoke production.

The smoke production predictions for the remaining five materials varied widely. The average smoke production rate for Materials 3 and 4 were within 10 percent of the experimental value. On the other hand, the smoke production for Material 5 was predicted to be 25 percent the measured value and for Material 8 it was predicted to be 25 times the experimental value.

These results are much worse that the heat release rate predictions. This may be partly due to the fact that the smoke production calculation uses the predicted heat release rate and the specific extinction area measure in the Cone Calorimeter. As such, there are additional sources of uncertainty in these predictions. Nevertheless, the results are unsatisfactory and are indicative of a lack of insight into smoke generation in these fires. It is possible that for the materials that do not cause flashover, the smoke generation is dominated by material pyrolysis, which is not ignited. This phenomena is not included in the model.

6.2 Model Sensitivity

The sensitivity of the flame spread model was evaluated by changing different input parameters. The parameters were modified according to the expected uncertainty in the particular parameter. Such uncertainty included reported error ranges in the data and potential user input errors when processing the Cone Calorimeter data for input into the flame spread model. In addition to the material properties, the convergence was verified by changing the number of elements and the solution time step size.

It was demonstrated that the flame spread model was not sensitive to the number of elements and the time step size for the ISO 9705 room/corner configuration predictions. Less elements or a larger time step could result in a non-convergent solution.

Two composites were used to test the model sensitivity to the material properties: Material 3 and Material 9. Material 3 represents a typical composite that results in flashover in the ISO 9705 room/corner tests when exposed to the 100 kW fire source. Material 9 represents a composite that does not flashover the ISO 9705 room/corner test when exposed to the 100 kW source fire but does when exposed to the 300 kW source fire. The model was shown to be sensitive to the ignition, the lateral flame spread, and the heat release rate parameters. Material 3 was more sensitive than Material 9 in all cases. The effect of room size and opening area were also noted to be very significant, primarily by changing the hot layer temperature.

7.0 REFERENCES

Alpert, R.L, “Turblent Ceiling Jet Induced by Large-Scale Fires,” *Combustion Science and Technology*, Vol. 11. Pp. 197-213, (1975).

Alpert, R. L. (1972), "Calculation of Response Time of Ceiling-Mounted Fire Detectors," *Fire Technology*, **8**(3), National Fire Protection Association, Quincy, MA, 1972.

ASTM E 1321-97A, “Standard Test Method for Determining Material Ignition and Flame Spread Properties,” *1997 Annual Book of ASTM Standards*, Vol 04.01: Building Seals and Sealants; fire Standards; Dimension Stone, American Society for Testing and Materials, Philadelphia, PA, pp. 620-635, (1997).

Back, G., Beyler, C., DiNenno, P., and Tatem, P., 1994, “Wall Incident Heat Flux Distribution Resulting from and Adjacent Fire,” *Fire Safety Science-Proceedings from the Fourth International Symposium*, Editor T. Kashiwagi, International Association for Fire Safety Science, pp. 241-252.

Beyler, C.L., Hunt, S.P., Iqbal, N., and Williams, F.W., “A Computer Model of Upward Flame Spread on Vertical Surfaces,” *Fire Safety Science-Proceedings of the Fifth International Symposium*, International Association of Fire Safety Science (IAFSS), Hasemi and Taukuba, Editors, Australia, March 307, 1997, pp. 297-308.

Deal, S. and Beyler, C. (1990), "Correlating Preflashover Room Fire Temperatures," *Journal of Fire Protection Engineering*, **2**(2), 1990.

Hasemi, T., Yokobayashi, S., Wakamatsu, T., and Ptchelintsev, A., “fire Safety of Building Components Exposed to a Localized Fire-Scope and Experiments on Ceiling/beam System Exposed to a Localized Fire,” *Proceedings from ASIAFLAM*, pp. 351-361 (1995).

Hasemi, T., Yoshida, M., Takashima, S., Kikuchi, R., and Yokobayashi, Y., “Flame Length and Flame Heat Transfer Correlations in Corner-Wall and Corner-Wall Ceiling Configurations,” *Proceedings of INTERFLAME''96*, Eds. Franks and Grayson, pp. 179-188 (1996).

Hirschler, M.M. (1992), "Plastics: A. Heat Release from Plastic Materials," *Heat Release in Fires*, Elsevier, London, 1992.

ISO 9705 (1990), "Fire Tests - full-scale Room Test for Surface Products," International Organization for Standards, Geneva, Switzerland, 1990.

Janssens, M. L. and Garabedian, A., and Gray, W. (1998), "Establishment of International Standards Organization Criteria for Fire Restricting Materials Used on High Speed Craft," USCG Report No. CG-D-22-98, 1998.

Karlsson, B. and Magnusson, S. E. (1991), "Combustible Wall Lining Materials: Numerical Simulation of Room Fire Growth and the Outline of a Reliability Based Classification Procedure," *Proceedings of the Third International Fire Safety Science Symposium*, Elsevier Applied Science, London, 1991.

Kokkala, M., “Characteristics of a Flame in an Open Corner of Walls,” *Proceedings from Interflam* ’93, pp. 13-24, (1993).

Laramee, R. C. (1987), "Forms and Properties of Composite Materials," Volume 1, Engineered Materials Handbook, Composites, American Society of Materials, Metals Park, Ohio, 1987.

Lattimer, B.Y., Hunt, S.P., Sorathia, U., Blum, M., Graciek, T., MacFarland, M., Lee, A., and Long, G. (1999), "Development of a Model for Predicting Fire Growth in a Combustible Corner," NSWCCD-64-TR-1999/XX, U.S. Navy, Naval Surface Warfare Center-Carderock Division, West Bethesda, MD, September 1999.

McCaffrey, B., Quintiere, J., and Harkleroad, M. (1981), "Estimating Room Fire Temperatures and the Likelihood of Flashover using Fire Test Data Correlations," *Fire Technology*, **17**(2), 1981.

Mowrer, F. and Williamson, B. (1987), "Estimating Room Temperatures from Fires along Walls and in Corners," *Fire Technology*, **23**(2), 1987.

Quintiere, J.G., Harkleroad, M., and Hasemi, T., “Wall Flames and Implications for Upward Flame Spread,” *Combustion Science and Technology*, **48** (1), (1986).

Quintiere, J.G. and Cleary, T.G., “Heat Flux from Flames to Vertical Surfaces,” *ASME-Heat and Mass Transfer in Fire and Combustion Systems*, HTD-Vol. 223, pp. 111-120, (1992)

Quintiere, J.G. (1993), "A Model for Fire Growth on Materials in a Room-Corner Test," *Fire Safety Journal*, Vol. **20** 1993.

Quintiere, J. and Harkleroad, M. (1985), "New Concepts for Measuring Flame Spread Properties," *Fire Safety Science and Engineering*, ASTM STP 882, American Society for Testing and Materials, Philadelphia, PA, 1985.

Resolution MSC.40(64) (1994), "Standard for Qualifying Marine Materials for High Speed Craft as Fire-Restricting Materials," International Maritime Organization, London, England, 1994.

Tewarson, A. (1995), "Generation of Heat and Chemical Compounds in Fires," Section 3, Chapter 4, *The SFPE Handbook of Fire Protection Engineering*, National Fire Protection Association, Quincy, MA, 1995.

Tu, K. M. and Quintiere, J. Q. (1991), "Wall Flame Heights and External Radiation," *Fire Technology*, **27**(3), 1991.

Williams, F. W., Beyler, C. L., Hunt, S. P., Iqbal (1997), "Upward Flame Spread on Vertical Surfaces," NRL/MR/6180-97-7908, Navy Technology Center for Safety and Survivability, Chemistry Division, Washington, DC, 1997.